

Amyloid fibrils are nanoparticles that target lysosomes

Toral Chandulal Jakhria

Submitted in accordance with the requirements for the degree of Doctor of Philosophy

The University of Leeds

School of Molecular and Cellular Biology

Faculty of Biological Sciences

September 2014

The candidate confirms that the work submitted is her own and that appropriate credit has been given where reference has been made to the work of others.

This copy has been supplied on the understanding that it is copyright material and that no quotation from the thesis may be published without proper acknowledgement.

The right of Toral Chandulal Jakhria to be identified as Author of this work has been asserted by her in accordance with the Copyright, Designs and Patents Act 1988.

© 2014 The University of Leeds and Toral Chandulal Jakhria

Acknowledgements

I would like to thank my supervisors Eric Hewitt and Sheena Radford for all their assistance, support and valued advice throughout my PhD. I would also like to thank past and present members of the Hewitt and Radford groups for their help over the past four years. I would especially like to thank Andrew Hellewell for showing me the ropes when I first started and for always being there with advice, support, coffee and bad puns. Special thanks also go to Rebecca Thompson for being so enthusiastic, helpful and supportive and Claire Sarell for her fantastic support and helping me keep things in perspective. I am grateful to Gareth Howell and Sally Boxall for advice on confocal microscopy and flow cytometry, Kevin Tipping for determining the fibril length of β_2m fibril samples, Timo Eichner for teaching me how to express and purify β_2m , Theodoros Karamanos for assistance with the AKTA, Sophie Goodchild for help with the PTI and James Ault for mass spectrometry analysis. I am grateful to members of the Whitehouse group for useful advice throughout my PhD and for making the laboratory an enjoyable place to work in; and special thanks go to Dave Hughes and Chris Owen for all their blotting advice. Thanks also to the BBSRC for funding my PhD studentship.

I am grateful to colleagues who have kindly supplied antibodies and materials which have been crucial to this work including Charles Glabe (University of California, Irvine) for the A11 antibody and $A\beta_{1-40}$ oligomers, Ronald Wetzel (University of Pittsburgh, Illinois) for the WO1 antibody and Nunilio Cremades (University of Cambridge) for the pET28b-Hsp70(1A) plasmid.

Extra special thanks goes to my family. I would not have been able to make the most of this fantastic opportunity had it not been for everything you've done to get me to where I am today. Thank you Dad for all the sacrifices you've made for me, I know they have been plenty and they have not gone by unnoticed. Thank you Mum for setting me all that extra Maths work all those years ago. You may not know it but all the energy, patience and love you devoted to me has got me here and I am eternally grateful. Thank you Meera for always being just a phone call away for sisterly advice. Finally, but by no means least, I am sincerely grateful to Dale. You've been nothing short of amazing and I do not know how I would have coped without your constant support and encouragement.

Abstract

The amyloidoses are a group of debilitating disorders which include neurodegenerative diseases such as Alzheimer's disease and systemic diseases such as dialysis-related amyloidosis (DRA). Amyloidoses are associated with the aggregation of proteins into amyloid fibrils with a highly organised cross- β structure. Amyloid fibrils are formed by a variety of proteins and peptides despite differences in sequence and native structure. Amyloid formation occurs by a nucleated growth mechanism and proceeds via oligomeric intermediates into mature fibrils. Despite intense research, the molecular mechanisms involved in disease pathogenesis remain unclear. This thesis discusses the mechanism by which amyloid fibrils cause cellular disruption.

Chapter 3 describes work performed to validate the use of β_2 -microglobulin (β_2m), the protein that self-associates into amyloid fibrils found in DRA deposits, as a model to study amyloidosis. Fragmentation of mature β_2m fibrils, increased their internalisation and access to intracellular compartments, and were therefore used to investigate mechanisms of cellular disruption. Building on previous work in the laboratory showing trafficking of β_2m fibrils to the lysosome, chapter 4 examined the effect of fragmented fibrils on lysosomal function and demonstrates that fragmented fibrils impair lysosome-mediated degradation of endocytosed proteins. Following on from this, chapter 5 discusses the effect of fragmented fibrils on membrane trafficking. Fragmented fibrils perturbed the trafficking of lysosomal membrane proteins and also reduced the trafficking of endocytosed cargo to lysosomes. This may rationalise the impairment in degradation of endocytosed proteins. The molecular chaperone, heat shock protein 70 (Hsp70) has been shown to be protective in amyloid disease. The role of Hsp70 in fibril-mediated cell disruption was investigated in chapter 6. Hsp70 protected fibril-treated cells from impairment in degradation of endocytosed protein but not from membrane trafficking defects. This work demonstrates that fragmented fibrils are nanoparticles which target lysosomes and implicates the lysosome in the pathogenesis of amyloidosis.

Table of Contents

| | |
|--|----|
| Acknowledgements..... | 3 |
| Abstract..... | 4 |
| List of figures..... | 10 |
| List of Tables | 13 |
| Abbreviations..... | 14 |
| 1 Introduction | 18 |
| 1.1 Amyloidosis | 18 |
| 1.1.1 Alzheimer’s disease..... | 20 |
| 1.1.2 Parkinson’s disease | 21 |
| 1.1.3 Type II diabetes mellitus | 23 |
| 1.1.4 Dialysis related amyloidosis..... | 24 |
| 1.2 Amyloid as a functional element | 28 |
| 1.2.1 Exploitation of the mechanical strength of amyloid fibrils..... | 28 |
| 1.2.2 Amyloid fibrils as self-replicative transmissible elements | 28 |
| 1.2.3 Functional amyloid fibrils in mammalian systems..... | 29 |
| 1.3 Amyloid | 31 |
| 1.3.1 Structure of amyloid fibrils | 31 |
| 1.3.2 Amyloid fibril formation pathway..... | 35 |
| 1.4 Association of amyloid with cell death and disease progression | 38 |
| 1.4.1 The role of oligomers in cell death and disease progression..... | 39 |
| 1.4.2 The role of amyloid fibrils in cell death and disease progression..... | 40 |
| 1.5 Mechanisms and consequences of cell death and disruption of cellular functions... | 43 |
| 1.5.1 Disruption due to aberrant interactions via hydrophobic surfaces..... | 43 |
| 1.5.2 Disruption via saturation of the central protein quality control and clearance systems | 44 |
| 1.5.3 Disruption via membrane permeation | 45 |
| 1.5.4 Disruption via organelle dysfunction | 48 |

| | | |
|-------|---|----|
| 1.6 | Aims..... | 54 |
| 1.7 | Objectives..... | 54 |
| 1.7.1 | Chapter 3 objectives | 54 |
| 1.7.2 | Chapter 4 objectives | 54 |
| 1.7.3 | Chapter 5 objectives | 54 |
| 1.7.4 | Chapter 6 objectives | 54 |
| 2 | Materials and methods..... | 55 |
| 2.1 | Expression and purification of β_2m | 55 |
| 2.1.1 | Expression of β_2m | 55 |
| 2.1.2 | Inclusion body isolation | 55 |
| 2.1.3 | Refolding by dialysis..... | 55 |
| 2.1.4 | Anion exchange chromatography..... | 56 |
| 2.1.5 | Size exclusion chromatography | 56 |
| 2.2 | Sodium dodecyl sulphate polyacrylamide gel electrophoresis (SDS-PAGE)..... | 57 |
| 2.3 | Statistical analysis | 59 |
| 2.4 | Generation and characterisation of β_2m fibrils | 59 |
| 2.4.1 | Production of β_2m fibrils..... | 59 |
| 2.4.2 | Fragmentation of β_2m fibrils..... | 59 |
| 2.4.3 | Thioflavin T fluorescence | 59 |
| 2.4.4 | Immunoblotting of fibril samples..... | 60 |
| 2.4.5 | Transmission electron microscopy | 61 |
| 2.4.6 | Fibril length determination by atomic force microscopy (AFM)..... | 61 |
| 2.5 | Cell culture | 62 |
| 2.5.1 | 3-(4,5-Dimethylthiazol-2yl)-2,5-diphenyltetrazolium bromide (MTT) assay | 62 |
| 2.5.2 | Phase contrast microscopy of cells incubated with MTT..... | 62 |
| 2.6 | Western blotting analysis | 63 |
| 2.6.1 | Preparation of cell lysates..... | 63 |
| 2.6.2 | Immunoblotting | 63 |

| | | |
|--------|---|----|
| 2.7 | Assays on lysosomal function | 65 |
| 2.7.1 | Analysis of lysosomal degradation of fluorescent protein substrates..... | 65 |
| 2.7.2 | Analysis of lysosomal proteolysis using Magic Red™..... | 67 |
| 2.7.3 | Analysis of β -glucocerebrosidase and β -galactosidase activity | 67 |
| 2.8 | Analysis of membrane trafficking | 68 |
| 2.8.1 | Analysis of the cell surface levels of LAMP-1 and CD63 | 68 |
| 2.8.2 | Immunofluorescence microscopy analysis of the intracellular distribution of LAMP-1 and CD63 | 69 |
| 2.8.3 | Analysis of the effect of fibrils on fluid phase endocytosis..... | 70 |
| 2.9 | Expression and purification of Hsp70 | 71 |
| 2.9.1 | Expression of Hsp70..... | 71 |
| 2.9.2 | Cell lysis..... | 71 |
| 2.9.3 | Ni-NTA affinity chromatography..... | 72 |
| 2.9.4 | Size exclusion chromatography | 72 |
| 2.9.5 | Anion exchange chromatography..... | 73 |
| 2.10 | Analysis of the effect of Hsp70 on fibril-mediated cell disruption | 73 |
| 2.10.1 | Analysis of intracellular localisation of recombinant Hsp70..... | 73 |
| 2.10.2 | MTT assay..... | 74 |
| 2.10.3 | Phase contrast microscopy analysis of cells incubated with MTT | 74 |
| 2.10.4 | Analysis of cell-surface expression of LAMP-1..... | 74 |
| 2.10.5 | Analysis of lysosomal degradation of fluorescently labelled ovalbumin..... | 75 |
| 3 | β_2 m as a model to study amyloid disease..... | 76 |
| 3.1 | Introduction | 76 |
| 3.1.1 | β_2 m structure | 76 |
| 3.1.2 | β_2 m amyloid formation and characterisation..... | 77 |
| 3.1.3 | β_2 m as a model to study amyloid disease..... | 80 |
| 3.2 | Results..... | 80 |
| 3.2.1 | Expression and purification of β_2 m..... | 80 |

| | | |
|-------|---|-----|
| 3.2.2 | Generation and characterisation of amyloid fibrils | 85 |
| 3.2.3 | Analysis of the effect of fibrils on the cellular reduction of MTT | 89 |
| 3.3 | Discussion..... | 95 |
| 4 | Analysis of the effect of amyloid fibrils on lysosome function | 98 |
| 4.1 | Introduction | 98 |
| 4.2 | Results..... | 100 |
| 4.2.1 | Analysis of the effect of fragmented fibrils on lysosomal proteolysis..... | 100 |
| 4.2.2 | Analysis of the effect of fibrils on autophagy | 119 |
| 4.2.3 | Analysis of the effect of fibrils on the lysosomal hydrolase, β -glucocerebrosidase | 120 |
| 4.2.4 | Analysis of the effect of fibrils on the lysosomal hydrolase, β -galactosidase .. | 122 |
| 4.3 | Discussion..... | 124 |
| 5 | Analysis of the effect of amyloid fibrils on membrane trafficking..... | 128 |
| 5.1 | Introduction | 128 |
| 5.2 | Results..... | 132 |
| 5.2.1 | Analysis of the effect of fibrils on the cell surface expression of LAMP-1 and CD63 | 132 |
| 5.2.2 | Immunoblotting analysis of the effect of fibrils on lysosomal protein expression | 135 |
| 5.2.3 | Immunofluorescence microscopy analysis of the effect of fibrils on the intracellular distribution of LAMP-1 and CD63 | 136 |
| 5.2.4 | Analysis of the effect of fibrils on the trafficking of newly synthesised LAMP-1 and CD63 | 139 |
| 5.2.5 | Analysis of the effect of fibrils on endocytosis | 142 |
| 5.3 | Discussion..... | 147 |
| 6 | Investigation of the role of the molecular chaperone, Hsp70 in fibril-mediated cell disruption..... | 151 |
| 6.1 | Introduction | 151 |
| 6.1.1 | Hsp70 and its role in amyloid disease..... | 151 |

| | | |
|-------|--|-----|
| 6.1.2 | Hsp70 and its role in lysosomal storage diseases | 152 |
| 6.2 | Results | 153 |
| 6.2.1 | Expression and purification of Hsp70 | 153 |
| 6.2.2 | Analysis of the intracellular localisation of recombinant Hsp70 | 159 |
| 6.2.3 | Investigation of the role of Hsp70 in amyloid-mediated disruption of MTT reduction..... | 159 |
| 6.2.4 | Investigation of the role of W90F Hsp70 in amyloid-mediated disruption of MTT reduction..... | 161 |
| 6.2.5 | Investigation of the effect of Hsp70 on fibril-mediated alteration in formazan trafficking | 165 |
| 6.2.6 | Further investigation into the effect of Hsp70 on fibril-mediated cell disruption | 167 |
| 6.3 | Discussion..... | 171 |
| 7 | Discussion and future work | 175 |
| 7.1 | Lysosome dysfunction and its role in amyloid disease | 175 |
| 7.2 | Membrane trafficking perturbations and their role in amyloid disease | 178 |
| 7.3 | Future therapeutic strategies for amyloid disease | 179 |
| 7.4 | Summary | 180 |
| 8 | References | 182 |

List of figures

| | |
|--|-----|
| Figure 1.1: Amyloid deposits in neurodegenerative diseases. | 23 |
| Figure 1.2: β_2m deposits in the joints in DRA. | 26 |
| Figure 1.3: Model for the pathogenesis of DRA. | 27 |
| Figure 1.4: Electron micrographs showing different fibril morphologies..... | 32 |
| Figure 1.5: Amyloid fibrils have a cross- β architecture. | 33 |
| Figure 1.6: Amyloid fibril structure at atomic resolution. | 34 |
| Figure 1.7: Schematic representation of two possible amyloid formation pathways: | 37 |
| Figure 1.8: Model of pathogenicity: | 42 |
| Figure 1.9: Schematic description of the proposed models of interactions resulting in membrane destabilisation and disruption..... | 47 |
| Figure 3.1: Structure of MHC I complex and β_2m monomer. | 76 |
| Figure 3.2: Structures of wild-type β_2m and β_2m variants displaying a β -bulge or continuous β - strand D..... | 77 |
| Figure 3.3: Morphological, structural and tinctorial characteristics of β_2m amyloid fibrils assembled at low pH and low ionic strength..... | 79 |
| Figure 3.4: Schematic of expression and purification strategy. | 81 |
| Figure 3.5: Anion exchange chromatography purification of solubilised inclusion bodies..... | 82 |
| Figure 3.6: SDS-PAGE analysis of β_2m expression and purification by anion exchange chromatography. | 82 |
| Figure 3.7: Further purification of β_2m by size exclusion chromatography. | 83 |
| Figure 3.8: SDS-PAGE analysis of purification of β_2m by size exclusion chromatography. | 83 |
| Figure 3.9: Analytical size exclusion chromatography to determine the purity of β_2m | 84 |
| Figure 3.10: Electrospray ionisation mass spectrometry (ESI-MS) analysis of the purified protein..... | 84 |
| Figure 3.11: Characterisation of amyloid fibrils by ThT fluorescence. | 86 |
| Figure 3.12: Analysis of β_2m fibril samples with amyloid-specific antibodies. | 87 |
| Figure 3.13: TEM images of fibrils generated from β_2m | 88 |
| Figure 3.14: Analysis of fibril length by AFM. | 89 |
| Figure 3.15: Schematic showing an overview of the MTT assay. | 91 |
| Figure 3.16: Analysis of the effect of fibrils on MTT reduction. | 92 |
| Figure 3.17: Phase contrast microscopy images of fibril treated cells incubated with MTT..... | 94 |
| Figure 3.18: Analysis of the effect of fibrils on cell viability. | 97 |
| Figure 4.1: Quantification of intracellular TMR labelled β_2m monomer and fibrils from confocal images. | 99 |
| Figure 4.2: Schematic of the lysosomal proteolysis assay. | 101 |
| Figure 4.3: Analysis of the effect of fibrils on the degradation of TMR- β_2m in RAW 264.7 cells. | 102 |
| Figure 4.4: Analysis of the effect of fibrils on the degradation of TMR- β_2m in SH-SY5Y cells.. | 103 |
| Figure 4.5: Analysis of the effect of fibrils on the degradation of Pumilio-GFP in RAW 264.7 cells. | 105 |
| Figure 4.6: Pumilio-GFP fluorescence intensity varies with pH..... | 106 |
| Figure 4.7: Analysis of the internalisation, localisation and degradation of fluorescently labelled ovalbumin in RAW 264.7 cells..... | 109 |

| | |
|---|-----|
| Figure 4.8: Analysis of the internalisation, localisation and degradation of fluorescently labelled ovalbumin in SH-SY5Y cells | 111 |
| Figure 4.9: Immunoblotting analysis to assess the degradation of ovalbumin in RAW 264.7 and SH-SY5Y cells. | 112 |
| Figure 4.10: Analysis of the effect of fibrils on the degradation of AF647-ovalbumin in RAW 264.7 cells. | 114 |
| Figure 4.11: Analysis of the effect of fibrils on the degradation of AF647-ovalbumin in SH-SY5Y cells. | 115 |
| Figure 4.12: Analysis of the internalisation and cleavage of Magic red™ cathepsin B substrate. | 117 |
| Figure 4.13: Analysis of the effect of fibrils on lysosomal cathepsin B activity. | 118 |
| Figure 4.14: Immunoblotting analysis of the effect of fibrils on autophagy with LC3B. | 119 |
| Figure 4.15: Analysis of the effect of fibrils on glucocerebrosidase activity. | 121 |
| Figure 4.16: Analysis of the effect of fibrils on β-galactosidase activity. | 123 |
| Figure 4.17: Analysis of the effect of fragmented fibrils on lysosomal membrane permeabilisation. | 126 |
| Figure 5.1: Overview of LAMP-1 and CD63 trafficking. | 131 |
| Figure 5.2: Analysis of the effect of fibrils on the cell surface expression of LAMP-1. | 133 |
| Figure 5.3: Analysis of the effect of fibrils on the cell surface expression of CD63..... | 134 |
| Figure 5.4: Immunoblotting analysis of the effect of fibrils on total levels of LAMP-1, CD63 and Cathepsin-D..... | 135 |
| Figure 5.5: Immunofluorescence microscopy analysis of the effect of fibrils on the distribution of LAMP-1..... | 137 |
| Figure 5.6: Immunofluorescence microscopy analysis of the effect of fibrils on the distribution of CD63..... | 138 |
| Figure 5.7: Analysis of the effect of cycloheximide on cell surface levels of LAMP-1..... | 140 |
| Figure 5.8: Analysis of the effect of cycloheximide on cell surface levels of CD63. | 141 |
| Figure 5.9: Analysis of the effect of fibrils on the uptake of fluorescently labelled dextran. .. | 143 |
| Figure 5.10: Live cell confocal microscopy analysis of the effect of fibrils on endocytosis..... | 145 |
| Figure 5.11: Colocalisation analysis of the effect of fibrils on endocytosis..... | 146 |
| Figure 5.12: Model of fibril-mediated perturbation in trafficking of LAMP-1, CD63 and endocytosed cargo..... | 148 |
| Figure 6.1: Schematic of Hsp70 expression and purification strategy. | 154 |
| Figure 6.2: Ni-NTA affinity chromatography purification of Hsp70..... | 155 |
| Figure 6.3: SDS-PAGE analysis of Hsp70 purification by Ni-NTA chromatography..... | 156 |
| Figure 6.4: Size exclusion chromatography purification of Hsp70. | 156 |
| Figure 6.5: SDS-PAGE analysis of size exclusion chromatography purification of Hsp70..... | 157 |
| Figure 6.6: Further purification of Hsp70 by anion exchange chromatography. | 157 |
| Figure 6.7: SDS-PAGE analysis of anion exchange chromatography purification of Hsp70. | 158 |
| Figure 6.8: Electrospray ionisation mass spectrometry (ESI-MS) analysis of purified Hsp70. . | 158 |
| Figure 6.9: Analysis of the internalisation and localisation of labelled Hsp70 in RAW 264.7 cells. | 159 |
| Figure 6.10: Analysis of the effect of Hsp70 on MTT reduction in fibril treated cells..... | 160 |
| Figure 6.11: Analytical size exclusion chromatography of purified W90F Hsp70. | 162 |

| | |
|---|-----|
| Figure 6.12: SDS-PAGE analysis of analytical size exclusion chromatography of purified W90F Hsp70..... | 162 |
| Figure 6.13: Analysis of the effect of W90F Hsp70 on the fibril-mediated disruption of MTT reduction. | 164 |
| Figure 6.14: Phase contrast microscopy analysis of the effect of Hsp70 on formazan trafficking. | 166 |
| Figure 6.15: Analysis of the effect of Hsp70 on the cell surface expression of LAMP-1. | 168 |
| Figure 6.16: Analysis of the effect of Hsp70 on the degradation of fluorescently labelled ovalbumin in fibril treated cells..... | 170 |
| Figure 6.17: Analysis of the effect of Hsp70 on disaggregation of β_2m fibrils..... | 172 |
| Figure 7.1: Model of cellular disruption by fragmented β_2m amyloid fibrils. | 181 |

List of Tables

| | |
|--|----|
| Table 1: Examples of amyloid diseases, their associated proteins, location of deposits and affected organs..... | 19 |
| Table 2.1: Details of the AKTA program used for size exclusion chromatography of β_2m | 56 |
| Table 2.2: Components of a Tris-tricine buffered gel..... | 57 |
| Table 2.3: Components of a Tris-glycine buffered gel..... | 57 |
| Table 2.4: Primary antibodies used in the immunoblotting protocol..... | 60 |
| Table 2.5: Secondary antibodies used in the immunoblotting protocol..... | 61 |
| Table 2.6: Primary antibodies used for probing western blots..... | 64 |
| Table 2.7: Secondary antibodies used for probing western blots..... | 64 |
| Table 2.8: Fluorescent protein substrates used for analysis of lysosomal degradation..... | 66 |
| Table 2.9: Antibodies used for flow cytometric analysis of LAMP-1 and CD63 cell surface expression..... | 69 |
| Table 2.10: Primary antibodies used for immunofluorescence microscopy..... | 69 |
| Table 2.11: Secondary antibodies used for immunofluorescence microscopy..... | 70 |
| Table 2.12: Details of the AKTA program used for the size exclusion chromatography purification of Hsp70..... | 73 |

Abbreviations

| | |
|-----------------|--|
| 17-AAG | 17-N-allylamino-17-demethoxygeldanamycin |
| AA | Amyloid A amyloidosis |
| AF568-dextran | Alexa Fluor® 568 labelled dextran |
| AF647-ovalbumin | Alexa Fluor® 647 labelled ovalbumin |
| AF680-dextran | Alexa Fluor® 680 labelled dextran |
| AFM | Atomic force microscopy |
| AGE | Advanced-glycation end products |
| AL | Amyloid light-chain |
| ALS | Amyotrophic lateral sclerosis |
| ANS | 1-anilinonapthalene 8-sulphonate |
| AP3 | Adaptor protein complex 3 |
| APP | Amyloid precursor protein |
| A β | Amyloid β |
| <i>BIN1</i> | Bridging integrator 1 |
| BMP | Bis(monoacylglycero)phosphate |
| BSA | Bovine serum albumin |
| CBE | conduritol B epoxide |
| CD | Circular Dichroism |
| CD63 | Cluster of differentiation 63 |
| CLEAR | Co-ordinated lysosomal expression and regulation |
| CMA | Chaperone-mediated autophagy |
| CNS | Central nervous system |

| | |
|--------|---|
| DAPI | 2-(4-amidinophenyl)-1H -indole-6-carboxamide |
| DMEM | Dulbecco's modified eagle's medium |
| DMSO | Dimethyl sulphoxide |
| DRA | Dialysis-related amyloidosis |
| DTT | Dithiothreitol |
| EDTA | Ethylene diamine tetra acetic acid |
| EEA1 | Early endosome antigen 1 |
| ER | Endoplasmic reticulum |
| ESI-MS | Electrospray ionisation mass spectrometry |
| FDA | Food and Drug Administration |
| FDG | Fluorescein di- β -D-galactopyranoside |
| FTIR | Fourier Transform Infrared |
| GAPDH | Glyceraldehyde-3-phosphate dehydrogenase |
| GFP | Green fluorescent protein |
| HRP | Horseradish peroxidase |
| Hsp | Heat shock protein |
| Hsp70 | Heat shock protein 70 |
| IAPP | Islet amyloid peptide |
| IPTG | isopropyl β -D-1-thiogalactopyranoside |
| LAMP-1 | Lysosomal-associated membrane protein 1 |
| LB | Lysogeny Broth |
| LC3 B | Microtubule-associated protein 1 light chain 3B |
| LMP | Lysosomal membrane permeabilisation |

| | |
|---------------|---|
| LRRK2 | Leucine-rich repeat kinase 2 |
| LSD | Lysosomal storage disorder |
| LTP | Long-term potentiation |
| M6P | Mannose-6-phosphate |
| MCC | Manders' colocalisation coefficient |
| MHC I | Major histocompatibility complex I |
| MTT | 3-(4,5-dimethylthiazol-2-yl)-2,5-diphenyltetrazolium bromide |
| MVB | Multivesicular body |
| MVBs | Multi-vesicular bodies |
| MW | Molecular weight |
| MWCO | Molecular weight cut off |
| NMDA | N-methyl-D-aspartic acid |
| NP-40 | Nonidet P-40 |
| PBS | Phosphate buffered saline |
| PFB-FDGlu | 5-(pentafluorobenzoylamino)fluorescein di- β -D-glucopyranoside |
| <i>PICALM</i> | Phosphatidylinositol-binding clathrin assembly protein |
| PMSF | Phenylmethylsulphonyl fluoride |
| PVDF | Polyvinylidene fluoride |
| QC | Quality control |
| rPRP | Recombinant mammalian prion protein |
| S.D. | Standard deviation |
| S.E.M. | Standard error of mean |
| SAP | Serum amyloid protein |

| | |
|-----------------|---|
| SBMA | Spinobulbar muscular atrophy |
| SDS | Sodium dodecyl sulphate |
| SDS-PAGE | Sodium dodecyl sulphate polyacrylamide gel electrophoresis |
| SNARE | Soluble <i>N</i> -ethylmaleimide-sensitive fusion attachment protein receptor |
| SOD1 | Superoxide dismutase-1 |
| <i>SORL1</i> | Sortilin-related receptor 1 |
| ssNMR | Solid state nuclear magnetic resonance |
| TEM | Transmission electron microscopy |
| TEMED | Tetramethylethylenediamine |
| TFEB | Transcription factor EB |
| TGN | Trans-Golgi network |
| ThT | Thioflavin T |
| TMR | 5-(and-6)-carboxytetramethylrhodamine |
| TMR- β_2m | Tetramethylrhodamine labelled β_2m monomer |
| TSE | Transmissible spongiform encephalopathies |
| UCHL1 | Ubiquitin carboxy-terminal hydrolase L1 |
| UPS | Ubiquitin-proteasome system |
| W90F Hsp70 | Single point mutation of Hsp70 which changes tryptophan 90 to a phenylalanine residue |
| WST-1 | 2-(4-iodophenyl)-3-(4-nitrophenyl)-5-(2,4-disulphophenyl)-2H-tetrazolium sodium salt |
| β_2m | β_2 -microglobulin |
| $\Delta N6$ | N terminally truncated β_2m (missing the first 6 residues) |

1 Introduction

1.1 Amyloidosis

The amyloidoses are a class of protein conformational diseases that are associated with the conversion of proteins/peptides from their soluble, functional forms into highly ordered β -sheet rich aggregates, known as amyloid, that deposit as extracellular plaques or intracellular inclusions [1]. The amyloidoses include a variety of diseases from severe debilitating neurodegenerative conditions such as Alzheimer's, Parkinson's, Huntington's and Creutzfeldt-Jacob diseases; to localised non-neurodegenerative diseases such as type II diabetes and light chain amyloidosis; and chronic systemic diseases such as dialysis-related amyloidosis [1]. With 5 million people currently estimated to be suffering from Alzheimer's disease in the United States alone and a prediction of increased prevalence to 13.8 million by 2050, the high prevalence of these diseases in the population has major implications for the economic burden on society as the population ages [2].

The ability to adopt the amyloid conformation is an inherent property of polypeptide chains, although the propensity to form such a structure can vary dramatically with sequence [3]. To date there are at least 30 known human extracellular fibril proteins (and 7 proteins found in intracellular inclusion bodies) associated with amyloidosis [4](Table 1). Interestingly, some organisms, including humans have been found to convert one or more of their endogenous proteins into amyloid fibrils that have functional, rather than disease-associated properties [1].

Remarkably, the disease-associated amyloid proteins have no evident similarity in the amino acid sequence, native conformations or biological functions [1]. Amyloid diseases target a variety of tissues and are accompanied by a variety of pathological symptoms (Table 1). To highlight the consequences of amyloid formation, the neurodegenerative diseases, Alzheimer's disease and Parkinson's disease will be discussed in detail in the following section, as will the non-neurodegenerative disorder type II diabetes mellitus. Dialysis-related amyloidosis (DRA), the chronic systemic disease associated with β_2 -microglobulin (β_2m) will also be discussed. Finally, examples where the amyloid structure is exploited for functional uses are briefly discussed.

| Disease | Aggregating protein or peptide | Extracellular amyloid deposits/ intracellular inclusions | Systemic or Organ-specific; Involved organ(s) |
|---|---|---|--|
| Alzheimer's Disease | Amyloid β peptide | Extracellular amyloid deposits | Organ-specific; Brain |
| Alzheimer's Disease | Tau | Intracellular inclusions | Organ-specific; Brain |
| Parkinson's Disease | α -synuclein | Intracellular inclusions | Organ-specific; Brain |
| Spongiform encephalopathies | Prion protein | Extracellular amyloid deposits | Organ-specific; Brain |
| Huntington's Disease | Huntingtin with polyglutamine expansion | Intracellular inclusions | Organ-specific; Brain |
| Amyloid Light-chain (AL) amyloidosis | Immunoglobulin light chain or fragments | Extracellular amyloid deposits | Systemic |
| Dialysis related amyloidosis | β_2 -microglobulin | Extracellular amyloid deposits | Systemic; Joints |
| Lysozyme amyloidosis | Lysozyme | Extracellular amyloid deposits | Systemic |
| Senile systemic amyloidosis | Transthyretin | Extracellular amyloid deposits | Systemic |
| Transthyretin amyloidosis | Transthyretin | Extracellular amyloid deposits | Systemic |
| Fibrinogen amyloidosis | Fibrinogen α -chain | Extracellular amyloid deposits | Systemic |
| Type II Diabetes | Amylin | Extracellular amyloid deposits | Organ-specific; Pancreas (Islets of Langerhans) |
| AA amyloidosis | Serum amyloid A protein | Extracellular amyloid deposits | Systemic |
| Medullary carcinoma of the thyroid | Calcitonin | Extracellular amyloid deposits | Organ-specific; Thyroid |
| Atrial amyloidosis | Atrial natriuretic factor | Extracellular amyloid deposits | Organ-specific; Heart |
| Cataract | γ -Crystallins | Extracellular amyloid deposits | Organ-specific; Eye |

Table 1: Examples of amyloid diseases, their associated proteins, location of deposits and affected organs. Adapted from [1] and [4].

1.1.1 Alzheimer's disease

Owing to its high prevalence, Alzheimer's disease has been well studied. Since it was first described in 1906, substantial progress has been made in terms of understanding the etiology of disease; however a cure is still unavailable [5, 6].

Alzheimer's disease patients experience an inevitable loss of control over thought and behaviour, leading to relentless cognitive decline [7]. This is accompanied with behavioural and psychological symptoms such as delusions, hallucinations, apathy, depression, anxiety and agitation; inescapably leading to a gradual loss of daily activities [7]. Accurate early diagnosis of Alzheimer's disease is difficult as patients not only present with varying degrees of these symptoms, but these symptoms are also shared with a variety of other disorders [8]. Despite a strong push in biomarker discovery research, biomarkers are still insufficient for a differential and unambiguous diagnosis between different dementia types, and the biological tools that do exist are not available to clinicians as they require expert knowledge for interpretation [8].

Alzheimer's disease is an organ-specific neurodegenerative disease and involves two major protein aggregates [9]. The amyloid β ($A\beta$) peptide, a proteolytic cleavage product of the amyloid precursor protein (APP), is found in extracellular aggregates known as amyloid plaques [10]. The microtubule-associated protein, tau, is found in intracellular aggregates called neurofibrillary tangles [11]. Amyloid plaques and neurofibrillary tangles are considered the pathological hallmarks of Alzheimer's disease [12](Figure 1.1).

The normal physiological function of APP is still not fully understood, however it is thought to relate to cell-cell interactions and cell-substrate adhesion [13, 14]. APP is required for migration of neuronal precursor cells in the developing brain as well as neuronal cell migration in the mature brain [14, 15]. It plays a part in neuronal calcium homeostasis which is essential for synaptic transmission [14]. Mutations in APP and in presenilins involved in the cleavage of APP are linked to familial Alzheimer's disease, implicating them in the pathogenesis of disease [16]. $A\beta$ is generated by the sequential cleavage of APP by β -secretase and γ -secretase [17]. The size of $A\beta$ can be 39-43 residues in length depending on the γ -secretase cleavage site. The longer moieties are more amyloidogenic, with $A\beta_{1-40}$ and $A\beta_{1-42}$ being the focus of most research efforts, as these peptides are found at high levels in amyloid plaques [18]. $A\beta_{1-40}$ is thought to be less aggregation prone and less toxic than $A\beta_{1-42}$, but is more prevalent than $A\beta_{1-42}$ [19]. The α -secretase mediated cleavage of APP followed by γ -secretase cleavage yields non-amyloidogenic peptide products [17].

Tau is a neuronal microtubule-associated protein mainly found in axons. It interacts with tubulin and stimulates its assembly into microtubules stabilising their structure [20]. Tau modulates microtubule-dependent axonal anterograde and retrograde transport of organelles and biomolecules [21]. It is also involved in programmed apoptosis as tau phosphorylation stabilises β -catenin to halt apoptotic death [22]. Hyperphosphorylation of Tau has been implicated in the pathogenesis of Alzheimer's disease, both due to loss of normal physiological function and enhanced aggregation propensity into neurofibrillary tangles [20]. Despite the prominent role of Tau in the pathogenesis of Alzheimer's disease, research efforts have mainly focused on A β . However, it is becoming increasingly clear that Alzheimer's disease therapies will have to recognise both Tau and A β as molecular players driving Alzheimer's disease [20].

Although there have been numerous clinical trials testing drugs that either modify the disease or relieve symptoms, there are few current U.S. Food and Drug Administration (FDA) approved therapies. Approved therapies currently include acetylcholinesterase inhibitors and N-methyl-D-aspartic acid (NMDA) receptor antagonists [6]. However, these current therapies do not target the underlying pathogenesis of Alzheimer's disease, but limit disease progression after neuronal damage has occurred [6]. Therapeutic strategies currently in development include those that modulate neurotransmission; alter Tau post-translational modifications and levels as well as APP processing and A β levels; target intracellular signalling cascades, oxidative stress and mitochondrial damage; and modulate calcium homeostasis and inflammation (reviewed in [6]).

1.1.2 Parkinson's disease

Parkinson's disease is the second most common neurodegenerative disease after Alzheimer's disease, affecting 1 % of the population over 65 and 5 % of the population over the age of 85 [23, 24]. Parkinson's disease is a chronic, slowly progressive disorder with an average life expectancy of about 15 years after diagnosis; however some patients live 20 years or longer post-diagnosis [25].

Parkinsonism is clinically described as a syndrome comprising combinations of motor problems such as bradykinesia, resting tremor, rigidity, postural instability and loss of postural reflexes [26]. Parkinson's disease is the major cause of parkinsonism, and it begins with parkinsonism usually affecting one side of the body before inevitably spreading to the other side [26]. Secondary symptoms include anxiety, depression, confusion, memory loss and dementia [26].

Mutations in *SNCA*, the gene encoding α -synuclein, are strongly associated with familial Parkinson's disease, whereas sporadic Parkinson's disease is associated with both single

nucleotide polymorphisms at the *SNCA* locus as well as mutations not associated with familial Parkinson's disease historically [25]. α -synuclein is a small, 140 residue protein, widely expressed throughout the nervous system and particularly enriched at presynaptic nerve terminals [27]. Although the precise function of α -synuclein is unknown, it is thought to be involved in synaptic vesicle trafficking, in particular the fast kinetics of synaptic vesicle endocytosis [28]. α -synuclein is thought to promote Parkinson's disease pathogenesis via gain-of-function mechanisms; through dominantly inherited mutations or via increased expression due to gene-multiplication or gene-promoter polymorphisms [25]. Mutations in the *LRRK2* gene encoding the leucine-rich repeat kinase 2 (LRRK2) protein are also associated with Parkinson's disease. LRRK2 is widely expressed in both neuronal and non-neuronal tissues [25]. *GBA*, the gene encoding glucocerebrosidase, a lysosomal hydrolase, is mutated in patients with Gaucher's disease. There's a strong association between Gaucher's disease and Parkinson's disease and *GBA* mutations are commonly found in patients with Parkinson's disease [25]. The relationship between Gaucher's disease and Parkinson's disease is discussed in Section 1.5.4.2.4.

A pathological loss in dopaminergic neurons within the substantia nigra pars compacta and the resultant dysfunction of the basal ganglia (responsible for the initiation and execution of movements) is associated with Parkinson's disease [29]. Neuronal cell loss is accompanied with the accumulation of intracellular, cytoplasmic, protein-rich inclusions called Lewy bodies which contain numerous proteins, including the fibrillar form of α -synuclein [30](Figure 1.1). Clinical diagnosis of Parkinson's disease relies on the identification of motor features associated with the disease as outlined above. However, non-motor symptoms such as a diminished sense of smell, disrupted sleep and constipation are thought to precede the diagnostic motor symptoms by as much as 20 years [31]. Motor symptoms of Parkinson's disease are manageable with dopamine replacement therapy such as levodopa which has been widely used since the late 1960's [32]. Although the therapies currently available delay disability and extend life expectancy, none of them are capable of significantly altering the neurodegenerative process and therefore targeted disease altering therapies are urgently needed [25].

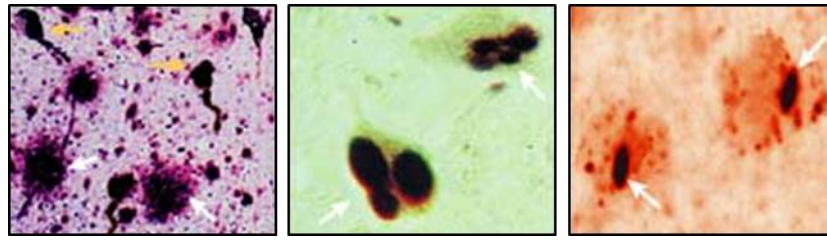


Figure 1.1: Amyloid deposits in neurodegenerative diseases. Post-mortem neuropathological analysis of patients suffering from Alzheimer's disease (left), Parkinson's disease (centre) and Huntington's disease (right) reveals amyloid deposits. Extracellular amyloid plaques (left, white arrows) and intracytoplasmic neurofibrillary tangles (left, yellow arrows) are the pathological hallmarks of Alzheimer's disease. Lewy bodies (centre, white arrows) are observed in the neurons of Parkinson's disease patients. Intranuclear inclusions (right, white arrows) are observed in Huntington's disease patients. Adapted from [33].

1.1.3 Type II diabetes mellitus

Type II diabetes is one of the most common metabolic diseases, with 346 million diabetic people worldwide at present, and with a doubling of diabetes-related deaths from 2009 and 2030 predicted [34]. Secondary complications such as heart attacks, strokes, blindness and renal failure are attributed to type II diabetes [35]. The increasing prevalence of type II diabetes in modern society combined with the debilitating secondary complications demonstrates an urgent need for investigation into the underlying mechanisms of this devastating disease.

The amyloidogenic protein amylin, also referred to as islet amyloid polypeptide (IAPP), is strongly associated with type II diabetes [36, 37]. IAPP is expressed exclusively in the pancreatic islet β -cells, the same cells responsible for insulin production [38]. IAPP and insulin are under the same regulatory elements and are co-expressed and co-secreted at a 20 to 1 molar ratio of insulin to amylin [39, 40]. Due to their co-regulation, an increased insulin requirement which occurs in states of insulin resistance, will inevitably lead to increased production of both IAPP and insulin. As high protein concentrations can induce aggregation of amyloidogenic proteins, resulting in amyloid fibril formation, insulin resistance is thought to promote islet amyloidosis leading to apoptotic death of β -cells [41]. Whether islet amyloid deposition is a cause or consequence of type II diabetes has long been debated, however evidence from *in vivo* experiments using transgenic mice with the human IAPP gene incorporated into their chromosomal DNA indicates that IAPP is an important pathogenic factor in the development of type II diabetes [41, 42].

There are a wide variety of U.S Food and Drug Administration (FDA) approved diabetes therapies, however they have limited efficacy, undesirable side-effects and are associated with

extortionate costs [43]. Although there are several classes of new drugs in development, these approaches involve lowering blood glucose, enhancing insulin sensitivity and insulin release and do not target amyloid fibril formation [43]. Developing therapies that target amyloid fibril formation could circumvent β -cell loss altogether and could thus prove to be more effective in halting disease progression [44].

1.1.4 Dialysis related amyloidosis

Another well-studied amyloid disease is the chronic systemic disease, dialysis related amyloidosis (DRA). β_2m is the all β -sheet protein that self-associates to form the amyloid fibrils that are found in DRA [45]. β_2m forms the non-covalently bound light chain of the major histocompatibility complex I (MHC I) which is expressed on the surface of all nucleated cells [46]. The role of MHC I is to present antigenic peptides to cytotoxic T cells. These antigenic peptides are typically 8 – 10 residues long and generated from a cytosolic pool of proteins by proteasomal proteolysis [47]. These peptides are trafficked to the endoplasmic reticulum where they associate non-covalently with the heavy chain (α -chain) and β_2m , thus forming the fully assembled MHC I complex which is transported to the cell surface [46].

Significant quantities ($2.4 \pm 0.7 \text{ mgkg}^{-1}\text{day}^{-1}$) of β_2m are synthesised *in vivo*, and upon dissociation from the MHC I complex, β_2m is dispersed in the extracellular space prior to transport to the kidneys via the serum [48]. In healthy individuals, the kidney eliminates β_2m from the vasculature. This is achieved by glomerular filtration, followed by proximal tubular resorption and proteolytic cleavage [49]. However, efficient clearance of β_2m from the blood is not achieved in disease states where the kidney function is reduced. This is because dialysis therapy, which is designed to function in the place of the kidney, does not effectively eliminate β_2m [50]. This results in an increase of serum β_2m concentration from 25 – 60 fold above normal levels ($1.2 \pm 0.6 \text{ mg l}^{-1}$), depending on the residual kidney function [50]. Different types of dialysis procedures are able to reduce serum β_2m concentrations to different extents; however none of them are able to efficiently remove all β_2m and thus serum β_2m concentrations remain at least 10-fold greater than in healthy individuals [51].

Elevated β_2m concentration over many years of renal insufficiency is thought to result in the self-association of β_2m into amyloid fibrils, which deposit mainly in osteoarticular tissues due to their affinity for collagen [52, 53](Figure 1.2 and Figure 1.3). The major component of DRA amyloid deposits is full-length β_2m , however truncated and modified versions of β_2m have been observed in *ex vivo* amyloid fibrils. These include, amongst others, truncation of the N-terminal six residues to generate highly amyloidogenic $\Delta N6 \beta_2m$ and modification of β_2m with

advanced-glycation end-products (AGE) (reviewed in [54]). Other components of DRA deposits include glycosaminoglycans, proteoglycans, collagen, apolipoprotein E, serum amyloid protein (SAP) and Cu^{2+} ions; these are thought to help stabilise fibril deposits and be involved in disease pathogenesis (reviewed in [54]).

Clinical symptoms usually present after 5 years of dialysis therapy; beginning with carpal tunnel syndrome and later progressing to chronic and destructive arthropathy, which can result in bone lesions and fractures as well as periarthritits in multiple joints including knee, hip, shoulder and ankle [55]. Currently treatment of DRA mainly focuses on the alleviation of symptoms such as chronic pain and inflammation [49]. Symptoms can also be alleviated by surgery to reduce fibril bulk thereby reducing nerve compression [54]. Kidney transplantation is the only curative procedure which prevents further fibril deposition but does not diminish existing fibril deposits [56]. Transplantation, however, is not always possible for all DRA patients due to limited availability of kidneys for transplant and the advanced age of patients [54]. Advances in dialysis membranes and filters, and incorporation of $\beta_2\text{m}$ adsorption columns in series with dialysis membranes to reduce circulating levels of $\beta_2\text{m}$, may have some benefit in preventing DRA or alleviating symptoms, however the long term impact of these is currently unknown [57].

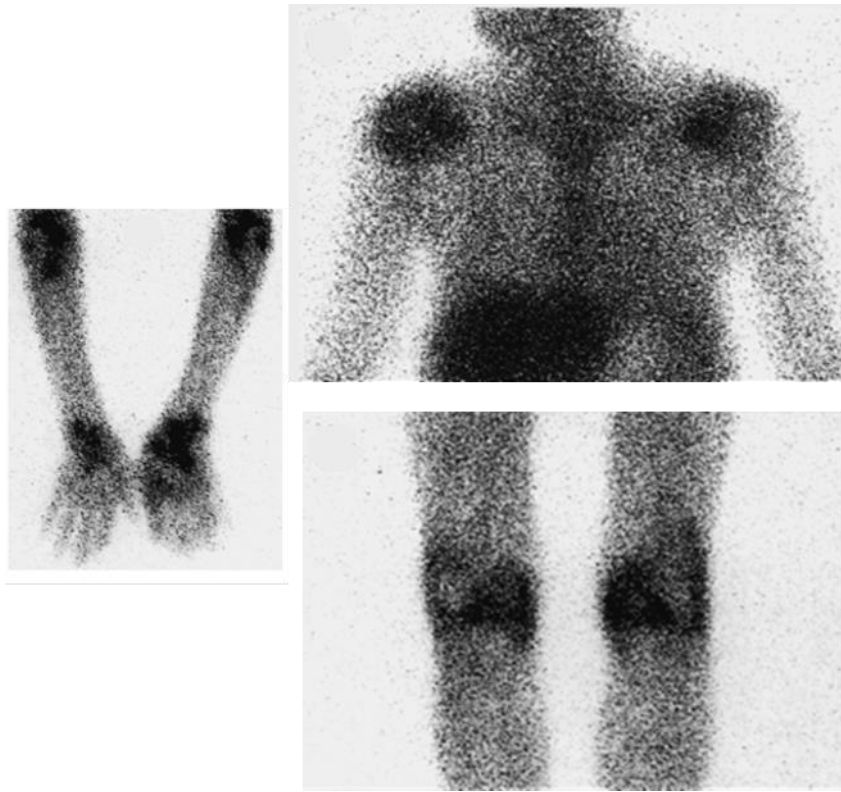


Figure 1.2: β_2m deposits in the joints in DRA. Scintograph of patient suffering from DRA using a ^{111}In - β_2m tracer. Accumulation of β_2m is observed in the wrists and elbows (left), shoulders (top right) and knees (bottom right). Accumulation in the liver (top right) results from uptake by the hepatic reticulo-endothelial system and does not indicate fibril deposition. Figure from [53].

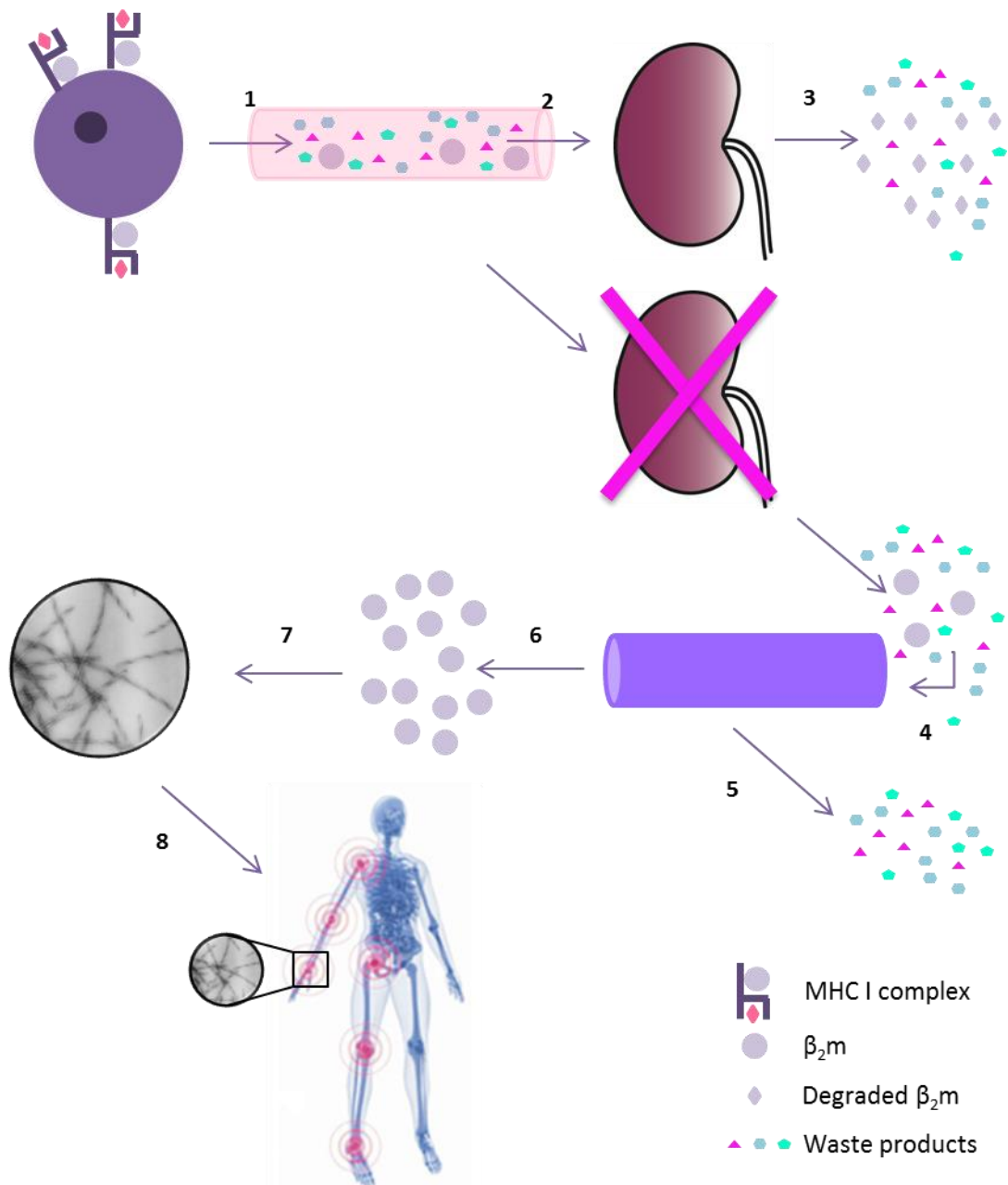


Figure 1.3: Model for the pathogenesis of DRA. (1) β_2m dissociates from the MHC I complex found on the surface of nucleated cells. (2) β_2m is transported in the vasculature to the kidneys. (3) In healthy individuals, β_2m is eliminated by glomerular filtration followed by proteolytic cleavage in the proximal tubules. Other waste products are also eliminated by the kidneys. (4) However, in patients with renal failure, dialysis replaces kidney function. (5) Waste products are removed by dialysis. (6) β_2m , however, is not removed by dialysis and plasma concentration increases 25-60 fold. (7) β_2m aggregates into amyloid fibrils. (8). Amyloid fibrils deposit in osteoarticular tissues. Figure adapted from [54].

1.2 Amyloid as a functional element

Although originally associated with disease, the amyloid structure has been employed by a range of organisms for functional roles. For example, by bacteria for protective and invasive purposes, by yeast to communicate epigenetic information and by mammals to control melanin biosynthesis [58]. Indeed, the amyloid fold is thought to have existed for as long as proteins have [59]. It therefore appears that organisms have evolved to exploit the canonical amyloid fold which confers proteolytic and detergent resistance, mechanical strength, self-replicative properties and molecular memory [58, 60].

1.2.1 Exploitation of the mechanical strength of amyloid fibrils

Amyloid fibrils have a high mechanical strength, with a yield-strength comparable to steel [61]. This mechanical strength has been exploited by bacteria such as *Escherichia coli* and *Salmonella* spp., via the formation of extracellular amyloid fibres known as curli [62, 63]. Amyloid formation is carefully controlled by two operons, the *csgBAC* and *csgDEFG* operons encoding 7 Csg proteins [64, 65]. CsgA, the major subunit of curli fibres is secreted to the cell surface before amyloid formation is catalysed by the nucleator, Csg B; thereby restricting amyloid formation to the extracellular milieu and preventing potential toxicity associated with both the intermediates formed during amyloid formation and the mature fibres [60, 65]. CsgG forms the outer membrane pore that facilitates secretion of CsgA and CsgB whereas CsgE and CsgF are chaperones that assist in secretion and attachment of curli fibres to the cell surface [65-68]. The role of CsgC is still unclear, however it is thought to regulate subunit secretion [65]. CsgD is a transcriptional regulator that positively regulates curli production [64]. Careful regulation of amyloid formation therefore results in the production of curli fibres at the cell surface which are involved in biofilm formation, host-cell adhesion and pathogenesis [58, 65].

1.2.2 Amyloid fibrils as self-replicative transmissible elements

Prions were initially identified as the causative agent of transmissible spongiform encephalopathies (TSEs) such as Creutzfeld-Jacob disease and kuru [69, 70]. Prion proteins usually exist in a soluble conformation but are capable of refolding and assembling into highly ordered, self-replicating prion polymers [71]. Although associated with disease in mammals, several amyloid-based prions with functional properties have been identified in unicellular organisms such as those formed by the proteins Sup35p and Ure2p in *Saccharomyces cerevisiae* [72-75]. Like their mammalian counterparts, prion proteins in lower eukaryotes are also capable of forming insoluble, self-perpetuating amyloid-like polymers both *in vitro* and *in vivo* [76]. Both Sup35p and Ure2p reversibly form cytoplasmic amyloid, conferring a particular

phenotype which is passed either vertically from mother to daughter cell during cell division or horizontally during mating [60, 71].

Soluble Sup35p is a translational termination factor that ensures termination of protein translation at nonsense (stop) codons [73]. Aggregated Sup35p, however, prevents translation termination, allowing stop codon read-through. This results in the extension of the C-termini of proteins and thus creates phenotypic diversity [73]. Clues to the biological importance of Sup35p, and its associated phenotype, are provided by its conservation across a diverse array of *Saccharomyces* spp. and the positive selection of the Sup35 prion domain [77]. Yeast populations with the aggregated form of Sup35p carry certain growth advantages [73]. Ure2p is another yeast prion protein, found in *Saccharomyces cerevisiae*. Soluble Ure2p controls nitrogen catabolism through its repressive action on the transcription factor, Gln3. Gln3 regulates genes required for the uptake of poor nitrogen sources. Aggregated Ure2p is unable to repress the activation of Gln3, thereby making it constitutively active and allowing the organism to grow in nitrogen poor conditions [78]. Like Sup35p, Ure2p also confers growth advantages which are epigenetically heritable [60].

1.2.3 Functional amyloid fibrils in mammalian systems

Examples of functional amyloid have also been identified in mammalian systems [79]. For example, amyloid formation plays a functional role in the biosynthesis of melanin in lysosome related organelles called melanosomes, in melanocytes found in skin [80]. The protein Pmel17 forms the amyloid fibres found in melanosomes [81]. Full-length Pmel17 is a transmembrane protein which is proteolytically degraded into two subunits, a transmembrane fragment (M β) and a luminal fragment (M α) [82]. M α rapidly self-assembles into amyloid fibres which catalyse melanin formation by providing a scaffold. The scaffold acts as a template for the polymerisation of highly reactive melanin precursors [81]. M α amyloid fibres, by sequestering toxic melanin precursors, are thought to reduce the toxicity associated with melanin synthesis [60, 81]. M α amyloid formation is carefully controlled by the requirement of the cleavage of the full length protein prior to amyloid formation in the melanosome thus protecting cellular compartments such as the ER and Golgi [60, 81]. This, along with the rapid rate of fibril formation is thought to minimise toxicity associated with amyloidogenesis [81].

Another example of functional amyloid in mammals is as a natural store for peptide hormones in pituitary secretory granules [83]. In a particular study, out of a total of 42 tested, 31 protein and peptide hormones found in secretory granules of the endocrine system were shown to form amyloid fibrils *in vitro* [83]. These *in vitro*-formed amyloid fibrils were shown to release functional monomer when the pH was increased from secretory granule pH to that

encountered upon secretion [83]. Furthermore, secretory granules containing amyloid-like material were identified in a mouse pituitary tumour neuroendocrine cell line as well as primary mouse and rat pituitary tissue. The amyloid-like material was shown to contain hormones such as adrenocorticotrophic hormone, β -endorphin, prolactin and growth hormone [83]. Amyloid formation is thus proposed as a method of sorting protein and peptide hormones into secretory granule cores, and concentrating hormones to the highest density possible thus separating them from non-aggregation prone secretory proteins [83]. Toxicity associated with such a storage tactic is thought to be contained by storage in membrane bound granules and via careful regulation of amyloid formation [83].

1.3 Amyloid

The term 'amyloid' was first coined by Rudolph Virchow in 1854 to describe the deposits in human tissue of protein that had starch-like tinctorial properties (reviewed in [84]). The definition of amyloid has since been adapted to describe highly ordered, insoluble, protein assemblies which are β -sheet rich and are characterised by their specific binding to dyes such as Congo Red and Thioflavin T as well as their characteristic X-ray diffraction patterns [1, 84-88]. Rather than being a rare phenomenon associated with a few diseases, the amyloid state is now recognised as being a well-defined structural conformation and is an alternative to the native state which can be adopted, in principle, by all polypeptide sequences [1, 79, 89, 90].

1.3.1 Structure of amyloid fibrils

Amyloid fibrils formed from different amino acid sequences share a striking resemblance at a nanometre scale [1, 88]. When observed by transmission electron microscopy (TEM) or atomic force microscopy (AFM), amyloid fibrils appear as long, unbranched, polymeric assemblies often a few microns in length [1, 79]. Fibrils usually consist of a number (2-6) of protofilaments, individually about 2-5 nm in diameter, which either twist together to form rope-like fibres typically 7-13 nm wide; or associate laterally to form long ribbons approximately 2-5 nm thick and up to 30 nm wide [1, 91-94] (Figure 1.4).

There are subtle differences in fibril structures formed from different precursor proteins and peptides due to the influence of side chains [95, 96]. Nevertheless, the core structure is remarkably similar in all fibrils, consisting of parallel or anti-parallel β sheets propagating along the fibril with β -strands perpendicular to the fibril axis. This gives rise to a cross- β arrangement with a distinctive and characteristic 'cross- β ' X-ray diffraction pattern [88, 97] (Figure 1.5). This pattern shows an intense reflection at 4.7 - 4.8 Å in the meridional direction and a broader reflection at 8 - 10 Å in the equatorial direction indicating a spacing of 4.7 - 4.8 Å between β -strands within β -sheets and 8 - 10 Å between β -sheets [88, 97].

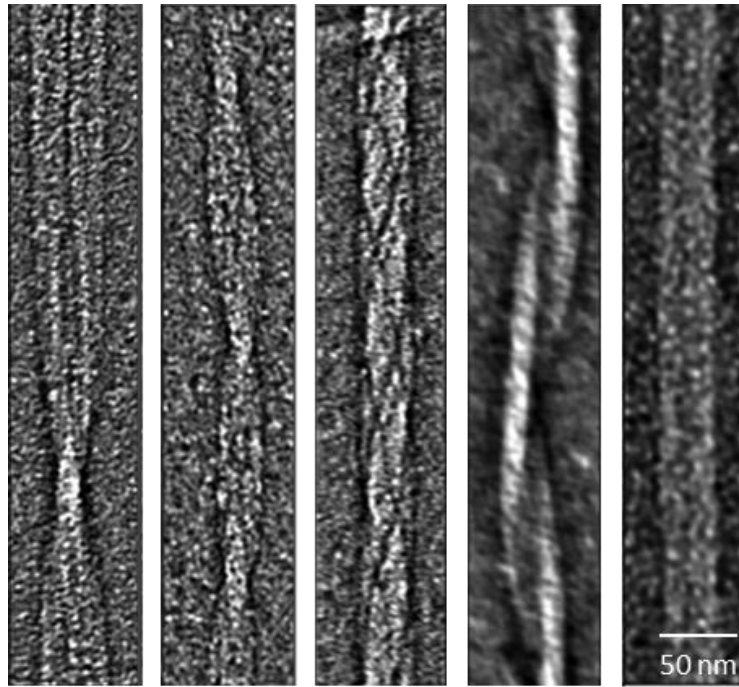


Figure 1.4: Electron micrographs showing different fibril morphologies. Negatively stained amyloid fibrils assembled from amyloidogenic peptides display different morphologies such as twisted ribbons, tapes, robes and tubes when analysed by electron microscopy. Adapted from [98].

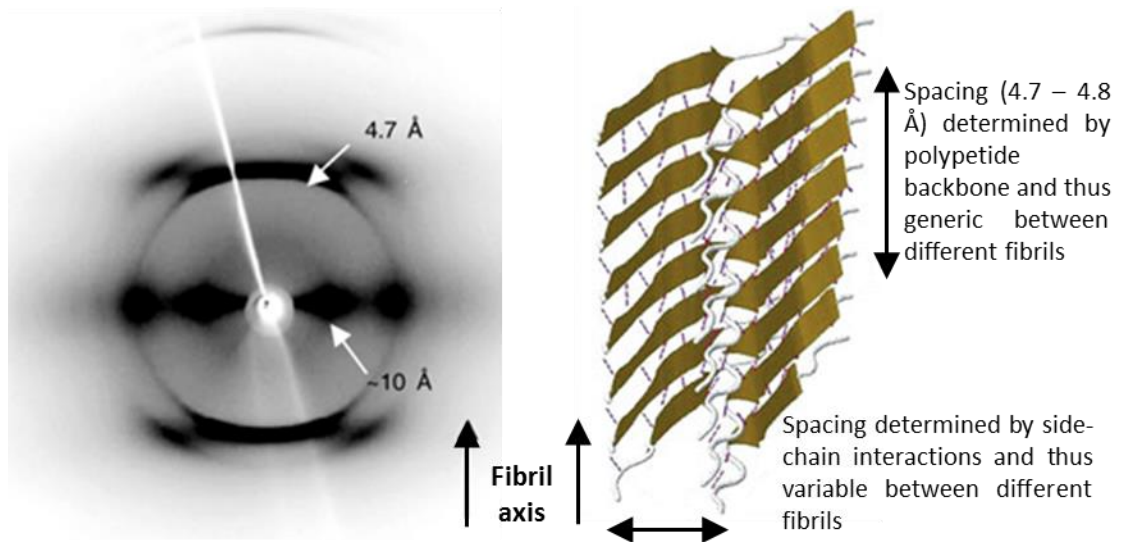


Figure 1.5: Amyloid fibrils have a cross- β architecture. Aligned islet amyloid polypeptide (IAPP) fibrils have been shown to display a characteristic cross- β diffraction pattern (left) with reflections (single headed white arrows) at 4.7 Å in the meridional direction and 10 Å in the equatorial direction [99]. The direction of the fibril axis is shown by single headed black arrows. A representation of the generic cross- β structure inferred from the X-ray diffraction pattern is shown (right) with the spacing between β -strands determined by the meridional reflections and that between β -sheets determined by equatorial reflections. Adapted from [99] and [100].

A detailed view of the molecular structure of amyloid fibrils has been made possible by developments in cryo-electron microscopy and solid-state nuclear magnetic resonance (ssNMR) spectroscopy [79, 101] (Figure 1.6). X-ray microcrystallography of amyloid fibril segments formed from small peptides provides further evidence for a common core structure, but also demonstrates how side-chains interlock between β -sheets [95]. This compatibility in side-chain interactions within β -sheets has also been shown by high resolution ssNMR studies as well as by X-ray fibre diffraction [102-107]. A combination of experimental techniques spanning five orders of magnitude in length was used to demonstrate at a molecular level the hierarchical assembly of a small peptide into mature polymorphic fibrils via protofilaments and filaments [100]. These studies support earlier work demonstrating a common core structure which can be attributed to the polypeptide backbone as well as explain the packing of side-chains and the basis of fibril polymorphism. An understanding of amyloid fibrils at the molecular level, and the species formed en route to mature fibrils, will undoubtedly aid the development of effective compounds that impede or accelerate fibril formation which could inform future targeted therapies.

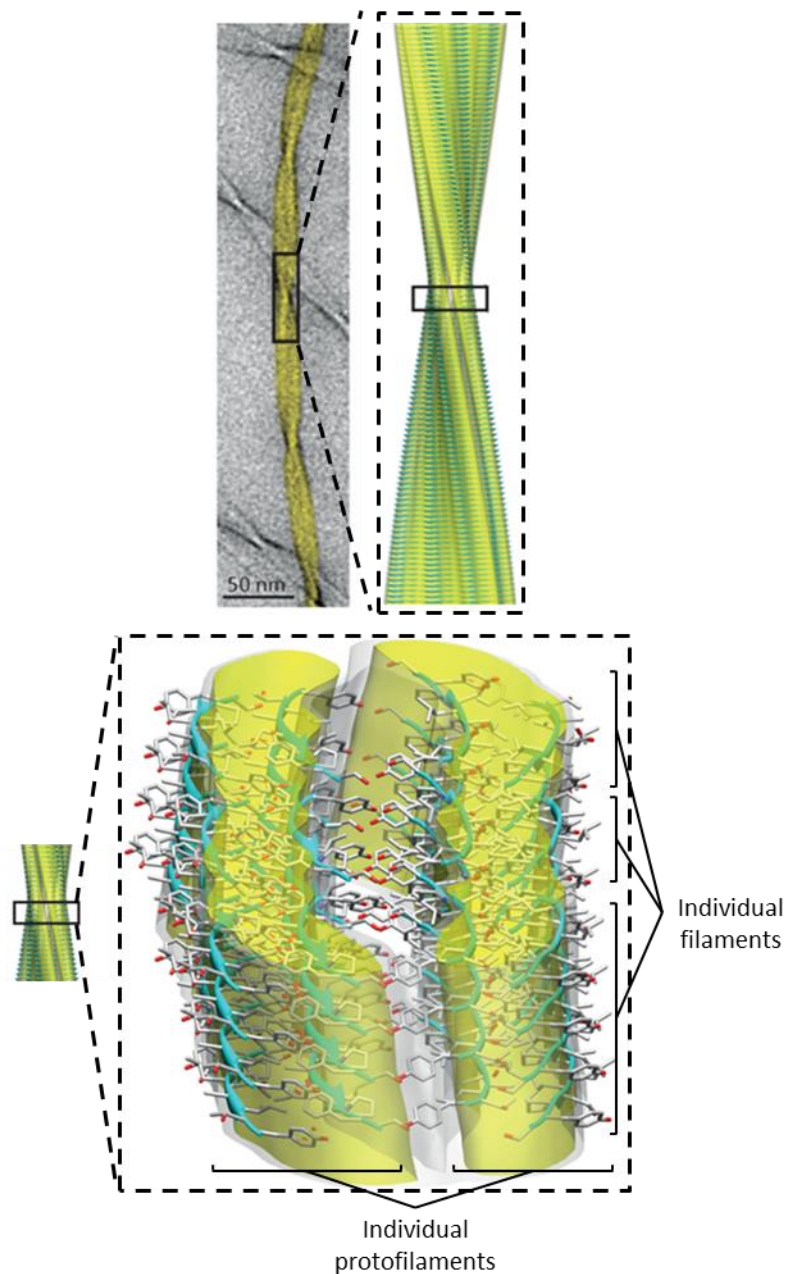


Figure 1.6: Amyloid fibril structure at atomic resolution. The structure of a polymorph of a mature fibril from a transthyretin fragment has been determined at atomic resolution [100]. Transmission electron microscopy (TEM) imaging (top left) in combination with cryo-electron microscopy allowed visualisation of fibril structure by cryo-electron microscopy reconstruction (top right). Cryo-electron microscopy imaging in combination with ssNMR analysis allowed the determination of an atomic level structure (bottom), demonstrating the hierarchical organisation of a mature fibril. Three individual filaments twist together to form the mature fibril. The filaments are composed of pairs of individual protofilaments which in turn are made up of pairs of β -sheets. β -sheets are shown in a ribbon representation and oxygen, carbon and nitrogen atoms are shown in red, grey and blue respectively. Figure adapted from [100].

1.3.2 Amyloid fibril formation pathway

Characterisation of the fibril formation process is challenging due to the heterogeneous nature of intermediate species formed en route to mature fibril formation, and the existence of polymorphisms in amyloid fibrils formed from the same starting protein [96, 108]. There is a potential discrepancy between *in vitro* studies performed on purified protein solutions, which are achievable on the timescale of days, compared to the crowded microenvironment in which fibrillation occurs *in vivo* over the course of decades [108]. Nevertheless, advances have been made in understanding the oligomerisation process with the aid of *in vitro* macroscopic techniques such as the use of amyloid-dyes for example, Congo Red and Thioflavin T, to follow the kinetics of fibril formation [86, 87]. As amyloid structures typically have a high β -sheet content, the use of spectroscopic techniques such as Circular Dichroism (CD) and Fourier Transform Infrared Spectroscopy (FTIR) has been exploited to monitor progression of fibril formation over time [86]. Despite the limited resolution of these techniques, a picture of the fibril formation pathway is beginning to form and is continuously being refined by the development of single molecule methods, advances in theoretical studies and the development of imaging techniques in living systems [79, 108-113].

Amyloid fibril growth is a hierarchical process, starting with monomers which are unfolded or have aggregation prone segments exposed [114, 115]. These monomers coalesce in solution resulting in the formation of short-lived, unstable, globular or tubular entities referred to as oligomers [115-117]. Oligomers are heterogeneous in size and conformational properties and have been described as frequently associating into beaded chains, curvy protofibrils, large enclosed rings and/or ribbons, collectively termed protofibrils [115, 117-120].

The oligomerisation process involves the formation of thermodynamically stable intermediates en route to mature fibril formation, which have been visualised by transmission electron microscopy and atomic force microscopy [121, 122]. Fibril formation proceeds via a rate-dependent formation of a nucleus, with the lag-phase thought to involve the conversion of monomers into a nucleus, which is followed by a rapid elongation phase as individual monomers add to fibril ends [109, 110, 123]. Monomers adopt the cross- β conformation upon addition to fibril ends, and fibrils thus function as templates [114]. Indeed, the addition of pre-formed fibrils as seeds significantly reduces and ultimately eliminates the lag phase [124]. When the amount of protein is limited, as is the case of *in vitro* fibril kinetics studies, the growth phase is followed by a plateau phase where the rate of reaction diminishes due to the depletion of monomer species (Figure 1.7).

Some protofibrils can be off-pathway intermediates, whereas others which are on-pathway intermediates are precursors of longer ribbons or protofilaments that ultimately assemble into mature fibrils [120]. Oligomeric species are thought to contain more exposed hydrophobic clusters than the native monomers or mature fibrils [117, 125]. A11 is a conformation-specific antibody which binds to a shared epitope found on soluble oligomers independent of protein sequence [18]. A11 does not bind to monomer or fibrils. OC is another antibody which also binds in a sequence-independent fashion; however it recognises a conformation found on both fibrils and soluble oligomers [126]. These oligomers are characterised as fibrillar oligomers as they are distinct from the pre-fibrillar oligomers recognised by A11. The aggregation pathway can therefore be simplified using conformation-dependent antibodies [127] (Figure 1.7). Monomer can follow one of two pathways depending on the conformation it adopts. One pathway involves the formation of pre-fibrillar oligomers recognised by A11 but not by OC. These pre-fibrillar oligomers may undergo a concerted conformation change 'en bloc' to form fibrils [127]. An alternate pathway involves the aggregation of amyloidogenic monomer to fibrillar oligomers, recognised by OC but not A11, which may represent nuclei or seeds that elongate by monomer addition to their ends [127]. Pre-fibrillar oligomers may also form off-pathway intermediates that do not mature into fibrils. The simplified model (Figure 1.7) describes two of an infinite number of possible pathways of amyloid formation.

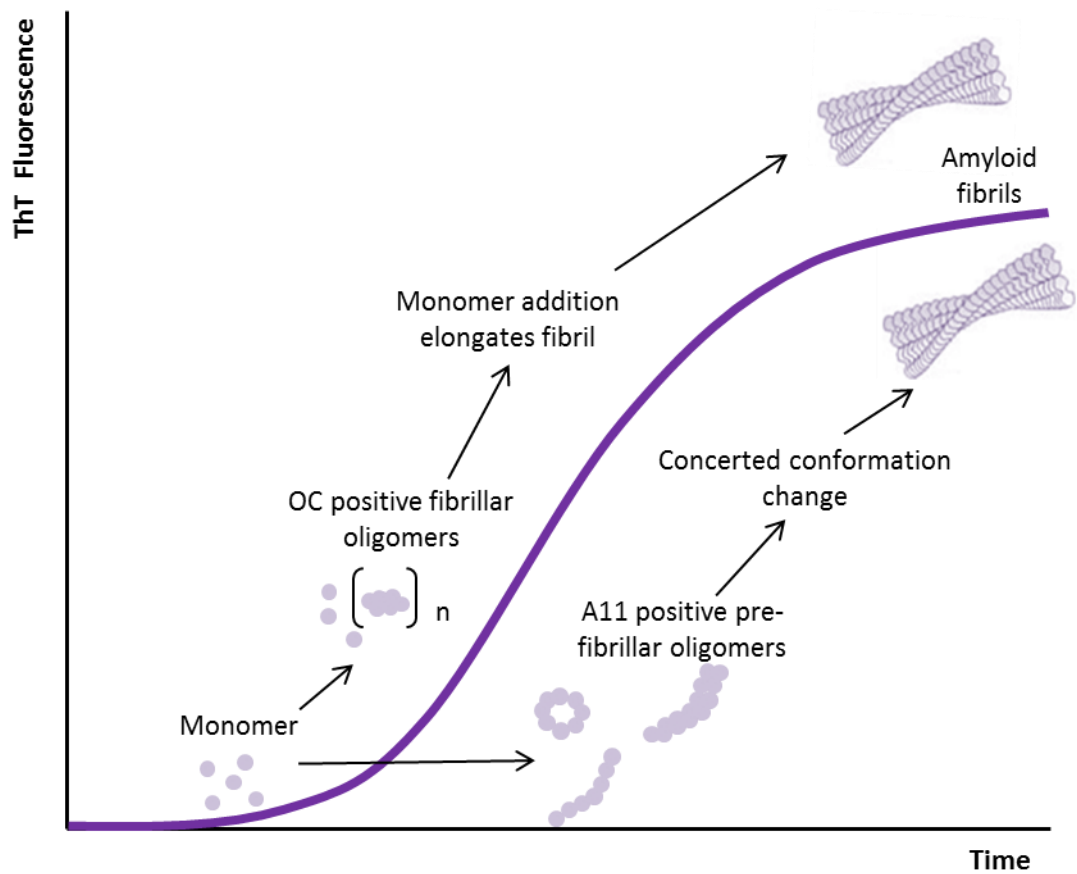


Figure 1.7: Schematic representation of two possible amyloid formation pathways: Monomer can either coalesce in solution to form fibrillar oligomers (OC-positive, A11-negative), or form pre-fibrillar oligomers (A11-positive, OC-negative). Fibrillar oligomers mature into amyloid fibrils by monomer addition (top pathway). Pre-fibrillar oligomers may undergo a concerted conformation change to form mature fibrils (bottom pathway) or form off-pathway intermediates (not shown in this schematic). Figure adapted from [127].

1.4 Association of amyloid with cell death and disease progression

The close association between the appearance of amyloid deposits and the beginning of pathological events in Alzheimer's disease has been established for many years [12]. The amyloid cascade hypothesis, put forward over 20 years ago, was based on neuropathological, genetic and biophysical information and implicates the deposition of A β as the primary insult driving pathogenesis in Alzheimer's disease [12]. This hypothesis has evolved over the years to account for the role of soluble A β species due to the lack of quantitative correlation between the number of insoluble amyloid deposits and the extent of cognitive decline [128]. The hypothesis has also been generalised over the years to include other amyloidoses as it has become clear that they are all characterised by amyloid protein aggregates, although of varying composition [129](Figure 1.1). Despite this long standing association, the specific mechanisms underlying pathogenesis remain unclear [79].

Originally, the observation of fibrillar deposits in the organs of patients suffering from amyloidosis led to the postulation that these deposits were the causative agents of disease [12]. Further evidence for this postulation came from the toxicity of amyloid fibrils assembled from A β_{1-42} , to cultured neuronal cells [130]. The incorporation of animal models provided additional proof as the injection of amyloid fibrils assembled from A β_{1-40} , into the cerebral cortex of aged rhesus monkeys led to microglia activation and neuronal loss [131]. In addition, amyloid fibrils generated from IAPP, implicated in type II diabetes, were also found to be toxic, in this case to insulin-producing beta-cells of the adult pancreas of rats and humans [132]. This combined with the observed neurotoxicity of A β amyloid fibrils, suggested a common cytotoxic effect of amyloid fibrils as a contributing factor to the pathogenesis of amyloid diseases [133].

The observation that the severity of cognitive decline in Alzheimer's disease correlated better with soluble A β compared to insoluble A β plaques (containing fibrillar A β), drew focus to the role of soluble low-molecular weight species in the pathogenesis of disease [134-137]. Transgenic mice models showing cognitive decline as well as impairments in cell function and synaptic plasticity prior to the accumulation of significant detectable quantities of amyloid plaques provided further support to the role of low-molecular weight species in disease pathogenesis [138]. The presence of amyloid plaques throughout the cortex of many healthy 70 year-olds unaccompanied by cognitive decline, further detracted the field from amyloid plaques being central to disease progression [139]. Extensive extracellular deposition of insoluble amyloid material, through its sheer bulk is likely to cause organ failure by disrupting tissue architecture, especially in systemic diseases where kilograms of amyloid deposits can accumulate in vital organs such as the liver and kidney [1]. However, in non-systemic

conditions such as neurodegenerative diseases and organ-specific diseases like type II diabetes, the soluble low-molecular weight species are thought to play a greater role in disease progression [79, 120, 140-142].

1.4.1 The role of oligomers in cell death and disease progression

The lack of correlation between fibrillar deposits and disease severity, sometimes even observed as an anti-correlation, led to the investigation of pre-fibrillar aggregates [135, 143-145]. Due to difficulties in extraction of non-fibrillar aggregates from the brains of patients with Alzheimer's disease, the first non-fibrillar A β aggregates were prepared from synthetic A β *in vitro* [146-148]. As discussed in section 1.3.2, oligomerisation is a heterogeneous process and a variety of pre-fibrillar aggregates, collectively referred to as oligomers have been described. Oligomers have been observed and described for a variety of disease-associated proteins such as α -synuclein, huntingtin and IAPP as well as for fibril forming proteins not associated with disease [141, 149-152].

Oligomer extraction methods have evolved over the years and this has enabled the purification of oligomers isolated from cell culture, brains of animal models and from diseased human brains [153-160]. It is important to note that the extraction and analysis methods used to study these oligomers utilise techniques that dissociate, or at least destabilise fibrillar proteins such as homogenisation and boiling as well as addition of reagents such as sodium dodecyl sulphate (SDS), β -mercaptoethanol and urea; thus making the occurrence of oligomers in the tissue of interest potentially unclear [129, 161]. However, bearing this limitation in mind, several reports have implicated oligomers in disease pathogenesis.

Oligomeric A β species have demonstrated toxicity to cultured neurons, inhibited hippocampal long-term potentiation (LTP), impaired synaptic function as well as disrupted cognition and learned behaviour in rats [120, 140, 157, 158, 162-165]. Oligomeric α -synuclein species also demonstrate toxicity via oxidative stress, Golgi fragmentation, synaptic loss and inhibition of proteasomal activity [166-169]. Toxicity has also been associated with oligomeric assemblies from other proteins such as huntingtin, IAPP, transthyretin, and lysozyme as well as non-amyloidosis associated proteins such as stefin B, hypF-N and p53 [141, 170-175]. The remarkable observation of toxicity associated with oligomers prepared from proteins that are not associated with amyloidosis implies an inherent toxicity of oligomeric species [142]. Interestingly, the conformation-specific, sequence-independent antibody, A11, binds to oligomers generated from amyloidogenic proteins and peptides such as A β ₁₋₄₂, A β ₁₋₄₀, α -synuclein, IAPP, polyglutamine and lysozyme and protects against their observed cytotoxicity;

providing further support for both the role of oligomeric species in disease pathogenesis and the inherent toxicity associated with oligomers [18] (Figure 1.8).

1.4.2 The role of amyloid fibrils in cell death and disease progression

Following the original formulation of the amyloid cascade hypothesis, evidence suggesting toxicity associated with the A β fibril began to appear, as discussed in section 1.4. Due to the lack of established characterisation methods, many of these early studies do not contain biophysical evidence of the presence of fibrils and the absence of oligomers in amyloid preparations; and therefore strictly speaking, do not exclude oligomer toxicity [176]. However, more recent studies with biophysical characterisation of amyloid aggregates show that fibrils do play a role in disease pathogenesis.

Fibril-associated toxicity has been reported for fibrils assembled from amyloid disease associated proteins or peptides such as A β , lysozyme, recombinant mammalian prion protein (rPRP) and IAPP as well as from proteins not associated with disease such as the yeast prion proteins Sup35 and Ure2p [173, 177-186]. In some instances toxicity has been associated with both oligomeric species and fibrils by side by side comparison of both entities [173, 179, 182, 185, 186]. Interestingly, oligomer and fibril have been shown to initiate cell death via distinct pathways. For example, oligomers and fibrils assembled from A β_{1-42} were both shown to initiate cell death via apoptosis, however fibrils induced apoptosis via a mechanism involving caspase 8 activation and oligomers via caspase 9 activation [179]. Studies on lysozyme amyloid oligomers and fibrils demonstrated a detrimental effect on cell viability associated with both species. In this instance, oligomers were shown to induce an apoptosis-like death in contrast to the necrosis-like death induced by fibrils [173]. These studies proposed that the widespread polymorphism observed in amyloid species, is indicative of a continuum of cross- β -sheet containing amyloid structures as perpetuators of disease progression, as opposed to a single uniform oligomer or fibril species [173] (Figure 1.8).

One observation that challenged the original amyloid cascade hypothesis was that the decline in cognition, cell function and synaptic plasticity was independent of the accumulation of significant detectable quantities of amyloid plaques [138]. This was supported by the observation of morphological abnormalities and alterations in axonal trafficking preceding plaque detection [187]. Developments in temporally resolved longitudinal *in vivo* multiphoton microscopy in combination with the availability of sensitive *in vivo* amyloid dyes have provided a different perspective. Although collectively, plaques take months to accumulate in Alzheimer's disease mouse models; individually, each plaque was shown to represent an acute

event and formed extraordinarily rapidly. Plaque formation preceded microglia recruitment and activation as well as the appearance of dysmorphic neurites. The authors propose that plaques act as critical mediators of neuritic pathology and the lengthy, sometimes decades-long degenerative process of Alzheimer's disease is marked by infinite acute changes in the cortex [188].

Amyloid polymorphism is a widely accepted phenomenon and there are several examples of fibrils formed from the same starting peptide or protein with different stabilities, morphologies and/or molecular structure [96, 117]. In some cases, these polymorphisms carry different biological activities. One example of this is the polymorphism observed in fibrils assembled from $A\beta_{1-40}$, where differences in both morphology and molecular structure are apparent. These differences are associated with differences in their toxicities in neuronal cell cultures [177]. Amyloid fibrils from lysozyme that differ in molecular structure, stability and size of the cross- β core also demonstrate differences in the degree of cytotoxicity to neuronal cultures [180]. Another example is the variation in fibril morphology observed in fibrils assembled from β_2m [189]. Depending on the assembly conditions, β_2m has been shown to assemble via competing pathways into rigid amyloid fibrils or semi-flexible worm-like fibrils. These fibrils have also been shown to differ in their biological activity [190]. These studies demonstrate that cytotoxic potential is governed by molecular structure and stability.

Indeed, the stability of amyloid fibrils and in particular, their disassembly process is an important factor [101, 161]. Fibrils have been shown to disaggregate and release oligomeric species and have thus been proposed to act as a reservoir of cytotoxic species [117, 166, 191, 192]. For example, natural lipids have been shown to destabilise and rapidly disaggregate mature $A\beta_{1-42}$ fibrils, releasing oligomers which demonstrate potent toxicity to primary neurons, and memory impairment in mouse models [191]. This phenomenon is not exclusive to $A\beta$ fibrils, as α -synuclein fibrils have also been shown to disaggregate into stable oligomers with toxic potential [166]. The mechanical stability of amyloid fibrils may also play an important role in pathogenesis. Indeed, previous work in our laboratory has shown that amyloid fibrils assembled from β_2m disrupt artificial lipid membranes and also inhibit the cellular reduction of the tetrazolium dye, 3-(4,5-dimethylthiazol-2-yl)-2,5-diphenyltetrazolium bromide (MTT), a substrate commonly used to assay cell viability. Interestingly, mechanical fragmentation of amyloid fibrils enhanced their ability to disrupt lipid membranes and inhibit MTT reduction, thus suggesting that particle size plays an important role in determining biological activity [190].

In light of this accumulating evidence, the role of amyloid fibrils in disease pathogenesis is being reappraised [176]. It is important to appreciate the limitation of the correlative studies conducted so far. These studies reduce a complex disease process which develops over years, perhaps decades, to a single, measurable phenotype; for example cognitive decline in Alzheimer's results from impairment in long term potentiation [129]. Although this oversimplification is essential to draw conclusions; it is worthwhile to remember that amyloid diseases probably result from an amalgamation of biochemical, cell biological and systemic events, each of which may be aggravated by one or more aggregated species [129] (Figure 1.8).

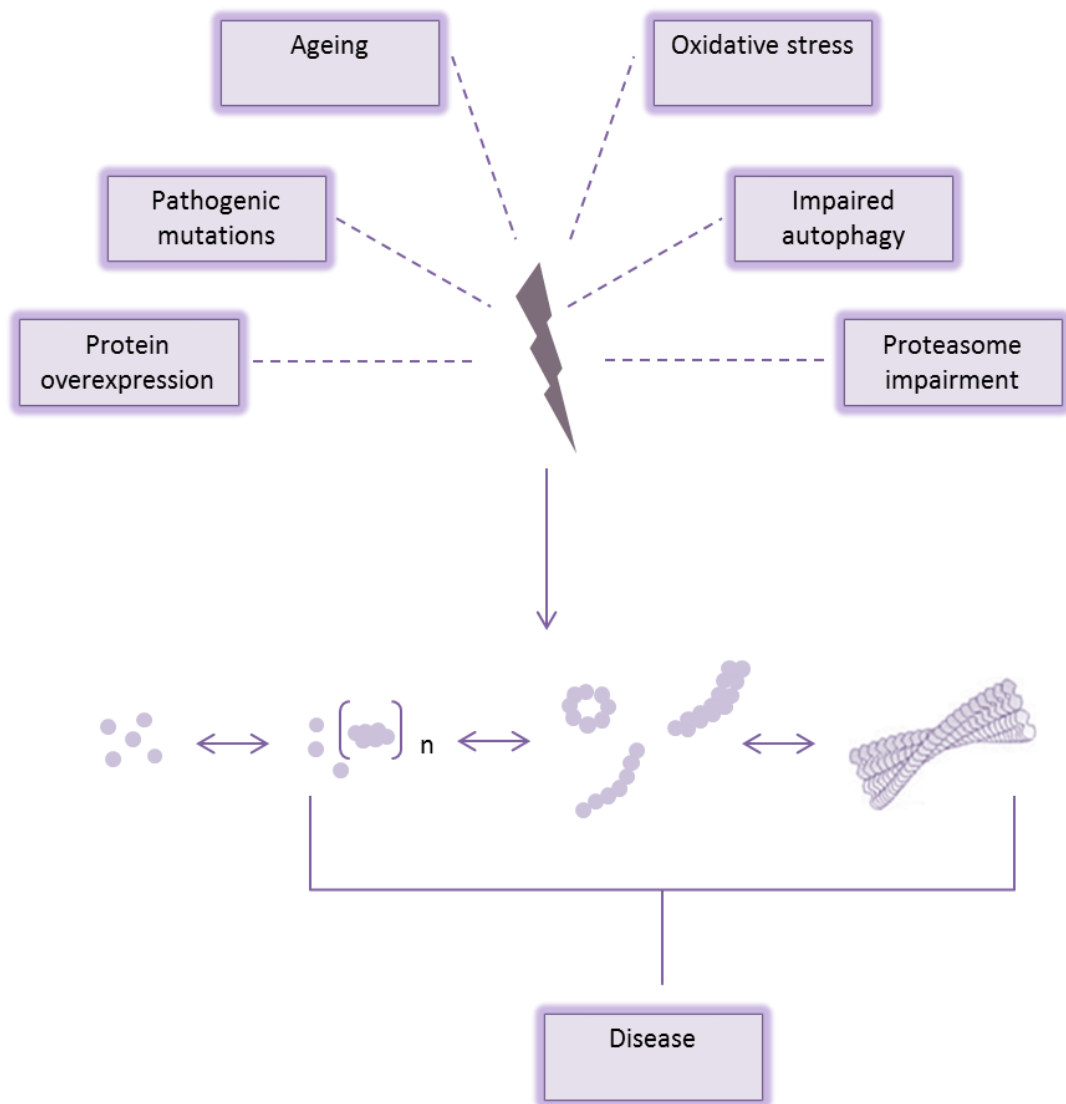


Figure 1.8: Model of pathogenicity: A number of factors have been proposed to trigger protein aggregation into amyloid fibrils [129]. A large body of evidence supports the role of oligomers in disease progression as discussed in section 1.4.1. Accumulating evidence also points to a role of fibrils in pathogenicity either directly or indirectly as discussed in section 1.4.2. It is therefore possible that the perpetuator of disease pathogenesis is not a single uniform species, but rather a continuum of species.

1.5 Mechanisms and consequences of cell death and disruption of cellular functions

The underlying mechanism of cell disruption in the pathogenesis of amyloid diseases is poorly understood. In light of the intense research focused on this, several models have been proposed. These models along with the evidence that led to their proposal will be discussed.

1.5.1 Disruption due to aberrant interactions via hydrophobic surfaces

A prominent hypothesis is one that focuses on the misfolded nature of aggregates, in particular the heterogeneous, soluble, oligomers. These misfolded aggregates expose on their surfaces a variety of groups and hydrophobic patches that would normally be either buried in globular proteins or dispersed in intrinsically disordered proteins and peptides [1, 125, 193, 194]. It is possible that these aggregates mediate aberrant interactions with other cellular components thus causing cell disruption via abnormal exposure of hydrophobic surfaces and reactive groups [141, 193-195]. Indeed, a study using 1-anilinonaphthalene 8-sulphonate (ANS), a dye widely used to measure exposed hydrophobic patches, showed an increase in exposure during the course of fibril formation of three different amyloid systems. Interestingly, the increase in hydrophobic exposure was shown to correlate with cell death, measured by the incorporation of propidium iodide in the neuronal cell line, SH-SY5Y; thus suggesting that the exposure of hydrophobic surfaces during amyloid aggregation is a generic toxic feature of amyloid proteins [194]. The role of hydrophobic interactions is further supported by studies on oligomer toxicity. Interestingly, when polymorphic oligomers are compared, where the fundamental differences lie in the degree of hydrophobic packing and exposure; toxicity was associated with the oligomer species which had a greater exposure of hydrophobic surfaces and a lower degree of hydrophobic packing [141, 195].

Exposed hydrophobic surfaces have been proposed to mediate aberrant interactions and studies have been conducted to identify these interaction partners with the aim of understanding the mechanisms of toxicity [193, 196]. A large number of proteins (324 out of 8100 tested) were identified to interact with oligomeric A β in an *in vitro* protein array based study, where the most highly impacted cellular system identified was the protein translation machinery [196]. Another study revealed a much larger set of proteins, approximately 2000, as interaction partners for amyloid-like aggregates formed from model proteins designed *de novo* and expressed in the cytosol [193]. The *de novo* design allowed for complete removal of bias from naturally occurring proteins and thus allowed investigation of interaction partners based on the amyloid conformation in human cells transfected with the *de novo* model amyloid construct. Co-aggregating proteins identified were found to occupy essential 'hub' positions in

cellular protein networks with important roles in protein quality control, chromatin organisation, transcription, translation and maintenance of cell architecture [193]. The authors propose that these aberrant interactions with amyloid aggregates can impair the normal functioning of the identified essential proteins by sequestering them, thereby causing the collapse of cellular functions and inevitably resulting in multifactorial toxicity [193].

1.5.2 Disruption via saturation of the central protein quality control and clearance systems

Protein homeostasis, also known as proteostasis, refers to the tight regulation that ensures that each protein in the cellular proteome is properly synthesised, folded, sub-compartmentalised and degraded [197, 198]. Proteostasis is maintained by a network of cellular systems and components, collectively referred to as the proteostasis network [197, 199]. The ubiquitin-proteasome system (UPS) is one pathway of the proteostasis network [197, 199]. Molecular chaperones play multiple key roles in the proteostasis network due to their ability to recognise misfolded proteins [199]. The capacity to maintain proteostasis is found to decline with age as well as in various neurodegenerative conditions [197]. The role of two aspects of the proteostasis network, the UPS and molecular chaperones will be discussed here; however many branches of the proteostasis network are thought to be affected in aging and disease and is the focus of intense research [197]. Molecules that regulate the network as a whole (proteostasis regulators) as well as those that control individual protein fates such as pharmacological chaperones and kinetic stabilisers are currently under development as therapeutic agents [197].

The normal role of the UPS is cellular quality control by degrading misfolded, unassembled or damaged proteins that could otherwise form potentially toxic aggregates [200]. Proteins tagged for degradation display poly-ubiquitin chains and are rapidly degraded by cellular proteasomes. The presence of elevated ubiquitin conjugates in the intracellular deposits of protein aggregates within diseased neurons in most sporadic and inherited neurodegenerative diseases has led to a long established link between UPS dysfunction and pathogenesis [201]. Indeed, mutations in genes encoding components of the UPS pathway such as parkin and ubiquitin carboxy-terminal hydrolase L1 (UCHL1) are associated with Parkinson's disease [202]. Importantly, protein aggregation of a pathogenic variant of huntingtin was shown to completely inhibit the UPS [201]. The injection of proteasome inhibitors into adult rats was shown to cause parkinsonian features, including Lewy body aggregates [203]. This suggests that protein aggregates are simultaneously inhibitors of the UPS as well as products that result

from its inhibition and this positive feedback mechanism may rationalise the neuronal loss characteristic of neurodegenerative diseases [201].

Despite the amino acid sequence containing all the necessary information required to facilitate proper folding into a functional three-dimensional structure, the highly crowded macromolecular environment *in vivo* promotes misfolding and aggregation [204, 205]. This has led to the evolution of highly conserved molecular chaperones [206]. Molecular chaperones function by preventing inappropriate interactions both within and between non-native polypeptides; as well as by increasing the efficiency of *de novo* protein folding; and refolding of existing proteins that have misfolded [207]. They were first discovered due to their increased synthesis in response to mild elevations in temperature, and were therefore named heat shock proteins (Hsps). Hsps are rapidly produced in response to stress such as elevated temperature, ischemia, oxidation; but a subset are constitutively expressed and are involved in conformational maintenance [207, 208]. Primary or secondary impairments in molecular chaperone function have been associated with a host of age-related pathologies [198]. Changes in chaperone content are indicative of the cellular attempt to overcome a pathogenic condition and preserve proteostasis [198]. For example, a stress inducible small Hsp, Hsp27, was detected at high levels in degenerating areas of brains from patients with Alzheimer's disease [209]. In addition, aging is associated with impairment in stress-induced synthesis of molecular chaperones [210-212]. Interestingly, in a study using *Caenorhabditis elegans* polyglutamine aggregation models, polyglutamine aggregates were shown to globally stress the cellular folding capacity by overwhelming it; resulting in the aggregation of several unrelated metastable proteins; which in turn further aggravated the aggregation of polyglutamine proteins [213]. This has led to the concept of protein 'metastasis' which describes a condition when initial aggregation events elicit a cascade of pathological events [79]. And finally, multiple lines of evidence demonstrate that pharmacological or genetic enhancement of molecular chaperones is protective in amyloid disease models [214-218].

1.5.3 Disruption via membrane permeation

Cellular membranes, in particular the plasma membrane, have been implicated as a target for amyloid cell disruption [117, 219, 220]. Amyloidogenic proteins and peptides, either as monomers or higher order aggregates have been shown to interact with membranes [184, 221-223]. The presence of lipids has been shown to modulate the fibril formation process. Fibril growth from α -synuclein, IAPP and A β is accelerated in a membrane environment when compared to growth in solution [221-223].

Amyloid aggregates have also been shown to permeabilise membranes and this has been proposed as a mechanism of cell disruption [117]. It is important to note that the ability of amyloid proteins to fibrillate on, interact with and to permeabilise cell membranes critically depends on the biophysical features of the membrane such as curvature, compactness, rigidity and charge density [117]. Various models have been put forward to explain membrane destabilisation and cell toxicity (Figure 1.9) [219, 220]. These include carpeting effects, detergent effects, pore formation, raft-like insertion and fibrillogenesis on the membrane [219, 220, 224].

The carpeting model suggests that the carpeting of the peptide on one edge of membrane applies asymmetric pressure between membrane leaflets resulting in the leakage of small molecules [225]. Evidence for this model comes from *in vitro* experiments showing dye leakage from model liposomes after incubation with human IAPP [226]. Incubation with non-amyloidogenic rat IAPP also resulted in membrane disruption leading to leakage and therefore this model is unlikely to explain the membrane perturbations associated with amyloid structures [184, 226]. Fibril formation of IAPP on the membrane, however, has been shown to damage membranes leading to their leakage; and the amyloid fibril formation process has been shown to be crucial to this disruption as manipulations that retard or accelerate fibril formation, retard or accelerate membrane disruption respectively [184].

The raft-like insertion model describes the extensive insertion of amyloid in the membrane resulting in a 'protein raft' inside the membrane [219]. Studies on a yeast toxic mutant of HET-s support the raft-like insertion model as amyloid aggregation was shown to result in a large insertion of amyloid in the membrane to form a 'protein raft' [227]. Whether amyloid aggregation occurs prior to membrane interaction, or as a result of membrane interaction as in the case of A β ; both result in a raft-like insertion of amyloid material which leads to membrane destabilisation [219, 227, 228].

Amyloid species are also proposed to have detergent like effects which may rationalise the potential to disrupt membranes. The model based on detergent-like effects is based on an initial electrostatic interaction allowing the peptide or aggregate to bind the charged phospholipid head group or membrane surface receptors and thus permitting the peptide or aggregate to orientate its hydrophobic residues in proximity to the hydrophobic core of the membrane [229]. This results in disruption of the bilayer curvature and thus leads to membrane disintegration. Human IAPP has been shown to extract lipids from cellular membranes in such a fashion [230]. β_2m fibrils have also been shown to interact with and

distort artificial lipid membranes. Distortion, mainly by fibril ends, was shown to coincide with the extraction of lipids from the membranes into tiny lipid vesicles [231].

Ca^{2+} is a universal intracellular messenger, and cytosolic Ca^{2+} regulates a multitude of cellular functions and reactions [232]. Disruptions to cytosolic Ca^{2+} concentrations could lead to apoptosis through caspase activation and cytochrome-c release [233]. Disruption of Ca^{2+} homeostasis following the formation of stable pores or ion channels in the membrane is perhaps the model with the most supporting evidence [219]. This model is based on observations of a certain type of annular amyloid oligomeric species which has a central cavity and resembles a pore or channel within model liposomes [224]. Remarkably, this type of oligomer has been observed in amyloid aggregates from disease associated amyloid proteins or peptides such as $\text{A}\beta$, α -synuclein and huntingtin amongst others [121, 224, 234-236]. Furthermore, a large body of evidence supporting pore or channel formation has been associated with $\text{A}\beta$, α -synuclein and polyglutamine proteins and implicates a disruption in Ca^{2+} homeostasis as the main mechanism of toxicity [224, 237-239].

Cell disruption due to membrane permeation need not be exclusively via one of the above proposed models [220]. It is possible that a combination of these proposed models are responsible for pathogenesis [219, 220]. Indeed, the biophysical properties of the membrane in question as well as the structure of the amyloid species will ultimately determine the nature of disruption [117].

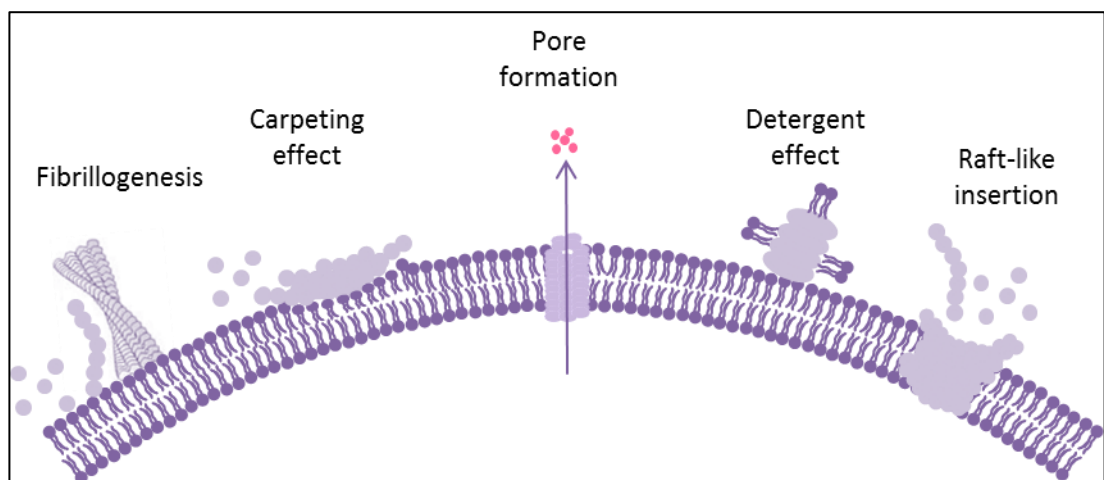


Figure 1.9: Schematic description of the proposed models of interactions resulting in membrane destabilisation and disruption. Pore formation may lead to the leakage of ions and small molecules depicted by pink spheres.

1.5.4 Disruption via organelle dysfunction

Increasing evidence points towards intracellular damage by amyloid aggregates. Extracellular amyloid aggregates either occurring *in vivo* or applied exogenously *in vitro* utilise the endocytic pathway to access intracellular compartments as demonstrated for A β , α -synuclein, polyglutamine and β_2m [240-248]. Once in the intracellular milieu, amyloid aggregates have been reported to induce ER stress, inhibit proteasomes, cause autophagic dysfunction and Golgi fragmentation [167, 201, 249-256]. Oxidative stress and mitochondrial damage have also been implicated [251, 257-259]. Lysosomal damage either via perturbation of the lysosomal membrane or accumulation of amyloid aggregates in the lysosome has also been reported [242, 245, 260-265]. The role of mitochondrial damage in amyloid disease will be briefly discussed. The role of lysosomes in amyloid disease including lysosomal membrane damage, lysosomal dysfunction and autophagy impairment will be discussed in more detail due to its prominence in this project.

1.5.4.1 Mitochondrial dysfunction in amyloid disease

The complex biosynthesis of mitochondria combined with their vital function of energy production contributes to their vulnerability to damage accumulation over their life cycles [266]. Neurons are particularly susceptible to mitochondrial damage as they require high levels of ATP to fuel transport of macromolecules and organelles across a range of distances along axons, and maintain ionic gradients, Ca²⁺ homeostasis and membrane potentials [266]. Due to their complex morphology and high energetic demand, mitochondria have to be transported away from the cell body (where most mitochondrial biogenesis occurs) along axons to regions with high energy and Ca²⁺ buffering requirements thus extending their life-span when compared to other post-mitotic cells [267-270]. This longer life-span results in accumulation of damage [266]. Most newly synthesised mitochondrial proteins are imported in to the mitochondria at the cell body and therefore the older mitochondria at the cell periphery may be less efficient at coping with misfolded proteins or Ca²⁺ overload [271, 272]. Removal of damaged mitochondria from the cell periphery by mitophagy can be an energetically demanding task in neurons as autophagosomes from the axons would need to travel the length of the axon to fuse with lysosomes at the cell body [273]. Therefore, although neurons share the same mitochondrial quality control (QC) systems as other cells they are faced with more arduous challenges [266]. Any mutations or accumulation of aggregates that affect mitochondrial QC capacity will thus preferentially affect neurons and are implicated in neurodegenerative diseases such as Parkinson's disease and Alzheimer's disease [251, 266, 274-276]. One example is the association of mutations in PINK1 and parkin with Parkinson's

disease. Mounting evidence points to the concerted involvement of PINK1 and parkin in mitophagy thus validating the role of mitochondria in disease pathogenesis [276, 277]. Mutant PINK1 and parkin disrupt mitophagy at several different steps [277].

1.5.4.2 Role of lysosomes in amyloid disease

Increasing evidence points towards lysosomal and autophagy dysfunction as one of the underlying mechanisms in amyloidoses such as Alzheimer's, Parkinson's and Huntington's diseases [278]. Amyloid aggregates accumulate in the endolysosomal system, making it the focus of many studies [242, 261, 263, 265].

1.5.4.2.1 Lysosomal membrane damage

Lysosomes, first described by Christian de Duve in 1955, are membrane-bound acidic organelles that house approximately 60 different lysosomal hydrolases responsible for the degradation and recycling of cellular waste [278, 279]. Lysosomes, however, are much more than just a cell waste disposal system, they are central organelles involved in secretion, plasma membrane repair, signalling, energy metabolism, antigen presentation, cholesterol homeostasis, cell death and autophagy pathways [278, 280]. Extracellular material targeted for degradation reaches the lysosome mainly via the endocytic pathway whereas intracellular material is targeted via autophagy [280, 281].

The acidic milieu of lysosomes is crucial for their function and is maintained by a vacuolar ATPase [282]. It is also crucial for the lysosomal membrane to remain intact, both to maintain an acidic lysosomal lumen and to protect the cell from the hydrolytic contents of the lysosome [283]. Lysosomal membrane permeabilisation (LMP) refers to the activation of controlled cell death via leakage of lysosomal proteases from the lysosomal lumen [283]. The lysosomal proteases that remain active at neutral pH such as cathepsins B, D and L have been implicated in activating cell death via caspase or mitochondria-dependent pathways [283].

Accumulating evidence supports lysosomal membrane damage as one of the main causes of cytotoxicity associated with amyloid aggregates. In Alzheimer's disease, A β_{1-42} has been reported to insert tightly into the lysosomal membrane and this has been suggested to cause lysosomal membrane instability leading to LMP [264]. Others have found that the accumulation of A β_{1-42} aggregates in the lysosome results in the rapid generation of free radicals which disrupt the lysosomal proton gradient resulting in cell death [263]. Enzyme leakage following damage to lysosomes culminating in cell death has also been described for exogenously applied A β_{42} oligomers [242]. Mouse models of Alzheimer's disease containing the aggressive Osaka mutation show lysosomal leakage in combination with ER stress and

mitochondrial dysfunction [251]. Lysosomal membrane rupture is also observed in studies involving α -synuclein. This rupture is particle size dependent such that α -synuclein oligomers are more efficient at causing damage than larger α -synuclein fibrillar assemblies [245].

1.5.4.2.2 Disruption of lysosomal function

Undoubtedly, damage to the lysosomal membrane mediated by amyloid aggregates would result in disruption to lysosomal function. Further evidence supporting the role of the lysosome in amyloid cytotoxicity comes from elegant studies looking at the effect of enhancing or disrupting lysosomal function [284, 285]. Interestingly, inhibition of lysosomal function in the absence of amyloid aggregates results in the same phenotype as observed in amyloid disease [284]. For example, inhibition of lysosomal proteolysis either by cathepsins or suppression of lysosomal acidification, retarded transport of late endosomes, lysosomes and autolysosomes along axons and resulted in their accumulation on dystrophic axonal swellings, as observed in Alzheimer's disease. These swellings resembled, in morphology and composition, those observed in mouse models of Amyloid disease [284]. *Scyllo*-Inositol inhibits accumulation of A β and Huntingtin aggregates by promoting proteasomal and lysosomal degradation, and thus inhibits toxicity [285, 286].

Further evidence is provided by fibroblasts from patients suffering from Kufor-Rakeb Syndrome. This disease is characterised by juvenile-onset Parkinsonism and dementia. These patients carry a mutation in PARK9 which results in a reduced ability to maintain Zn²⁺ homeostasis resulting in lysosomal dysfunction [287]. This disruption leads to accumulation of α -synuclein and inhibition of glucocerebrosidase, which is reminiscent of the pathogenic association observed between Parkinson's disease and Gaucher's disease [287, 288]. And lastly, disruption of lysosomal function is also observed in non-neurodegenerative diseases. Human-IAPP disrupts lysosome-dependent degradation which in turn impairs autophagy in mouse models of type II diabetes [289].

1.5.4.2.3 Autophagy dysfunction

As alluded to in section 1.5.4.1 above, neurons are particularly sensitive to accumulation of damaged organelles due to their unusual morphology and high energy demands. It is unsurprising therefore, that autophagy plays a crucial role in neurons and autophagic dysfunction is reported across a host of neurodegenerative diseases. Gathering evidence points to lysosomal and autophagy dysfunction as the central underlying mechanisms in common neurodegenerative diseases such as Alzheimer's, Parkinson's and Huntington's disease [278]. Autophagy is a complex process requiring several different steps and the

involvement of many molecular players. Understanding the reasons behind autophagic failure in neurodegenerative diseases thus requires identification of the pathway(s) affected in each disease [255]. Differences in pathways involved may explain differences in disease pathology and progression. Identification of these differences is therefore crucial to developing targeted therapies [255].

Altered autophagy is a common theme in neurodegenerative diseases and the first clue to this alteration is the accumulation of autophagosomes in diseased neurons in Alzheimer's, Parkinson's and Huntington's diseases [255, 261, 290, 291]. However, accumulation of autophagosomes does not necessarily signify increased degradation through autophagy, as cells could accumulate autophagosomes when autophagy is upregulated (due to increased autophagosome formation) or when clearance of autophagosomes is disrupted [255, 292, 293]. Disrupted autophagic clearance via autophagosome accumulation uncoupled with increased autophagic flux, has been reported for an increasing number of neurodegenerative diseases [255]. This perturbation could be due to disrupted autophagosome trafficking, decreased fusion with endosomes/lysosomes or decreased proteolysis inside lysosomes [255]. Decreased proteolysis could be attributed to altered lysosomal pH, accumulation of undigested by-products or impaired activity and/or expression of lysosomal hydrolases; thus drawing striking parallels between amyloid diseases and the neurodegenerative symptoms observed in lysosomal storage disorders [255, 294].

There are different types of autophagy and three of the main sub-types are macroautophagy, microautophagy and chaperone-mediated autophagy (CMA). The main difference between them is the method of delivery of cargo to the lysosome [295, 296]. In the case of microautophagy and macroautophagy, whole areas of the cytosol are directly engulfed either by invagination at the lysosomal membrane (microautophagy) or by formation of a membrane that seals around the cargo to form an autophagosome (macroautophagy) [255]. CMA involves selective recognition of cargo and direct delivery to the lysosome by specific cytosolic chaperones [297]. All three pathways function simultaneously alongside other proteolytic mechanisms in a co-ordinated manner, for example, macroautophagy is upregulated during blockage of both UPS and CMA [298, 299]. Mutated pathogenic variants of α -synuclein bind tightly to the CMA translocation complex but are not delivered to the lysosome; thus interfering with the CMA translocation complex by sequestering it and preventing degradation of other CMA substrates [300]. Mutated forms of Tau, but not wild-type Tau, are targeted to the lysosomes via CMA where they are abnormally cleaved into amyloidogenic peptides; some

of these peptides form oligomeric structures at the lysosomal membrane which interfere with normal CMA functioning [301].

Connections between macroautophagy and non-autophagic lysosomal pathways such as endocytosis also exist. ESCRT-III dysfunction in the late endosomal membrane disrupts the formation of multi-vesicular bodies (MVBs), which reduces autophagic flux and results in autophagosome accumulation in models of frontotemporal dementia [302]. Disruption of endosome biogenesis causing autophagic failure leads to accumulation of poly-ubiquitinated amyloid proteins such as Huntingtin and TDP-43 [303].

In summary, identification of the nature of the autophagic defect and the cellular response to that defect will inform targeted therapies [255]. An ideal approach would involve enhancing autophagosome clearance by upregulating the lysosome, as demonstrated by upregulating lysosomal biogenesis via overexpression of the transcription factor EB (TFEB) [255, 304].

1.5.4.2.4 Parallels between lysosomal storage diseases and amyloid disease

Lysosomal storage diseases (LSDs) are a group of over 40 metabolic disorders attributed to mutations in lysosomal proteins such as hydrolases and integral membrane proteins as well as proteins involved in modification and trafficking of lysosomal proteins [305, 306]. Over 65 % of LSDs have defects in the central nervous system (CNS) leading to progressive cognitive and motor decline [305]. LSDs exist in infantile, juvenile and adult forms [307].

Over the years, an increased interest in the involvement of autophagy in LSD pathogenesis has developed. Indeed, in mouse models of two LSDs (Multiple Sulfatase Deficiency and Mucopolysaccharidosis type IIIA) striking parallels with Alzheimer's disease are drawn such as an accumulation of autophagosomes [294], reduced degradation of endogenous and exogenous autophagic substrates [308] and defective organelle turnover [306]. Also, autophagic impairment leading to pathological protein aggregate accumulation was detected in LSD neurons [309]. In combination, these observations show similarities between LSDs and amyloid diseases such as Alzheimer's, Parkinson's and Huntington's disease [306]. The similarities between LSDs and neurodegenerative diseases not only suggest a potential central role of lysosomes in amyloid disease, but in some cases are informative of the pathogenesis of the amyloid disease. In particular, the similarities between Parkinson's and Gaucher's diseases, as well as Niemann-Pick Type C and Alzheimer's will be briefly discussed.

Parkinson's and Gaucher's diseases

Gaucher's disease is an autosomal recessive disorder that results from loss-of-function mutations in *GBA1*, the gene encoding glucocerebrosidase, a lysosomal enzyme that cleaves the β -glucosyl linkage of glucoceramide [288]. Gaucher's disease has three subtypes which are based on the aggressiveness of the disease and neurological involvement [310]. Gathering clinical, pathological and genetic evidence points to an association between Gaucher's and Parkinson's diseases [311].

The clinical presentation of parkinsonism in type 1 Gaucher's disease patients, further supported by genetic evidence, suggests a strong link [312-314]. α -synuclein aggregation was implicated in the pathogenesis of Gaucher's disease upon discovery of α -synuclein positive Lewy bodies in the brains of Gaucher's disease patients [315]. The discovery that parkinsonism patients had an increased incidence of *GBA1* mutations from genetic studies in large patient cohorts makes *GBA1* the most common genetic risk factor for Parkinson's disease known to date [288, 316]. And finally, accumulation of toxic α -synuclein species has been shown to deplete lysosomal glucocerebrosidase, leading to accumulation of glucocerebroside which in turns stabilises α -synuclein aggregates. This self-propagating positive feedback loop has been proposed as a mechanism that connects the two diseases [288].

Niemann-Pick type C and Alzheimer's diseases

Niemann-Pick type C is also an autosomal recessive disorder, involving disruption in cholesterol trafficking within the endolysosomal pathway [317]. Although fundamentally different from Alzheimer's disease, Niemann-Pick type C disease draws some interesting parallels with it. Endosomal abnormalities reminiscent of those observed at the earliest stage in Alzheimer's disease are observed in neuronal populations in Niemann-Pick type C disease [317]. Strikingly, this is also combined with endosomal accumulation of APP and A β peptides [317-319]. Also of remarkable interest, is the observation of neurofibrillary tangles in the brains of NPC patients in the absence of mutations in tau or abnormal A β deposition [320, 321]. Cholesterol is another common theme between the two diseases, cholesterol trafficking disruption being the primary pathogenic cause in Niemann-Pick type C disease and elevated cholesterol being a risk factor in Alzheimer's disease [317, 322].

1.6 Aims

The first aim of the thesis was to analyse the effect of β_2m amyloid fibrils on lysosomal function, with particular focus on lysosomal proteolysis. This was based on the large body of literature implicating lysosomes as key cellular targets of amyloid pathogenesis (discussed in 1.5.4.2) as well as emerging evidence from our laboratory. The second aim was to analyse the effect on membrane trafficking. The precedence for this comes from genome wide association studies implicating endocytic trafficking and observations of impaired endolysosomal trafficking [323, 324]. The third aim was to investigate the role of the molecular chaperone, Hsp70, in fibril-mediated cell disruption based on the increased incidence of amyloid disease with diminished proteostasis (discussed in 1.5.2).

1.7 Objectives

1.7.1 Chapter 3 objectives

The objective of this chapter was to validate the use of β_2m as a model to study amyloid-cell interactions. β_2m amyloid fibrils were generated and subsequently characterised based on their biophysical, tinctorial and immunological characteristics. In addition, the effect of β_2m fibrils on the cell viability assay, the MTT assay was analysed.

1.7.2 Chapter 4 objectives

Building on previous work in the laboratory which shows that fragmentation of β_2m fibrils enhances their internalisation and trafficking to the lysosome, the objective of chapter 4 was to investigate the effect of fragmented β_2m fibrils on lysosomal function. This included analysis of lysosomal proteolysis and autophagy, as well as the activity of the lysosomal hydrolases β -glucocerebrosidase and β -galactosidase.

1.7.3 Chapter 5 objectives

The objective of chapter 5 was to investigate the effect of fragmented β_2m fibrils on membrane trafficking. This was based on literature precedence as well as observations from experiments described in chapters 3 and 4. Investigation of membrane trafficking involved the analysis of the localisation of the lysosomal membrane proteins, LAMP-1 and CD63, and analysis of fluid-phase endocytosis.

1.7.4 Chapter 6 objectives

The objective of chapter 6 was to investigate the role of Hsp70 in fibril-mediated cellular disruption. Building on observations in chapters 3, 4, and 5, this involved analysis of the effect of Hsp70 on cellular reduction, lysosomal proteolysis and LAMP-1 trafficking in fibril-treated cells.

2 Materials and methods

All materials used were from Sigma-Aldrich unless otherwise stated in the text.

2.1 Expression and purification of β_2m

2.1.1 Expression of β_2m

β_2m was expressed in BL21 (DE3) pLysS cells transformed with the designated pINK plasmid containing the gene for human β_2m [325]. 10 μ l of a glycerol stock of BL21 (DE3) pLysS cells transformed with pINK was streaked out onto a fresh Lysogeny Broth (LB)-agar plate containing 100 μ g/ml carbenicillin (Melford). The LB-agar plate was incubated at 37 °C for 16 h. A single colony was picked and used to inoculate a starter culture of 100 ml LB containing 100 μ g/ml carbenicillin. The starter culture was incubated in an orbital shaker (Stuart S150) at 37 °C for 16 h whilst shaking at 200 rpm.

11 l of pre-warmed LB were inoculated with the starter culture (5 ml of starter culture per litre of LB containing 100 μ g/ml carbenicillin). The bacterial cultures were incubated at 37°C whilst shaking at 200 rpm. The OD₆₀₀ was monitored regularly and when an OD of 0.6 was reached, the cultures were induced by the addition of isopropyl β -D-1-thiogalactopyranoside (IPTG) at a final concentration of 1 mM. The bacterial cultures were incubated at 37°C whilst shaking at 200 rpm for 16 h, after which the cells were harvested using a continual action centrifuge (Heraeus Contifuge Stratos # 3049 with a continuous flow rotor) at 15,000 rpm. The supernatant was discarded and the pellet was resuspended as described below.

2.1.2 Inclusion body isolation

The cell pellet was resuspended in 100 ml lysis buffer (25 mM Tris.HCl pH 8.0 containing 100 μ g/ml lysozyme, 50 μ g/ml PMSF, 20 μ g/ml DNaseA and 1 mM EDTA) by stirring at room temperature for 30 min. The cells were homogenised by passing through a small blunt needle and then further lysed using a cell disrupter (Constant Systems Cell Disrupter). Cell lysates were centrifuged for 30 min at 4 °C (Beckman Coulter, JLA 16.250 rotor, 15,000 rpm). The cell pellet containing the protein as inclusion bodies was washed five times with 100 ml wash buffer (25 mM Tris.HCl pH 8.0). The pellet was then solubilised in 200 ml solubilisation buffer (25 mM Tris.HCl pH 8.0 containing 8 M urea) by stirring at 25 °C for 16 h.

2.1.3 Refolding by dialysis

Solubilised protein was then dialysed six times against 5 l of 25 mM Tris.HCl pH 8.0 using 3500 molecular weight cut off (MWCO) dialysis tubing at 4 °C. The dialysed protein was centrifuged for 1 h at 4 °C (Beckman Coulter, JLA 16.250 rotor, 15,000 rpm) to remove any precipitate.

2.1.4 Anion exchange chromatography

The refolded protein was further purified by anion exchange chromatography using a XK50 column (GE Healthcare) containing 200 ml (bed volume) fast-flow Q-Sepharose (GE Healthcare) previously equilibrated with 25 mM Tris.HCl pH 8.0 and connected to an AKTA prime chromatography system (GE Healthcare). The resolubilised protein was loaded onto the column, and washed with five column volumes of 25 mM Tris.HCl pH 8.0. The protein was eluted with a linear gradient of 0-400 mM NaCl in 25 mM Tris.HCl pH 8.0 over 1 l. The fractions containing β_2m , as judged by the elution profile and sodium dodecyl sulphate polyacrylamide gel electrophoresis (SDS-PAGE) analysis, were pooled and dialysed five times against 5 l of 18 M Ω purite water before lyophilising for storage at -20°C.

2.1.5 Size exclusion chromatography

The protein was further purified by size exclusion chromatography using a Superdex 75 HiLoad 26/60 size exclusion column (GE Healthcare) mounted on an AKTA prime chromatography system (GE Healthcare). The lyophilised protein was dissolved in 20 ml of 10 mM sodium phosphate buffer pH 7.2 and filtered using a 0.2 μ m filter (Sartorius). The protein was loaded onto the column (5 ml of ~10 mg/ml per run) and the following program (Table 2.1) on the AKTA prime system was used to purify the protein.

| Breakpoint (ml) | % B | Flow rate | Fraction size | Buffer valve position | Inject valve position | Set peak collect | Auto zero | Event mark |
|-----------------|-----|-----------|---------------|-----------------------|-----------------------|------------------|-----------|------------|
| 0 | 0 | 2ml/min | 0ml | 1 | Load | No | No | No |
| 10 | 0 | 2ml/min | 0ml | 1 | Inject | No | Yes | Yes |
| 20 | 0 | 2ml/min | 0ml | 1 | Load | No | No | Yes |
| 110 | 0 | 2ml/min | 3ml | 1 | Load | No | No | Yes |
| 360 | 0 | 2ml/min | 0ml | 1 | Load | No | No | No |

Table 2.1: Details of the AKTA program used for size exclusion chromatography of β_2m .

The fractions corresponding to monomeric β_2m as judged by SDS-PAGE analysis were pooled and dialysed five times against 5 l of 18 M Ω purite water before lyophilising for storage at -20°C. The precise molecular weight of the protein was determined using electrospray ionisation mass spectrometry (ESI-MS) performed by James Ault (Astbury mass spectrometry facility manager).

2.2 Sodium dodecyl sulphate polyacrylamide gel electrophoresis (SDS-PAGE)

Tris-tricine or Tris-glycine buffered SDS-PAGE gels were used to separate proteins according to their molecular weight. Two glass plates were assembled according to the manufacturer's instructions using a 1.5 mm spacer (Bio-Rad for Tris-tricine gels and Hoefer for Tris-glycine gels). A two-layered gel system consisting of a stacking and resolving gel was made using the components in Table 2.2 or Table 2.3.

| Solution Component | Resolving gel | Stacking gel |
|--|--------------------|--------------------|
| | Volume to add (ml) | Volume to add (ml) |
| 30% (w/v) Acrylamide: 0.8% (w/v) bis-acrylamide | 7.5 | 0.83 |
| 3 M Tris.HCl, 0.3% (w/v) SDS pH 8.45 | 5.0 | 1.55 |
| H₂O | 0.44 | 3.72 |
| Glycerol | 2.0 | - |
| 10% (w/v) ammonium persulphate | 0.05 | 0.10 |
| Tetramethylethylenediamine (TEMED) | 0.005 | 0.005 |

Table 2.2: Components of a Tris-tricine buffered gel.

| Solution Component | Resolving gel | Stacking gel |
|--|--------------------|--------------------|
| | Volume to add (ml) | Volume to add (ml) |
| 30% (w/v) Acrylamide: 0.8% (w/v) bis-acrylamide | 3.33 | 0.83 |
| 3 M Tris.HCl, 0.8% (w/v) SDS, pH 8.8 | 1.35 | - |
| 1 M Tris.HCl, 0.8% (w/v) SDS, pH 6.8 | - | 0.63 |
| H₂O | 5.31 | 3.4 |
| 10% (w/v) ammonium persulphate | 0.05 | 0.10 |
| TEMED | 0.005 | 0.005 |

Table 2.3: Components of a Tris-glycine buffered gel.

For Tris-tricine gels:

The resolving gel mixture was made and rapidly poured to within 2 cm of the top of the glass plates. The stacking gel mixture was made and then poured on top of the resolving gel. A comb was inserted to create wells for sample loading. The gels were left for a minimum of 1 h to set.

Gel samples were diluted two-fold into 2X modified Laemmli buffer (100 mM Tris.HCl pH 6.8 containing 20 % (v/v) glycerol, 4 % (w/v) SDS, 0.2 % (w/v) bromophenol blue and 100 mM dithiothreitol (DTT)) and incubated at 95 °C for 5 min before loading onto the gel. To obtain comparative loadings of bacterial cell lysates, 100 µl of the modified Laemmli buffer was added to the cell pellet (obtained from the volume of bacterial culture corresponding to 1.0 OD₆₀₀ units) and 15 µl was loaded per lane. A lane containing 15 µl of protein marker (Invitrogen Mark 12) was included.

The proteins were electrophoresed using a cathode buffer (200 mM Tris-HCl, 200 mM Tricine, 0.2% (w/v) SDS pH 8.25) and an anode buffer (400 mM Tris-HCl pH 8.8). A constant current of 30 mA was applied until the samples entered the resolving gel, and then the current was adjusted to 60 mA until the dye front reached the bottom of the gel. Gels were stained, de-stained and imaged as described below.

For Tris-glycine gels:

The resolving gel mixture was made and rapidly poured to within 2 cm of the top of the glass plates. A layer of water-saturated butan-1-ol was applied onto the surface of the first layer to exclude oxygen and to aid polymerisation. Once the resolving gel had set, the surface was rinsed with water before the stacking gel mixture was poured on top of it. A comb was inserted immediately after pouring the stacking gel. The stacking gel was allowed to set for approximately 45 min.

Samples were prepared for loading as described above. A lane containing 15 µl protein marker (ColorPlus Prestained Protein Marker, New England Biolabs) or 5 µl protein marker (Precision Plus Dual Xtra Pre-stained Standards, Bio-Rad) was included.

The gels were electrophoresed in running buffer (25 mM Tris-HCl, pH 8.0, 192 mM glycine, 0.1 % (w/v) SDS) through the stacking gel at 15 mA and through the resolving gel at 25 mA. The gels were stained, de-stained and imaged as described below or western blotted (Section 0).

For both gel types:

The gels were stained in 50% methanol (v/v), 10% acetic acid (v/v) and 0.25% (w/v) Coomassie Brilliant Blue for 1 h at room temperature whilst rocking. After staining, the gels were rinsed and destained in 50% methanol (v/v) and 10% acetic acid (v/v) for approximately 16 h or until the bands were clearly visible and the background stain diminished. The gels were photographed using the InGenius gel documentation system (Syngene).

2.3 Statistical analysis

Where appropriate, statistical analysis was performed using the two-tailed, independent, two-sample t test between sample pairs. Where appropriate, p values of <0.05, <0.01 and <0.001 are indicated by (*), (**) and (***) respectively. When $p > 0.05$, p values are not quoted and the lack of significant difference is indicated in the text.

2.4 Generation and characterisation of β_2m fibrils

2.4.1 Production of β_2m fibrils

β_2m fibrils were generated using an established protocol [190]. The lyophilised protein was dissolved in 10 mM sodium phosphate buffer pH 2.0 containing 50mM NaCl to a concentration of approximately 5 mg/ml. The protein solution was filtered using a 0.2 μ m filter (Sartorius). 10 μ l of the protein solution was unfolded in 20 mM sodium phosphate buffer pH 6.5 containing 6 M guanidine.HCl and the OD₂₈₀ was measured spectrophotometrically. The extinction coefficient of 20065M⁻¹cm⁻¹ was used to calculate the concentration of the protein solution [326]. The protein concentration was adjusted to 120 μ M. Fibrils were generated by seeding with 0.1% (v/v) fragmented fibrils and quiescent incubation at room temperature for 72 h.

2.4.2 Fragmentation of β_2m fibrils

Fragmented β_2m fibrils were generated by stirring 500 μ l of β_2m fibrils in a 1.5 ml glass vial containing a 3 x 8 mm polytetrafluoroethylene-coated magnetic stirring bar, using a custom-made precision stirrer (custom built by the workshop of the School of Physics and Astronomy, University of Leeds).

2.4.3 Thioflavin T fluorescence

The end point Thioflavin T (ThT) fluorescence of fibril samples was measured. Each sample (β_2m monomer, unfragmented fibrils or fragmented fibrils) was diluted to a final monomer equivalent concentration of 1.2 μ M in ThT buffer (0.5 M Tris.HCl pH 8.5 containing 10 μ M ThT). Samples were excited at 440 nm and fluorescence was measured immediately after dilution for 60 s by recording emission at 480 nm (slit widths of 3 nm each, acquisition temperature of

37 °C). Fluorescence was measured on a fluorimeter (Quantamaster, Photon Technology International). An average fold increase in fluorescence of fibril samples over β_2m monomer was calculated.

2.4.4 Immunoblotting of fibril samples

Fibril samples or controls (2 μ l) were applied to nitrocellulose membrane (Hybond-Enhanced Chemiluminescence, GE Healthcare) and allowed to dry at room temperature. Controls included, Hsp70 as a negative control for anti- β_2m , β_2m monomer as a negative control for WO1 and A11 and as a positive control for anti- β_2m , and $A\beta_{1-40}$ oligomer (kind gift from Charles Glabe, University of California, Irvine) as a positive control for A11. The membranes were blocked with 10 % (w/v) skimmed milk powder (Marvel) in immunoblot buffer (Table 2.4) for 16 h at 4 °C (β_2m and A11 blots) or 1 h at 25 °C (WO1 blots). For WO1 blots, samples were incubated with primary antibody in immunoblot buffer containing 3 % (w/v) bovine serum albumin (BSA) for 16 h at 4 °C. For A11 and anti- β_2m dot blots, samples were incubated with primary antibody in immunoblot buffer containing 5 % (w/v) skimmed milk powder for 1 h at 25 °C. The membranes were washed three times in immunoblot buffer before incubation with horseradish peroxidase (HRP) conjugated secondary antibody, in the same buffers as the primary antibodies, for 1 h at 25 °C (Table 2.5). The membranes were washed three times with immunoblot buffer, before visualisation of antibody binding using Supersignal West Pico chemiluminescent substrate (Perbio) and medical imaging film (Fujifilm), developed on the Konica SRX-101A developer.

| Antibody | Host, clonality | Supplier/source | Concentration used | Immunoblot buffer |
|---------------------|--------------------|--|--------------------|--------------------------------------|
| Anti- β_2m | Rabbit, Polyclonal | DakoCytomation | 11 μ g/ml | PBS containing 0.2 % (v/v) Tween 20 |
| Anti-oligomer (A11) | Rabbit, polyclonal | Charles Glabe, University of California, Irvine [18] | 0.5 ng/ml | PBS containing 0.05 % (v/v) Tween 20 |
| Anti-fibril (WO1) | Mouse, monoclonal | Ronald Wetzel, University of Pittsburgh [327] | 1 μ g/ml | PBS containing 0.2 % (v/v) Tween 20 |

Table 2.4: Primary antibodies used in the immunoblotting protocol.

| Antibody | Supplier | Concentration used |
|-----------------|----------------|--------------------|
| Anti-rabbit HRP | BD Biosciences | 0.4 µg/ml |
| Anti-mouse HRP | BD Biosciences | 0.4 µg/ml |

Table 2.5: Secondary antibodies used in the immunoblotting protocol.

2.4.5 Transmission electron microscopy

20 µl of unfragmented or fragmented β_2m fibril samples at a final monomer equivalent concentration of 12 µM was applied to carbon coated copper grids and allowed to dry for 30 s. Excess fibril sample was blotted using filter paper. The grids were then stained with 20 µl of 4% (w/v) uranyl acetate for 30 s. Excess uranyl acetate was blotted using filter paper. The fibril samples were imaged using a Phillips CM10 electron microscope (100 KeV).

2.4.6 Fibril length determination by atomic force microscopy (AFM)

Fibril length distribution was determined by Kevin Tipping, University of Leeds. Samples were prepared for tapping-mode AFM by dilution in 18 MΩ purite water to a final monomer equivalent concentration of 0.4 µM. Samples were diluted to ensure good sample dispersion and uniform distribution on the imaging surface. 20 µl of diluted sample was applied to a freshly cleaved mica surface and allowed to dry for 5 min at room temperature. Mica surfaces were then washed with 1 ml of 18 MΩ purite water and dried under a gentle stream of N₂ gas. Samples were imaged using a Dimension 3100 scanning probe microscope (Veeco Instruments) and PPP-NCLR silicon cantilever probes (Nanosensors) with a nominal force constant of 48 N/m. Typically, 10 µm² images at a pixel ratio of 1024 x 1024 were collected for analysis. Image analysis was performed using scripts generated in Matlab (MathWorks) by Wei-Feng Xue (University of Kent) [328]. Fibrils were selected automatically using the script to avoid subjective bias in analysis.

2.5 Cell culture

RAW 264.7 and SH-SY5Y cells were cultured in Dulbecco's modified eagle's medium (DMEM) with 10 % (v/v) foetal bovine serum (Biosera), 2 mM L-glutamine, 100 IU/ml penicillin and 100 µg/ml streptomycin in 75 cm³ flasks (OrFlask, Orange Scientific). Cells were incubated at 37 °C, 5 % CO₂. SH-SY5Y cells were passaged using 1 % Trypsin-EDTA solution and RAW 264.7 cells with a cell scraper (Grenier Bio-one) when they reached 60–80 % confluency.

2.5.1 3-(4,5-Dimethylthiazol-2yl)-2,5-diphenyltetrazolium bromide (MTT) assay

Cells were plated out at 5,000 cells/well (RAW 264.7) or 10,000 cells/well (SH-SY5Y) in 96 well plates (RAW 264.7 in Corning Costar plates and SH-SY5Y in NUNC plates) and cultured for 16 h. Cells were then incubated with 1.2 µM (monomer equivalent) β₂m fibril samples, or controls (1.2 µM β₂m monomer, fibril growth buffer or 0.1 % (w/v) sodium azide) for 24 h. 20 µl of 5 mg/ml MTT solution was added to the cells and incubated for 1.5 h. The media was then discarded and the resulting formazan crystals were resuspended in dimethyl sulfoxide (DMSO). Absorbance was measured spectrophotometrically (PowerWave HT Microplate Spectrophotometer, BioTek) at 570 nm with absorbance due to background cell debris subtracted at 650 nm. Results were normalised to 0.1 % (w/v) sodium azide (0 %) and fibril growth buffer (100 %).

2.5.2 Phase contrast microscopy of cells incubated with MTT

RAW 264.7 cells were plated out at 500,000 cells/well and SH-SY5Y cells at 1,000,000 cells/well in 6 well plates (Corning Costar) and cultured for 16 h. Cells were incubated with 1.2 µM (monomer equivalent) β₂m fibril samples or controls (1.2 µM β₂m monomer or fibril growth buffer) for 24 h. Cells were then incubated with MTT at a final concentration of 0.5 mg/ml for 1.5 h. The cell culture medium was replaced with PBS and cells were imaged with an inverted contrasting microscope (Leica DM IL connected to a Leica DC 300F camera, Leica Microsystems).

2.6 Western blotting analysis

2.6.1 Preparation of cell lysates

RAW 264.7 and SH-SY5Y cells were plated out at 500,000 cell/swell and 1,000,000 cells/well respectively in 6 well plates (Corning Costar) and cultured for 16 h. Cells were incubated with either fragmented β_2m fibrils at a final monomer equivalent concentration of 1.2 μ M or 1.2 μ M β_2m monomer as a control for 2 h or 24 h. Cells were then washed three times with PBS, prior to lysis in lysis buffer (50 mM Tris.HCl pH 7.6 containing 150 mM NaCl, 1 % (v/v) nonidet P-40 (NP-40) and EDTA-free complete protease inhibitor cocktail (Roche, as described in manufacturer's instructions)) for 30 min on ice. Cell lysates were centrifuged at 500 g for 10 min at 4 °C (Microcentrifuge 5415R, Eppendorf) and the supernatant was retained. Protein concentration in the supernatant was determined by an adapted version of the Lowry assay, the DC protein assay (Bio-Rad), as described in the manufacturer's instructions. Protein concentration was assayed for all samples in the experiment at the same time. All sample concentrations were adjusted with lysis buffer to match the lowest sample concentration. All samples were further diluted in an equal volume of 2X modified Laemmli buffer (100 mM Tris.HCl pH 6.8 containing 20 % (v/v) glycerol, 4 % (w/v) SDS, 0.2 % (w/v) bromophenol blue and 100 mM dithiothreitol (DTT)) and incubated at 95 °C for 5 min. Samples were then resolved by SDS-PAGE and immunoblotted as described below.

2.6.2 Immunoblotting

Tris-glycine SDS-PAGE was carried out as described in section 2.2. 10 % Tris-glycine SDS-PAGE gels were transferred onto polyvinylidene fluoride (PVDF) membranes (GE Healthcare) using a trans-blot semi-dry electrophoretic Transfer cell (Bio-Rad) as described in the manufacturer's instructions, with transfer buffer (15 mM Tris-HCl, 150 mM glycine, 0.02 % (w/v) SDS, 20 % (v/v) methanol) at 12 V for 1 h. Membranes were blocked with 5 % (w/v) skimmed milk powder (ovalbumin, LC3B and GAPDH blots) or 3 % (w/v) BSA (LAMP-1, CD63 and cathepsin D blots) for 16 h rocking at 4 °C. Membranes were incubated with primary antibody for the times specified (Table 2.6). Membranes were then washed three times for 5 min whilst rocking with PBS containing 0.2 % (v/v) Tween20. This was followed by incubation with secondary antibodies (Table 2.5) for 1 h whilst rocking at room temperature. Membranes were washed three times for 5 min whilst rocking with PBS containing 0.2 % (v/v) Tween 20. Excess buffer was blotted and membranes were developed by chemiluminescence detection using Supersignal West Pico chemiluminescent substrate (Perbio) and medical imaging film (Fujifilm), on a Konica SRX-101A developer.

| Antibody | Host, clone | Supplier | Incubation period | Concentration used |
|----------------------|--------------------|--------------------------|--------------------------|---------------------------|
| Ovalbumin-HRP | Rabbit, polyclonal | GeneTex | 16 h, 4 °C | 1 in 2000 |
| Anti-LC3B | Rabbit, polyclonal | Abcam | 16 h, 4 °C | 0.5 µg/ml |
| Anti-LAMP-1 | Mouse, H4A3 | Santa Cruz Biotechnology | 16 h, 4 °C | 0.4 µg/ml |
| Anti-CD63 | Rabbit, EPR5702 | Abcam | 16 h, 4 °C | 1 in 200 |
| Cathepsin D | Mouse, CTD-19 | GeneTex | 16 h, 4 °C | 1 in 500 |
| GAPDH | Mouse, 6C5 | Abcam | 1 h, 25 °C | 0.4 µg/ml |

Table 2.6: Primary antibodies used for probing western blots.

| Antibody | Supplier | Incubation period | Concentration used |
|------------------------|-----------------|--------------------------|---------------------------|
| Anti-mouse HRP | BD Biosciences | 1 h, 25 °C | 0.4 µg/ml |
| Anti-rabbit HRP | DakoCytomation | 1 h, 25 °C | 0.4 µg/ml |

Table 2.7: Secondary antibodies used for probing western blots.

2.7 Assays on lysosomal function

2.7.1 Analysis of lysosomal degradation of fluorescent protein substrates

2.7.1.1 Preparation of fluorescent protein substrates

β_2m was fluorescently labelled as described below. Pumilio-GFP was a kind gift from Thomas Edwards (University of Leeds). Alexa Fluor® 647 ovalbumin was purchased from Molecular Probes.

2.7.1.1.1 Labelling of β_2m monomer with tetramethylrhodamine.

A ten-fold molar excess of 5-(and-6)-carboxytetramethylrhodamine-succinimidyl ester (TMR, Molecular Probes) over β_2m was dissolved in DMSO at a concentration of 1 mg/ml, and added drop wise to β_2m (10 mg/ml in 1 M sodium bicarbonate buffer) whilst stirring in the dark for 1 h. A PD10 desalting column (GE Healthcare) was equilibrated using 25 ml of 100 mM Tris.HCl pH 8.0. 2.5 ml of the TMR- β_2m conjugate was loaded onto the column and eluted using 3.5 ml of 100 mM Tris.HCl pH 8.0. The eluted TMR- β_2m conjugate was dialysed against 18 M Ω purite water, lyophilised and stored at -20 °C. β_2m monomer was labelled with 2, 3, 4 or 5 TMR molecules per monomer with a ratio of \approx 1:2:2:1 as determined by electrospray ionisation mass spectrometry performed by James Ault (University of Leeds, Astbury mass spectrometry facility manager).

2.7.1.2 Analysis by flow cytometry

RAW 264.7 and SH-SY5Y cells were plated out at 25,000 and 150,000 cells/well respectively in 12 well plates (Corning Costar) and cultured for 16 h. Cells were incubated with either fragmented β_2m fibrils at a final monomer equivalent concentration of 1.2 μ M, or controls (1.2 μ M β_2m monomer and/or fibril growth buffer) for 24 h. Following fibril incubation, cells were pulsed with fluorescent protein substrate (Table 2.8) for 4 h (RAW 264.7 cells) or 6 h (SH-SY5Y cells). At the end of the pulse, cells were washed thoroughly and either analysed for cell-associated fluorescence immediately (0 h chase) or cultured for a further 24 h in the absence of fluorescent protein substrate and then analysed (24 h chase). The cell population was gated to exclude dead cells and debris and 10,000 gated events were recorded. Because SH-SY5Y cells have a tendency to clump, SH-SY5Y cells were gated further to exclude cell clumps. Results were corrected for background fluorescence using cells incubated in the absence of fluorescent protein substrate. Results were normalised to 0 h chase (100 %) for each condition and the percentage remaining fluorescence of protein substrate was determined (background corrected fluorescence at 24 h chase/background corrected fluorescence at 0 h chase). Cells were analysed using a BD LSRFortessa analyser (Becton Dickinson).

| Protein | Fluorophore | Concentration used | Excitation laser |
|-------------|-------------------------------|--|------------------|
| β_2m | Tetramethylrhodamine (TMR) | 14 $\mu\text{g/ml}$ (RAW 264.7) or 28 $\mu\text{g/ml}$ (SH-SY5Y); 10 % labelled: 90 % unlabelled | 488 nm |
| Pumilio-GFP | Green fluorescent protein GFP | 20 $\mu\text{g/ml}$ | 488 nm |
| Ovalbumin | Alexa Fluor [®] 647 | 15 $\mu\text{g/ml}$; 40 % labelled: 60 % unlabelled | 640 nm |

Table 2.8: Fluorescent protein substrates used for analysis of lysosomal degradation.

2.7.1.2.1 In vitro measurement of GFP-fluorescence variation with pH

Pumilio-GFP was diluted to a final concentration of 150 $\mu\text{g/ml}$ into a citrate-phosphate buffer (50 mM citric acid, 50 mM sodium phosphate, 100 mM NaCl, 1 mM EDTA) at pH 4.5, 5.5 or 7.4 respectively. Diluted Pumilio-GFP was excited at a wavelength of 395 nm and emission spectra were collected on a fluorimeter (Quantamaster, Photon Technology International). Excitation and emission slit widths were set to 3 nm. Background correction was applied by subtracting the fluorescence spectra acquired from a citrate-phosphate buffer control.

2.7.1.3 Analysis by live cell confocal microscopy

RAW 264.7 and SH-SY5Y cells were seeded at 50,000 and 250,000 cells/well respectively in 3 cm glass bottomed imaging dishes (Iwaki) and cultured for 16 h. Cells were incubated with β_2m fibril samples at a final monomer equivalent concentration of 1.2 μM , or controls (1.2 μM β_2m monomer or fibril growth buffer) for 24 h. Cells were then washed and pulsed with 15 $\mu\text{g/ml}$ Alexa Fluor[®] 647 ovalbumin (40 % labelled, 60 % unlabelled) for 4 h (RAW 264.7) or 6 h (SH-SY5Y). Following thorough washing, cells were either imaged by live cell confocal microscopy immediately (0 h chase) or cultured for a further 24 h and then imaged (24 h chase). Cells were stained with 50 nM (RAW 264.7) or 75 nM (SH-SY5Y) LysoTracker Green (Molecular Probes) 30 min prior to imaging. Images were acquired on an inverted confocal microscope (Zeiss LSM700) with a heated stage (37 °C).

2.7.2 Analysis of lysosomal proteolysis using Magic Red™

2.7.2.1 Live cell confocal microscopy analysis of Magic Red™ cathepsin B substrate cleavage

SH-SY5Y cells were plated at 1,000,000 cells/well in 3 cm imaging dishes (Iwaki) and were cultured for 16 h. Following thorough washing, cells were incubated with Magic Red™ cathepsin B substrate (ImmunoChemistry Technologies) according to the manufacturer's protocol (Magic Red™ cathepsin B substrate was re-constituted in DMSO and diluted 260-fold into cell culture media before incubation with cells at 37 °C for 1 h). Cells were then washed and stained with 75 nM LysoTracker Green (Molecular Probes) 30 min prior to imaging, and Hoechst (Immunochemistry Technologies) immediately before imaging. Images were acquired on an inverted confocal microscope (Zeiss LSM700) with a heated stage (37 °C).

2.7.2.2 Flow cytometric quantification of cathepsin B activity using Magic Red™

RAW 264.7 and SH-SY5Y cells were plated at 250,000 and 500,000 cells/well in 12 well plates (Corning Costar) and cultured for 16 h. Cells were incubated with either fragmented β_2m fibrils at a final monomer equivalent concentration of 1.2 μ M, or controls (1.2 μ M β_2m monomer or fibril growth buffer) for 24 h. Cells were washed and incubated in the presence or absence of Magic Red™ cathepsin B substrate as described in 2.7.2.1. Cells were washed prior to analysis for cell-associated fluorescence by flow cytometry. The cell population was gated to exclude dead cells and debris and 10,000 gated events were recorded. Because SH-SY5Y cells have a tendency to clump, SH-SY5Y cells were gated further to exclude cell clumps. Results were corrected for background fluorescence using cells incubated in the absence of Magic Red™ cathepsin B substrate. Results were normalised to controls incubated with fibril growth buffer (100 %). Cells were analysed using a BD LSRFortessa analyser (Becton Dickinson).

2.7.3 Analysis of β -glucocerebrosidase and β -galactosidase activity

SH-SY5Y cells were plated at 500,000 cells/well in 12 well plates (Corning Costar) and cultured for 16 h. Cells were incubated with either fragmented β_2m fibrils at a final monomer equivalent concentration of 1.2 μ M, or controls (1.2 μ M β_2m or fibril growth buffer) for 24 h. Cells were then washed and incubated with either 50 μ g/ml 5-(pentafluorobenzoylamino)fluorescein di- β -D-glucopyranoside (PFB-FDGlu, Molecular Probes) or 50 μ M fluorescein di- β -D-galactopyranoside (FDG, Molecular Probes) respectively for 1 h at 37 °C. β -glucocerebrosidase cleaves the non-fluorescent substrate PFB-FDGlu to yield the green-fluorescent PFB-F dye. β -galactosidase cleaves the non-fluorescent substrate FDG to yield highly fluorescent fluorescein. For analysis of β -glucocerebrosidase activity, the inhibitor

conduritol B epoxide (CBE) was included as an additional control. Cells were pre-incubated with 1 μ M CBE for 2 h prior to incubation with PFB-FDGlu. Cells were then washed and cell-associated fluorescence was quantified by flow cytometry. The cell population was gated to exclude dead cells and debris and 10,000 gated events were recorded. As SH-SY5Y cells have a tendency to clump, SH-SY5Y cells were gated further to exclude cell clumps. Results were corrected for background fluorescence using cells incubated in the absence of PFB-FDGlu or FDG. Results were normalised to controls incubated with fibril growth buffer (100 %). Cells were analysed using a BD LSRFortessa analyser (Becton Dickinson).

2.8 Analysis of membrane trafficking

2.8.1 Analysis of the cell surface levels of LAMP-1 and CD63

SH-SY5Y cells were plated at 1,000,000 cells/well in 6 well dishes (Corning Costar) and cultured for 16 h. Cells were incubated with either 1.2 μ M (monomer equivalent) fragmented β_2 m fibril samples or controls (1.2 μ M β_2 m monomer or fibril growth buffer) for 2 h or 24 h. To inhibit protein synthesis, cells were pre-incubated for 1 h with 100 μ g/ml cycloheximide prior to the addition of β_2 m. After incubation with β_2 m, cells were washed and then blocked by resuspension in PBS with 0.2% (w/v) BSA containing 10% Mouse Seroblock FcR (AbD Serotec) and incubation for 30 min on ice.

To detect cell surface expression of LAMP-1 and CD63, cells were stained with fluorescently labelled anti-LAMP-1 or anti-CD63 antibodies at the recommended concentrations (Table 2.9). To measure non-specific background antibody staining, isotype controls were included in which cells were stained with the relevant isotype matched antibodies (Table 2.9). The cell population was gated to exclude dead cells and debris, and 10,000 gated events were recorded. Due to the tendency of SH-SY5Y cells to clump, an additional gate to exclude cell clumps was included. The geometric mean fluorescence for the isotype controls was subtracted from the geometric mean fluorescence for the samples for each respective treatment. The corrected geometric mean fluorescence was then normalised to buffer treated controls (100 %). Cell-associated antibody fluorescence was quantified by flow cytometry with a BD-LSRFortessa analyser (Becton Dickinson).

| Antibody | Host, clone | Isotype | Supplier | Fluorescent label |
|--|----------------|--------------------|----------------|-------------------|
| Anti-LAMP-1 | Mouse, H4A3 | IgG ₁ κ | BD Biosciences | PE-Cy5 |
| Mouse IgG₁ κ isotype control (control for anti-LAMP-1) | Mouse, MOPC-21 | IgG ₁ κ | BD Biosciences | PE-Cy5 |
| Anti-CD63 | Mouse, MEM-259 | IgG ₁ κ | GeneTex | FITC |
| Mouse IgG₁ κ isotype control (control for anti-CD63) | Mouse, 15H6 | IgG ₁ κ | Genetex | FITC |

Table 2.9: Antibodies used for flow cytometric analysis of LAMP-1 and CD63 cell surface expression.

2.8.2 Immunofluorescence microscopy analysis of the intracellular distribution of LAMP-1 and CD63

SH-SY5Y cells were plated on to coverslips (pre-treated with 0.01 % poly-L-lysine) at 75,000 cells/well in 24 well plates (Nunc) and cultured for 16 h. Cells were then incubated with either fragmented β_2m fibrils at a final monomer equivalent concentration of 1.2 μ M, or fibril growth buffer as a control for 2 h or 24 h. Cells were then washed and fixed with 4 % formaldehyde for 10 min. Following three washes with PBS, cells were incubated with PBS containing 15 mM glycine for 10 min. Cells were then washed with PBS and were simultaneously blocked and permeabilised for 3 h in blocking buffer (PBS containing 1 % (w/v) fish skin gelatin and 0.2 % saponin). This was followed by three washes with PBS. Cells were incubated with primary antibody (Table 2.10) in blocking buffer for 1 h at 37 °C. Following three washes with PBS, cells were incubated with secondary antibody in blocking buffer for 1 h at 37 °C in the dark. After incubation with secondary antibody (Table 2.11), cells were washed three times with PBS prior to mounting on to glass slides with mounting medium (VectaShield containing DAPI, Vector Laboratories). Images were acquired on an inverted confocal microscope (Zeiss LSM700).

| Antibody | Host, clone | Supplier | Concentration used |
|--------------------|--------------------|---------------|--------------------|
| Anti-LAMP-1 | Rabbit, polyclonal | Sigma-Aldrich | 1 in 50 |
| Anti-CD63 | Mouse, MEM-259 | GeneTex | 1 in 50 |

Table 2.10: Primary antibodies used for immunofluorescence microscopy.

| Antibody | Host, clonality | Supplier | Concentration used |
|---------------------------|-----------------------------|------------------|--------------------|
| Anti-rabbit Fluor® 546 | Alexa Goat, polyclonal | Molecular Probes | 1 in 200 |
| Anti-mouse Fluor® 546 | Alexa Donkey, polyclonal | Molecular Probes | 1 in 200 |

Table 2.11: Secondary antibodies used for immunofluorescence microscopy.

2.8.3 Analysis of the effect of fibrils on fluid phase endocytosis

2.8.3.1 Analysis by flow cytometry

SH-SY5Y cells were plated at 150,000 cells/well in 12 well plates (Corning Costar) and were cultured for 16 h. Cells were incubated with either fragmented β_2m fibrils or controls (1.2 μM β_2m monomer or fibril growth buffer) for 24 h. Cells were then washed prior to incubation with Alexa Fluor® 680 10,000 molecular weight (MW) dextran (Molecular Probes) at a final concentration of 0.25 mg/ml for 24 h. Following incubation with labelled dextran, cells were washed thoroughly and analysed for cell-associated fluorescence by flow cytometry. The cell population was gated to exclude dead cells and debris and 10,000 gated events were recorded. Because SH-SY5Y cells have a tendency to clump, SH-SY5Y cells were gated further to exclude cell clumps. Results were corrected for background fluorescence using cells incubated in the absence of labelled dextran. Cell-associated dextran (%) was normalised to cells incubated with fibril growth buffer (100 %). Cells were analysed using a BD LSRFortessa analyser (Becton Dickinson).

2.8.3.2 Analysis by live cell confocal microscopy

SH-SY5Y cells were plated at 500,000 cells/well in 3 cm imaging dishes (Iwaki) and cultured for 16 h. Cells were then washed and incubated with Alexa Fluor® 568 10,000 MW dextran (Molecular Probes) at a final concentration of 0.5 mg/ml for 24 h. Following incubation with labelled dextrans, cells were washed thoroughly prior to incubation with either fragmented β_2m fibrils at a final monomer equivalent concentration of 1.2 μM or fibril growth buffer as a control for 24 h. This was followed by incubation with a second labelled dextran, Alexa Fluor® 680 10,000 MW dextran (Molecular Probes) at a final concentration of 0.5 mg/ml for 24 h. Cells were then washed thoroughly prior to analysis by live cell confocal microscopy. Images were acquired on an inverted confocal microscope (Zeiss LSM700) with a heated stage (37 °C).

Images were analysed for colocalisation of the two labelled dextrans with Image J using the JACoP plugin [329]. Colocalisation analysis was performed by following established guidelines

[330]. Background fluorescence which would result in over-estimation of correlation, was subtracted using the Costes' threshold method using the Costes' subtraction feature in JACoP [329, 331]. Correlation was quantified by calculating Manders' colocalisation coefficients (MCC) [332]. MCC allows quantification of the fraction of one fluorophore that colocalises with a second fluorophore [332]. For example, for two probes, denoted as R and G, two different MCC values, M1 and M2 are derived. M1 represents the fraction of R in compartments containing G. M2 represents the fraction of G in compartments containing R. M1 and M2 values were calculated for 20 images per condition.

2.9 Expression and purification of Hsp70

2.9.1 Expression of Hsp70

Hsp70 (UniProtKB P08107.5) was expressed in BL21 (DE3) pLysS cells transformed with the designated pET28b-Hsp70(1A) plasmid containing the gene for human, stress-inducible, cytosolic Hsp70 (kind gift from Nunilo Cremades, University of Cambridge). Hsp70 was expressed and purified using a previously described protocol [333]. 10 µl of a glycerol stock of BL21 (DE3) pLysS cells transformed with pET28b-Hsp70(1A) was streaked out onto a fresh LB-agar plate containing 50 µg/ml kanamycin. The LB-agar plate was incubated at 37 °C for 16 h. A single colony was picked and used to inoculate a starter culture of 100 ml LB containing 50 µg/ml kanamycin. The starter culture was incubated in an orbital shaker (Stuart S150) at 37 °C for 16 h whilst shaking at 200 rpm.

11 l of pre-warmed LB were inoculated with the starter culture (5 ml of starter culture per litre of LB containing 50 µg/ml kanamycin). The bacterial cultures were incubated at 37 °C whilst shaking 200 rpm. The OD₆₀₀ was monitored regularly and when an OD of 0.7 was reached, the cultures were induced by addition of IPTG at a final concentration of 1 mM. The bacterial cultures were incubated at 28 °C whilst shaking at 200 rpm for 16 h, after which the cells were harvested by centrifugation (Beckman Coulter, JLA-10.500 rotor, 6000 rpm, 4 °C, 40 min). The supernatant was discarded and the cell pellet was stored at -20 °C.

2.9.2 Cell lysis

The cell pellet was thawed on ice and resuspended in 100 ml of lysis buffer (50 mM Tris.HCl pH 7.4, 150 mM KCl, 2 mM MgCl₂ and 10 mM imidazole) containing EDTA-free complete protease inhibitor cocktail (Roche, according to the manufacturer's instructions). The cells were lysed further with a cell disrupter (Constant Systems Cell Disrupter). 5 mg of DNaseA was added to the cells post-lysis. Cell lysates were then centrifuged for 30 min at 4 °C (Beckman Coulter, JLA

16.250 rotor, 15,000 rpm). The supernatant was retained and filtered through a 0.4 µM filter (Sartorius) prior to purification by Ni-NTA affinity chromatography.

2.9.3 Ni-NTA affinity chromatography

The filtered supernatant was loaded onto an XK26 column (GE Healthcare) containing 25 ml (bed volume) Ni Sepharose High Performance (GE Healthcare) previously equilibrated with lysis buffer (50 mM Tris.HCl pH 7.4, 150 mM KCl, 2 mM MgCl₂ and 10 mM imidazole). The column was mounted on an AKTA prime chromatography system (GE Healthcare) at 4 °C. The column was washed with a mixture of 6 % elution buffer (lysis buffer containing 500 mM imidazole) and 94 % lysis buffer (final imidazole concentration of 40 mM). The protein was then eluted with a mixture of 40 % elution buffer and 60 % lysis buffer (final imidazole concentration of 200 mM). The column was finally washed with 100 % elution buffer. The fractions corresponding to the peak eluted with 200 mM imidazole were pooled and dialysed five times against 2 l of 50 mM Tris.HCl pH 7.4 containing 150 mM KCl and 2 mM MgCl₂.

2.9.4 Size exclusion chromatography

The dialysed protein was further purified by size exclusion chromatography using a Superdex 75 HiLoad 26/60 size exclusion column (GE Healthcare) previously equilibrated with 50 mM Tris.HCl pH 7.4 containing 150 mM KCl and 2 mM MgCl₂, and connected to an AKTA prime chromatography system (GE Healthcare) at 4 °C. The dialysed protein was loaded onto the column (5 ml of ~12 mg/ml per run) and the following program (Table 2.1) on the AKTA prime system was used to purify the protein.

| Breakpoint (ml) | % B | Flow rate ml/min | Fraction size | Buffer valve position | Inject valve position | Set peak collect | Auto zero | Event mark |
|-----------------|-----|------------------|---------------|-----------------------|-----------------------|------------------|-----------|------------|
| 0 | 0 | 2 ml/min | 0 | 1 | Load | No | No | No |
| 10 | 0 | 0.5 ml/min | 0 | 1 | Inject | No | Yes | Yes |
| 20 | 0 | 2 ml/min | 0 | 1 | Load | No | No | Yes |
| 30 | 0 | 2 ml/min | 2.5 | 1 | Load | No | No | Yes |
| 260 | 0 | 2 ml/min | 0 | 1 | Load | No | No | Yes |

Table 2.12: Details of the AKTA program used for the size exclusion chromatography purification of Hsp70.

2.9.5 Anion exchange chromatography

Size exclusion chromatography did not successfully separate the protein as judged by SDS-PAGE analysis, the protein was therefore further purified by anion exchange chromatography. The protein fractions from size exclusion chromatography were pooled and dialysed five times against 2 l of 20 mM Tris.HCl pH 8.0. The dialysed protein was loaded onto a ResourceQ column (GE Healthcare) previously equilibrated with loading buffer (20 mM Tris.HCl pH 8.0) and connected to an AKTA prime chromatography system (GE Healthcare) at 4 °C. The column was washed with 10 ml of loading buffer, and protein was eluted with a linear gradient of 0 – 700 mM NaCl in 20 mM Tris.HCl pH 8.0 over 60 ml. Finally, the column was washed with 1M NaCl in 20 mM Tris.HCl pH 8.0 to remove any remaining bound protein and regenerate the column. The fractions corresponding to pure Hsp70 as judged by SDS-PAGE analysis were pooled and dialysed five times against 2 l of 50 mM Tris.HCl pH 7.4 containing 150 mM KCl and 2 mM MgCl₂, prior to storage at -80 °C.

2.10 Analysis of the effect of Hsp70 on fibril-mediated cell disruption

2.10.1 Analysis of intracellular localisation of recombinant Hsp70

Purified wild-type Hsp70 was fluorescently labelled with Alexa Fluor® 405 using Alexa Fluor® 405-succinimidyl ester (Molecular Probes) at a five-fold molar excess over Hsp70. Alexa Fluor® 405-succinimidyl ester was dissolved in DMSO at a concentration of 1 mg/ml, and added drop wise to Hsp70 (12 mg/ml in 1 M sodium bicarbonate buffer) whilst stirring in the dark for 1 h. The reaction was quenched by addition of 500 µl 10 mM Tris.HCl pH 8.0. A PD10 desalting

column (GE Healthcare) was equilibrated with 25 ml of 100 mM Tris.HCl pH 8.0. The Alexa Fluor® 405-Hsp70 conjugate was loaded onto the column and eluted using 3.5 ml of 100 mM Tris.HCl pH 8.0. The eluted Alexa Fluor® 405-Hsp70 conjugate was dialysed against PBS. Approximately 30 % of the Hsp70 was labelled with one dye molecule per Hsp70 monomer as determined by electrospray ionisation mass spectrometry performed by James Ault (University of Leeds, Astbury mass spectrometry facility manager).

RAW 264.7 cells were incubated with 3 μ M Alexa Fluor® 405-Hsp70 for 4 h. Cells were then washed and stained with 50 nM LysoTracker Green prior to analysis by live cell confocal microscopy. Images were acquired on an inverted confocal microscope (Zeiss LSM510) using a heated stage (37 °C).

2.10.2 MTT assay

Cells were plated out at 5,000 cells/well (RAW 264.7) or 10,000 cells/well (SH-SY5Y) in 96 well plates (RAW 264.7 in Corning Costar plates and SH-SY5Y in NUNC plates) and cultured for 16 h. Cells were then pre-incubated with either Hsp70 or W90F Hsp70 at a final concentration of 0 μ M, 0.3 μ M or 3 μ M for 4 h (RAW 264.7) or 6 h (SH-SY5Y). Controls cultured in the absence of Hsp70 were incubated with PBS instead. This was followed by incubation with either 1.2 μ M (monomer equivalent) fragmented β_2 m fibrils or controls (1.2 μ M β_2 m or fibril growth buffer) for 24 h. Cells were assayed for MTT reduction as described in 2.5.1.

2.10.3 Phase contrast microscopy analysis of cells incubated with MTT

SH-SY5Y cells were plated at 1,000,000 cells/well in 6 well plates (Corning Costar) and cultured for 16 h. Cells were pre-incubated with either Hsp70 at a final concentration of 3 μ M or PBS as a control. This was followed by incubation with either 1.2 μ M (monomer equivalent) fragmented β_2 m fibrils or fibril growth buffer as a control for 24 h. Cells were then incubated with MTT and imaged by phase contrast microscopy as described in 2.5.2.

2.10.4 Analysis of cell-surface expression of LAMP-1

SH-SY5Y cells were plated at 1,000,000 cells/well in 6 well plates (Corning Costar) and cultured for 16 h. Cells were pre-incubated with either Hsp70 at a final concentration of 3 μ M or PBS as control for 6 h prior to incubation with either fragmented β_2 m fibrils at a final monomer equivalent concentration of 1.2 μ M or controls (1.2 μ M β_2 m monomer or fibril growth buffer) for 24 h. Cell-surface LAMP-1 levels were quantified as described in 2.8.1.

2.10.5 Analysis of lysosomal degradation of fluorescently labelled ovalbumin

SH-SY5Y cells were plated at 250,000 cells/well in 12 well plates (Corning Costar) and cultured for 16 h. Cells were pre-incubated with either Hsp70 at a final concentration of 3 μ M or PBS as control for 6 h prior to incubation with either 1.2 μ M (monomer equivalent) fragmented β_2 m fibrils or controls (1.2 μ M β_2 m monomer or fibril growth buffer) for 24 h. Ovalbumin degradation was assayed as described in 2.7.1.2.

3 β_2m as a model to study amyloid disease

3.1 Introduction

3.1.1 β_2m structure

β_2m is a 99 residue protein which exhibits a typical immunoglobulin fold consisting of seven β strands arranged into a β -sandwich stabilised by a disulphide bond between residues 25 and 80 (Figure 3.1) [334]. The β strands are arranged in an all antiparallel organisation with the edge strand, 'D' exhibiting a β -bulge as observed in crystal structures of β_2m within the MHC I complex or as a free monomer in solution (Figure 3.2)[335, 336]. A conformation in which the edge 'D' strand does not exhibit a β -bulge but instead displays a straight D-strand has also been reported several times, and has been implicated in facilitating aggregation (Figure 3.2 and reviewed in [337]). Four out of five of the proline residues found within the β_2m sequence are in the *trans* conformation, whereas proline 32 is in the *cis* conformation in the native state. The isomerisation of proline 32 is thought to be important in controlling β_2m aggregation into amyloid fibrils [338].

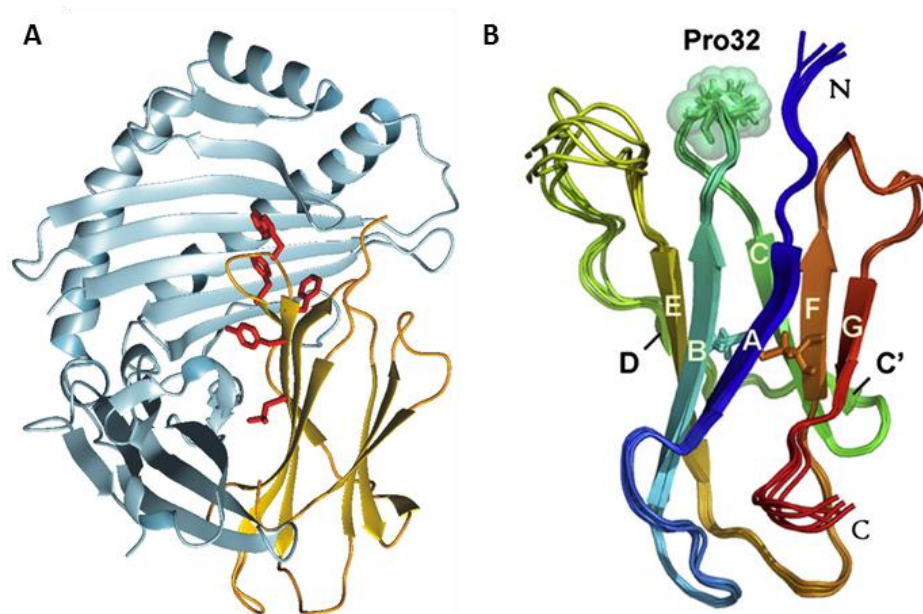


Figure 3.1: Structure of MHC I complex and β_2m monomer. (A) Ribbon representation of human MHC I (PDB code 3MYJ)[339] showing the heavy chain (silver) and the light chain, β_2m (gold). Hydrophobic residues present in β -strand E (Phe56, Trp60, Tyr62, Tyr63 and Leu65) that contact the heavy chain are highlighted. (B) Ribbon representation of the solution structure of native β_2m monomer (PDB code 2XJS)[340] showing β -strands A (residues 6-11), B (residues 21-28), C (residues 36-41), C' (residues 44-45), D (residues 50-51), E (residues 64-70), F (residues 79-83) and G (residues 91-94). Figure adapted from [337, 341].

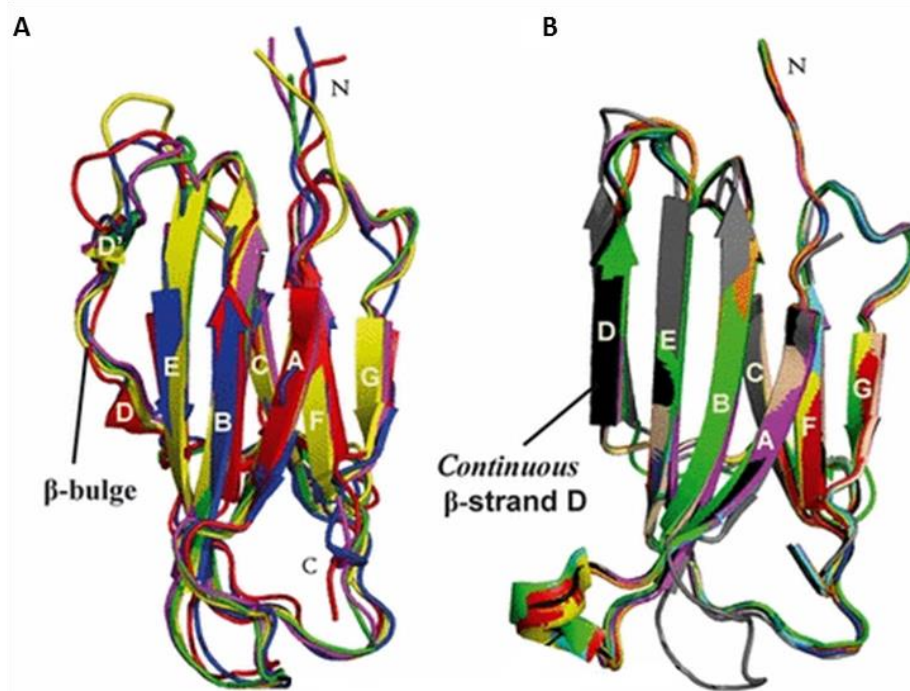


Figure 3.2: Structures of wild-type β_2m and β_2m variants displaying a β -bulge or continuous β -strand D. (A) Structures displaying a β -bulge. Wild-type β_2m is displayed in red (PDB code 1JNJ)[336], H31Y β_2m in green (PDB code 1PY4)[342], W60G β_2m in blue (PDB code 2VB5)[343], H13F β_2m in yellow (PDB code 3CIQ)[344] and β_2m bound to the MHC I complex in magenta (PDB code 3MYJ)[339]. (B) Structures displaying a continuous β -strand D. Wild-type β_2m is displayed in red (PDB code 1LDS)[334], L39W/W60F/W95F β_2m in green (PDB code 2D4D)[345], wild-type β_2m in blue (PDB code 2YXF)[345], wild-type β_2m in yellow (PDB code 2YXFF)[346], W60G β_2m in magenta (PDB code 2Z9T)[343], W60C β_2m in cyan (PDB code 3DHJ)[347], D59P β_2m in orange (PDB code 3DHM)[347], W60G β_2m in wheat (PDB code 3EKC)[347], K58P/W60G β_2m in black (PDB code 3IB4)[348] and P32A β_2m in grey (PDB code 2F8O)[349]. Figure adapted from [337].

3.1.2 β_2m amyloid formation and characterisation

It is important to note that wild-type human β_2m , does not form amyloid fibrils at physiological temperature and pH *in vitro*, without the aid of external factors such as Cu^{2+} , SDS or trifluoroethanol [350-352]. *In vitro* studies of β_2m amyloid fibril formation have been made possible by the finding that agitation at low pH results in rapid β_2m fibril formation [189, 325, 353]. Perturbation of the β_2m sequence controls the amyloid fibril-forming propensity of the unfolded state at low pH, thus implicating several regions in amyloid formation [54]. Peptide fragments that correspond to residues 21-40 (spanning β strands B and C) have been shown to aggregate into amyloid fibrils in isolation [354]. Another study involving the systematic investigation of peptide fragments spanning the entire sequence of β_2m , implicated residues

59-71 (encompassing β strand E) [355]. This region is highly enriched in aromatic residues and is capable of forming amyloid fibrils in isolation. It has also been shown to play an important role in nucleation and elongation of fibrils as well as the rate of fibril formation [355-357]. Residues in the loop connecting β strands D and E, as well as residues 83-89 (corresponding to the C terminal region) have also been reported to promote aggregation [343, 358]. In contrast, β strand A has been reported to disfavour aggregation and stabilise the native state [359].

Accumulating evidence points to increased conformational dynamics as a common feature in the assembly of β_2m monomers into amyloid fibrils at neutral pH, analogous to observations from other amyloidogenic proteins that also assemble into amyloid fibrils via conformational changes in their folded monomeric states (reviewed in [337]). Wild-type β_2m and its variants such as $\Delta N6$ β_2m (a truncated variant where six N terminal residues are cleaved), $\Delta K58$ β_2m and $\Delta K58$ β_2m (variants where Lys58 is cleaved with or without removal of Lys58, respectively), have all been demonstrated to exhibit increased local and global unfolding events, decreased solubility and enhanced amyloidogenicity at pH values close to physiological pH (reviewed in [337]).

$\Delta N6$ β_2m is of particular interest because it is found in *ex vivo* fibril deposits, of which it forms a significant component (~ 26 %) [360]. $\Delta N6$ β_2m is highly amyloidogenic and exhibits a greater affinity for collagen than wild-type β_2m [360, 361]. Collagen is highly enriched in osteoarticular tissues, the main site of damage in DRA, thus implicating $\Delta N6$ β_2m in the pathogenesis of DRA [360, 361]. Proline 32 in $\Delta N6$ β_2m is in the *trans* conformation compared to the *cis* conformation observed in wild-type β_2m ; this is particularly relevant as the non-native *trans* conformation of proline 32 is thought to be the link between the native and aggregation-prone states [338, 362]. Although $\Delta N6$ β_2m forms a significant component of *ex vivo* β_2m amyloid deposits, it is not found in the serum of DRA patients [363]. Cleavage has thus been suggested to occur after incorporation of full-length β_2m into amyloid fibrils [364]. However, recent studies have demonstrated that $\Delta N6$ β_2m is not only able to nucleate fibrillogenesis efficiently *in vitro* at physiological pH, but is also able to convert wild-type β_2m into an aggregation-competent state by bimolecular collision [340]. Catalytic amounts of $\Delta N6$ β_2m (1 %) are sufficient to convert wild-type β_2m into amyloid fibrils, therefore implicating $\Delta N6$ β_2m as an important initiating factor for amyloid formation in DRA [340].

β_2m fibril formation *in vitro* has been shown to proceed via both nucleation-dependent and nucleation-independent polymerisation pathways under different fibrillation conditions [189, 365]. At low pH and low ionic strength (pH 2.0, 50 mM NaCl), β_2m monomers assemble via a

nucleation-dependent pathway to generate amyloid fibrils of a long straight morphology with a characteristic periodic twist classically associated with amyloid [189](Figure 3.3). By contrast, at higher pH and higher ionic strength (pH 3.5, 200 mM NaCl), β_2m monomers rapidly assemble via a non-nucleated pathway to generate shorter, 'worm-like' fibrils [189]. Long straight β_2m amyloid fibrils exhibit a characteristic cross- β diffraction pattern, Congo Red birefringence and ThT binding [341, 366](Figure 3.3). β_2m fibrils are also bound by the anti-fibril antibody, WO1, which recognises a fibrillar epitope found on amyloid fibrils independent of the precursor protein sequence [327, 367](Figure 3.3). In contrast, β_2m fibril samples are not recognised by the anti-oligomer antibody, A11 [367](Figure 3.3). A11 recognises soluble oligomers, and like, WO1, is also generic in that it binds independently of precursor protein sequence [18].

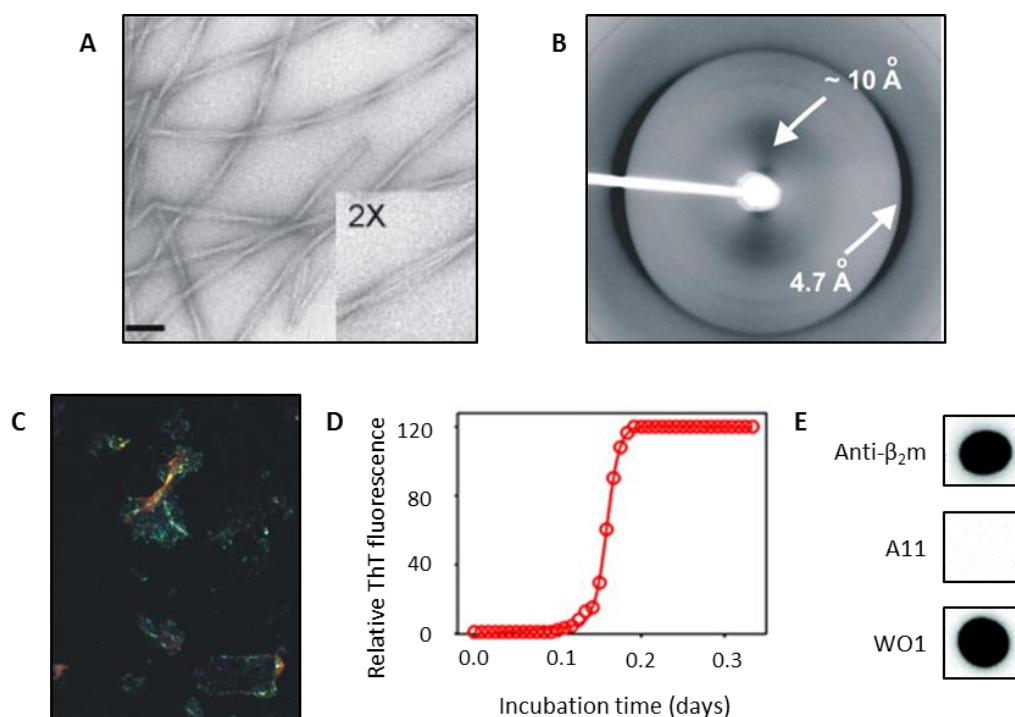


Figure 3.3: Morphological, structural and tinctorial characteristics of β_2m amyloid fibrils assembled at low pH and low ionic strength. (A) β_2m amyloid fibrils have a long straight morphology when visualised by TEM (scale bar 100 nm). Image from [366]. (B) β_2m amyloid fibrils display a characteristic cross- β X-ray diffraction pattern. Image from [341]. (C) The characteristic red-green birefringence of Congo Red under polarised light is observed when bound to β_2m amyloid fibrils. Image from [341]. (D) β_2m amyloid fibril growth kinetics visualised by ThT fluorescence. Image from [366]. (E) Immunoblotting of β_2m amyloid fibrils with anti- β_2m , A11 and WO1 antibodies. Image from [367]. Adapted with permission from [367]. Copyright (2006) American Chemical Society.

3.1.3 β_2m as a model to study amyloid disease

β_2m amyloid fibrils assembled at low pH and low ionic strength have been shown to share structural characteristics with fibrils assembled *in vitro* at physiological pH as well as *ex vivo* β_2m amyloid fibrils [366]. In addition, β_2m amyloid fibrils exhibit amyloid characteristics which are shared by all amyloid fibrils irrespective of the starting protein (Figure 3.3 and section 1.3). The β_2m amyloid fibril formation pathways, the various intermediate species and amyloid fibrils have been well studied and characterised [125, 189, 340, 341, 368]. Indeed, β_2m fibrils with a long straight morphology are readily formed (within 72 h) at low pH and low ionic strength with well characterised yield, morphology and fibril length [190, 366]. Mature β_2m fibril preparations do not contain detectable levels of soluble oligomer species [190]. The starting conformation of each fibril preparation prior to addition to cells is thus known. Furthermore, purification of recombinant β_2m is straightforward and results in a high yield of pure protein (approximately 40 mg per litre of bacterial culture). β_2m thus serves as a useful model to study amyloid disease.

3.2 Results

3.2.1 Expression and purification of β_2m

In order to generate β_2m to make amyloid fibrils for subsequent experiments, recombinant β_2m was expressed in BL21 (DE3) pLysS cells carrying the pINK plasmid using an established protocol [325] (Section 2.1 and Figure 3.4). Cells were lysed after induction of protein expression with isopropyl β -D-1-thiogalactopyranoside (IPTG) and the inclusion bodies containing β_2m were isolated and solubilised as described (Section 2.1.2).

β_2m was purified from the inclusion bodies by anion exchange chromatography (Figure 3.5). β_2m eluted in fractions corresponding to peak 1 as confirmed by SDS-PAGE analysis (Figure 3.6). Fractions corresponding to peak 1 were pooled, dialysed against 18 M Ω purite water and lyophilised. The lyophilised protein was re-solubilised in 25 mM sodium phosphate buffer pH 8.0 prior to further purification by size exclusion chromatography (Figure 3.7). Size exclusion chromatography was performed to separate monomeric β_2m from dimeric β_2m , higher order β_2m aggregates and other contaminants. Peak 2 corresponds to pure β_2m as confirmed by SDS-PAGE analysis (Figure 3.8). Fractions corresponding to peak 2 were pooled, dialysed against 18 M Ω purite water and lyophilised for storage at -20°C.

Analytical gel filtration was used to check the purity of β_2m upon reconstitution from lyophilised powder stored at -20 °C (Figure 3.9). A single symmetrical peak was observed and is consistent with a pure preparation of β_2m . Electrospray ionisation mass spectrometry (ESI-MS)

was used to determine the molecular weight of purified protein (Figure 3.10). A molecular mass of $11,859.48 \pm 0.66$ Da is consistent with the purified protein being monomeric β_2m (expected mass = 11,860 Da). The additional low intensity peaks correspond to mono- and bi-phosphate adducts.

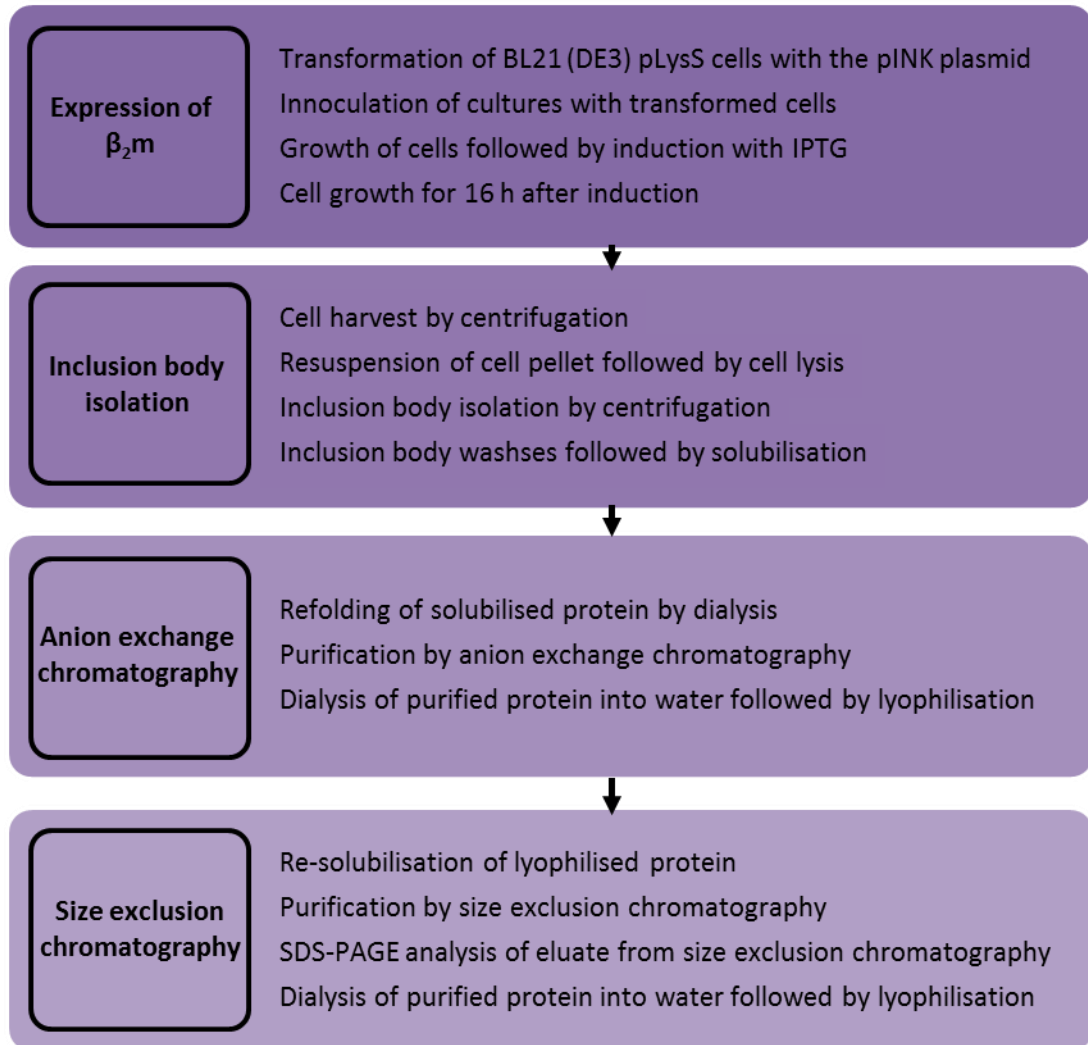


Figure 3.4: Schematic of expression and purification strategy.

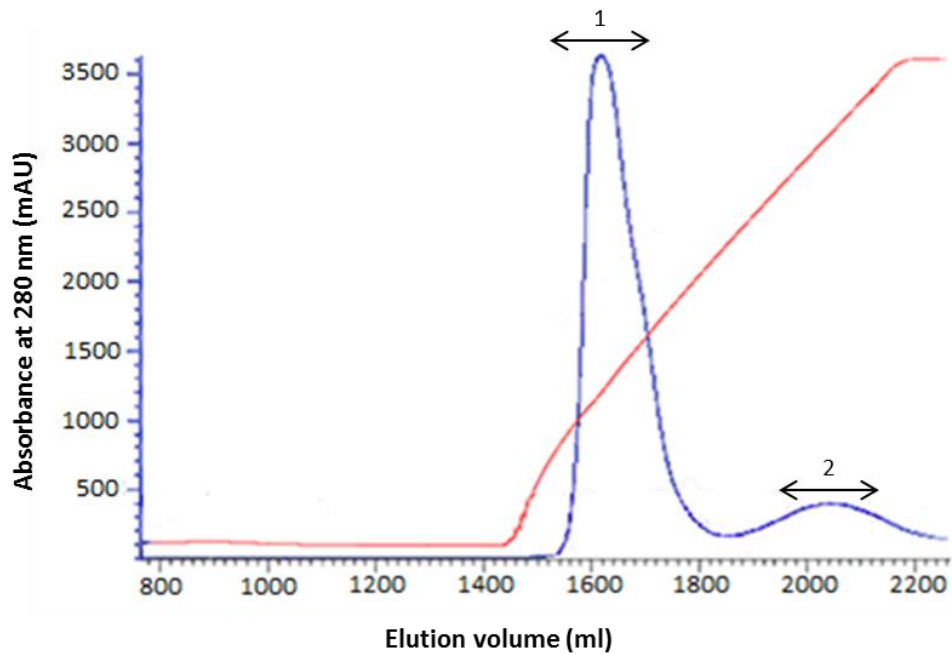


Figure 3.5: Anion exchange chromatography purification of solubilised inclusion bodies. After isolation from IPTG induced BL21 DE3 pLysS cells carrying the pINK plasmid [325], inclusion bodies were solubilised in 25 mM Tris.HCl pH 8.0 containing 8 M urea. β_2m was refolded by dialysis into 25 mM Tris.HCl pH 8.0 and purified from the inclusion bodies by anion exchange chromatography using a Q-Sepharose column. The protein was eluted with a linear gradient of 0 – 400 mM NaCl in 25 mM Tris.HCl pH 8.0 over 650 ml. β_2m elutes in peak 1. The corresponding fractions were pooled and dialysed against 18 M Ω purite water. Samples spanning peaks 1 and 2 were collected for analysis by SDS-PAGE.

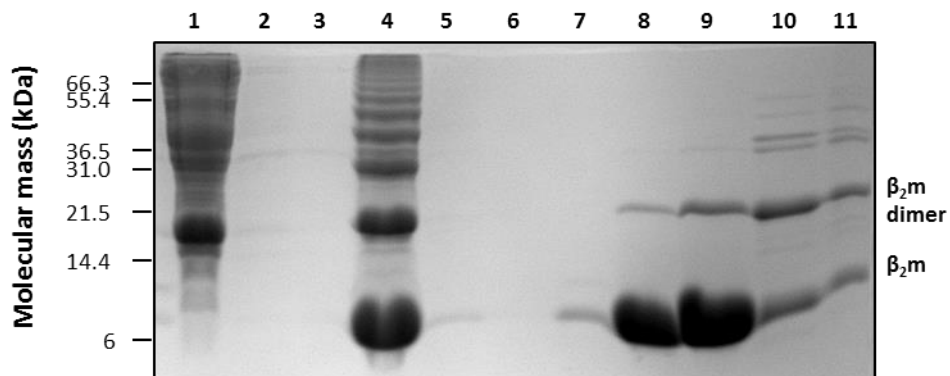


Figure 3.6: SDS-PAGE analysis of β_2m expression and purification by anion exchange chromatography. Samples were resolved by 15% Tris-Tricine SDS-PAGE and proteins were visualised with Coomassie Blue. Lane 1 – Soluble fraction of cell lysate post cell-lysis; 2 and 3 – Post-wash supernatant of inclusion body washes; 4 – Protein loaded onto anion exchange column after refolding by dialysis; 5 and 6 - Flow-through of anion exchange column; 7 to 11 – samples spanning first peak of anion exchange chromatographic purification (1 from Figure 3.5)

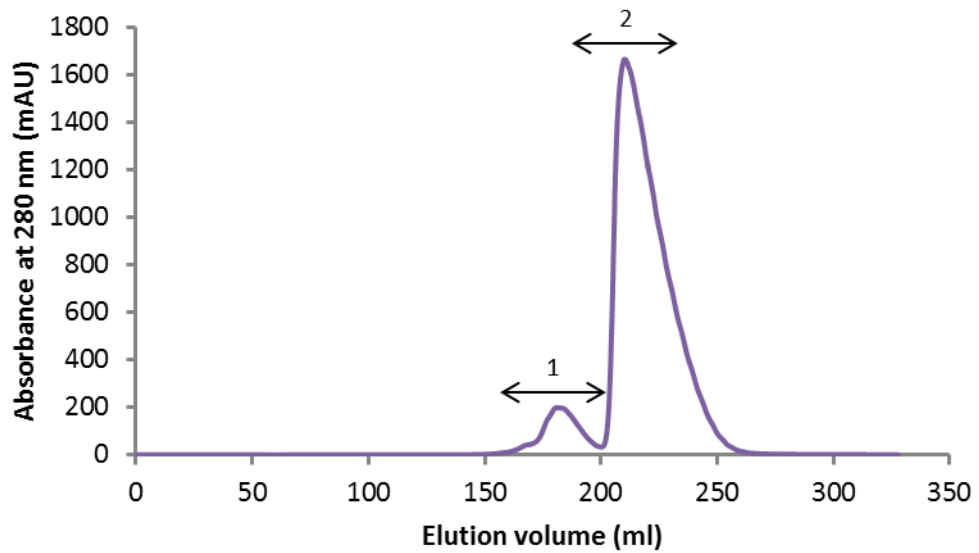


Figure 3.7: Further purification of β_2m by size exclusion chromatography. The lyophilised protein was dissolved in 10mM sodium phosphate buffer pH 7.2 to a concentration of approximately 1 mg/ml. 5ml of protein was loaded onto a Superdex 75 HiLoad 26/60 column per run. Samples spanning both peaks 1 and 2 were collected for SDS-PAGE analysis.

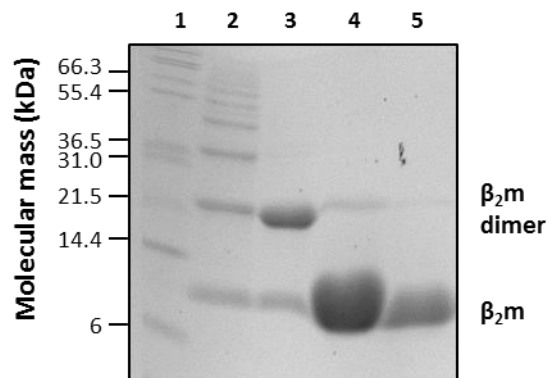


Figure 3.8: SDS-PAGE analysis of purification of β_2m by size exclusion chromatography. Samples were resolved by 15% Tris-Tricine SDS-PAGE and proteins were visualised with Coomassie Blue. Lane 1- marker; 2 - sample from the second anion exchange chromatography peak (2 in Figure 3.5); 3 - sample from the first size exclusion chromatography (1 in Figure 3.7); 4 and 5 – samples spanning the second size exclusion chromatography peak (2 in Figure 3.7).

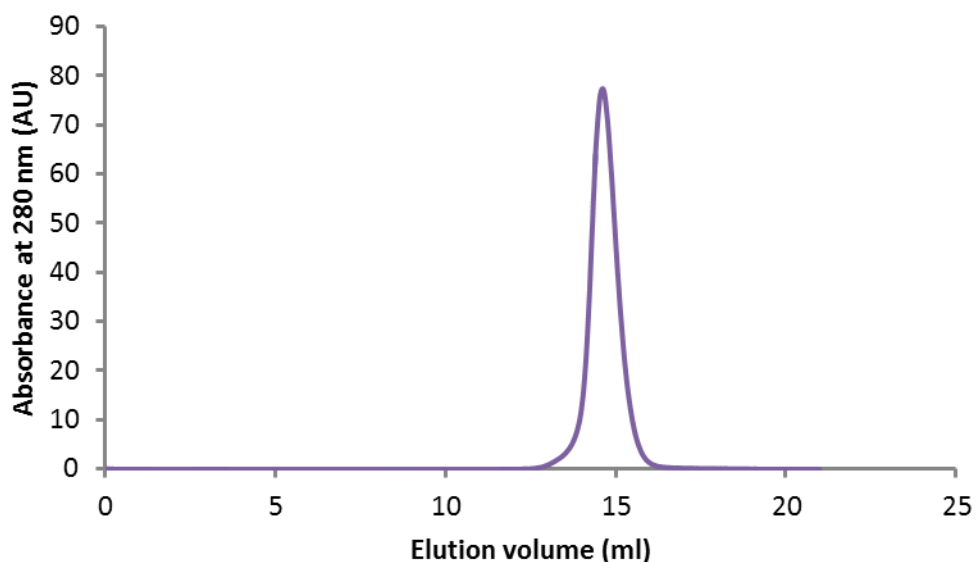


Figure 3.9: Analytical size exclusion chromatography to determine the purity of β_2m . Lyophilised β_2m stored at -20°C was dissolved in 10 mM sodium phosphate buffer pH 7.2 and then loaded onto a Superdex 75 HiLoad 16/10 column.

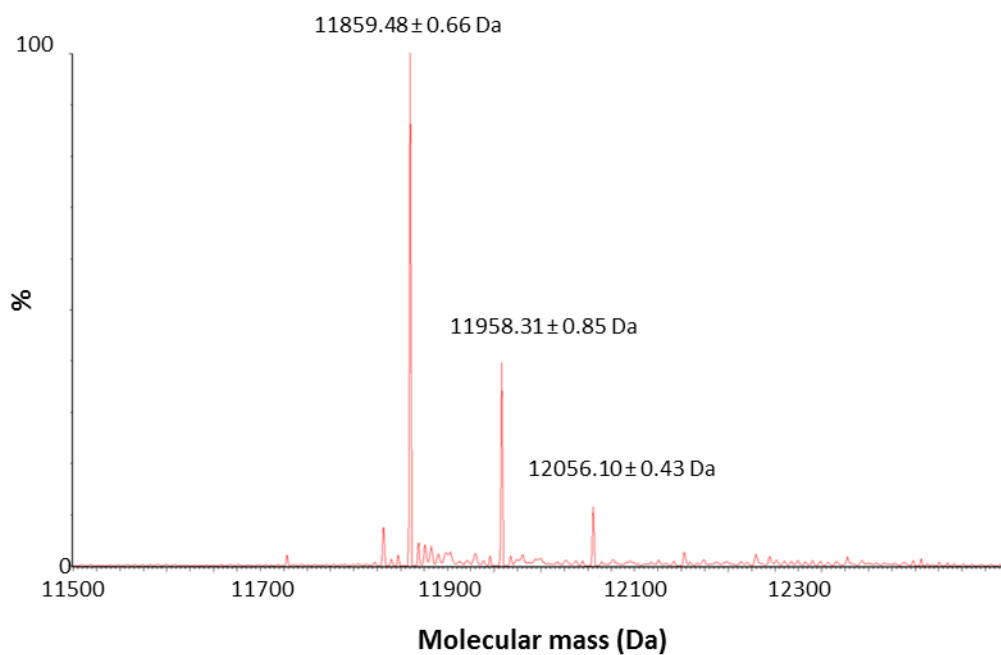


Figure 3.10: Electrospray ionisation mass spectrometry (ESI-MS) analysis of the purified protein. Mass profiles generated by Maximum Entropy processing of the ESI-MS m/z spectra. The peak corresponding to 11859.48 ± 0.66 Da represents full-length wild-type β_2m . The peaks to the right correspond to β_2m bound to sodium and potassium ions. ESI-MS analysis was performed by Dr James Ault (University of Leeds, Astbury mass spectrometry facility manager).

3.2.2 Generation and characterisation of amyloid fibrils

β_2m amyloid fibrils with the previously described long, straight morphology were generated from purified monomeric β_2m according to an established protocol (Section 2.4.1)[190]. Pure lyophilised β_2m was resuspended in fibril growth buffer (10 mM sodium phosphate pH 2.0, containing 50 mM NaCl) and passed through a 0.2 μm filter (Sartorius). Protein concentration was adjusted to 120 μM prior to the addition of 0.1 % (v/v) seeds (fragmented β_2m fibrils). Fibril formation was allowed to proceed quiescently at room temperature for 72 h.

Fragmented fibrils can be used to model fibrils that are formed early on in the polymerisation process or those that fragment post-assembly. Previous work in our laboratory has shown that fragmentation of fibrils results in fibrils of shorter length but otherwise unchanged molecular architecture. These fragmented fibrils inhibit the cellular reduction of a commonly used cell viability substrate, 3-(4,5-dimethylthiazol-2-yl)-2,5-diphenyltetrazolium bromide (MTT), to a greater extent than their unfragmented counterparts [190]. Fragmented fibrils were generated by fragmentation of mature long straight β_2m amyloid fibrils for 48 h using a custom built precision stirrer (Section 2.4.2)[190].

To confirm fibrils generated in this project have the same properties as described previously, fragmented and unfragmented fibrils were characterised based on their biophysical, tinctorial and immunological properties. Thioflavin T (ThT) is an amyloid dye widely used for over 50 years to monitor amyloid formation [369]. It is a fluorescent dye that fluoresces more intensely when bound to amyloid fibrils *in vitro* [86]. Samples of fragmented and unfragmented fibrils were characterised based on their binding to ThT, relative to monomer control (Section 2.4.3). An increase in ThT fluorescence over monomer control was observed for both fragmented (60-fold) fibrils and unfragmented (110-fold) fibrils (Figure 3.11). The enhanced increase in ThT fluorescence for unfragmented fibrils over fragmented fibrils is consistently observed, however the mechanism for this is currently unknown. Despite many studies, the exact binding mechanism of ThT to amyloid fibrils has not yet been determined [369]. The enhanced ThT fluorescence of unfragmented fibrils compared to unfragmented fibrils could be due to the longer length providing more ThT binding sites in close proximity to each other compared to fragmented fibrils.

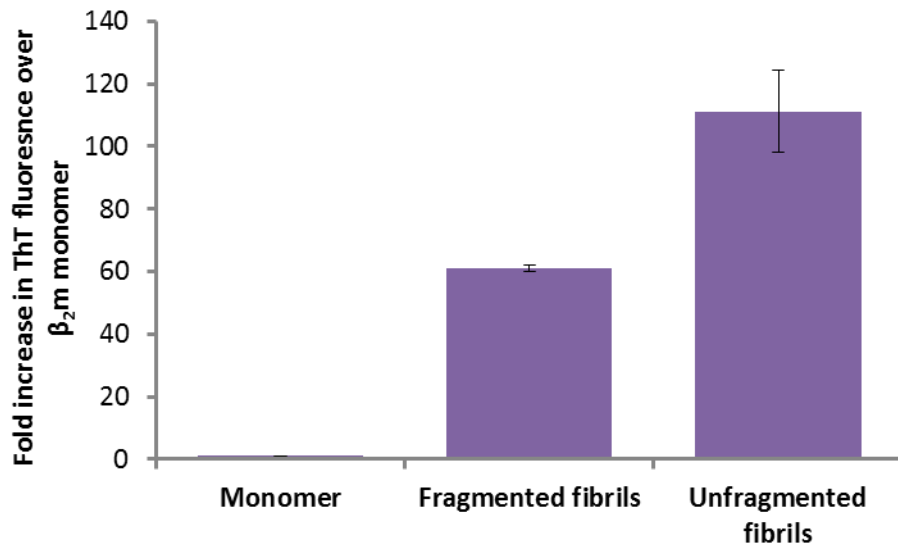


Figure 3.11: Characterisation of amyloid fibrils by ThT fluorescence. Samples of 1.2 μM β_2m monomer, 1.2 μM (monomer equivalent) fragmented or unfragmented fibrils were incubated with 10 μM ThT and the fluorescence measured. 60 readings were taken over 1 minute and the average fold increase over β_2m monomer calculated. Error bars represent one standard deviation (S.D).

The development of amyloid conformation-specific antibodies has created an additional experimental tool to characterise amyloid material (reviewed in [127]). Monomeric β_2m , as well as fragmented and unfragmented fibril samples were dotted onto nitrocellulose membrane and immunoblotted with A11, WO1 and anti- β_2m antibodies (Section 2.4.4). $A\beta_{1-40}$ oligomers were used as a positive control for the A11 antibody and Hsp70 as a negative control for the anti- β_2m antibody. Both fragmented and unfragmented fibrils were bound by WO1, but not by A11 (Figure 3.12). Consistent with previously published work, this confirms the presence of an amyloid fibril epitope in both fragmented and unfragmented fibril samples as well as the absence of detectable oligomers recognised by A11 [190].

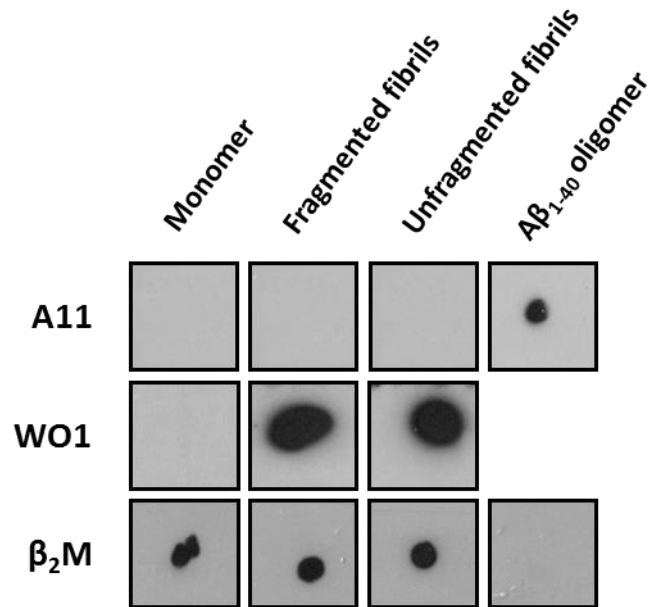


Figure 3.12: Analysis of β_2m fibril samples with amyloid-specific antibodies. Samples of β_2m monomer, unfragmented, or fragmented β_2m fibrils were analysed by immunoblotting with the anti-oligomer antibody A11 (top), the anti-fibril antibody WO1 (middle) and the anti- β_2m antibody (bottom). A β_{1-40} oligomers (kind gift from Charles Glabe, University of California, Irvine) were used as a positive control for the A11 antibody. Antibody binding was detected with secondary anti-rabbit IgG-HRP (A11, β_2m) or anti-mouse IgM-HRP (WO1) respectively and visualised by chemiluminescence. Hsp70 was used as a negative control for the anti- β_2m antibody. Each dot contains 2.8 μg (β_2m and Hsp70) or 1.1 μg (A β_{1-40}) of protein/peptide.

Fragmented and unfragmented fibril samples were analysed by negative stain transmission electron microscopy (TEM) to confirm the presence of fibrils and to visualise fibril morphology. Carbon coated copper grids were incubated with fragmented and unfragmented fibril samples prior to imaging (Section 2.4.5). Images for both fibril samples show rope-like, twisted fibrils with fragmented fibrils being qualitatively of a reduced length compared to their unfragmented counterparts (Figure 3.13).

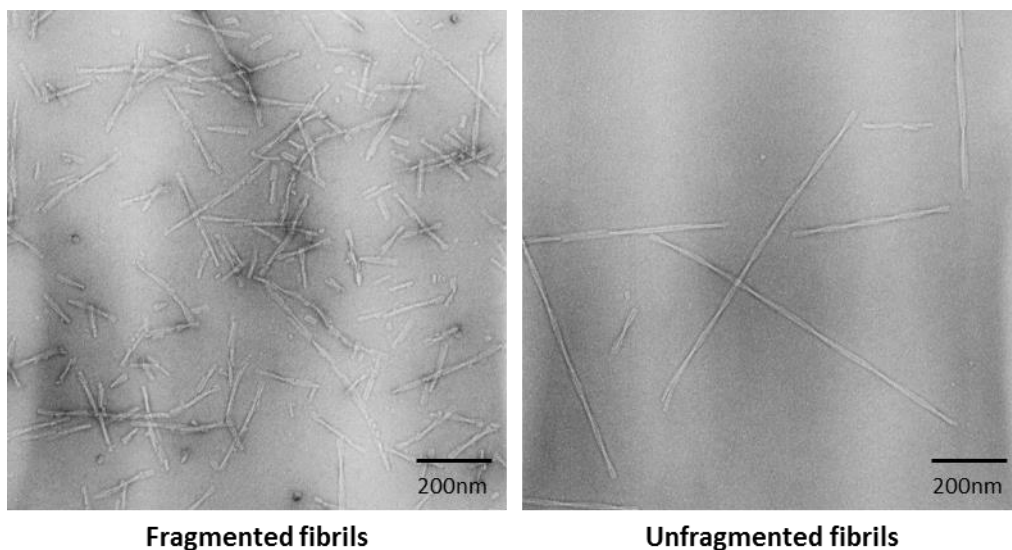


Figure 3.13: TEM images of fibrils generated from β_2m . Fibril samples were diluted to 6 μM (monomer equivalent) before incubation on carbon coated copper grids for 30 s. Grids were dried after fibril incubation and negatively stained with 4 % (w/v) uranyl acetate. Imaging was performed with a Phillips CM10 electron microscope at a magnification of 52,000. The scale bars represent 200 nm.

The effect of fragmentation on the structure of β_2m amyloid fibrils has been previously characterised extensively [190]. However for the purpose of this chapter, the effect of fragmentation on fibril length was determined by atomic force microscopy (AFM) (Section 2.4.6). Fibrils were imaged by tapping mode AFM and fibril length was quantified using automated scripts generated by Wei-Feng Xue (University of Kent)[328]. The fibril length distribution for unfragmented fibrils is broad and shallow with an average length of $1.30 \pm 0.05 \mu m$, whilst that for fragmented fibrils is narrower with an average length of $0.30 \pm 0.01 \mu m$ (Figure 3.14).

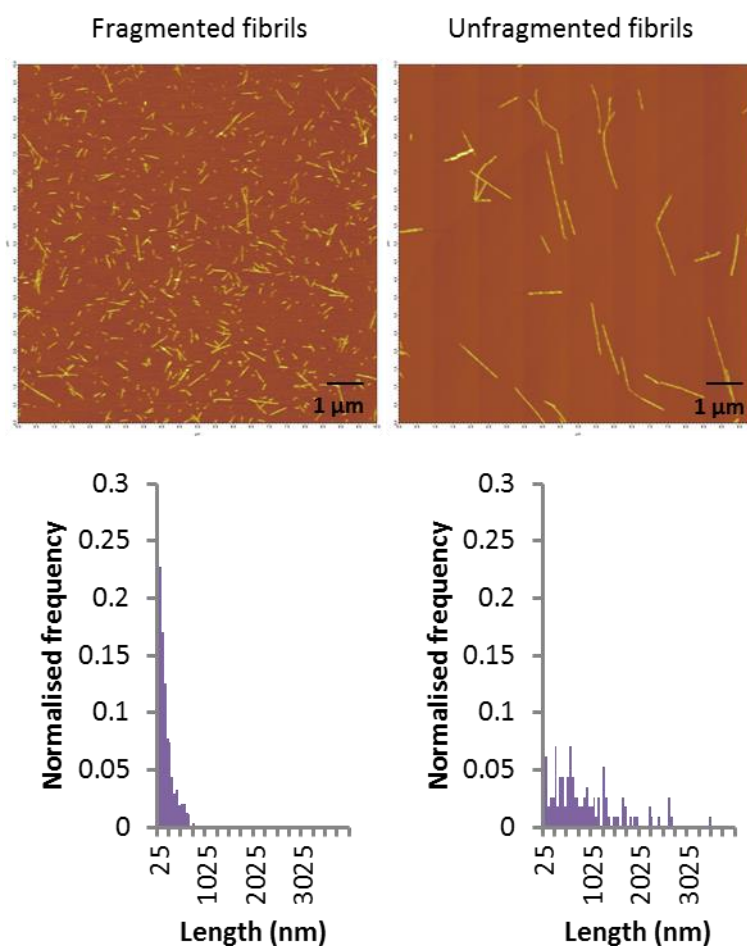


Figure 3.14: Analysis of fibril length by AFM. AFM images (top) of fragmented (left) and unfragmented (right) β_2m fibrils. Scale bars represent 1 μm . Histograms (bottom) showing the fibril length distribution calculated from >200 particles. Images acquired and calculations performed by Kevin Tipping, University of Leeds.

3.2.3 Analysis of the effect of fibrils on the cellular reduction of MTT

Having generated fibrils of defined length, and biophysical and immunological characteristics, the next step was to analyse the effect of fibrils on cellular viability. This involved the use of two cell lines, the human neuroblastoma cell line, SH-SY5Y and the mouse macrophage cell line, RAW 264.7. SH-SY5Y cells are widely used to study amyloid-cell interactions [242, 370, 371]. Macrophages have been implicated in disease progression in DRA and therefore RAW 264.7 cells serve as a good model to study macrophage interactions with amyloid [247, 372].

Cell viability was analysed using the commonly used viability assay, the MTT assay [373-376](Figure 3.15). The MTT assay measures the ability of viable cells to internalise the yellow tetrazolium salt (MTT) and reduce it to a dark blue product (formazan) [373]. MTT is thought to be reduced by mitochondrial dehydrogenases [377]. Spectroscopic measurement of the dark

blue product of reduction allows quantification of cell viability. The yellow MTT salt is internalised by endocytosis and the reduced formazan accumulates in intracellular-granule like structures prior to exocytosis to the cell surface where it accumulates as needle-like crystals [378].

Cells were incubated with β_2m monomer, fragmented or unfragmented β_2m fibrils at a final monomer equivalent concentration of 1.2 μM for 24 h (Section 2.5.1). β_2m monomer serves as control as it is the same protein however it is natively folded and lacks the cross- β architecture of amyloid fibrils. Additional controls were included to allow data normalisation; these were 0.1 % (w/v) sodium azide (0 % MTT reduction) and fibril growth buffer alone (100 % MTT reduction). As reported previously for both RAW 264.7 and SH-SY5Y cells, fragmented fibrils inhibited MTT reduction to a greater extent than unfragmented fibrils (Figure 3.16)[190].

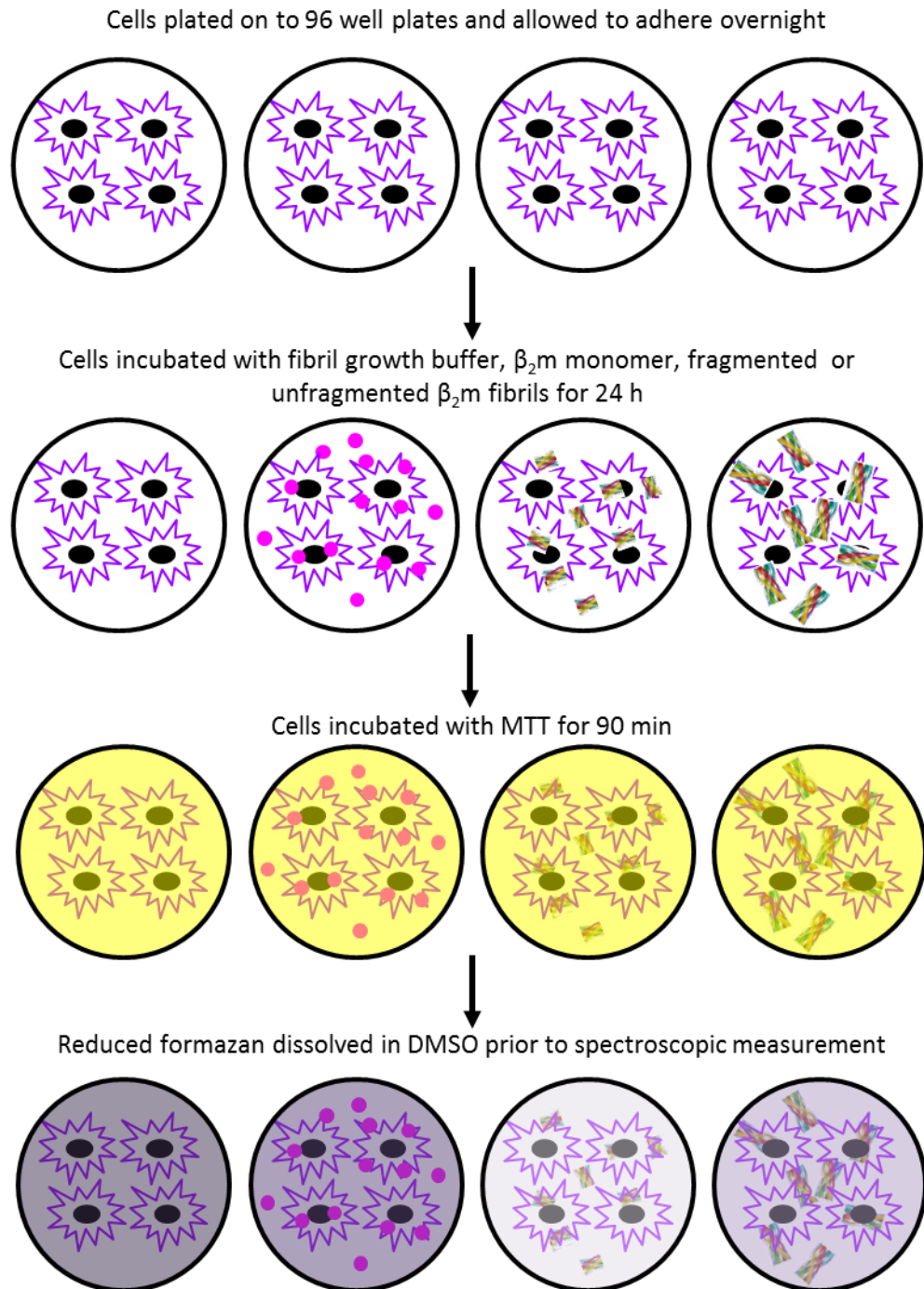


Figure 3.15: Schematic showing an overview of the MTT assay. Cells were plated on to 96 well plates prior to incubation with fibril growth buffer (left), β_2m monomer (centre left), fragmented β_2m fibrils (centre right) or unfragmented β_2m fibrils (right). Cells were then incubated with MTT which is a yellow salt. Reduced formazan is a dark blue product. Spectroscopic measurement of reduced formazan allows quantification of MTT reduction.

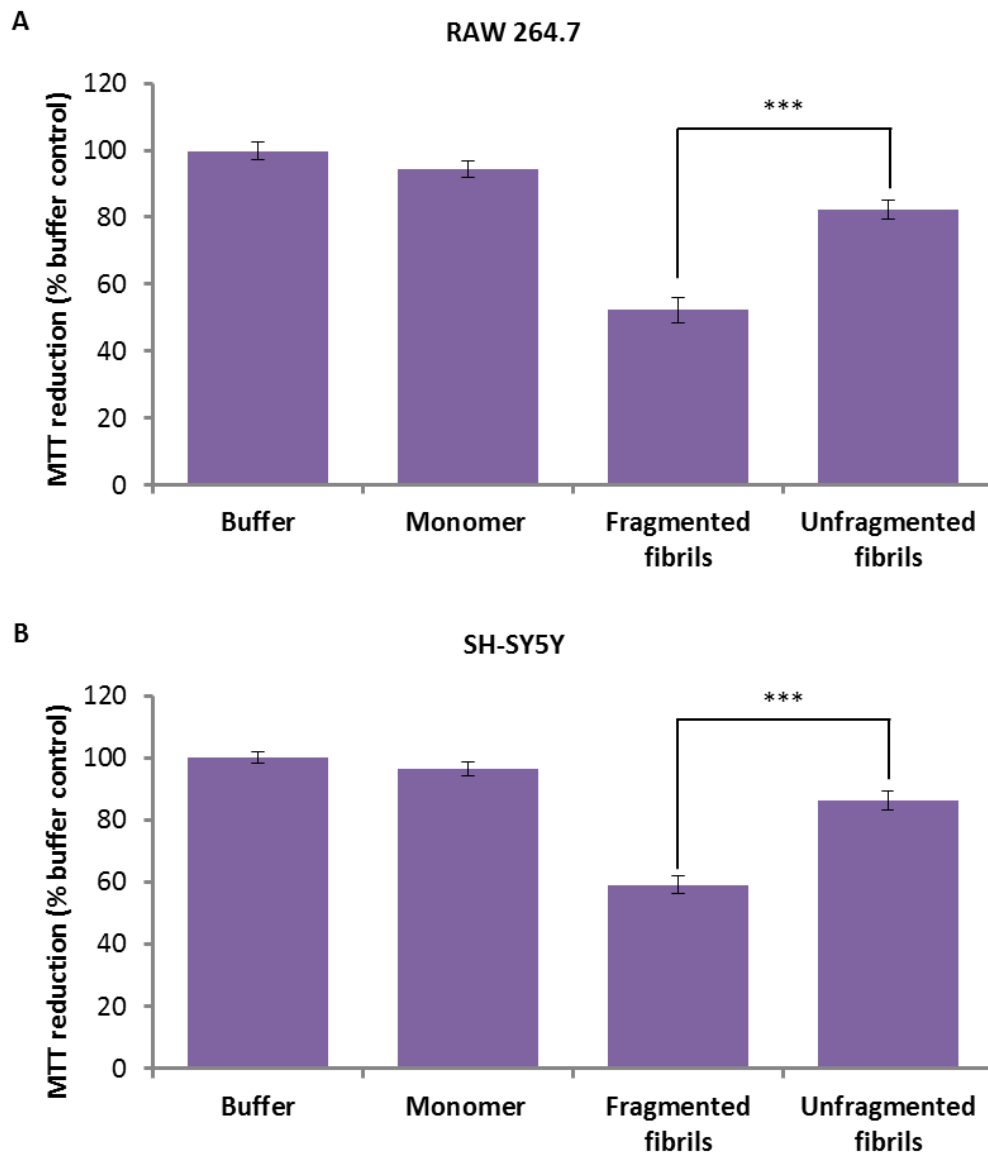


Figure 3.16: Analysis of the effect of fibrils on MTT reduction. MTT assays were performed using β_2m monomer, fragmented and unfragmented β_2m fibrils at a final monomer equivalent concentration of 1.2 μM . RAW 264.7 cells (A) and SH-SY5Y cells (B) were incubated with fibrils or controls for 24 h before being tested for MTT reduction. MTT reduction (%) was calculated by normalising the signal from cells incubated with fibril growth buffer as 100% and cells treated with 0.1% (w/v) NaN_3 as 0%. The error bars represent one standard error of mean (S.E.M.) over five independent experiments each containing five replicates. *** signifies a p value <0.001.

The use of the MTT assay in assessing the cytotoxicity of amyloid material must be approached with care. Previous work with A β peptides and amylin has shown that amyloid preparations inhibit MTT reduction, however, this inhibition is associated with an increase in formazan exocytosis [379-383]. Increased formazan exocytosis is visualised by an increased amount of needle-like formazan crystals at the cell surface [380] and has been proposed to impair cell membrane integrity [382, 383]. This inhibition in MTT reduction is uncoupled from any effect on cell death when assayed by alternative viability assays [380-382]. Indeed, analysis of RAW 264.7 and SH-SY5Y cells incubated with fibrils or controls demonstrated that formazan accumulates primarily in intracellular granule-like structures in fibril growth buffer or β_2m monomer controls (Figure 3.17 and Section 2.5.2). Both fragmented and unfragmented fibrils, however, markedly increased the deposition of formazan as extracellular needle-like crystals (Figure 3.17).

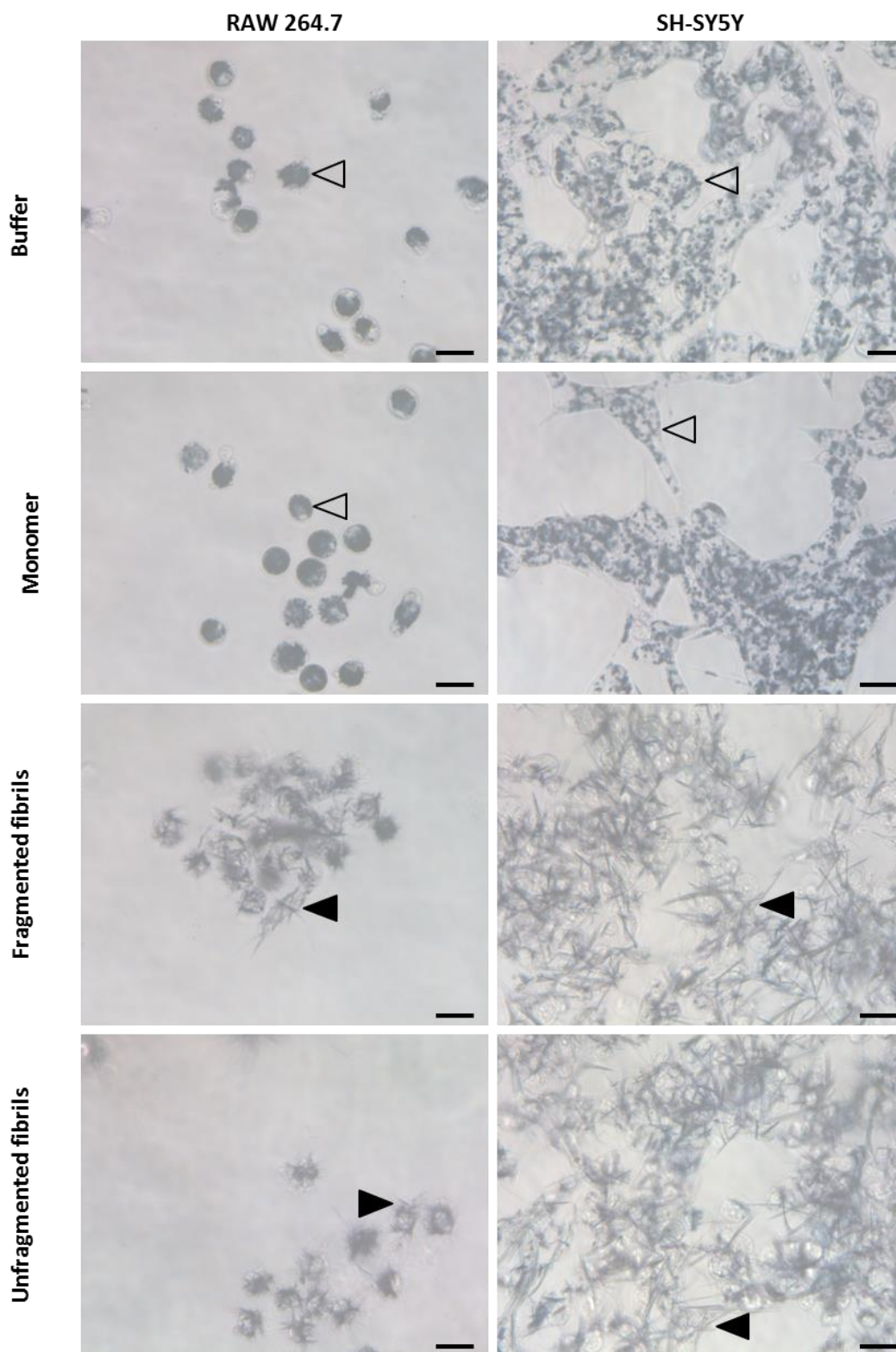


Figure 3.17: Phase contrast microscopy images of fibril treated cells incubated with MTT. RAW 264.7 cells (left) and SH-SY5Y cells (right) were incubated with β_2m monomer or fibrils at a final monomer equivalent concentration of $1.2 \mu M$ for 24h. Cells were incubated with MTT 90 min prior to imaging by phase contrast microscopy. Reduced formazan was visualised as dark intracellular granules as observed in buffer and monomer treated cells (open triangle) or extracellular needles as observed in fibril treated cells (filled triangle). The scale bar represents $20 \mu m$.

3.3 Discussion

The thermodynamic and kinetic stability of amyloid fibrils, with particular focus on the reversibility of amyloid formation and fibril disassembly to release potentially cytotoxic species, has been implicated as an important factor in determining amyloid cytotoxicity [101, 117, 161, 166, 177, 180, 191, 192]. The mechanical stability of amyloid fibrils may also be an important factor [101, 384]. Fragmentation of preformed amyloid fibrils may occur *in vivo* in the joints of DRA patients due to shear forces and mechanical stress [384]. Fibril fragmentation may also be caused by enzymatic action, for example, the molecular chaperone Hsp104 has been shown to fragment fibrils from the yeast prion protein Sup35 [385]. In addition, fragmented (i.e. short) fibrils may represent species that are formed during fibril elongation *in vivo*.

Fragmentation of β_2m amyloid fibrils alters their biological characteristics without changing their structural characteristics. Fragmented β_2m amyloid fibrils display the same biophysical and immunological characteristics (Figure 3.12 and Figure 3.13) but have a reduced average length (Figure 3.14)[190]. This reduction in length is an important factor in the inhibition of MTT reduction (Figure 3.16). Reduced fibril length has also been shown to be an important factor in the disruption of artificial lipid membranes [190]. Although beyond the scope of this thesis, an extensive characterisation on fragmented and unfragmented β_2m fibrils has been performed previously [190, 386]. This includes immunoblotting with WO1 and A11, of increasing concentrations of fragmented and unfragmented β_2m fibril samples up to 2400 μM (20 times the concentration tested in Figure 3.12). Oligomers bound by A11 were still undetectable at these high concentrations. Fibril architecture and fibril height were also analysed by Fourier transform infrared (FTIR) spectroscopy and AFM and were shown to be unchanged by fragmentation [190]. This characterisation is important to aid rationalisation of the differences in cellular effects between oligomer and fibril populations.

The MTT assay is a widely used cellular viability assay, however the use of it in determining the cytotoxicity of amyloid preparations has been questioned [379-383]. Amyloid aggregates of A β and amylin have been shown to inhibit MTT reduction in the absence of a loss in cell viability as mentioned above [380-382]. The inhibition in MTT reduction is thought to be linked to the enhanced exocytosis of formazan needles. This increase in extracellular formazan needles is thought to prevent endocytosis of the MTT salt, thereby inhibiting further reduction of MTT into formazan [379]. Indeed, the inhibition of MTT reduction by β_2m fibrils is coupled with an increase in extracellular formazan needles comparable to those reported with aggregated A β peptide (Figure 3.17) [380].

To investigate whether the inhibition of MTT reduction by β_2m amyloid fibrils was accompanied by a loss in cell viability, two additional viability assays were employed in our laboratory. Cellular ATP levels, which can be used as a measure of cell viability, were measured after incubation with fibrils or controls [387]. β_2m amyloid fibrils were shown to have no effect on cellular ATP levels, suggesting that the inhibition of MTT reduction is not due to loss in cell viability (Morwenna Porter, personal communications and Figure 3.18). Another cellular viability assay using the tetrazolium salt, 2-(4-iodophenyl)-3-(4-nitrophenyl)-5-(2,4-disulphophenyl)-2H-tetrazolium sodium salt (WST-1), employs the use of cellular reduction as a measure of cell viability. However, in this instance, reduction is thought to occur at the plasma membrane as opposed to the intracellular reduction of MTT [377]. WST-1 reduction was also measured after incubation with fibrils or controls. β_2m amyloid fibrils were also shown to have no effect on WST-1 reduction indicating no impairment in the overall cellular reductive capacity (Morwenna Porter, personal communications and Figure 3.18). Although β_2m amyloid fibrils do not affect cell viability, their effect on MTT reduction, in particular, the exocytosis of formazan needles provides clues of altered cell biology. Experiments designed to investigate these alterations are discussed in chapters 4 and 5.

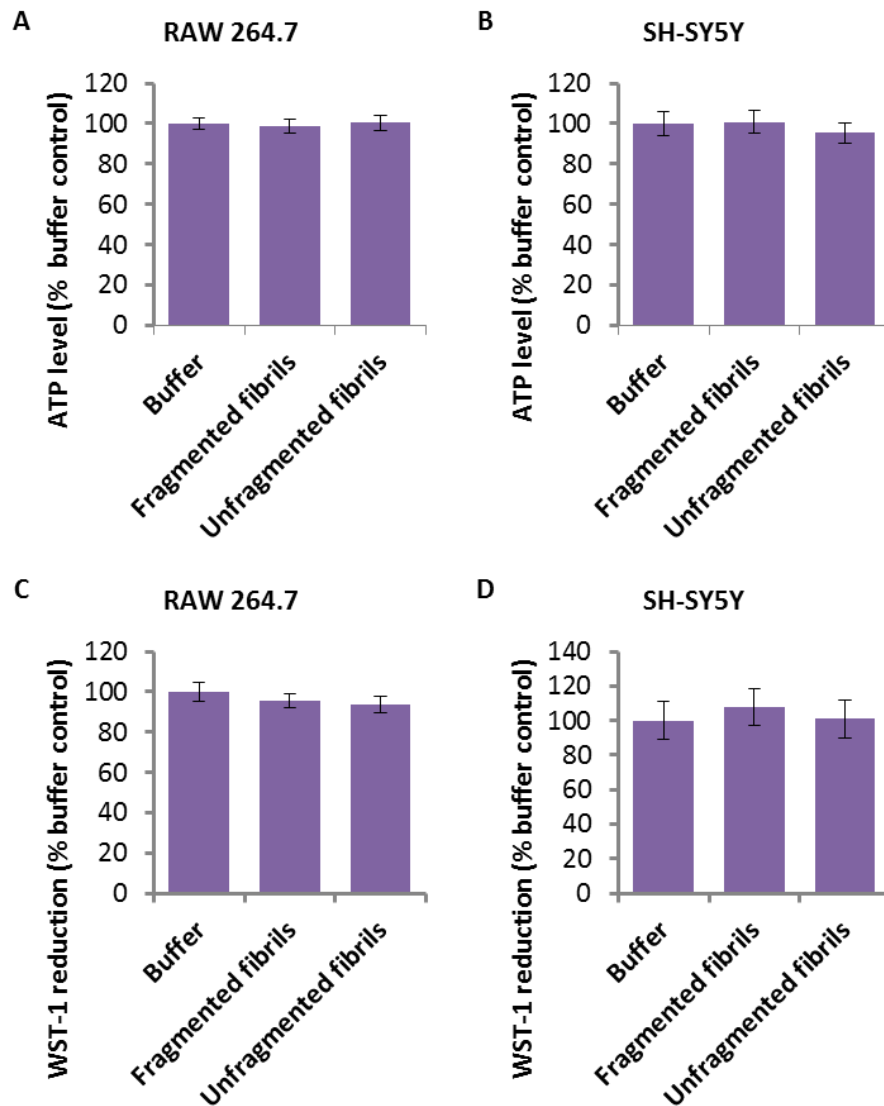


Figure 3.18: Analysis of the effect of fibrils on cell viability. ATP (A,B) and WST-1 (C,D) assays were performed using fragmented and unfragmented fibrils at a final monomer equivalent concentration of 1.2 μ M. RAW 264.7 cells (A,C) and SH-SY5Y cells (B,D) were incubated with fibrils or controls for 24 h before being assayed for cellular ATP levels or WST-1. ATP levels and WST-1 reduction (%) was calculated by normalising the signal from cells incubated with fibril growth buffer as 100% and cells treated with 0.1% (v/v) NaN_3 as 0%. The error bars represent one S.E.M. over two to three independent experiments each containing five replicates. Assays performed by Morwenna Porter.

4 Analysis of the effect of amyloid fibrils on lysosome function

4.1 Introduction

Increasing evidence points towards disruption of the lysosomal compartment in amyloid disease, in particular, lysosome and autophagy dysfunction have been consistently reported as mechanisms underlying pathogenesis in Alzheimer's, Parkinson's and Huntington's disease (reviewed in [255, 278, 388, 389]). Further evidence for lysosomal involvement comes from studies which demonstrate that inhibition of lysosomal function leads to neuronal dystrophy reminiscent of that observed in Alzheimer's disease [284]. Indeed, amyloid aggregates have been reported to accumulate in the endolysosomal system and this accumulation is associated with lysosomal dysfunction [242, 261, 263, 265]. Accumulation of amyloid aggregates in the endolysosomal system has also been demonstrated for β_2m . Analysis of amyloid deposits from DRA patients shows an accumulation of β_2m fibrils in the lysosomes of surrounding macrophages [390]. This is further supported by previous work from our laboratory. Macrophages were shown to internalise β_2m fibrils [247]. However, unlike β_2m monomer, β_2m fibrils were shown to be resistant to lysosomal degradation resulting in their persistence in the lysosome [247]. This lysosomal accumulation and persistence has also been shown for fibrils formed by the truncated form of β_2m , $\Delta N6 \beta_2m$, in primary human monocytes [248]. This chapter examines whether β_2m fibrils, upon trafficking to the lysosome, perturb lysosomal function.

Interestingly, β_2m fibril internalisation has been shown to be length dependent. Fragmented β_2m fibrils are internalised to a much greater extent than their unfragmented counterparts (Andrew Hellewell, personal communications and Figure 4.1). Fragmented fibrils would thus have greater access to intracellular compartments such as the lysosome where it has been shown to be trafficked to. Experiments were therefore focussed on fragmented β_2m fibrils. Unless explicitly stated otherwise, the experiments described in this chapter and subsequent chapters were performed with fragmented β_2m fibrils.

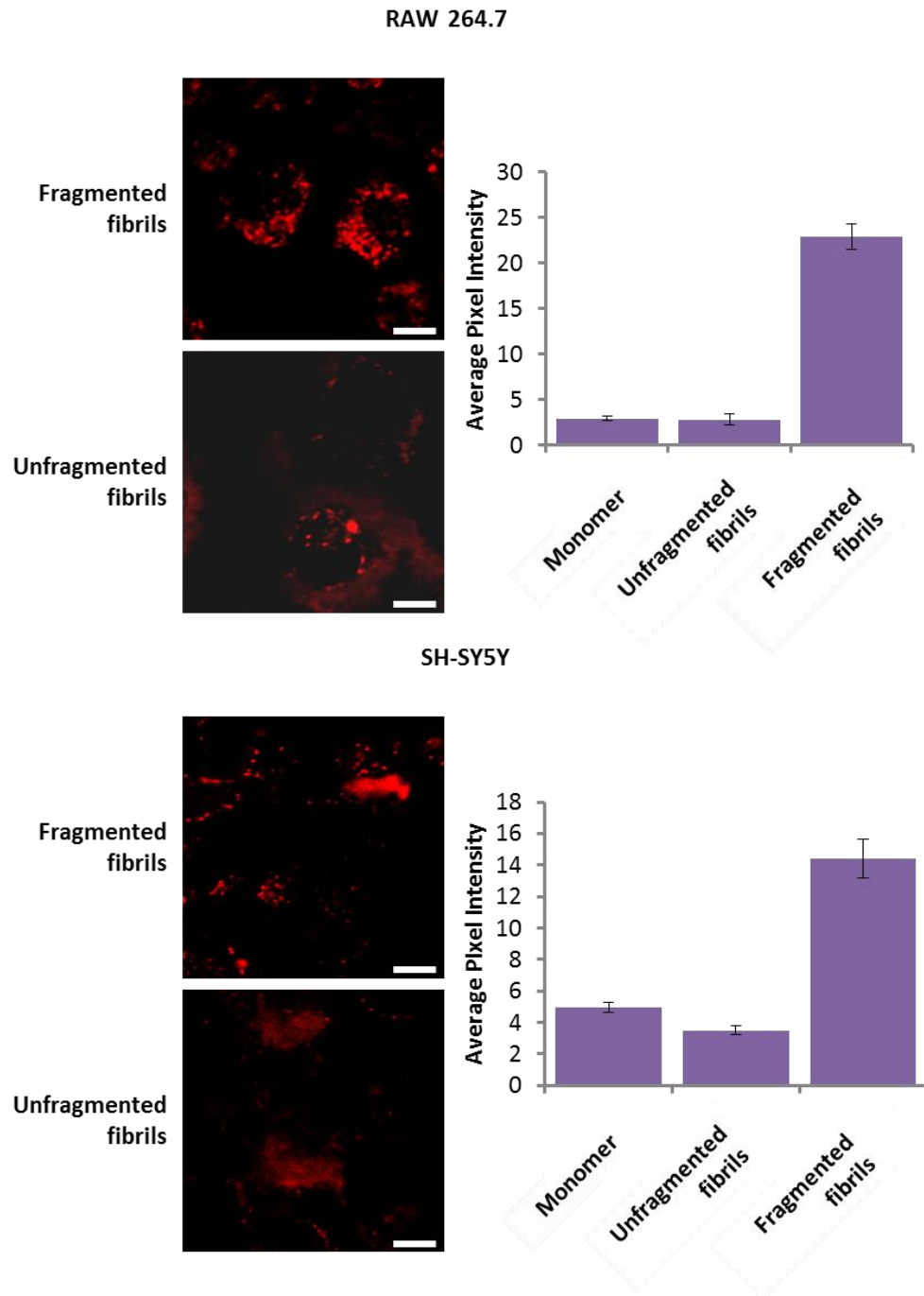


Figure 4.1: Quantification of intracellular TMR labelled β_2m monomer and fibrils from confocal images. Intracellular fluorescence from confocal images of RAW 264.7 (top) and SH-SY5Y cells (bottom) incubated with TMR labelled β_2m monomer, fragmented or unfragmented β_2m fibrils for 4 h was quantified using Image J. Ten images were collected for each condition and cell boundaries were delineated by hand using the phase contrast images. Images were acquired on a Zeiss LSM510 confocal microscope with a 40X objective. Representative images of cells treated with fibrils are shown on the left. The mean pixel intensity from the red channel (TMR) was calculated and is graphically shown on the right. Error bars represent one S.E.M. 158 RAW 264.7 and 60 SH-SY5Y cells were analysed. Experiment performed by Andrew Hellewell.

As degradation and recycling of macromolecules is one of the primary functions of the lysosome, the effect of fragmented fibrils on the ability of lysosomes to perform this crucial function was investigated [391]. Indeed, disruption to lysosome mediated degradation has been reported as a mechanism involved in the pathogenesis of amyloid disease [284, 285, 289](Section 1.5.4.2.2). The effect of fragmented β_2m amyloid fibrils on lysosome mediated protein degradation was studied and will be discussed here. In addition, the effect of fragmented β_2m fibrils on the activities of two other lysosomal hydrolases, β -glucocerebrosidase and β -galactosidase was examined.

4.2 Results

4.2.1 Analysis of the effect of fragmented fibrils on lysosomal proteolysis

4.2.1.1 TMR-labelled β_2m monomer as a lysosomal protease substrate

In order to investigate the effect of fragmented β_2m fibrils on lysosomal proteolysis, cells were incubated with fluorescently labelled substrates and their hydrolysis was followed by measuring cell-associated fluorescence by flow cytometry. β_2m monomer labelled with tetramethylrhodamine (TMR- β_2m) was initially selected for use as a substrate as previous work using RAW 264.7 cells and primary human monocytes revealed that exogenously added β_2m monomer is trafficked to the lysosome where it is degraded by lysosomal proteases [247, 248].

RAW 264.7 and SH-SY5Y cells were incubated with either fragmented β_2m fibrils or fibril growth buffer as a control for 24 h. Cells were then pulsed with fluorescent protein substrate (TMR- β_2m) for 4 h (RAW 264.7) or 6 h (SH-SY5Y) (Section 2.7.1). At the end of TMR- β_2m pulse, cells were either analysed for cell-associated fluorescence (0 h chase) or cultured for a further 24 h in the absence of TMR- β_2m . Cell-associated fluorescence was also measured 24 h after TMR- β_2m pulse (24 h chase). Cell-associated fluorescence at 0 h chase gives a measure of uptake of fluorescent protein substrate, in this case TMR- β_2m . The cell-associated fluorescence at 24 h chase gives a measure of the amount of fluorescent protein substrate remaining in cells 24 h after pulse. A comparison of fluorescence at 24 h chase to that at 0 h chase would therefore allow an estimation of lysosome-mediated degradation of fluorescent protein substrate over 24 h (Figure 4.2).

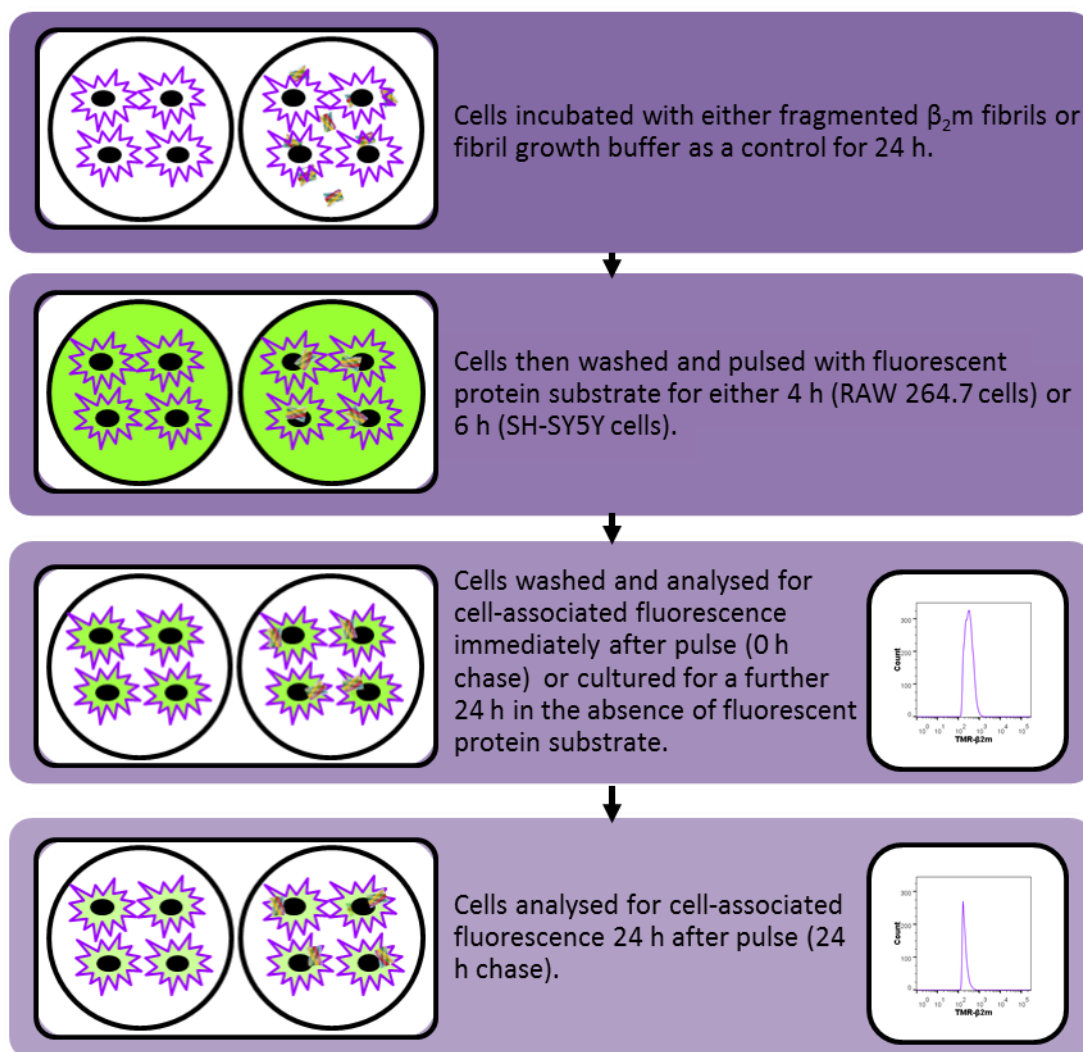


Figure 4.2: Schematic of the lysosomal proteolysis assay.

Cell-associated fluorescence at 24 h chase in both RAW 264.7 and SH-SY5Y cells was higher in cells incubated with fragmented β_2m fibrils than those incubated with fibril growth buffer (Figure 4.3 and Figure 4.4). This suggests that β_2m fibrils impair lysosomal proteolysis. However, as fragmented fibrils also contain β_2m , the possibility that TMR- β_2m is incorporated into proteolytically resistant fibrils in the lysosome could not be excluded [247]. The increased cell-associated fluorescence at 24 h chase in fibril-treated cells could therefore be due to an incorporation of TMR- β_2m into fibrils and may not necessarily reflect disruption in lysosomal proteolysis.

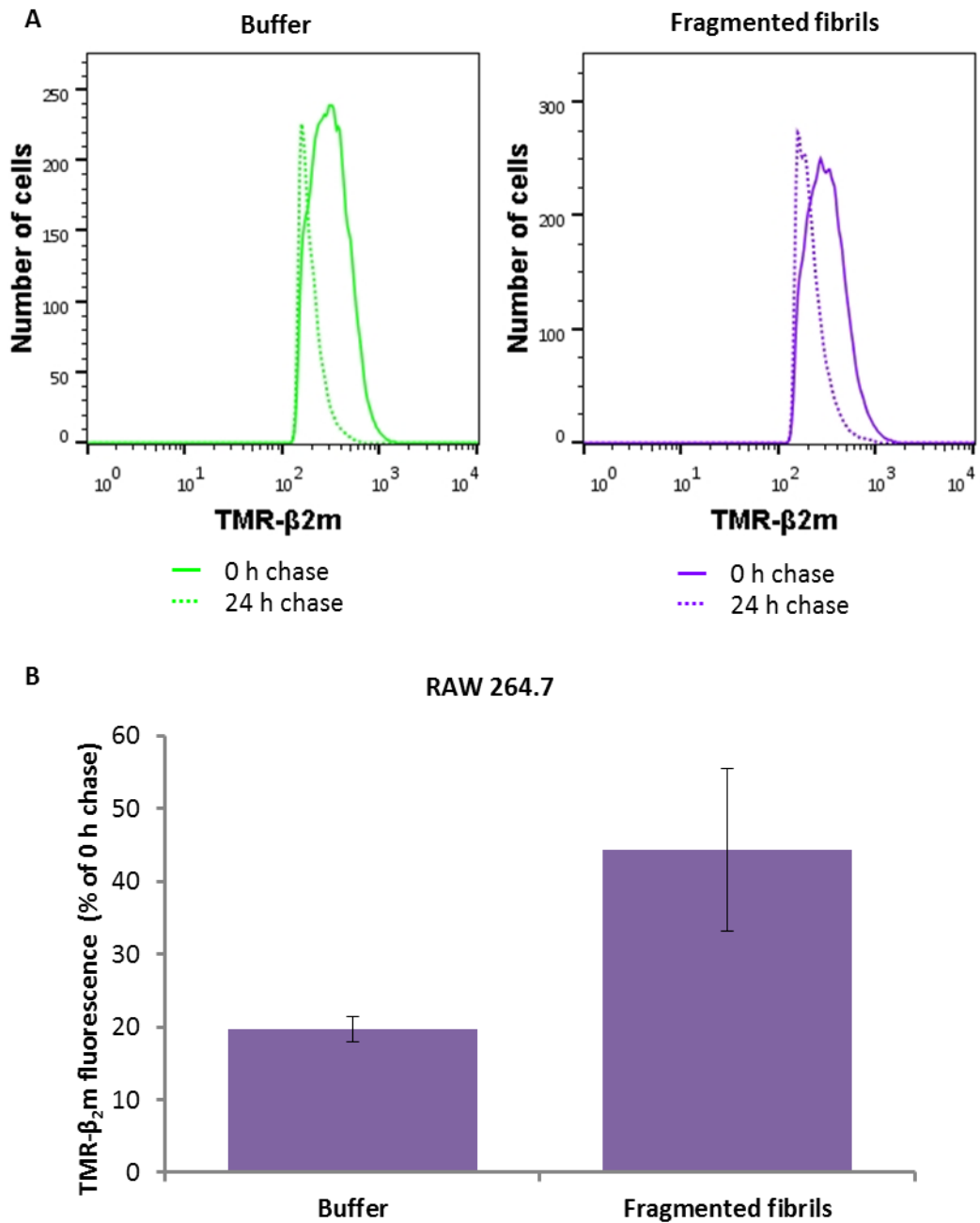


Figure 4.3: Analysis of the effect of fibrils on the degradation of TMR- β ₂m in RAW 264.7 cells. Cells were incubated with either fragmented fibrils at a final monomer equivalent concentration of 1.2 μ M or fibril growth buffer for 24 h. Cells were then pulsed with TMR- β ₂m and analysed for cell-associated fluorescence immediately after pulse (0 h) or cultured for a further 24 h in the absence of TMR- β ₂m and analysed (24 h chase). (A) Representative flow cytometry data comparing cell-associated fluorescence at 24 h chase with that at 0 h chase for each experimental condition. (B) Quantification of flow cytometry data. TMR- β ₂m fluorescence (%) was calculated by normalising the fluorescence at 24 h chase to the fluorescence at 0 h chase for each treatment. Error bars represent one S.E.M. over two independent experiments containing three replicates each. Flow cytometry data was collected on a BD LSRFortessa analyser (Becton Dickinson).

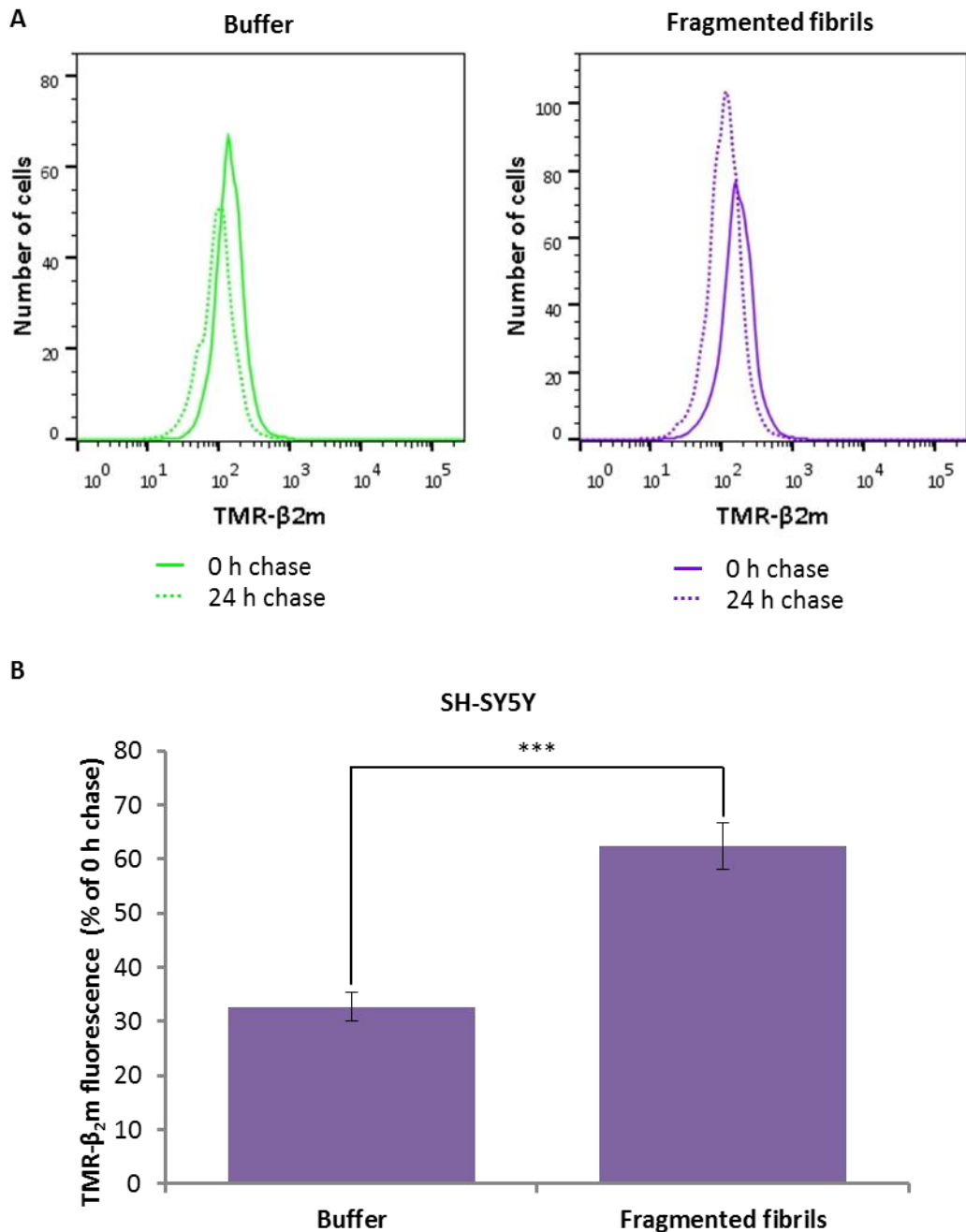


Figure 4.4: Analysis of the effect of fibrils on the degradation of TMR-β₂m in SH-SY5Y cells. Cells were incubated with either fragmented fibrils at a final monomer equivalent concentration of 1.2 μM or fibril growth buffer for 24 h. Cells were then pulsed with TMR-β₂m and analysed for cell-associated fluorescence immediately after pulse (0 h) or cultured for a further 24 h in the absence of TMR-β₂m and analysed (24 h chase). (A) Representative flow cytometry data comparing cell-associated fluorescence at 24 h chase with that at 0 h chase. (B) Quantification of flow cytometry data. TMR-β₂m fluorescence (%) was calculated by normalising the fluorescence at 24 h chase to the fluorescence at 0 h chase for each treatment. Error bars represent one S.E.M. over three independent experiments containing three replicates each. *** signifies a p value of <0.001. Flow cytometry data was collected on a BD LSRFortessa analyser (Becton Dickinson).

4.2.1.2 Pumilio-GFP as a lysosomal protease substrate

Due to the complications associated with using TMR- β_2m as a lysosomal protease substrate, an unrelated protein, Pumilio conjugated to GFP was selected. Pumilio, from *Drosophila Melanogaster* is a 157 KDa cytoplasmic protein [392]. Degradation of GFP is predicted to be coupled with a loss of fluorescence. The loss in cell-associated fluorescence can therefore be used as an estimate of Pumilio-GFP degradation. RAW 264.7 cells were incubated with either fragmented β_2m fibrils or fibril growth buffer as a control for 24 h. Cells were then pulsed with fluorescent protein substrate, in this case, Pumilio-GFP (Section 2.7.1). Cell-associated fluorescence was quantified by flow cytometry, immediately after pulse (0 h chase) or cells were cultured for a further 24 h in the absence of Pumilio-GFP. Cell-associated fluorescence was also measured 24 h after pulse (24 h chase). Cells incubated with fragmented β_2m fibrils had a greater amount of cell-associated fluorescence at 24 h chase than buffer controls (Figure 4.5). In combination with experiments using TMR- β_2m , this suggests that fragmented fibrils disrupt lysosomal proteolysis.

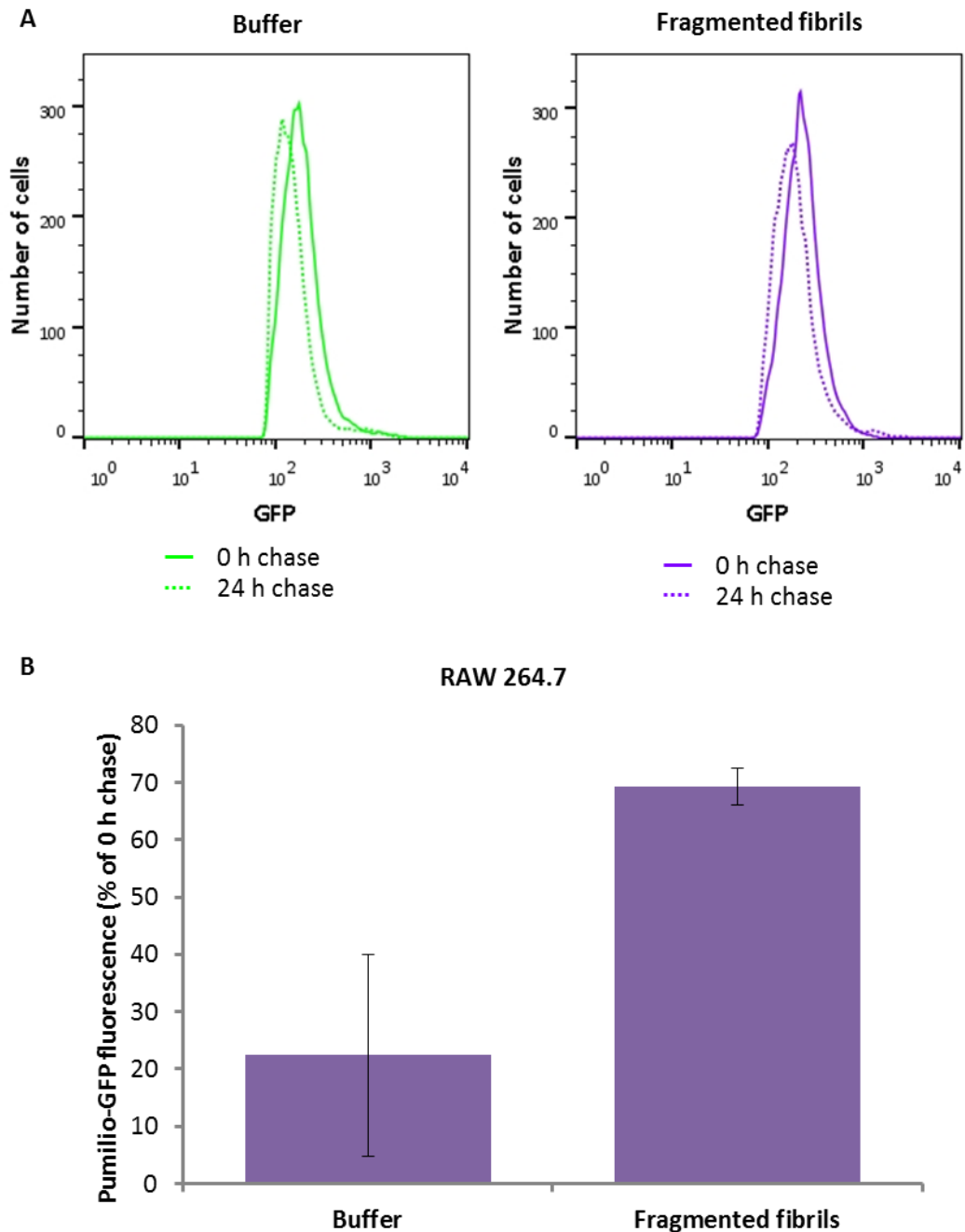


Figure 4.5: Analysis of the effect of fibrils on the degradation of Pumilio-GFP in RAW 264.7 cells. Cells were incubated with either fragmented fibrils at a final monomer equivalent concentration of 1.2 μM or fibril growth buffer for 24 h. Cells were then pulsed with Pumilio-GFP and analysed for cell-associated fluorescence immediately after pulse (0 h chase) or cultured for a further 24 h in the absence of Pumilio-GFP and analysed (24 h chase). (A) Representative flow cytometry data comparing cell-associated fluorescence at 24 h chase with that at 0 h chase. (B) Quantification of flow cytometry data. Pumilio-GFP fluorescence (%) was calculated by normalising the fluorescence at 24 h chase to the fluorescence at 0 h chase for each treatment. Error bars represent one S.D. over two replicates. Flow cytometry data was collected on a BD LSRFortessa analyser (Becton Dickinson).

Two caveats present themselves with this experiment. The first, although Pumilio-GFP is predicted to be internalised by fluid phase endocytosis; unlike β_2m , its internalisation and trafficking to the lysosome as well as degradation in the lysosome has not been characterised. The second caveat is that GFP fluorescence varies with pH and is diminished at acidic pH. Indeed, when Pumilio-GFP fluorescence was measured *in vitro*, a significant decrease in fluorescence intensity was observed when pH was reduced from 7.4 (cytosolic pH) to both 5.5 (late endosomal pH) and 4.5 (lysosomal pH) (Figure 4.6 and Section 2.7.1.2.1). The increased cell-associated fluorescence in fibril-treated cells could therefore also be due an increase in lysosomal pH. It is not possible, therefore, to distinguish between the effect of fibrils on lysosomal proteolysis and on lysosomal pH in these experiments.

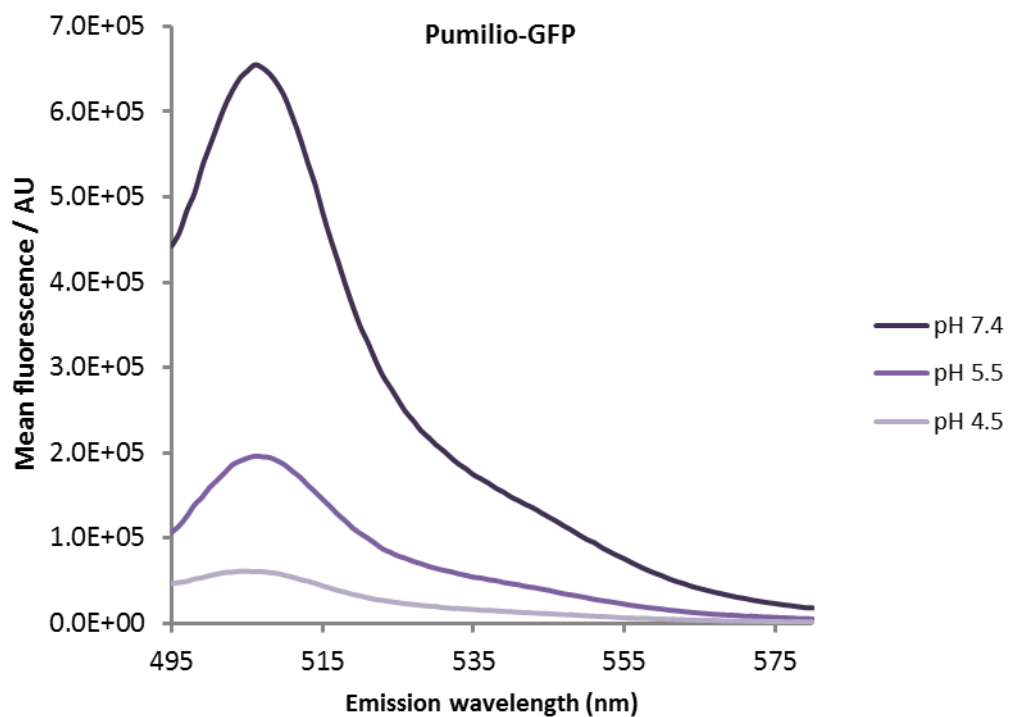


Figure 4.6: Pumilio-GFP fluorescence intensity varies with pH. Fluorescence emission spectra of 150 $\mu\text{g/ml}$ Pumilio-GFP at pH 4.5, 5.5 and 7.4. Pumilio-GFP was diluted in buffer immediately before fluorescence emission spectra were collected. The background corrected mean fluorescence is shown.

4.2.1.3 Alexa Fluor® 647 ovalbumin as a lysosomal protease substrate

In order to overcome the limitations of using TMR- β_2m and Pumilio-GFP as fluorescent protein substrates, a third substrate, Alexa Fluor® 647 labelled ovalbumin (AF647-ovalbumin) was selected for use in subsequent experiments. Ovalbumin has been shown to be trafficked via the endocytic pathway to the lysosome where it is degraded [393]. The fluorescence of the conjugated fluorophore, Alexa Fluor® 647, is pH insensitive. AF647-ovalbumin is therefore a better suited substrate to analyse the effect of fragmented β_2m fibrils on lysosomal proteolysis.

To confirm that ovalbumin is internalised and trafficked to the lysosome, cells were analysed by live cell confocal microscopy (Section 2.7.1.3). RAW 264.7 cells were incubated with either fragmented β_2m fibrils or controls (fibril growth buffer and β_2m monomer). Cells were then pulsed with AF647-ovalbumin for 4 h and imaged by live cell confocal microscopy immediately after pulse (0 h chase) or cultured for a further 24 h in the absence of AF647-ovalbumin and then imaged (24 h chase). Cells were stained with LysoTracker Green 30 min prior to imaging. LysoTracker Green is a fluorescent lysosomal marker used for its ability to accumulate in acidic vesicles.

AF647-ovalbumin was localised to intracellular punctate structures which co-stained with LysoTracker Green at 0 h chase (Figure 4.7, part 1). Images taken at 24 h chase show reduced AF647-ovalbumin fluorescence when compared to those at 0 h chase (Figure 4.7, part 2). This suggests that ovalbumin is degraded in the lysosome. Interestingly, AF647-ovalbumin fluorescence at 24 h chase in cells treated with fragmented fibrils was greater than in buffer or β_2m monomer controls (Figure 4.7, part 2).

RAW 264.7, 0 h chase

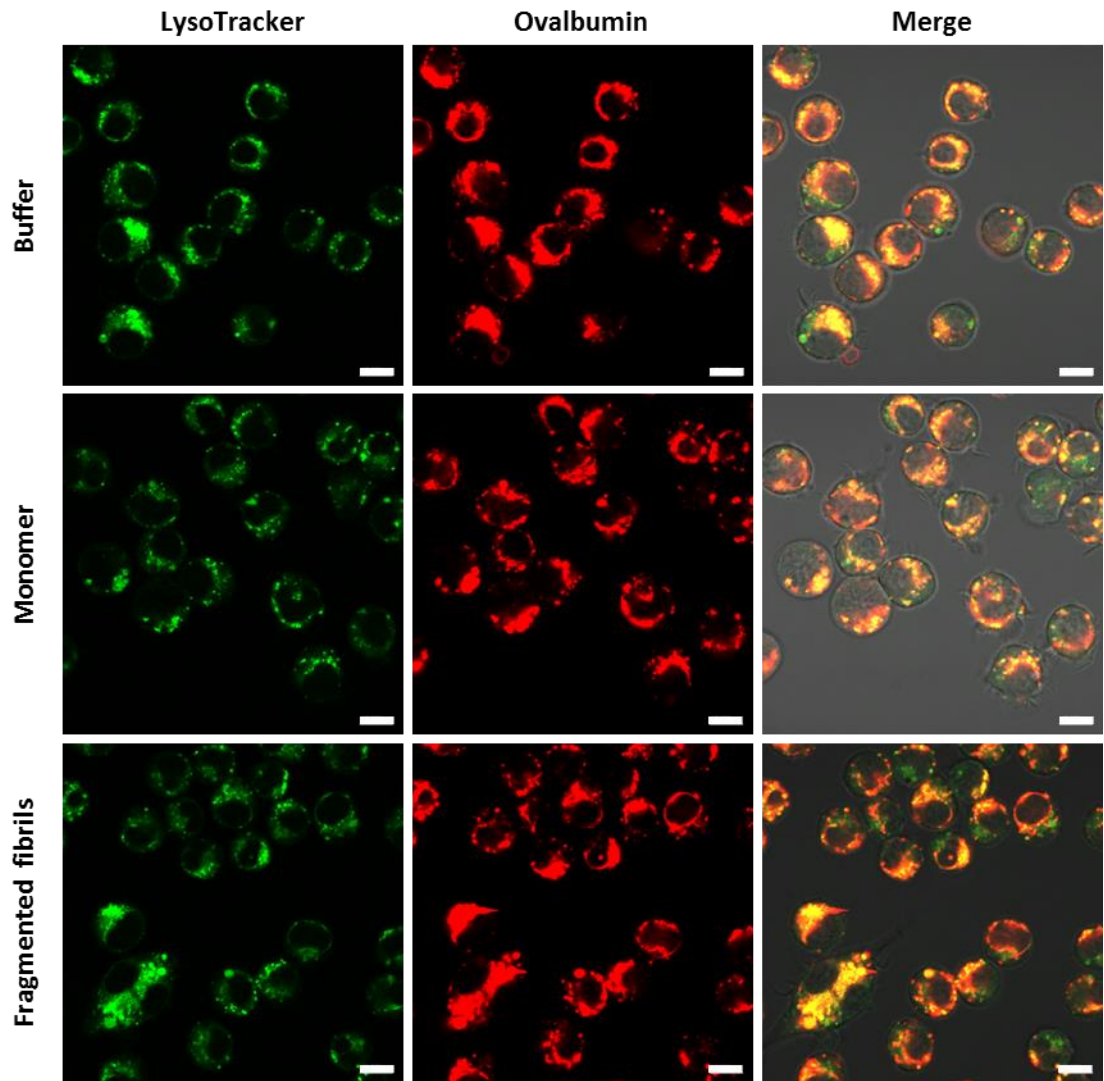


Figure 4.7: Analysis of the internalisation, localisation and degradation of fluorescently labelled ovalbumin in RAW 264.7 cells (part 1 of 2). For legend, see next page.

RAW 264.7, 24 h chase

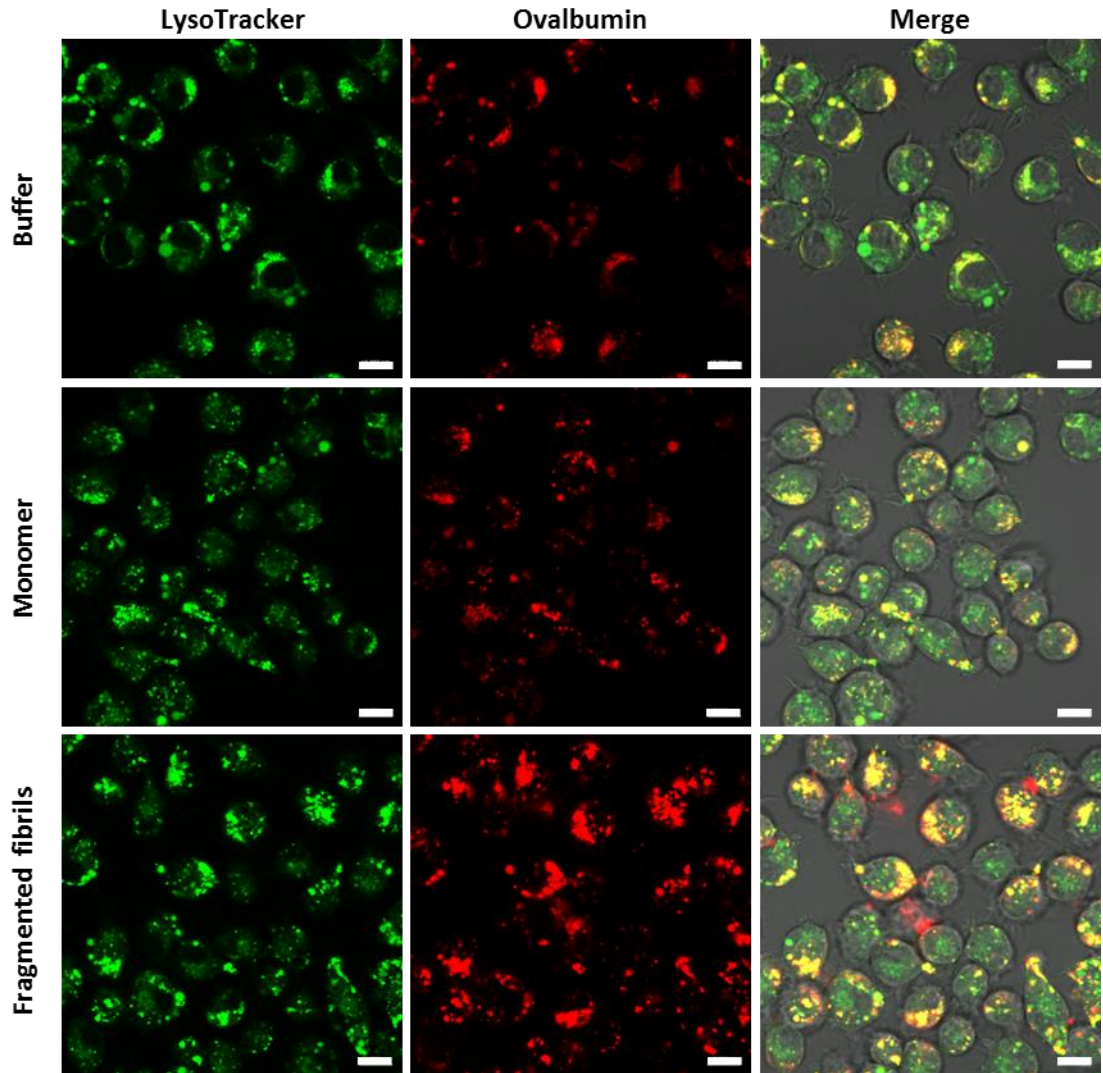


Figure 4.7: Analysis of the internalisation, localisation and degradation of fluorescently labelled ovalbumin in RAW 264.7 cells (part 2 of 2). Cells were incubated with 1.2 μM (monomer equivalent) fragmented $\beta_2\text{m}$ fibrils or 1.2 μM $\beta_2\text{m}$ monomer and fibril growth buffer as controls for 24 h. Cells were then pulsed with 15 $\mu\text{g}/\text{ml}$ AF647-ovalbumin (40 % labelled: 60 % unlabelled) for 4 h. Cells were washed and imaged immediately after pulse (0 h chase, part 1) or cultured in the absence of AF647-ovalbumin for 24 h and imaged (24 h chase, part 2). Cells were stained with 50 nm LysoTracker Green 30 min prior to imaging. Images were acquired with a Zeiss LSM700 confocal microscope and a 63X objective. Representative confocal images for each condition are shown. Scale bar represents 10 μm .

When the uptake and degradation of AF647-ovalbumin was analysed in SH-SY5Y cells, ovalbumin was also found to localise to punctate structures which co-stain with LysoTracker Green (Figure 4.8, part 1). As observed in RAW 264.7 cells, reduced ovalbumin fluorescence was observed at 24 h chase in SH-SY5Y cells. Cells treated with fragmented fibrils also showed greater ovalbumin fluorescence at 24 h chase than cells treated with fibril growth buffer or β_2m monomer controls (Figure 4.8, part 2).

SH-SY5Y, 0 h chase

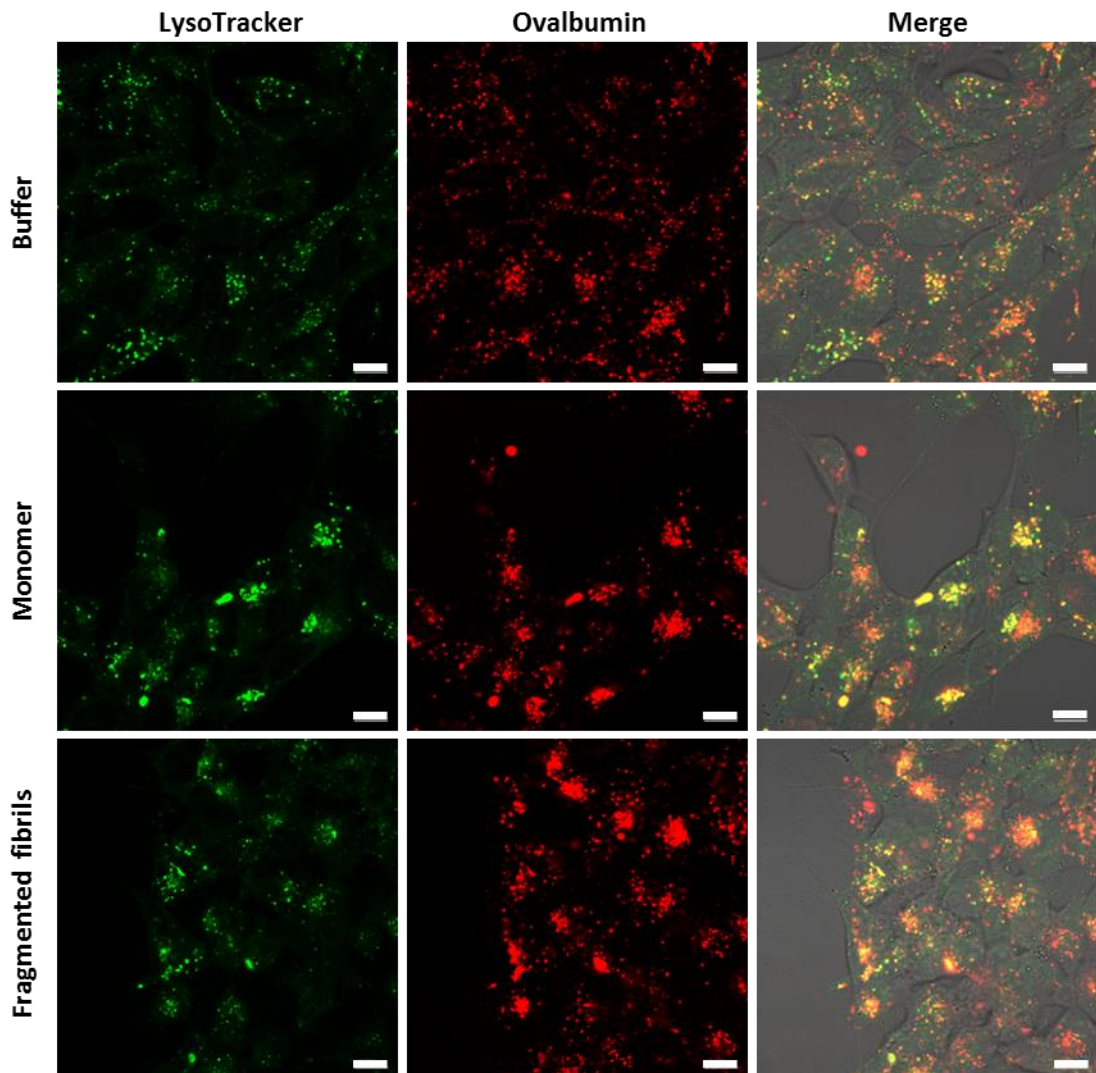


Figure 4.8: Analysis of the internalisation, localisation and degradation of fluorescently labelled ovalbumin in SH-SY5Y cells (part 1 of 2). For legend, see next page.

SH-SY5Y, 24 h chase

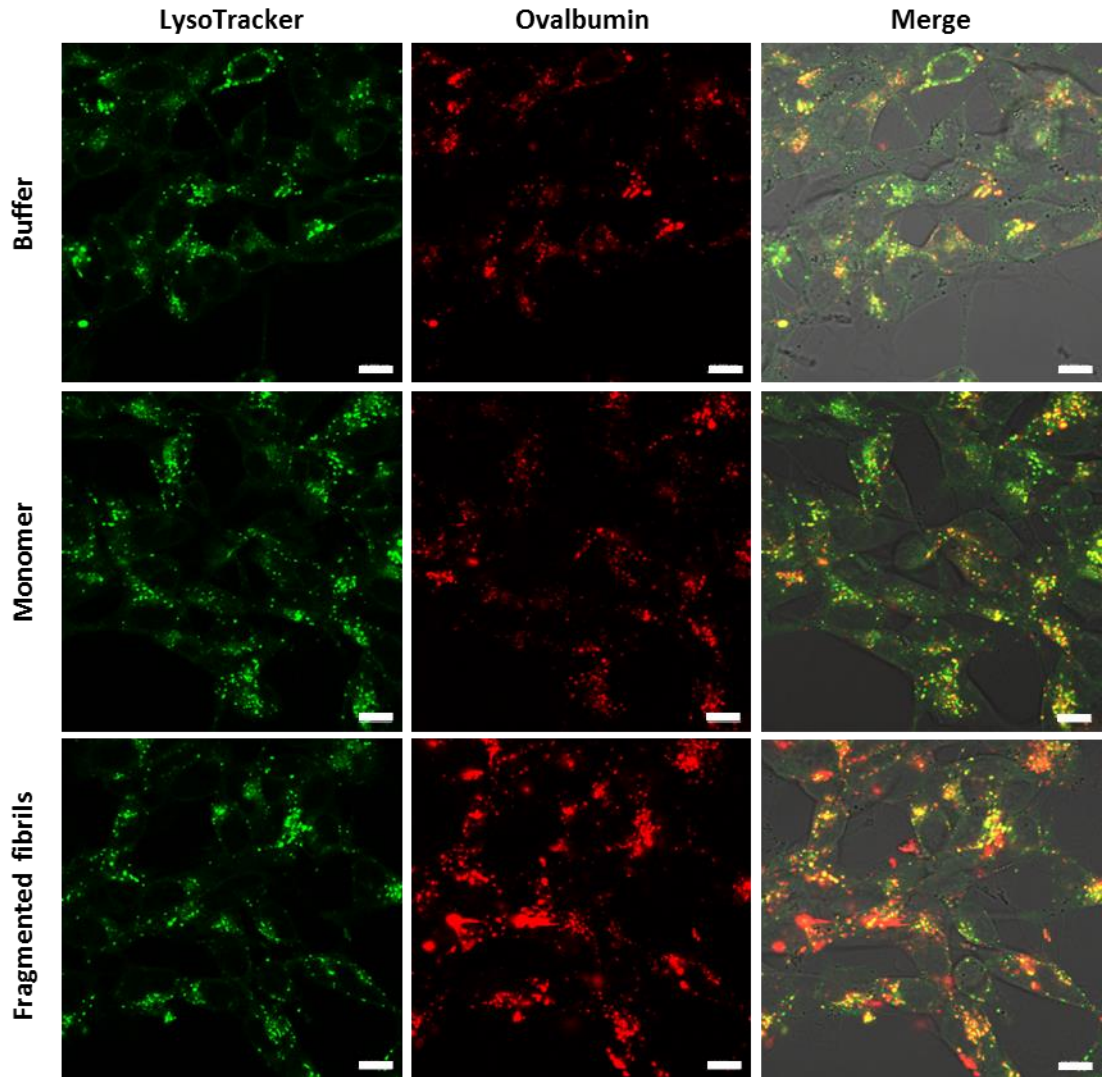


Figure 4.8: Analysis of the internalisation, localisation and degradation of fluorescently labelled ovalbumin in SH-SY5Y cells (part 2 of 2). Cells were incubated with 1.2 μM (monomer equivalent) fragmented $\beta_2\text{m}$ fibrils or 1.2 μM $\beta_2\text{m}$ monomer and fibril growth buffer as controls for 24 h. Cells were then pulsed with 15 $\mu\text{g}/\text{ml}$ AF647-ovalbumin (40 % labelled: 60 % unlabelled) for 6 h. Cells were washed and imaged immediately after pulse (0 h chase, part 1) or cultured in the absence of AF647-ovalbumin for 24 h and imaged (24 h chase, part 2). Cells were stained with 75 nm LysoTracker Green 30 min prior to imaging. Images were acquired with a Zeiss LSM700 confocal microscope and a 63X objective. Representative confocal images for each condition are shown. Scale bar represents 10 μm .

In order to ensure that the decrease in ovalbumin fluorescence was due to a decrease in protein levels and not due to photobleaching of AF674, RAW 264.7 and SH-SY5Y cells were pulsed with unlabelled ovalbumin and analysed by immunoblotting. Cells were lysed immediately after pulse with ovalbumin (0 h chase) or cultured for a further 24 h in the absence of ovalbumin and lysed (24 h chase). Cell lysates were immunoblotted for ovalbumin using an HRP-conjugated anti-ovalbumin antibody (anti-ovalbumin-HRP) (Section 0). Detection of ovalbumin in cell lysates was limited by the poor sensitivity of anti-ovalbumin HRP. A ten-fold increase in concentration (over that used for confocal microscopy analysis) was required to enable detection by immunoblotting of cell-associated ovalbumin at 0 h chase. Ovalbumin was detected in 0 h chase cell lysates from cells pulsed with 150 $\mu\text{g/ml}$ ovalbumin but not in those pulsed with 15 $\mu\text{g/ml}$ ovalbumin (Figure 4.9). In cell lysates from cells pulsed with 150 $\mu\text{g/ml}$ ovalbumin, ovalbumin was no longer detected at 24 h chase. Ovalbumin levels were detectable by confocal live cell microscopy at 24 h chase, yet undetectable by immunoblotting within the same time frame. This may reflect differences in the sensitivity of techniques. Nevertheless, the disappearance of the ovalbumin band in cell lysates immunoblotted for ovalbumin at 24 h chase indicates a reduction in ovalbumin levels. This suggests that the decrease in ovalbumin fluorescence observed by confocal microscopy is due to a decrease in protein levels.

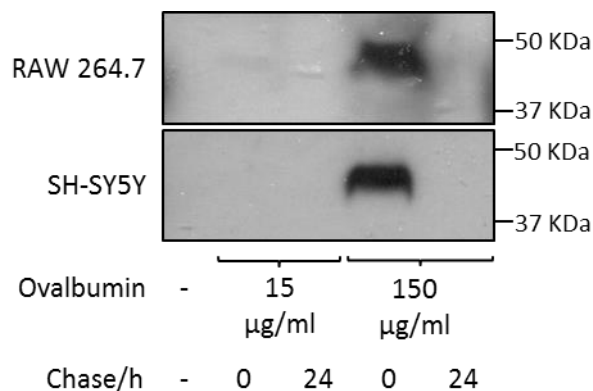


Figure 4.9: Immunoblotting analysis to assess the degradation of ovalbumin in RAW 264.7 and SH-SY5Y cells. RAW 264.7 (top) and SH-SY5Y (bottom) cells were pulsed with ovalbumin at the indicated concentrations for 4 h and 6 h respectively. Cells were then washed and lysed either immediately (0 h chase) after pulse or cultured for a further 24 h and lysed (24 h chase). Cell lysates were analysed by immunoblotting with an HRP-conjugated ovalbumin-specific antibody.

Flow cytometry was used to quantify lysosomal proteolysis of AF647-ovalbumin as described for TMR- $\beta_2\text{m}$ and Pumilio-GFP (Section 2.7.1.2). Cells were incubated with either fragmented $\beta_2\text{m}$ fibrils or controls ($\beta_2\text{m}$ monomer and fibril growth buffer). Cells were pulsed with AF647-

ovalbumin and analysed for cell-associated fluorescence immediately after pulse (0h chase) or cultured for a further 24 h in the absence of AF647-ovalbumin and analysed (24 h chase). Cell-associated ovalbumin fluorescence at 24 h chase was greater in fibril treated cells compared to controls for both RAW 264.7 and SH-SY5Y cells (Figure 4.10 and Figure 4.11). This suggests that ovalbumin degradation is impaired in fibril-treated cells. In combination, data from experiments with TMR- β_2m , Pumilio-GFP and AF647-ovalbumin, strongly indicate an inhibition in the lysosomal degradation of endocytosed proteins by fragmented fibrils.

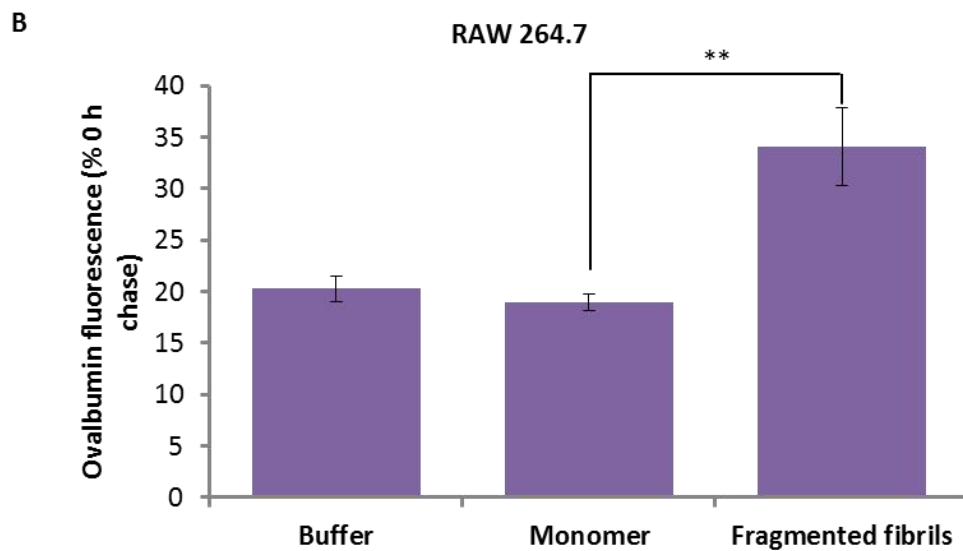
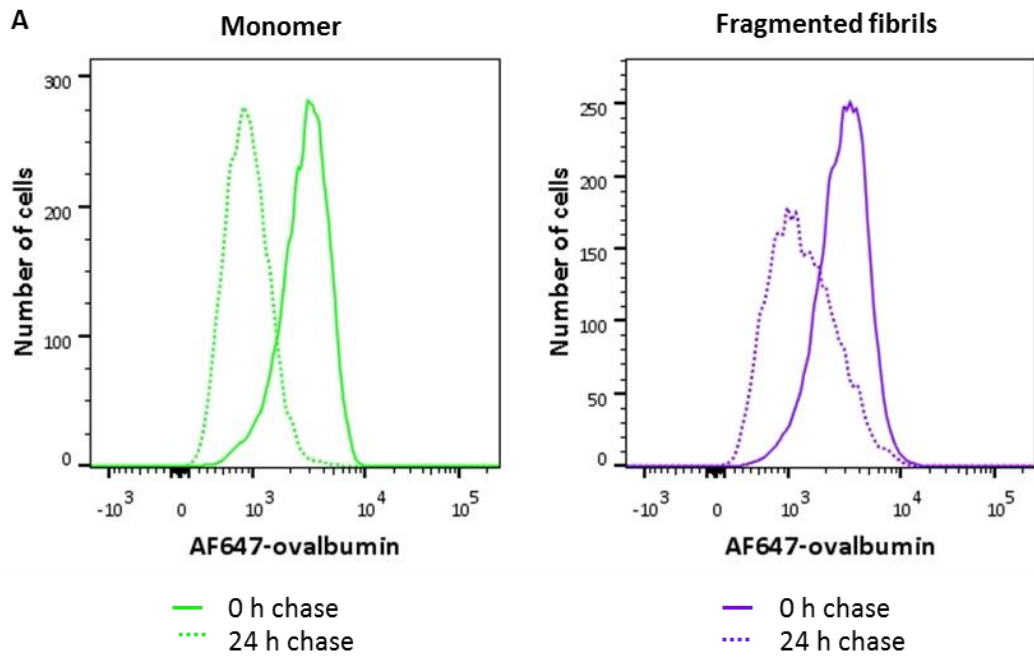


Figure 4.10: Analysis of the effect of fibrils on the degradation of AF647-ovalbumin in RAW 264.7 cells. Cells were incubated with either fragmented fibrils at a final monomer equivalent concentration of 1.2 μM , 1.2 μM $\beta_2\text{m}$ monomer or fibril growth buffer for 24 h. Cells were then pulsed with AF647-ovalbumin for 4 h and analysed for cell-associated fluorescence immediately after pulse (0 h chase) or cultured for a further 24 h in the absence of AF647-ovalbumin and analysed (24 h chase). (A) Representative flow cytometry data comparing cell-associated fluorescence at 24 h chase with that at 0 h chase. (B) Quantification of flow cytometry data. Ovalbumin fluorescence (%) was calculated by normalising the fluorescence at 24 h chase to the fluorescence at 0 h chase for each treatment. Error bars represent one S.E.M. over three independent experiments containing three replicates each. Flow cytometry data was collected on a BD LSRFortessa analyser (Becton Dickinson). ** signifies a p value of <0.01 .

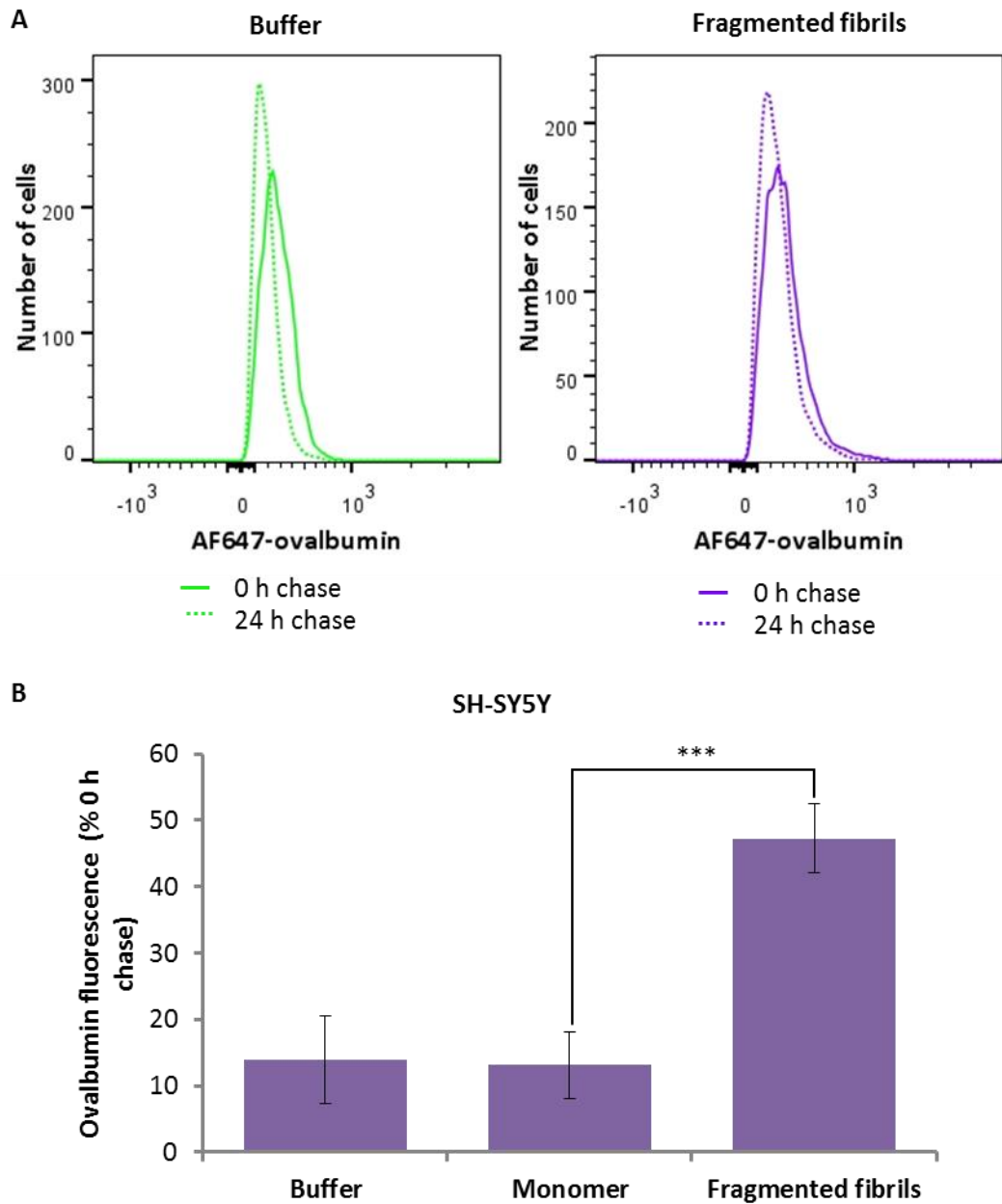


Figure 4.11: Analysis of the effect of fibrils on the degradation of AF647-ovalbumin in SH-SY5Y cells. Cells were incubated with either fragmented fibrils at a final monomer equivalent concentration of 1.2 μM , 1.2 μM $\beta_2\text{m}$ monomer or fibril growth buffer for 24 h. Cells were then pulsed with AF647-ovalbumin for 6 h and analysed for cell-associated fluorescence immediately after pulse (0 h chase) or cultured for a further 24 h in the absence of AF647-ovalbumin and analysed (24 h chase). (A) Representative flow cytometry data comparing cell-associated fluorescence at 24 h chase with that at 0 h chase. (B) Quantification of flow cytometry data. Ovalbumin fluorescence (%) was calculated by normalising the fluorescence at 24 h chase to the fluorescence at 0 h chase for each treatment. Error bars represent one S.E.M. over three independent experiments containing three replicates each. Flow cytometry data was collected on a BD LSRFortessa analyser (Becton Dickinson). *** signifies a p value of <0.001 .

4.2.1.4 Magic Red™ as a lysosomal protease substrate

All of the assays on lysosomal proteolysis described above rely on internalisation of the labelled protein substrate by endocytosis. Impairment in the lysosome-mediated degradation of these labelled proteins could be due to inhibition of lysosomal proteases or a disruption in delivery of cargo to lysosomes. In order to distinguish between these two possibilities, lysosomal proteolysis was assayed using a commercially available substrate, Magic Red™ cathepsin B substrate. Like in the assays described above, this substrate provides a method to assay varying levels of lysosomal hydrolase (in this case cathepsin B) activity in intact and living cells. The substrate, which is conjugated to a cresyl violet fluorophore, is non-fluorescent when uncleaved. It contains a cathepsin B targeting sequence. Cathepsin B cleaves the substrate releasing the fluorophores which are then free to fluoresce. Cresyl violet fluorescence can therefore be used as a measure of cathepsin B activity in cells. Crucially, because the Magic Red™ cathepsin B substrate is cell membrane permeable, it does not require endocytosis for targeted delivery to the lysosome.

Disruption in delivery of cargo to lysosomes as discussed in section (Section 1.5.4.2.3) and endolysosomal trafficking has been heavily implicated in neurodegenerative diseases [255, 256, 292, 323, 324, 394, 395]. For this reason, experiments were focused on analysis of the effect of fragmented fibrils on a model neuronal cell line, SH-SY5Y.

In order to confirm that the Magic Red™ cathepsin B substrate is cleaved in the lysosome, SH-SY5Y cells were incubated with Magic Red™ cathepsin B substrate and cresyl violet fluorescence was visualised by live cell confocal microscopy. SH-SY5Y cells were incubated with or without Magic Red™ cathepsin B substrate (Section 2.7.2.1). Cells were then stained with LysoTracker Green prior to imaging. Cresyl violet fluorescence co-localised with LysoTracker green positive compartments (Figure 4.12), indicating that the Magic Red™ cathepsin B substrate is cleaved in acidic compartments that presumably correspond to lysosomes.

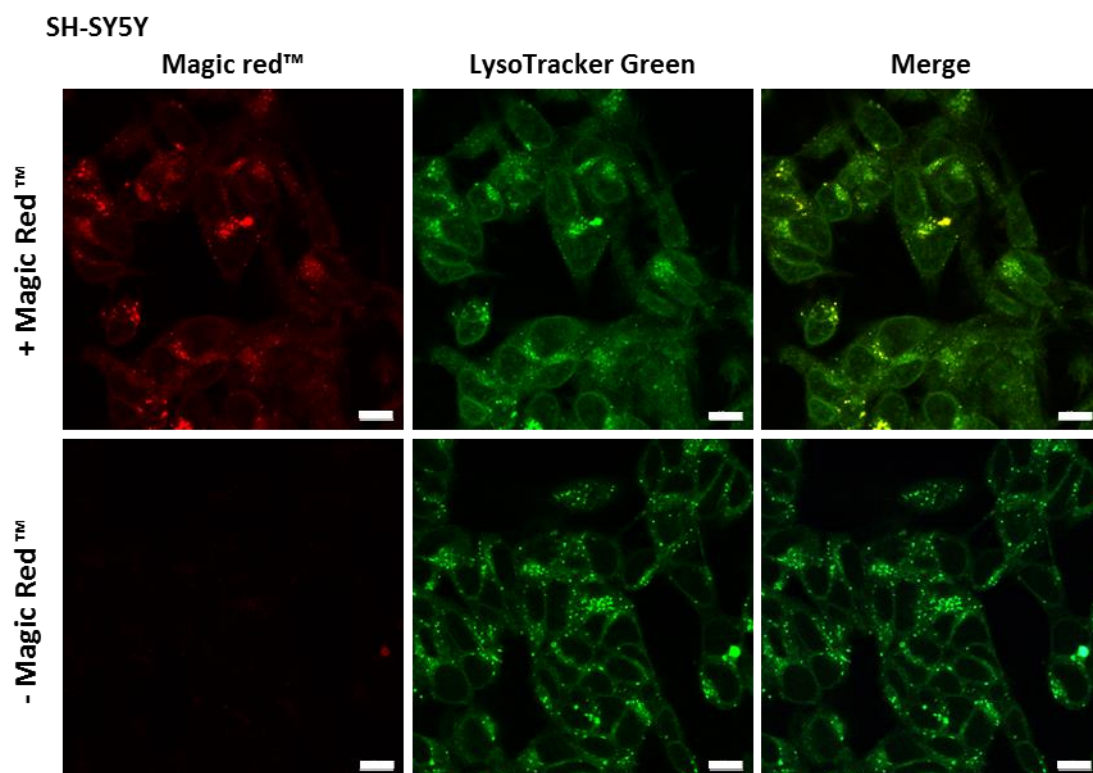


Figure 4.12: Analysis of the internalisation and cleavage of Magic red™ cathepsin B substrate. SH-SY5Y cells were incubated with Magic Red™ cathepsin B substrate (top panel) or in the absence of Magic Red™ cathepsin B substrate (bottom panel) for 1 h. Magic red™ is fluorescent upon cleavage. Cells were washed and stained with LysoTracker Green prior to imaging. Cells were imaged using a Zeiss LSM700 confocal microscope and a 63X objective. Representative confocal images for each condition are shown. Scale bar represents 10 μm .

Having established that Magic Red™ cathepsin B substrate is cleaved in acidic compartments, SH-SY5Y cells were incubated with either fragmented $\beta_2\text{m}$ fibrils or controls (fibril growth buffer and $\beta_2\text{m}$ monomer controls) for 24 h. Cells were then incubated with the Magic Red™ cathepsin B substrate and cell-associated fluorescence was quantified by flow cytometry (Section 2.7.2.1). Cleavage of Magic Red™ cathepsin B substrate was not significantly affected by fragmented fibrils in SH-SY5Y cells (Figure 4.13), suggesting that fibrils do not inhibit cathepsin B activity. Since the Magic Red™ cathepsin B substrate is cell permeable and thus does not require targeted delivery to the lysosome, the decreased lysosome-mediated degradation observed with TMR- $\beta_2\text{m}$, Pumilio-GFP and AF647-ovalbumin could therefore be due to: 1) inhibition of other lysosomal proteases and hydrolases, 2) disruption in endolysosomal trafficking or 3) disruption in targeted delivery of cargo to lysosomes.

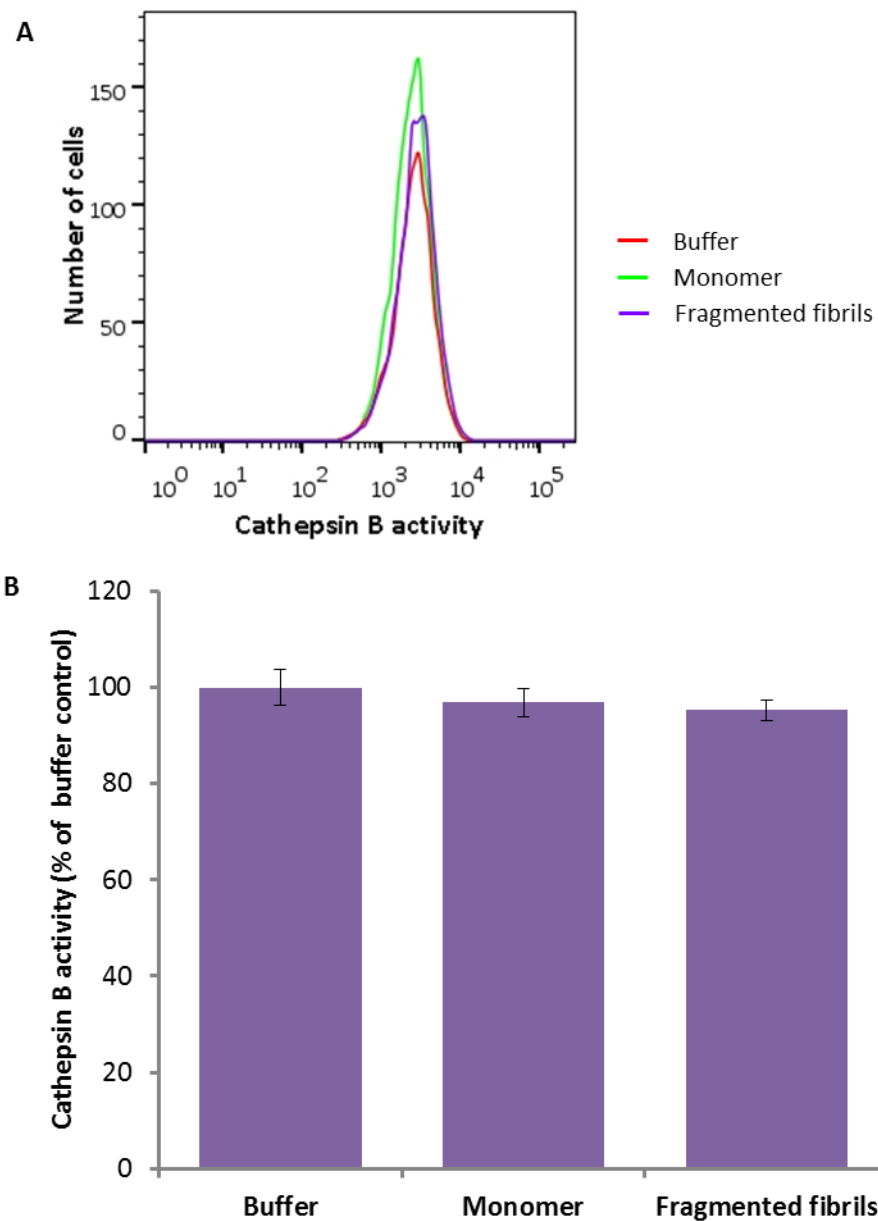


Figure 4.13: Analysis of the effect of fibrils on lysosomal cathepsin B activity. SH-SY5Y cells were incubated with either fragmented β_2m fibrils at a final monomer equivalent concentration of 1.2 μM , 1.2 μM β_2m monomer or fibril growth buffer for 24 h. Cells were then washed and incubated with Magic Red™ cathepsin B substrate for 1 h. Magic Red™ cathepsin B substrate is fluorescent upon cleavage and therefore cell-associated fluorescence gives a measure of cathepsin B activity in cells. Cells were washed and analysed for cell-associated fluorescence by flow cytometry. (A) Representative flow cytometry data comparing cathepsin B activity in buffer, monomer and fibril treated cells. (B) Quantification of flow cytometry data. Cathepsin B activity (%) was calculated by normalising against signal from cells that were incubated with fibril growth buffer (100 %). Error bars represent one S.E.M. over three independent experiments each containing three replicates per condition. Flow cytometry data was collected on a BD LSRFortessa analyser (Becton Dickinson).

4.2.2 Analysis of the effect of fibrils on autophagy

Disruption in autophagy has been heavily implicated in neurodegenerative amyloid diseases (discussed in Section 1.5.4.2.3)[255, 256, 292]. With this precedent in mind, the impairment of the lysosome mediated degradation of exogenously added protein substrates but not of the cell permeant Magic Red™ cathepsin B substrate could indicate disruption in cargo delivery to lysosomes or endolysosomal trafficking. The effect of fibrils on endolysosomal trafficking will be discussed in chapter 5. One of the proposed mechanisms of autophagy disruption in amyloid disease is a perturbation in the delivery of cargo (autophagosomes) to lysosomes which is essential for the formation of functional autolysosomes [255]. Another proposed mechanism is the inhibition of lysosomal mediated degradation in autolysosomes [255]. A preliminary investigation of the effect of fibrils on autophagy was conducted by immunoblotting with an antibody against the B form of LC3, a commonly used autophagy marker [396]. LC3-II is the lipidated form of LC3-I. Lipidation is required for recruitment to autophagosomes and is therefore used as an indicator of autophagy activation. The anti-LC3 B antibody recognises both, LC3-I and LC3-II.

SH-SY5Y cells were incubated with fragmented β_2m fibrils or β_2m monomer as a control for the times indicated. Cells were then lysed and immunoblotted with LC3 B (Section 2.6). Cells incubated with fibrils had an increased amount of LC3-II present (Figure 4.14). Fibrils increase the amount of LC3-II present, as early as 2 h post-treatment. This could be symptomatic of enhanced autophagy, perhaps as a protective mechanism to cope with fibril load but could also be indicative of blocked autophagy due to disruption in the delivery of autophagosomes to lysosomes. A detailed investigation of autophagy is required to be able to distinguish between the two possibilities.

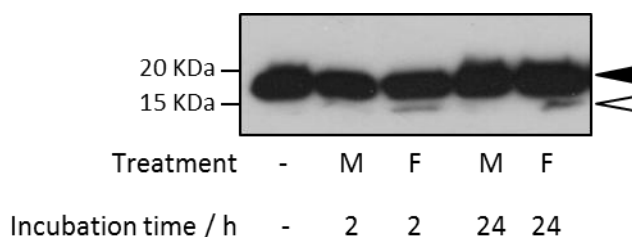


Figure 4.14: Immunoblotting analysis of the effect of fibrils on autophagy with LC3B. SH-SY5Y cells were incubated with 1.2 μ M monomer (M) or 1.2 μ M (monomer equivalent) fragmented fibrils (F) for the times indicated. Cells were then lysed and immunoblotted with LC3B. LC3-I (filled arrow) and LC3-II (open arrow) are detected in the cell lysates.

4.2.3 Analysis of the effect of fibrils on the lysosomal hydrolase, β -glucocerebrosidase

In order to investigate whether fragmented β_2m fibrils had an effect on other lysosomal hydrolases, β -glucocerebrosidase was selected for further analysis into lysosomal function. β -glucocerebrosidase is a lysosomal hydrolase that cleaves glucocerebroside to yield glucose and ceramide. β -glucocerebrosidase is mutated in Gaucher's disease, and it is of particular interest due to the association of Parkinson's disease and Gaucher's disease (discussed in Section 1.5.4.2.4)[288, 311, 312, 316].

The effect of fibrils on β -glucocerebrosidase activity was investigated (Section 2.7.3). This was achieved by using 5-(pentafluorobenzoylamino)fluorescein di- β -D-glucopyranoside (PFB-FDGlu), a commercially available non-fluorescent substrate for β -glucocerebrosidase. PFB-FDGlu is cleaved by glucocerebrosidase to yield the green fluorescent PFB-F product. As fluorescence is dependent on cleavage, cell-associated fluorescence can be used as a measure of β -glucocerebrosidase activity [397].

β -glucocerebrosidase activity was measured in intact and living SH-SY5Y cells. Glucocerebroside is primarily cleaved in the cell by β -glucocerebrosidase. However, a non-lysosomal glucocerebrosidase, termed β -glucosidase 2, also exists and may account for a small percentage of the cleavage of PFB-FDGlu [398]. The two enzymes differ in their sensitivity to conduritol B epoxide (CBE) which inhibits β -glucocerebrosidase but has no effect on β -glucosidase 2 [398]. CBE therefore serves as a tool to distinguish between PFB-F fluorescence due to specific cleavage of PFB-FDGlu by β -glucocerebrosidase and cleavage due to β -glucosidase 2. CBE inhibits glucocerebrosidase activity by 70 % therefore indicating that 70 % of total PFB-FDGlu is cleaved by β -glucocerebrosidase, the lysosomal glucocerebrosidase (Figure 4.15). In contrast to the enzyme inhibitor, CBE, fragmented fibrils do not have a significant effect on β -glucocerebrosidase activity.

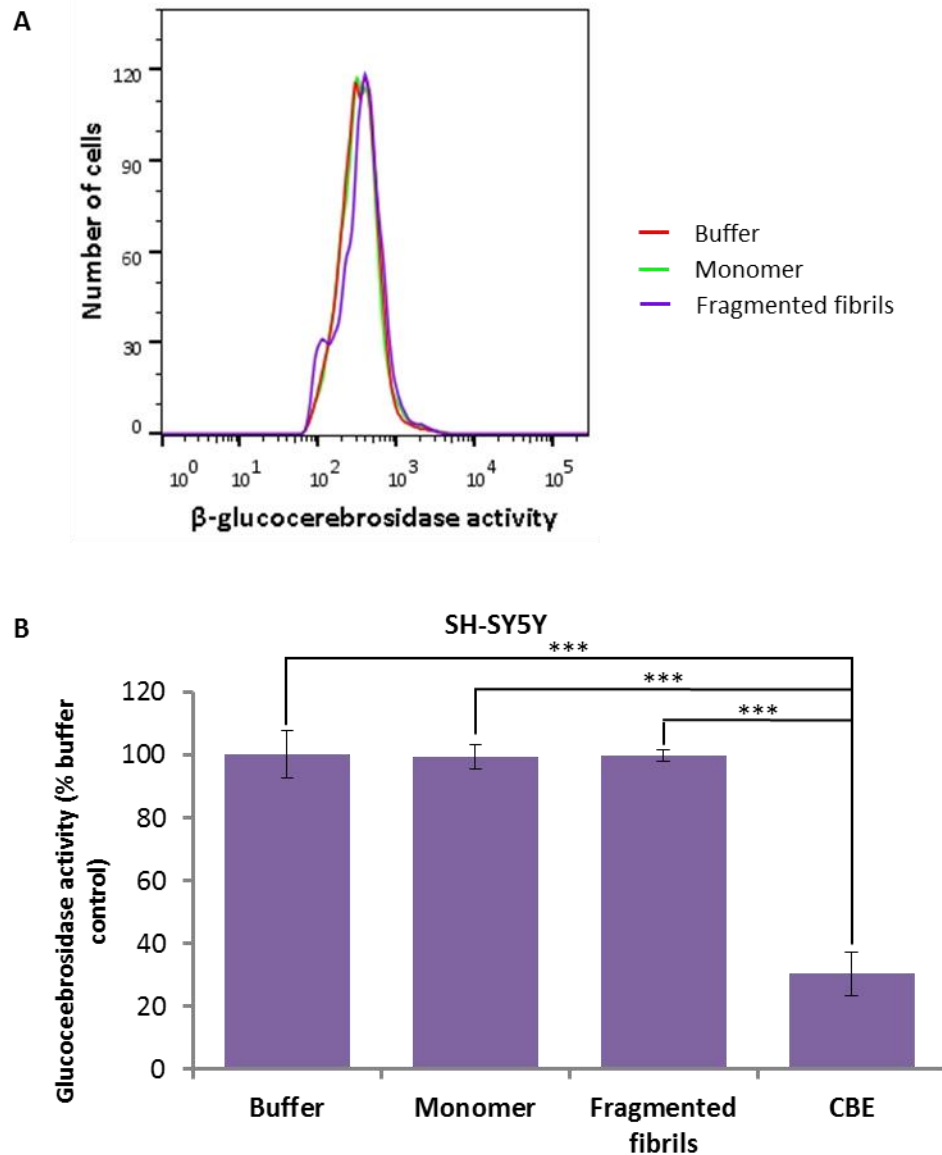


Figure 4.15: Analysis of the effect of fibrils on glucocerebrosidase activity. SH-SY5Y cells were incubated with either fragmented β_2m fibrils at a final monomer equivalent concentration of $1.2 \mu\text{M}$ or $1.2 \mu\text{M}$ β_2m monomer for 24 h. Fibril growth buffer and CBE treated cells were included as controls. Cells were then washed and incubated with β -glucocerebrosidase substrate (PFB-FDGlu) for 1 h. PFB-FDGlu is fluorescent upon cleavage, therefore cell-associated fluorescence gives a measure of glucocerebrosidase activity in cells. Cells were washed and analysed for cell-associated fluorescence by flow cytometry. (A) Representative flow cytometry data comparing glucocerebrosidase activity in fibril, monomer and buffer-treated cells. (B) Quantification of flow cytometry data. Glucocerebrosidase activity (%) was calculated by normalising against signal from cells incubated with fibril growth buffer (100 %). Error bars represent one S.E.M. over two independent experiments each containing three replicates per condition. Flow cytometry data was collected on a BD LSRFortessa analyser (Becton Dickinson). *** indicates a p value of <0.001 .

4.2.4 Analysis of the effect of fibrils on the lysosomal hydrolase, β -galactosidase

Analysis of the effect of fibrils on lysosomal function was extended by assaying the activity of another lysosomal hydrolase, β -galactosidase. β -galactosidase is a glycosidase which cleaves the commercially available non-fluorescent substrate fluorescein di- β -D-galactopyranoside (FDG) to yield fluorescein. FDG has been used as a substrate to measure β -galactosidase activity in intact and living cells by flow cytometry [399].

SH-SY5Y cells were incubated with either fragmented β_2m fibrils or controls (fibril growth buffer and β_2m monomer) as controls for 24 h. This was followed by incubation with FDG for 1 h prior to analysis by flow cytometry (Section 2.7.3). Fragmented fibrils have a small but significant inhibitory effect on β -galactosidase activity when compared to cells treated with fibril growth buffer (Figure 4.16).

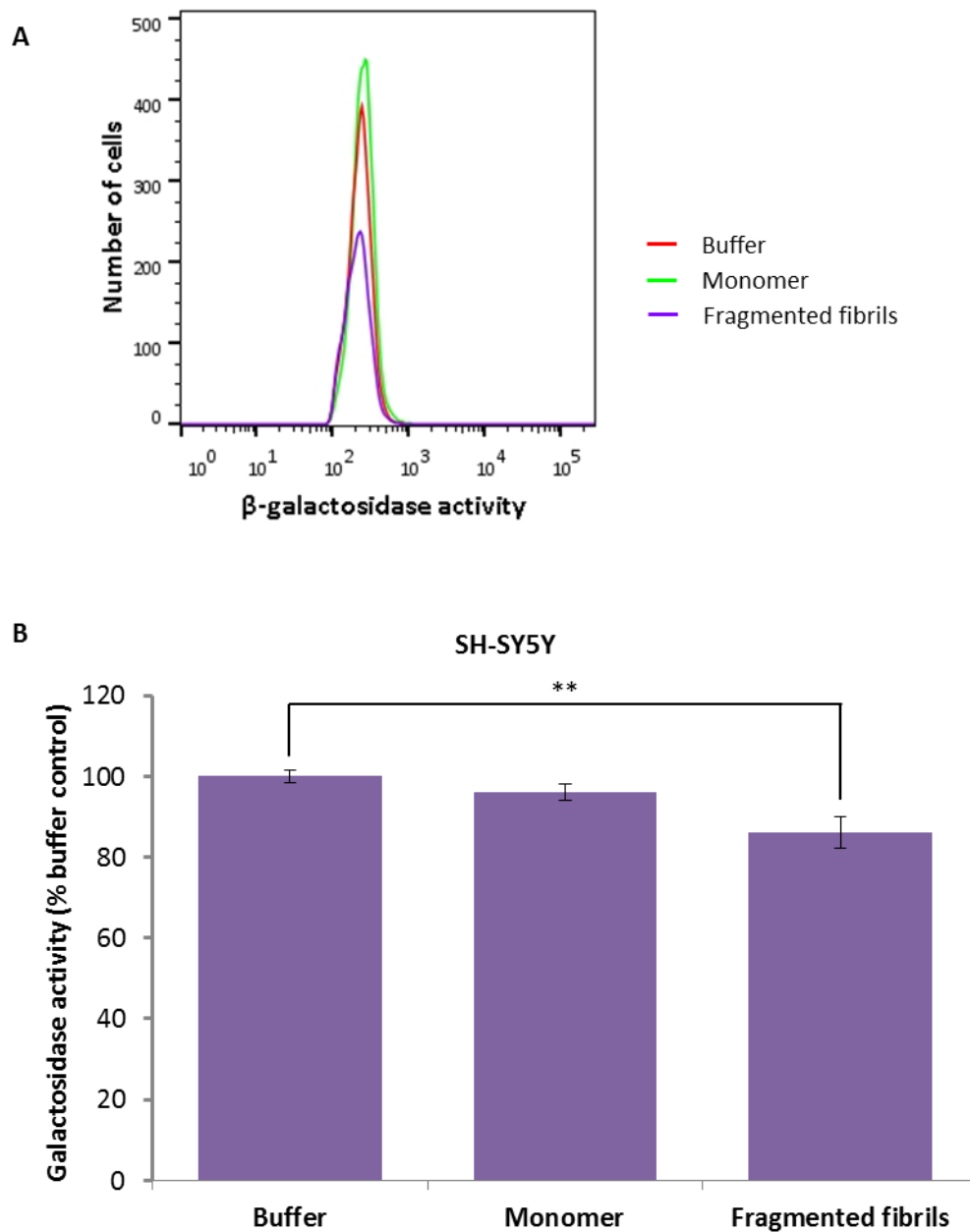


Figure 4.16: Analysis of the effect of fibrils on β -galactosidase activity. SH-SY5Y cells were incubated with either fragmented β_2m fibrils at a final monomer equivalent concentration of 1.2 μ M, 1.2 μ M β_2m monomer or fibril growth buffer for 24 h. Cells were then washed and incubated with β -galactosidase substrate (FDG) for 1 h. FDG is fluorescent upon cleavage, therefore cell-associated fluorescence gives a measure of β -galactosidase activity in cells. Cells were washed and analysed for cell-associated fluorescence by flow cytometry. (A) Representative flow cytometry data comparing β -galactosidase activity in fibril, monomer and buffer-treated cells. (B) Quantification of flow cytometry data. β -galactosidase activity (%) was calculated by normalising against signal from cells incubated with fibril growth buffer (100 %). Error bars represent one S.E.M. over three independent experiments each containing three replicates per condition. Flow cytometry data was collected on a BD LSRFortessa analyser (Becton Dickinson). ** indicates a p value of <0.01.

4.3 Discussion

Internalisation of exogenously applied amyloid material *in vitro* allowing access to endocytic compartments has been widely reported in the literature for a range of disease-associated amyloid aggregates [240-245, 247, 248, 400]. This could be relevant to extracellular amyloid aggregates that accumulate *in vivo* such as A β , IAPP and β_2m amongst others. Internalisation of amyloid aggregates and access to endocytic compartments may also be relevant to disease-associated amyloid proteins which form intracellular inclusions *in vivo* such as α -synuclein. α -synuclein has been reported to be secreted into cerebrospinal fluid, thus allowing for the potential to aggregate extracellularly prior to internalisation [401]. Furthermore, intracellular α -synuclein amyloid aggregates have been reported to induce neuronal death, which then facilitates leakage of α -synuclein amyloid aggregates into the extracellular space, resulting in spread to neighbouring cells which internalise these aggregates allowing access to endocytic compartments (reviewed in [402]). Upon internalisation, amyloid aggregates accumulate in the lysosome and increasing evidence points towards disruption of the lysosomal compartment in amyloid disease. This has been discussed in detail in (Section 1.5.4.2). Based on this precedent, and the trafficking of fragmented β_2m fibrils to the lysosome, the lysosome was selected for further investigation. Experiments were limited to fragmented fibrils due to their greater access to the lysosome.

One of the reported mechanisms of lysosomal dysfunction in amyloid disease is perturbation of lysosomal degradation. For example, overexpression of human IAPP in rodent models leads to the formation of IAPP oligomers, which have been shown to inhibit lysosome dependent degradation, which in turn impairs autophagy [289]. Lysosomal degradation is a key function of the lysosome and its impairment has been shown to be detrimental to cell health. Inhibition of lysosomal proteolysis in primary neurons has been shown to retard axonal transport of autolysosomes, late endosomes and lysosomes resulting in their accumulation in axonal swellings causing an Alzheimer's like axonal dystrophy [284]. On the other hand, enhancement of proteasomal and lysosomal mediated degradation results in the rescue of toxicity from A β and Huntingtin aggregates [285, 286]. Impairment of lysosomal proteolysis could therefore have significant consequences on cell health and disease progression.

The effect of fragmented fibrils on lysosomal degradation was therefore assayed. Fragmented fibrils inhibit the degradation of endocytosed proteins, but do not inhibit cleavage of the membrane permeant Magic Red™ cathepsin B substrate (Figure 4.3, Figure 4.4, Figure 4.5, Figure 4.10, Figure 4.11 and Figure 4.13). This could be due to a saturation of the proteolytic machinery with fibrils overwhelming lysosomal proteases other than cathepsin B; or due to a

disruption in endolysosomal trafficking by fibrils without significantly inhibiting lysosomal proteases. Impaired endolysosomal trafficking would disrupt delivery of cargo containing lysosomal substrates to the lysosome. Future experiments on other lysosomal proteases such as cathepsins K and L using membrane permeant substrates, would help establish whether or not fibrils saturate the proteolytic machinery. In addition, disruption to the lysosomal membrane has been frequently reported as a mechanism underlying both Alzheimer's disease and Parkinson's disease [242, 245, 251, 263] (Section 1.5.4.2.1). Lysosomal membrane damage would result in alteration of lysosomal pH and globally inhibit lysosomal hydrolases. Fragmented fibrils, however, do not have a significant effect on β -glucocerebrosidase activity and only have a modest effect on β -galactosidase activity. This provides evidence against gross damage to the lysosomal membrane as a mechanism for impairment in degradation of endocytosed proteins. Further evidence for this comes from ongoing work by other members of the laboratory which demonstrates that fragmented fibrils do not have a detectable effect on the integrity of the lysosomal membrane (Eric Hewitt, personal communications and Figure 4.17).

Autophagy dysfunction has been repeatedly connected to neurodegenerative diseases and has been proposed as an underlying mechanism for disease progression [255, 256]. The effect of fragmented fibrils on autophagy was therefore analysed by immunoblotting in preliminary experiments. One of the first clues to altered autophagy is the accumulation of autophagosomes [255]. Indeed, autophagosomal accumulation has been reported in neurodegenerative diseases [255, 261, 290, 291]. Active autophagosomes recruit LC3-II and the level of LC3-I and LC3-II relative to each other is used as a marker to report autophagy [396]. An increase in LC3-II levels could result from upregulated autophagy (due to increased production of autophagosomes) but paradoxically could also result from impaired autophagy (due to a block in delivery of autophagosomes to lysosomes or impaired autolysosomal clearance) [255, 293]. Interpretation of upregulated autophagy or blocked autophagy should therefore be approached with caution. Immunoblotting analysis with an anti-LC3-B antibody provides interesting preliminary evidence of altered autophagy in response to fibrils (Figure 4.14). In combination with data from experiments showing a fibril-mediated disruption in degradation of endocytosed proteins but not of the membrane permeant Magic Red™ cathepsin B substrate; this fibril-mediated increase in autophagosomes could indicate a disruption of cargo delivery to the lysosome. However, further experiments need to be conducted before an assessment of the direction of effect on autophagy can be made. Future

experiments should aim to distinguish between defects in autophagy induction, cargo sequestration and autophagosome clearance.

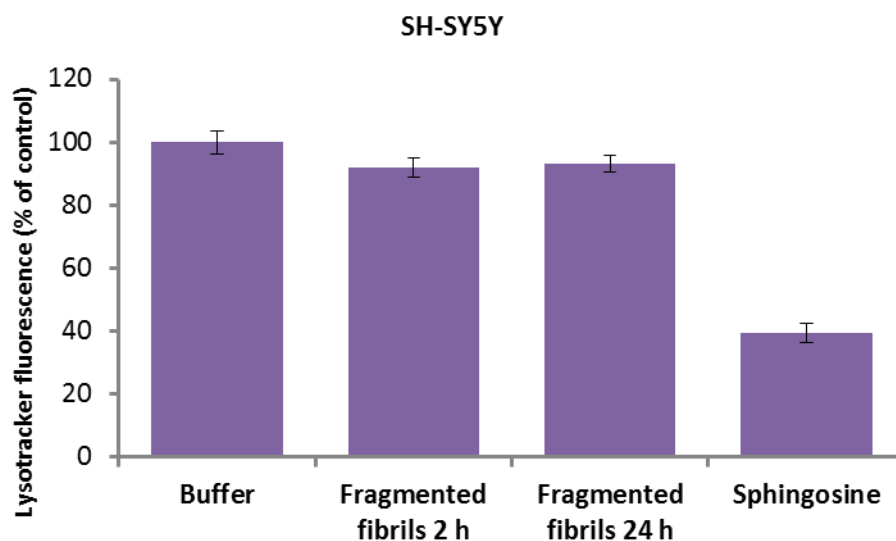


Figure 4.17: Analysis of the effect of fragmented fibrils on lysosomal membrane permeabilisation. SH-SY5Y cells were incubated with fragmented fibrils at a final concentration of 1.2 μM (monomer equivalent) for 2 or 24 h. Cells were then incubated with LysoTracker Green and cell-associated fluorescence was quantified by flow cytometry. Sphingosine, which causes lysosomal rupture and thus disrupts lysosomal pH was included as a positive control. Cells were incubated with 15 μM sphingosine for 15 min prior to LysoTracker Green staining. As LysoTracker Green accumulates in acidic vesicles, LysoTracker green staining reflects the amount of intact lysosomes in a cell. LysoTracker green fluorescence (%) was calculated by normalising against signal from control cells incubated with fibril growth buffer (100 %). Error bars represent one S.E.M. over three independent experiments containing three replicates each. Flow cytometry data was collected on a BD LSRFortessa analyser. Experiment performed by Eric Hewitt, University of Leeds.

A decrease in lysosome mediated degradation through the delivery of cargo to lysosomes, could impact upon autophagy. Autophagosome clearance relies on delivery of autophagosomes to lysosomes, and alterations in autophagosome clearance have been recurrently implicated in neurodegenerative disorders [255]. Accumulation of undigested substrates and the decreased content or activity of lysosomal hydrolases could result in degradative failure of lysosomes leading to defective autophagosome clearance [255]. The accumulation of autophagosomes is proposed to be detrimental to cellular function by interfering with intracellular trafficking [403]. In addition, autophagosomes have been shown to act as an endogenous source of $\text{A}\beta_{1-42}$ in cellular and animal models due to the accumulation of APP and proteases in autophagosomes [403]. Aged autophagosomes that persist in the

cytosol can suffer from a loss of membrane integrity and can release enclosed aggregating proteins which could induce aggregation of cytosolic proteins [255].

This chapter demonstrates that fragmented β_2m fibrils disrupt lysosomal mediated degradation of endocytosed proteins, but do not have a general inhibitory effect on lysosomal hydrolases. Defects in endolysosomal trafficking would impair delivery of cargo to lysosomes and may rationalise the observed differences on the effect of fibrils on lysosomal proteolysis (Figure 4.3, Figure 4.4, Figure 4.5, Figure 4.10, Figure 4.11 and Figure 4.13). The effect of fibrils on endolysosomal trafficking is discussed in the following chapter.

5 Analysis of the effect of amyloid fibrils on membrane trafficking

5.1 Introduction

Membrane trafficking describes the journey that proteins make, beginning with entry into the early secretory pathway at the ER, followed by transition via the Golgi apparatus to their final destination such as the extracellular milieu, plasma membrane or other intracellular organelles [404]. It also includes the internalisation of proteins from the plasma membrane, their recycling back to the plasma membrane or targeted delivery to the lysosome after movement through the late endosome and multivesicular body (MVB) compartments [404]. Proteins are mainly transferred through the cell in many different vesicular bodies. These vesicles can undergo fission, docking and fusion events between donor and acceptor compartments [405]. These vesicles, whether derived from the ER, other intracellular organelles or the plasma membrane, are decorated with unique protein complexes, as well as tethering and regulatory factors which target the vesicle to its acceptor compartment [404]. For example, the SNARE (soluble *N*-ethylmaleimide-sensitive fusion attachment protein receptor) proteins are a highly conserved group of proteins which have been found to regulate membrane trafficking [406]. SNARE proteins are present on both the vesicle and the acceptor and contain coiled-coiled domains which come together to enable vesicle docking and fusion [407]. Ras-related Rab GTPases are another family of proteins which in conjunction with SNARE proteins have been shown to be involved in the regulation of membrane trafficking [408].

Alterations in membrane trafficking are associated with the pathogenesis of amyloid diseases such as Parkinson's disease and Alzheimer's disease [394, 395]. Evidence of the association of Parkinson's disease and trafficking defects first came from the observation of abnormal interactions of Rab3a, Rab5 and Rab8 with mutant (A30P) but not wild-type α -synuclein in transgenic mice models [409]. In studies using a yeast model of Parkinson's disease, α -synuclein was shown to block ER-to-Golgi vesicular trafficking. Interestingly, the overexpression of Rab1, which is involved in the forward ER-to-Golgi trafficking process, rescued α -synuclein induced-toxicity in yeast, *Drosophila* and *C. elegans* models as well as in primary rat neurons [410]. In a follow up study from the same group, α -synuclein was shown to impair multiple trafficking steps *in vitro*, and Rab3a and Rab8a were demonstrated to ameliorate toxicity in neuronal models of Parkinson's disease [411]. Genome wide association studies have identified genes encoding LRRK2 and Rab7L1 as risk factors in Parkinson's disease.

Importantly, disease-associated defects in Rab7L1 and LRRK2 were shown to cause endolysosomal and Golgi sorting defects [412].

Genome wide association studies have also demonstrated links between defects in membrane trafficking and Alzheimer's disease. For example, several genes involved in the recycling of endosomal vesicles have been implicated, such as bridging integrator 1 (*BIN1*), phosphatidylinositol-binding clathrin assembly protein (*PICALM*) and sortilin-related receptor 1 (*SORL1*) (reviewed in [394]). Like with Parkinson's disease, yeast models of Alzheimer's disease have been useful in connecting disruptions in membrane trafficking to disease pathogenesis. Endocytic trafficking defects, in particular disruptions in clathrin-mediated endocytosis were highlighted as pathogenic factors in a genome-wide toxicity screen in a yeast model of Alzheimer's disease [323]. The demonstration of small molecules which restore endocytosis to ameliorate toxicity in yeast models of Alzheimer's disease provides further evidence for a pathogenic role of membrane trafficking defects [413]. Lastly, perturbations in membrane trafficking are implicated in other amyloid diseases. Aggregates from the amyloidogenic proteins huntingtin, ataxin-1 and superoxide dismutase-1 (*SOD1*) have been shown to inhibit clathrin-mediated endocytosis in mammalian cells [414].

A closer investigation of the effect of fragmented β_2m fibrils on membrane trafficking was prompted by two observations. The first was the observation of a greater amount of formazan needles in response to fibril treatment (Figure 3.17). This suggests an alteration in the trafficking of MTT and/or its reduced form, formazan, in fibril-treated cells. The second was the demonstration of fibril-mediated impairment in lysosomal degradation of endocytosed proteins, which could potentially be due to altered endolysosomal trafficking (Figure 4.10 and Figure 4.11). Investigation of membrane trafficking was achieved by analysing the localisation of the lysosomal membrane proteins LAMP-1 (lysosomal associated membrane protein 1) and CD63 (cluster of differentiation 63). LAMP-1 is an abundant lysosomal membrane protein which is involved in lysosomal trafficking by mediating attachment of lysosomes to transport machinery [280]. CD63, also known as LAMP-3, is a tetraspanin which interacts either directly or indirectly with many different proteins such as cell surface receptors, adaptor proteins, integrins and other tetraspanins [415]. LAMP-1 and CD63 are not static components of the lysosomal membrane; they have been shown to be in dynamic equilibrium between lysosomes, endosomes and the plasma membrane [416]. The trafficking of LAMP-1 and CD63 has been studied in some detail (Figure 5.1). Newly synthesised LAMP-1 and CD63 are transported from the TGN to the endolysosomal compartment mainly via an intracellular route [416]. A small portion of newly synthesised LAMP-1 and CD63 is trafficked to the plasma

membrane [415, 417]. Although most LAMPs mainly reside in the lysosome, their cell surface expression has been reported; for example during the activation of platelets and cytotoxic T cells as well as in highly malignant tumour cells [280]. The elevated cell surface expression of CD63 impacts other local protein concentrations due to its ability to interact with an array of proteins [415]. The consequences of increased levels of LAMP-1 at the cell surface are not well understood but have been associated with lysosomal exocytosis [418]. Lysosomal exocytosis is required for plasma membrane repair and the correct functioning of cytotoxic lymphocytes [419, 420].

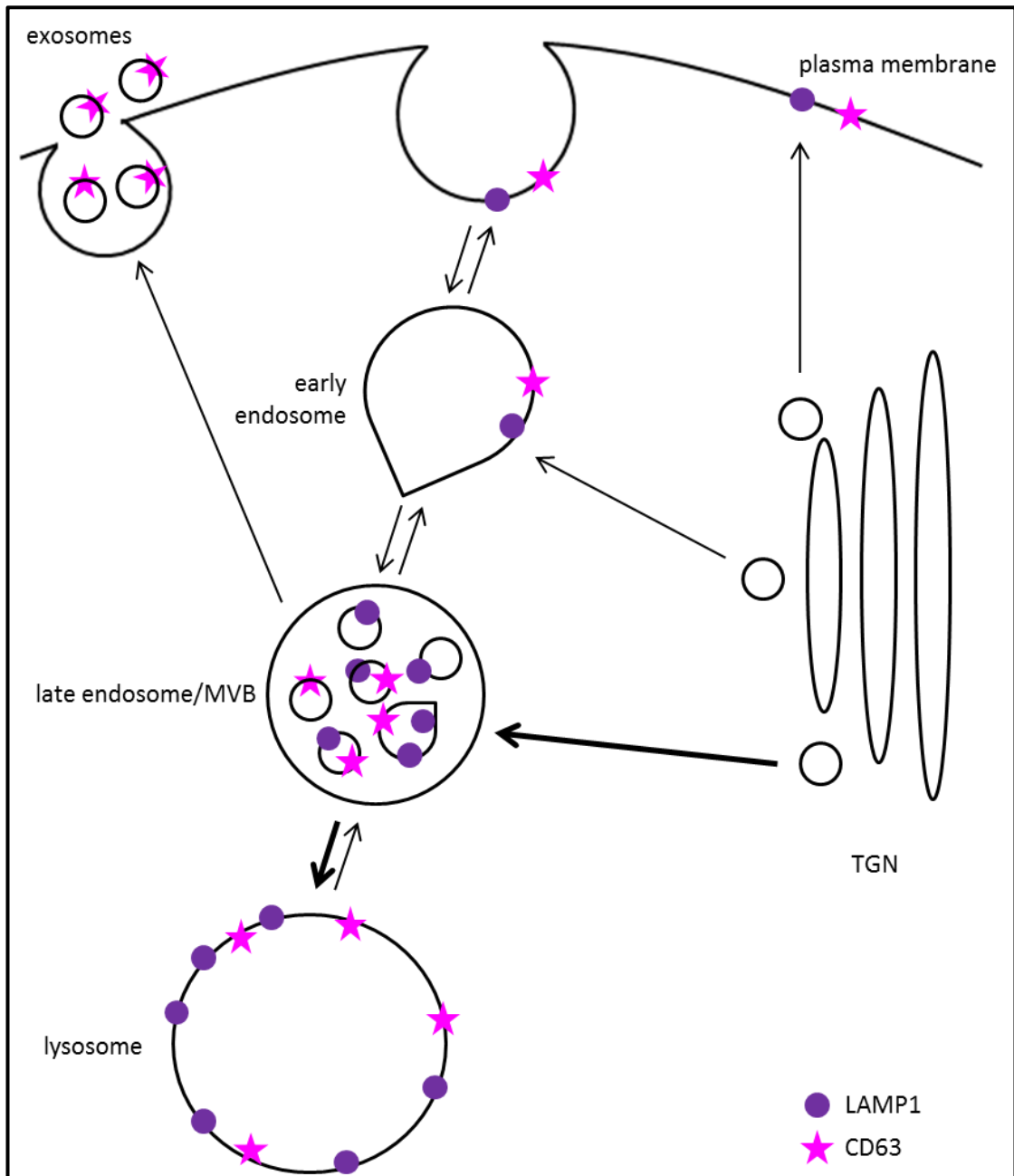


Figure 5.1: Overview of LAMP-1 and CD63 trafficking. After biosynthesis, newly synthesised LAMP-1 and CD63 are transported from the TGN predominantly to endosomes via a direct intracellular pathway, or to the plasma membrane via an exocytic pathway. At the plasma membrane, LAMP-1 and CD63 are endocytosed and progress to mature lysosomes via late endosomes/multivesicular bodies (MVBs); however CD63 can also be recycled to the cell surface. In late endosomes/MVBs, CD63 is enriched in the intraluminal vesicles, which in certain conditions can be released into the extracellular space as exosomes. Adapted from [415-417].

This chapter describes experiments that investigate the effect of fragmented fibrils on membrane trafficking. This was achieved by investigating the cell surface expression, subcellular localisation and total cellular levels of LAMP-1 and CD63. In order to examine

whether the impaired degradation of endocytosed proteins by fragmented β_2m fibrils (Figure 4.10 and Figure 4.11) was due to compromised delivery of cargo to the lysosome, a preliminary investigation on the effect of fibrils on fluid phase endocytosis was undertaken and will also be discussed.

5.2 Results

5.2.1 Analysis of the effect of fibrils on the cell surface expression of LAMP-1 and CD63

Newly synthesised LAMP-1 and CD63 are trafficked to the lysosome predominantly via an intracellular route, however, a small amount of LAMP-1 and CD63 is trafficked to the plasma membrane [415, 417](Figure 5.1). LAMP-1 and CD63 may play a functional role at the plasma membrane or transit through the plasma membrane. These proteins are internalised from the plasma membrane and directed towards the lysosome or recycled back to the plasma membrane (Figure 5.1). A comparison of the levels of LAMP-1 and CD63 at the plasma membrane between controls and fibril treated cells may provide insights into the effect of fibrils on membrane trafficking. The cell-surface levels of LAMP-1 and CD63 were measured by incubation of non-permeabilised cells with fluorescently labelled antibodies followed by flow cytometric analysis (Section 682.8.1).

SH-SY5Y cells were incubated with fragmented β_2m fibrils or β_2m monomer as a control. Blocking agents were used to minimise non-specific binding before incubation with LAMP-1 or CD63 specific antibodies. Additional controls incubated with matched isotype control antibodies (which are of the same isotype and have the same fluorescent label, but are not specific for any cellular proteins) were included for each experimental condition. Isotype controls were used to subtract any non-specific binding of antibodies. Cells incubated with fragmented fibrils have a significant increase in the cell surface expression of LAMP-1 (Figure 5.2). This effect is observed after just 2 h of fibril incubation as well as 24 h after fibril incubation. Incubation with fragmented fibrils also significantly enhances the cell-surface expression of CD63 (Figure 5.3). This increase is more pronounced, and is also observed as early as 2 h after fibril incubation and still detected after 24 h of fibril incubation.

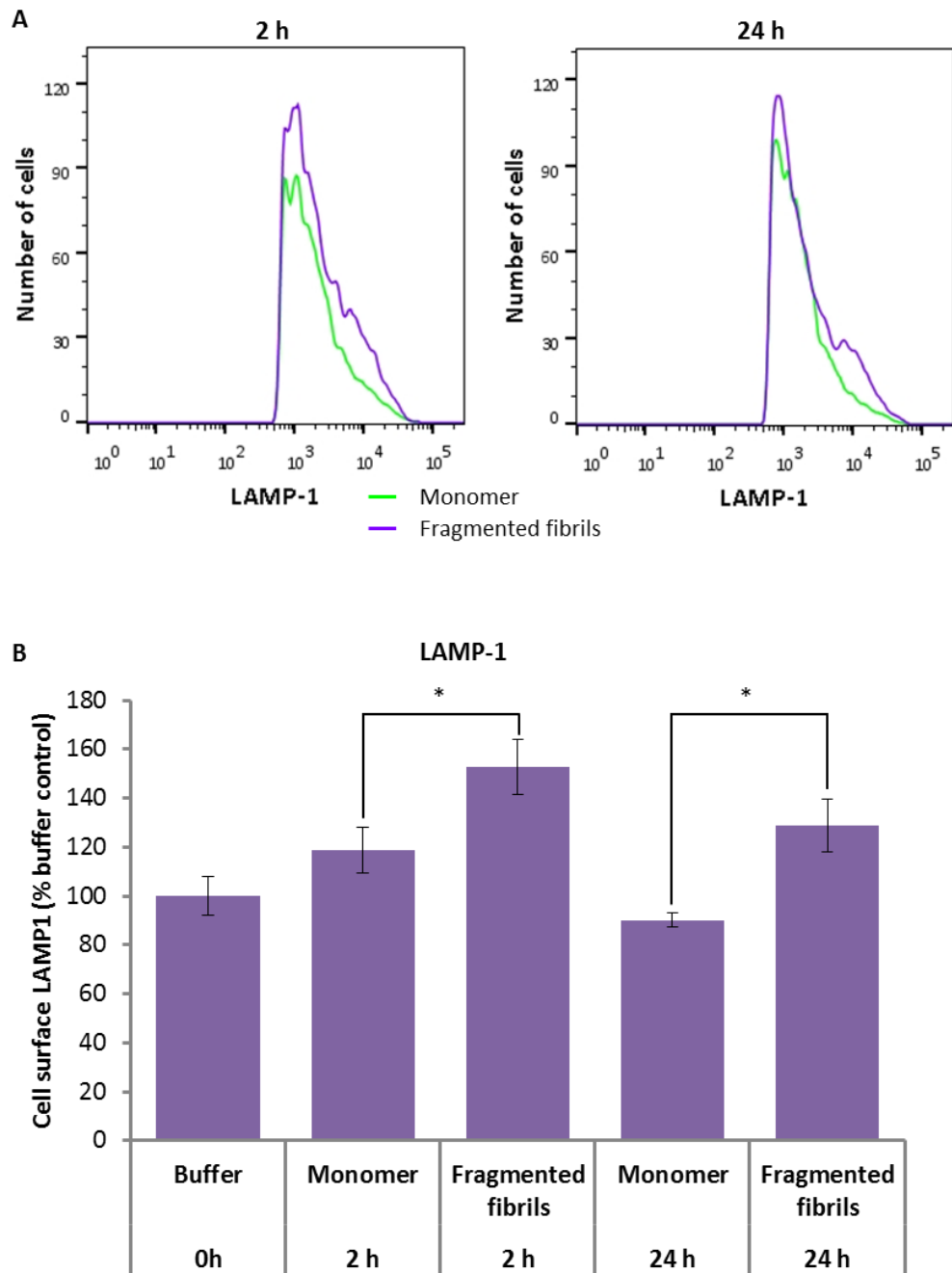


Figure 5.2: Analysis of the effect of fibrils on the cell surface expression of LAMP-1. SH-SY5Y cells were incubated with 1.2 μM $\beta_2\text{m}$ monomer or 1.2 μM (monomer equivalent) fragmented $\beta_2\text{m}$ fibrils for the times indicated. Cells were then stained with a fluorescently labelled antibody specific for LAMP-1 and cell-associated fluorescence was quantified by flow cytometry. (A) Representative flow cytometry data comparing cell surface LAMP-1 expression between monomer and fibril treated cells. (B) Quantification of flow cytometry data. Cell surface LAMP-1 (%) was calculated by normalising to signal from cells that were incubated with fibril growth buffer for 0 h (100 %). Error bars represent one S.E.M. over three independent experiments each containing three replicates each. * signifies a p value of <0.05. Flow cytometry data was collected on a BD LSRFortessa analyser (Becton Dickinson).

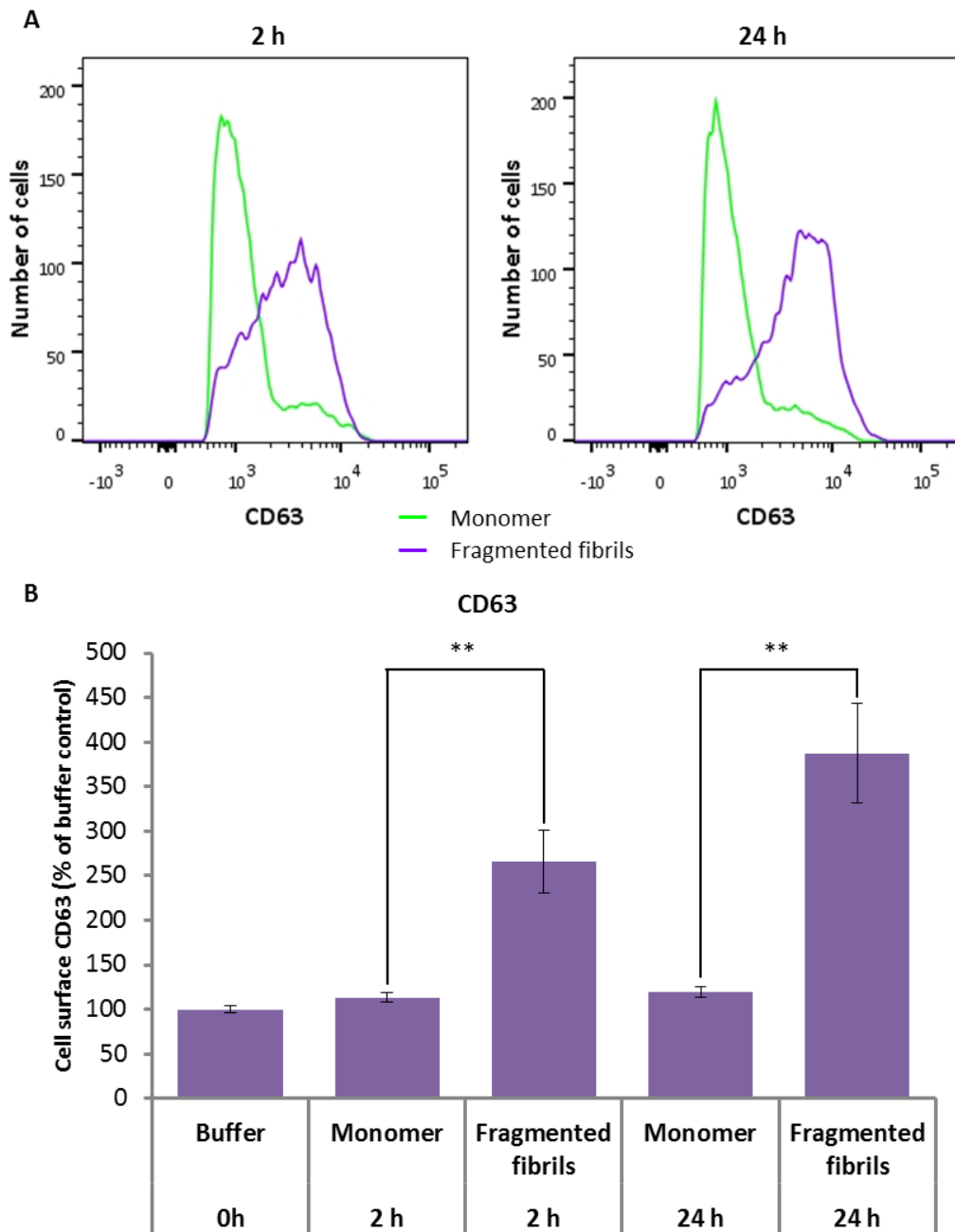


Figure 5.3: Analysis of the effect of fibrils on the cell surface expression of CD63. SH-SY5Y cells were incubated with 1.2 μM $\beta_2\text{m}$ monomer or 1.2 μM (monomer equivalent) fragmented $\beta_2\text{m}$ fibrils for the times indicated. Cells were then stained with a fluorescently labelled antibody specific for CD63 and cell-associated fluorescence was quantified by flow cytometry. (A) Representative flow cytometry data comparing cell surface CD63 expression between monomer and fibril treated cells. (B) Quantification of flow cytometry data. Cell surface CD63 (%) was calculated by normalising to signal from cells that were incubated with fibril growth buffer for 0 h (100 %). Error bars represent one S.E.M. over three independent experiments each containing three replicates each. ** signifies a p value of <0.01. Flow cytometry data was collected on a BD LSRFortessa analyser (Becton Dickinson).

5.2.2 Immunoblotting analysis of the effect of fibrils on lysosomal protein expression

The increased cell surface expression of LAMP-1 and CD63 could be due to an increase in the overall expression of LAMP-1 and CD63, or due to a re-distribution of LAMP-1 and CD63. In order to investigate whether fragmented fibrils increased the overall expression of LAMP-1 and CD63, the total cellular levels of these proteins were assessed by immunoblotting. SH-SY5Y cells were incubated with fragmented β_2m fibrils or β_2m monomer as a control. Cell lysates were immunoblotted with antibodies specific for LAMP-1 and CD63 (Section 2.6) and for GAPDH as a loading control. Total levels of LAMP-1 and CD63 were comparable for monomer and fibril treated cells indicating that fragmented fibrils do not increase the expression of LAMP-1 and CD63 (Figure 5.4). In order to investigate whether fragmented fibrils induced a compensatory increase in proteins involved in lysosomal degradation, the total cellular levels of the lysosomal hydrolase, cathepsin D were also analysed by immunoblotting (Section 2.6). As with LAMP-1 and CD63, levels of cathepsin-D were not affected by fibril treatment (Figure 5.4).

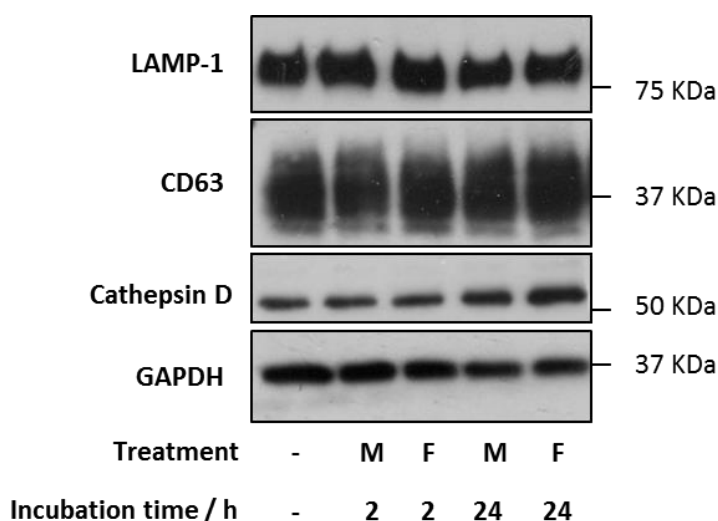


Figure 5.4: Immunoblotting analysis of the effect of fibrils on total levels of LAMP-1, CD63 and Cathepsin-D. SH-SY5Y cells were incubated with 1.2 μ M β_2m monomer (M) or 1.2 μ M (monomer equivalent) fragmented β_2m fibrils (F) for the times indicated. Cells were then lysed and probed with antibodies specific for LAMP-1, CD63 or cathepsin D. Representative blots from three independent experiments are shown.

5.2.3 Immunofluorescence microscopy analysis of the effect of fibrils on the intracellular distribution of LAMP-1 and CD63

In order to investigate whether the increased expression of LAMP-1 and CD63 at the cell surface was due to a major re-distribution of existing pools of LAMP-1 and CD63 by fragmented fibrils, the intracellular distributions of LAMP-1 and CD63 were analysed by immunofluorescence microscopy. SH-SY5Y cells were cultured on coverslips and incubated with fragmented β_2m fibrils or β_2m monomer as a control. Cells were permeabilised and stained with anti-LAMP-1 or anti-CD63 antibodies. Despite subtle variations in antibody staining, a gross change in the intracellular distribution of LAMP-1 and CD63 was not observed (Figure 5.5 and Figure 5.6). The increase in the cell-surface levels of LAMP-1 and CD63 measured by flow cytometry (Figure 5.2 and Figure 5.3) is therefore likely to represent a small percentage of total LAMP-1 and CD63.

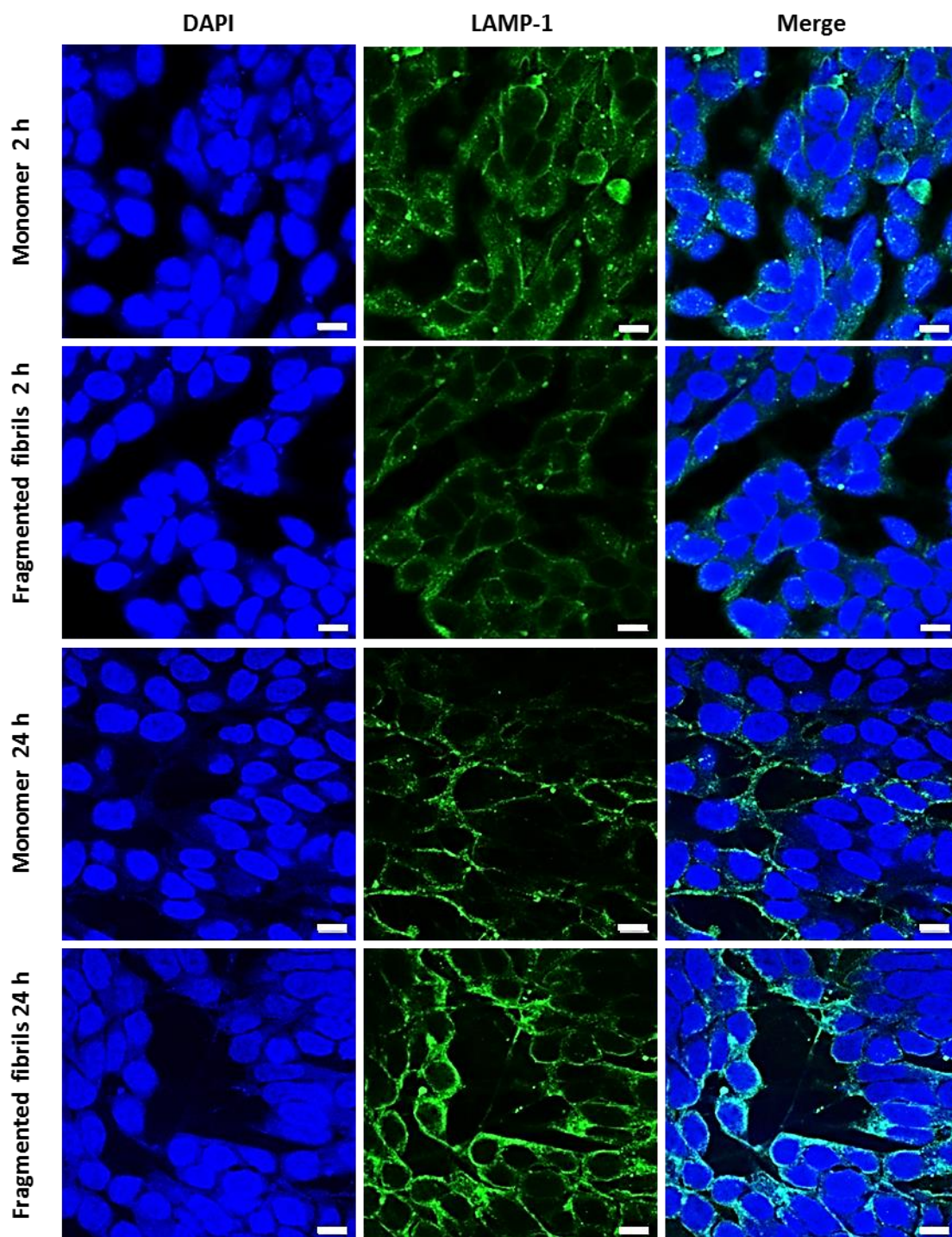


Figure 5.5: Immunofluorescence microscopy analysis of the effect of fibrils on the distribution of LAMP-1. SH-SY5Y cells were incubated with 1.2 μM $\beta_2\text{m}$ monomer or 1.2 μM (monomer equivalent) fragmented $\beta_2\text{m}$ fibrils for the indicated times. Cells were then fixed, permeabilised and stained with an anti-LAMP-1 antibody followed by a fluorescently labelled anti-mouse secondary antibody. Coverslips were imaged using a Zeiss LSM700 confocal microscope and a 63X objective. Representative confocal images for each condition are shown. Scale bar represents 10 μm .

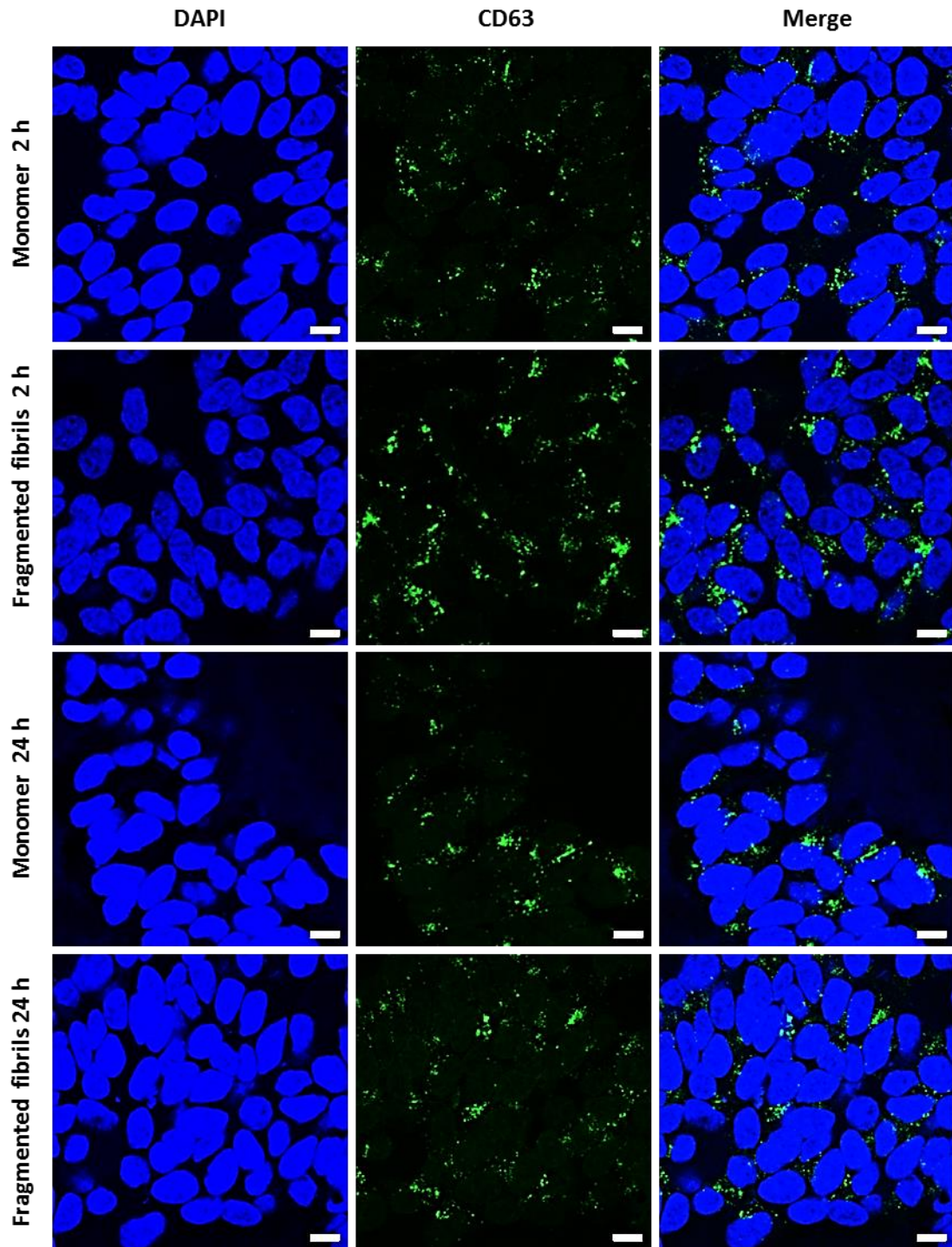


Figure 5.6: Immunofluorescence microscopy analysis of the effect of fibrils on the distribution of CD63. SH-SY5Y cells were incubated with 1.2 μM $\beta_2\text{m}$ monomer or 1.2 μM (monomer equivalent) fragmented $\beta_2\text{m}$ fibrils for the indicated times. Cells were then fixed, permeabilised and stained with an anti-CD63 antibody followed by a fluorescently labelled anti-mouse secondary antibody. Coverslips were imaged using a Zeiss LSM700 confocal microscope and a 63X objective. Representative confocal images for each condition are shown. Scale bar represents 10 μm .

5.2.4 Analysis of the effect of fibrils on the trafficking of newly synthesised LAMP-1 and CD63

In order to investigate whether the small percentage of total LAMP-1 and CD63 at the cell-surface corresponded to newly synthesised protein, the effect of fibrils on the trafficking of newly synthesised LAMP-1 and CD63 was investigated. As described in Figure 5.1, majority of the newly synthesised LAMP-1 and CD63 is directly trafficked to the lysosome; however a minority is trafficked via the plasma membrane [415, 417]. The protein synthesis inhibitor, cycloheximide, was employed to distinguish between effects on newly synthesised being diverted to, or retained at, the plasma membrane; and existing protein being redistributed to the plasma membrane. Cycloheximide inhibits proteins synthesis by blocking the translation of mRNA on cytosolic 80S ribosomes.

SH-SY5Y cells were pre- incubated for 1 h with cycloheximide to inhibit protein synthesis. Cells were then incubated with fragmented β_2m fibrils or β_2m monomer as a control. After incubation with fibrils or monomer, cells were stained with a fluorescently labelled antibody specific for LAMP-1 or CD63 (Section 2.8.2). Cycloheximide treatment has a significant decrease in the expression of LAMP-1 at the cell surface of fibril treated cells (Figure 5.7). A significant decrease in the cell surface expression of CD63 was also observed upon pre-treatment with cycloheximide in fibril treated cells (Figure 5.8). These results demonstrate that at least a portion of the increase in LAMP-1 and CD63 at the cell surface in response to fibril treatment is from newly synthesised protein. This therefore suggests that fibrils alter the trafficking of newly synthesised LAMP-1 and CD63 by diverting them to the plasma membrane.

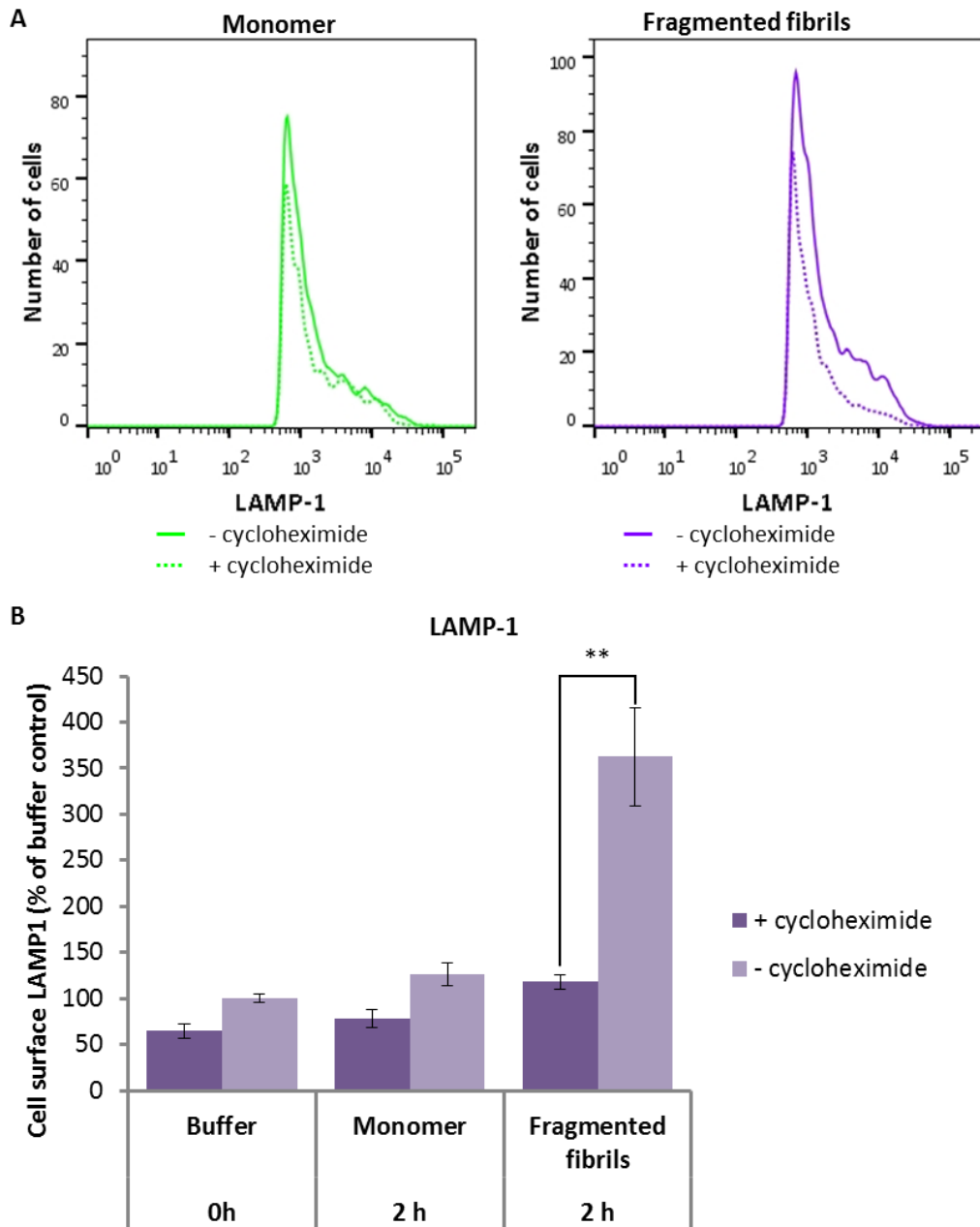


Figure 5.7: Analysis of the effect of cycloheximide on cell surface levels of LAMP-1. SH-SY5Y cells were pre-treated with cycloheximide for 1 h before incubation with 1.2 μ M β_2 m monomer or 1.2 μ M (monomer equivalent) fragmented β_2 m fibrils for 2 h. Cells were then stained with a fluorescently labelled antibody specific for LAMP-1 and cell-associated fluorescence was quantified by flow cytometry. (A) Representative flow cytometry data showing the effect of cycloheximide on cell surface LAMP-1 expression. (B) Quantification of flow cytometry data. Cell surface LAMP-1 (%) was calculated by normalising to signal from cells that were incubated with fibril growth buffer for 0 h (100 %). Error bars represent one S.E.M. over three independent experiments containing three replicates each. ** signifies a p value of <0.01. Flow cytometry data was collected on a BD LSRFortessa analyser (Becton Dickinson).

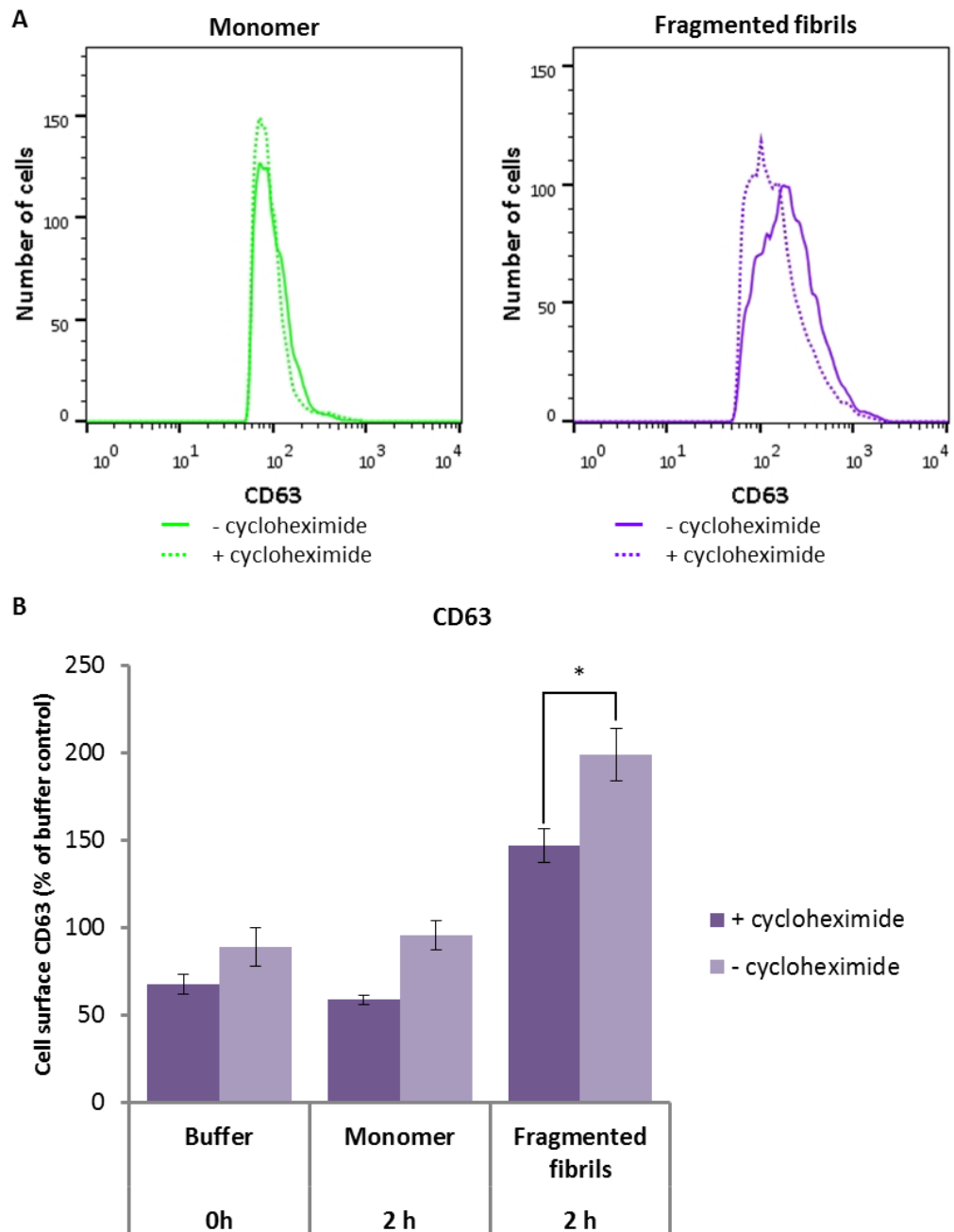


Figure 5.8: Analysis of the effect of cycloheximide on cell surface levels of CD63. SH-SY5Y cells were pre-treated with cycloheximide for 1 h before incubation with 1.2 μ M β_2 m monomer or 1.2 μ M (monomer equivalent) fragmented β_2 m fibrils for 2 h. Cells were then stained with a fluorescently labelled antibody specific for CD63 and cell-associated fluorescence was quantified by flow cytometry. (A) Representative flow cytometry data showing the effect of cycloheximide on cell surface CD63 expression. (B) Quantification of flow cytometry data. Cell surface CD63 (%) was calculated by normalising to signal from cells that were incubated with fibril growth buffer for 0 h (100 %). Error bars represent one S.E.M. over 3 independent experiments containing three replicates each. * signifies a p value of <0.05. Flow cytometry data was collected on a BD LSRFortessa analyser (Becton Dickinson).

5.2.5 Analysis of the effect of fibrils on endocytosis

Fragmented β_2m fibrils impair the trafficking of LAMP-1 and CD63 (Figure 5.2 and Figure 5.3). Perturbations in trafficking would rationalise the inhibition in degradation of endocytosed proteins in fibril-treated cells (Figure 4.10 and Figure 4.11). In order to investigate the effect of fragmented β_2m fibrils on fluid-phase endocytosis, the endocytosis of fluorescently labelled dextrans was assayed by measuring cell-associated fluorescence by flow cytometry. SH-SY5Y cells were incubated with either fragmented β_2m fibrils or controls (fibril growth buffer and β_2m monomer) for 24 h. Cells were then washed and incubated with a fluorescently labelled dextran, Alexa Fluor® 680 dextran (AF680-dextran) of molecular weight (MW) 10, 000 Da for 24 h. Dextrans are relatively inert polysaccharides which are resistant to cleavage in eukaryotic cells due to their uncommon α -1,6-polyglucose linkages [421]. Due to their resistance to cleavage and therefore their accumulation in cells, cell-associated fluorescence of dextrans can be used as a measure of uptake. Following thorough washing, cells were analysed for cell-associated fluorescence by flow cytometry (Section 2.8.3.1).

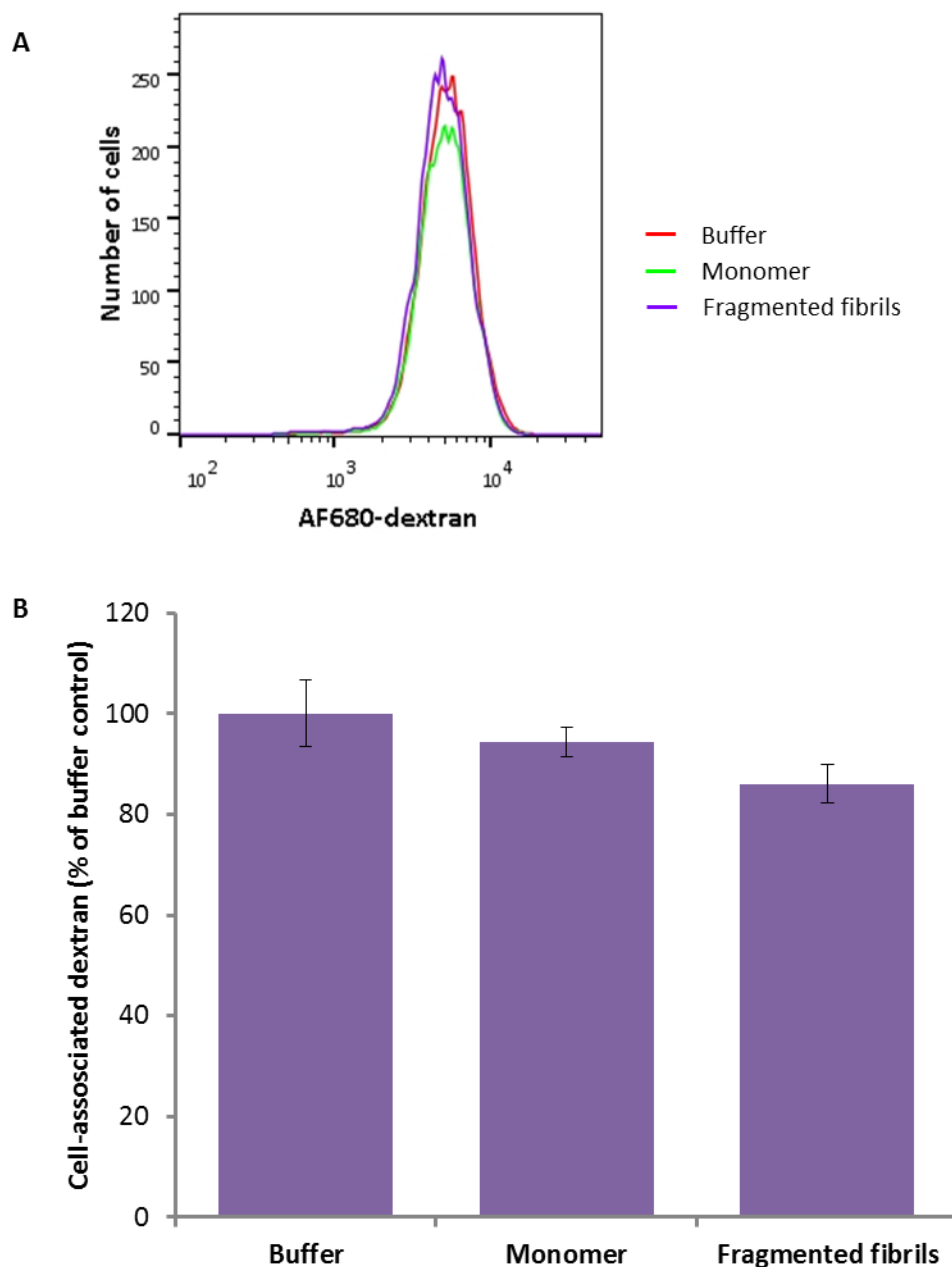


Figure 5.9: Analysis of the effect of fibrils on the uptake of fluorescently labelled dextran. SH-SY5Y cells were incubated with 1.2 μM $\beta_2\text{m}$ monomer or 1.2 μM (monomer equivalent) fragmented $\beta_2\text{m}$ fibrils for 24 h. Cells were then washed and incubated with AF680-dextran for 24 h. Cell-associated fluorescence was quantified by flow cytometry. (A) Representative flow cytometry data comparing AF680-dextran uptake. (B) Quantification of flow cytometry data. Cell-associated ovalbumin (%) was calculated by normalising against signal from cells that were incubated with fibril growth buffer (100 %). Error bars represent one S.D. over three replicates. Flow cytometry data was collected on a BD LSRFortessa analyser (Becton Dickinson).

Fragmented fibrils did not have a significant effect on the endocytosis of labelled dextran when compared to buffer and monomer treated cells (Figure 5.9). However, these data do not

provide any information on the trafficking of dextrans after internalisation by cells. For instance, if the trafficking of dextran is disrupted after internalisation, i.e. the delivery of cargo to the lysosomes is impaired, cell-associated fluorescence by flow cytometry would not distinguish between dextran accumulation in early endosomes, late endosomes, MVBs and lysosomes. For this reason, a preliminary investigation into the trafficking of labelled dextran to lysosomes was performed (Section 2.8.3.2). This was achieved by pre-incubation of SH-SY5Y cells with Alexa Fluor® 568 10,000 MW dextran, (AF586-dextran). As dextrans are resistance to cleavage by lysosomal hydrolases and accumulate in lysosomes, AF586-dextran fed before the addition of fibrils, can act as a marker for lysosomes. Cells were then washed thoroughly and incubated with fragmented β_2m fibrils or fibril growth buffer as a control. Following thorough washing, cells were incubated with a second fluorescently labelled dextran of a different colour, Alexa Fluor® 680 10,000 MW dextran (AF680-dextran). The degree of overlap between the two dextrans could therefore be indicative of delivery of cargo to the lysosome and can thus be used to determine if fibrils disrupt the sorting of endocytosed material to the lysosome. When such a degree of overlap was analysed by live cell confocal microscopy, and Manders' colocalisation coefficients (MCC) quantified using Image J, a significant reduction in the overlap of AF586-dextran and AF680-dextran was observed when cells were treated with fibrils compared to cells incubated with fibril growth buffer (Figure 5.10, Figure 5.11 and Section 2.8.3.2). MCC is independent of signal proportionality i.e. the absolute levels of AF568-dextran and AF680-dextran and is therefore unaffected by differences (if any) in levels of uptake of the two dextrans [330]. This suggests that fibrils impair delivery of endocytosed material to lysosomes.

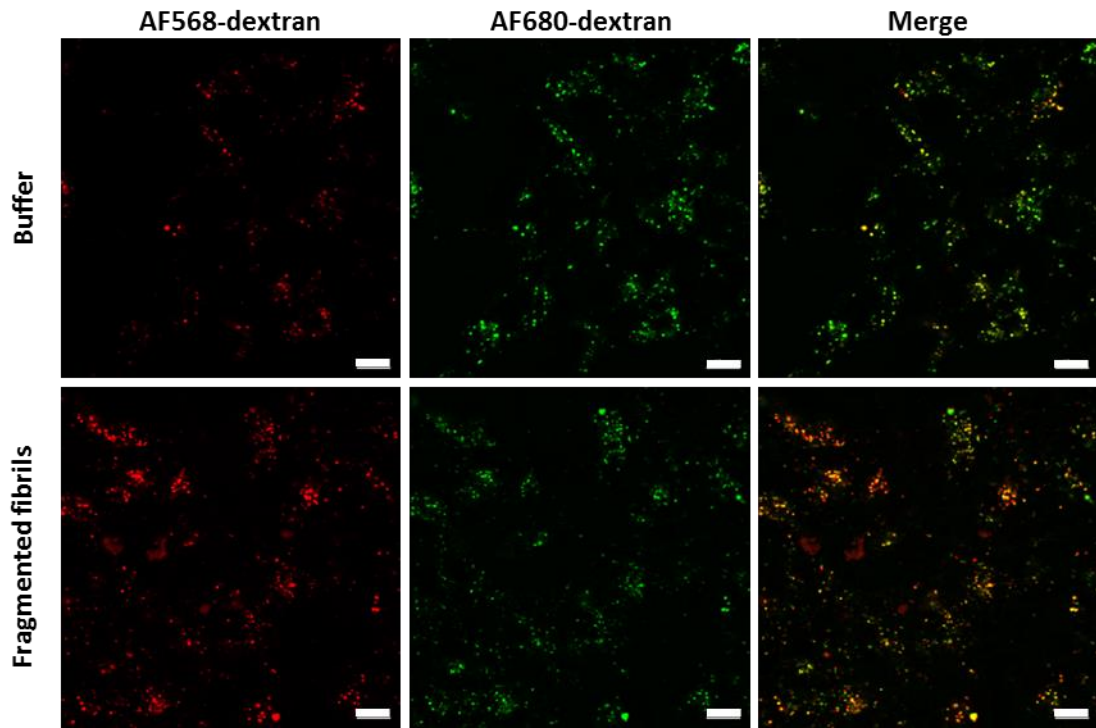


Figure 5.10: Live cell confocal microscopy analysis of the effect of fibrils on endocytosis. SH-SY5Y cells were incubated with AF568-dextran for 24 h. Cells were then thoroughly washed and incubated with either fibril growth buffer or 1.2 μ M (monomer equivalent) fragmented β_2 m fibrils for 24 h. This was followed by washing and incubation with a second fluorescently labelled dextran, AF680-dextran for 24 h. Cells were washed thoroughly prior to imaging using a Zeiss LSM700 confocal microscope with a 63X objective. Representative confocal images for each condition are shown. Scale bar represents 10 μ m.

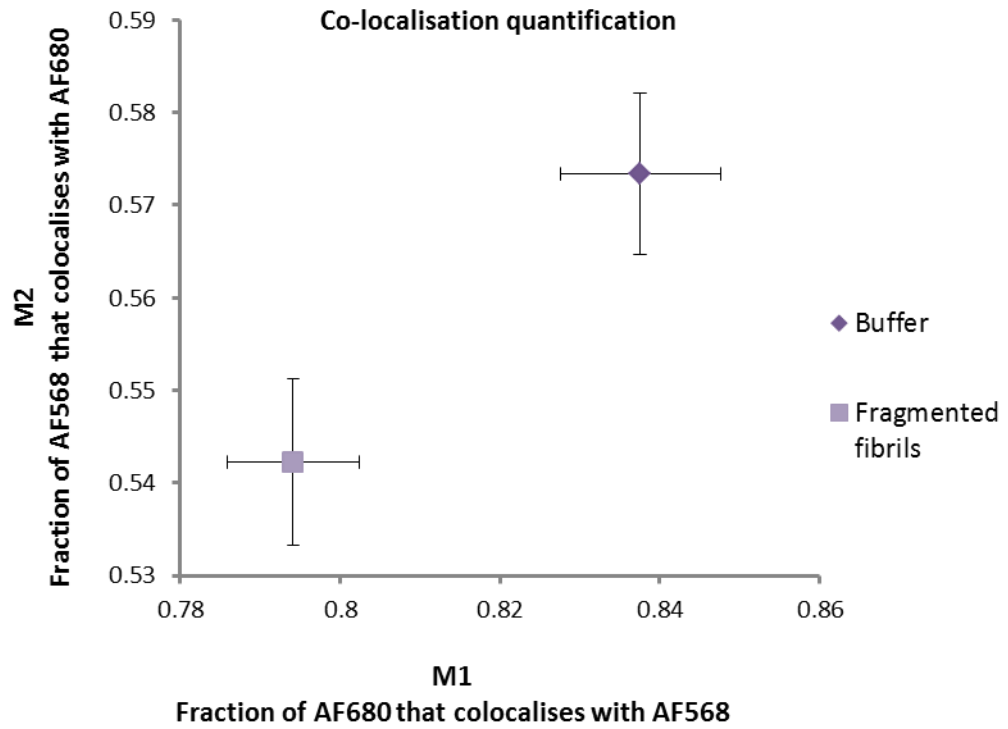


Figure 5.11: Colocalisation analysis of the effect of fibrils on endocytosis. Colocalisation analysis was performed on the experiment shown in (Figure 5.10) with Image J using the JACoP plugin. Costes' threshold was subtracted from the images before MCC analysis was performed. M1 and M2, Manders' coefficients were calculated from 20 images per condition. M1 represents the fraction of AF680-dextran that colocalises with AF568-dextran. M2 represents the fraction of AF568-dextran that colocalises with AF680-dextran. Error bars indicate one S.E.M. over twenty images. Both M1 ($p < 0.01$) and M2 ($p < 0.05$) are significantly different in fibril treated cells compared to buffer treated cells.

5.3 Discussion

The membrane trafficking system including endocytosis, exocytosis and intracellular trafficking is a finely controlled system which regulates many cellular processes. Cellular health and function relies on the system and there are several examples of disease associated with defects in membrane trafficking [404]. For example, the importance of proper trafficking of lysosomal proteins is demonstrated by the lysosomal storage disorder (LSD), mucopolipidosis type II (I-cell disease) [404]. The enzyme N-acetylglucosamine phosphotransferase, which catalyses the incorporation of a mannose-6-phosphate (M6P) moiety on newly synthesised lysosomal enzymes is mutated in patients suffering from mucopolipidosis type II [422, 423]. Lysosomal enzymes are targeted to lysosomes via this M6P moiety and mutations in N-acetylglucosamine phosphotransferase result in the improper trafficking of lysosomal enzymes to the extracellular space [424]. Accumulating evidence also suggests that trafficking may be altered in amyloid diseases such as Alzheimer's, Parkinson's and Huntington's disease (reviewed in [394, 395, 404]). Disruptions to membrane trafficking could therefore have significant pathogenic consequences.

The fibril-induced increase in extracellular formazan needles in the MTT assay suggests an alteration in the trafficking of MTT and/or formazan (Figure 3.17). This prompted a closer investigation of membrane trafficking. Indeed, β_2m fibrils enhance the expression of LAMP-1 and CD63 at the cell surface without increasing their production or inducing a gross redistribution of existing protein pools (Figure 5.2, Figure 5.3, Figure 5.4, Figure 5.5 and Figure 5.6). Fibrils exert their effect, in part, on the trafficking of newly synthesised LAMP-1 and CD63 (Figure 5.7 and Figure 5.8). A portion of existing CD63 is also trafficked to the plasma membrane in fibril-treated cells. This could involve a block in the trafficking of newly synthesised protein from the TGN to late endosomes resulting in more newly synthesised LAMP-1 and CD63 being trafficked to the lysosome via the plasma membrane. Indeed, depletion of the adaptor protein complex, AP-3, which is involved in the transport of lysosomal membrane proteins to late endosomes/lysosomes, has been shown to enhance the cell-surface expression of LAMP-1 and CD63 [415, 425]. Alternatively, this could be due to an increase in newly synthesised protein being trafficked to the plasma membrane or the retention of protein at the plasma membrane due to reduced endocytosis of LAMP-1 and CD63 (Figure 5.12).

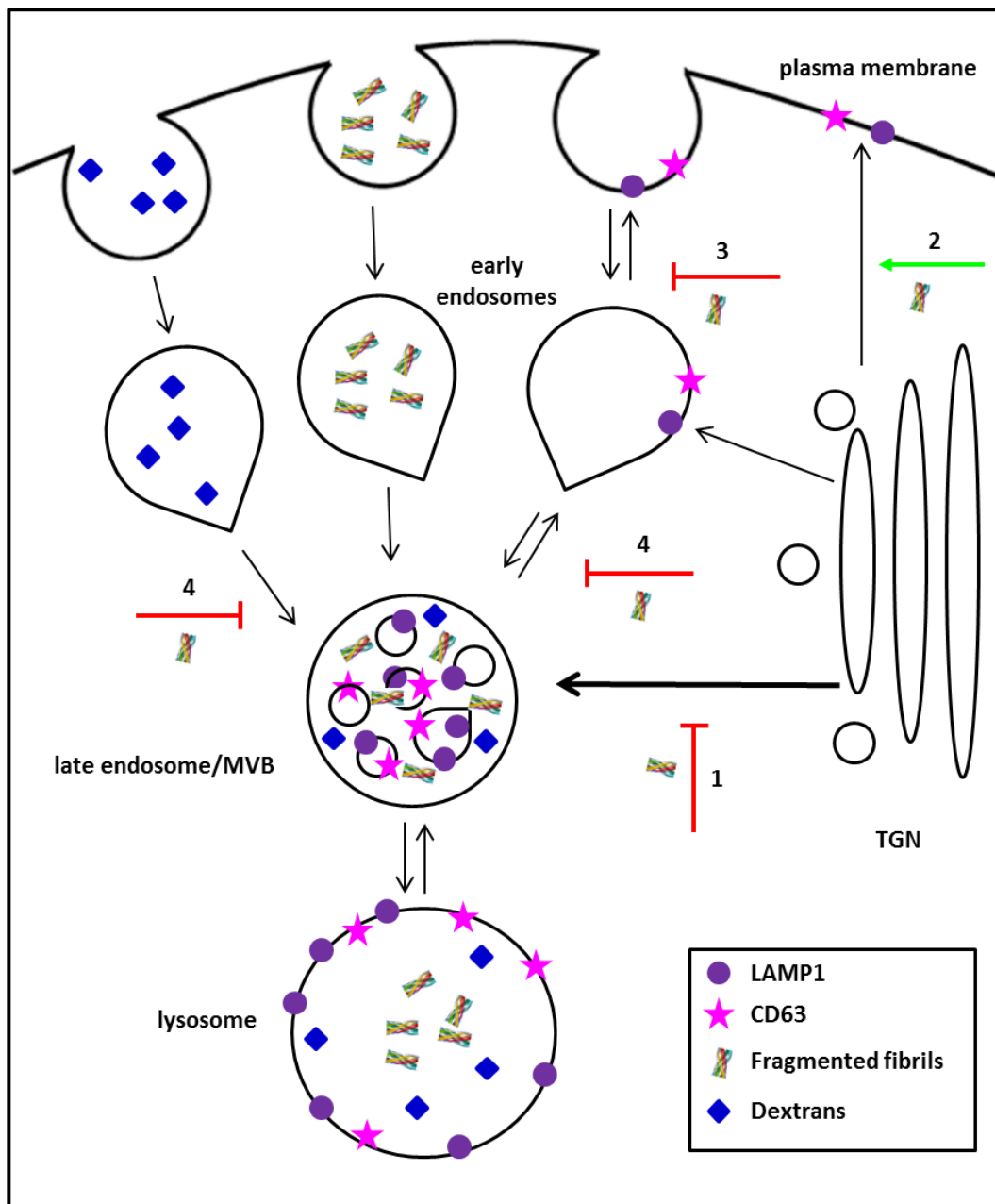


Figure 5.12: Model of fibril-mediated perturbation in trafficking of LAMP-1, CD63 and endocytosed cargo. Upon internalisation, fragmented fibrils perturbed membrane trafficking. This perturbation could be due to a block in trafficking of LAMP-1 and CD63 from the TGN to late endosomes (1). Alternatively, it could be due to increased trafficking of LAMP-1 and CD63 to the plasma membrane (2), or reduced endocytosis (3). Fragmented fibrils also impaired delivery of endocytosed cargo to lysosomes (4).

Trafficking defects have been reported in association with Parkinson's disease. α -synuclein was shown to not only block trafficking from the ER to the Golgi, but also block multiple trafficking steps [410, 411]. Although these studies were performed by overexpressing α -synuclein in yeast models and investigating membrane trafficking interactions *in vitro* from purified cell components, important parallels are apparent. The trafficking steps implicated in α -synuclein

mediated disruption, include, but are not limited to, trafficking between secretory vesicles and the plasma membrane, early endosomes and late endosomes, and between late endosomes and lysosomes [411]. The direction of the effect of α -synuclein on these trafficking steps is not known.

It is possible that fragmented fibrils are capable of interacting with accessory and regulatory proteins which mediate trafficking. For example, a disease-associated mutant (A30P) α -synuclein, has been shown to interact abnormally with the regulatory proteins Rab3a, Rab5 and Rab8 [409]. The rescue of amyloid-induced toxicity by overexpression of Rab1, Rab3a and Rab8 in yeast models provides further evidence for abnormal interactions between amyloid aggregates and regulatory proteins [410, 411]. However, these interactions would require the presence of amyloid aggregates in the cytosol. As evidence of lysosomal rupture has not been detected in our laboratory (Eric Hewitt, personal communications and Figure 4.17), it is unlikely that fibrils escape into the cytosol from the lysosome. However, these interactions may be mediated by fibrils inside trafficking vesicles, by interacting with adaptor proteins directly or indirectly via other cargo proteins.

Although preliminary, the investigation into the effect of fibrils on endocytosis was informative. Fibrils did not affect the fluid phase internalisation of cargo as demonstrated by the flow cytometry analysis of dextran uptake (Figure 5.9). However, it is possible that other forms of endocytosis are affected or trafficking of endocytosed cargo is disrupted after internalisation by cells. A fibril-mediated reduction in endocytosis could explain why LAMP-1 and CD63 accumulate at the cell surface. Fibrils appear to inhibit the delivery of cargo to lysosomes (Figure 5.10 and Figure 5.11). A reduction in delivery of endocytosed cargo to lysosomes could explain why the degradation of endocytosed proteins is impaired in fibril-treated cells but the degradation of cell membrane permeable Magic Red™ cathepsin B is unaffected (Figure 4.7, Figure 4.8 and Figure 4.13). Ovalbumin was shown to co-stain with LysoTracker Green when its internalisation and intracellular localisation was analysed by live cell confocal microscopy (Figure 4.7 and Figure 4.8). As LysoTracker Green accumulates in acidic compartments, and cannot distinguish between lysosomes and late endosomes, it is not possible to determine whether trafficking of endocytosed ovalbumin was impaired.

Other studies have demonstrated an inhibition of clathrin-mediated endocytosis by amyloid aggregates [413, 414]. It is possible that fibrils may indeed inhibit clathrin-mediated endocytosis but have no effect on fluid phase uptake. Future work should investigate the effects of fibrils on different forms of endocytosis. For example, clathrin-mediated endocytosis

and caveolae-mediated endocytosis are implicated in the internalisation of CD63 from the plasma membrane [415]. Investigation into the effect of fibrils on the endocytosis of known cargo for clathrin-mediated and caveolae-mediated endocytosis such as the transferrin receptor, and the SV40 virion respectively could be informative [426]. A more thorough investigation into the block in intracellular trafficking could be guided by the combination of dextrans with markers to early endosomes, late endosomes and MVBs. Fibrils may have a temporal dependent effect on endocytosis, and therefore analysis of endocytosis at shorter time points than 24 h may be instructive. The data described in this chapter demonstrate that fragmented β_2m fibrils impair the trafficking of lysosomal membrane proteins and of endocytosed cargo to lysosomes.

6 Investigation of the role of the molecular chaperone, Hsp70 in fibril-mediated cell disruption

6.1 Introduction

6.1.1 Hsp70 and its role in amyloid disease

The activation of the heat shock response and in particular, the elevation of Hsp70 levels, has been shown to have a neuroprotective effect in several models of neurodegeneration. This protective effect is thought to be principally due to its role as a chaperone (reviewed in [427]). Hsp70 is a 70 kDa protein which performs its role as a chaperone by interacting with exposed hydrophobic amino acids in various proteins. It directs its substrates into a variety of distinct fates by hydrolysing ATP. Hsp70 acts at multiple steps in a protein's life cycle; from folding, trafficking, remodelling and degradation (reviewed in [428]). Hsp70 is composed of three major domains: the N-terminal nucleotide binding domain (NBD); the substrate binding domain (SBD) and a C-terminal α -helical lid. All three domains are required for Hsp70 to function as a molecular chaperone [428]. In humans, there are 11 genes recognised as encoding Hsp70 family members. These include amongst others, the constitutive cytosolic member Hsc70, the stress-induced cytosolic Hsp70, ER-localised Grp78 and mitochondria-localised Grp 75 [429]. In addition to its role in cellular protein quality control and proteostasis, Hsp70 has been shown to promote cell survival by inhibiting lysosomal membrane permeabilisation (LMP), enhancing lysosomal catabolism and preventing apoptosis (reviewed in [430]).

Members of the Hsp40 and Hsp70 families have been found to colocalise with nuclear aggregates in poly-glutamine diseases, as observed in human and mouse brains (reviewed in [427]). This suggests that cellular protein quality control mechanisms are activated in poly-glutamine diseases. Indeed, overexpression of Hsp70 has been shown to be protective in a drosophila model of the poly-glutamine disease, spinocerebellar ataxia 3, as well as mouse models of the poly-glutamine diseases, spinocerebellar ataxia 1 and spinobulbar muscular atrophy (SBMA) [431-433]. A neuroprotective role for Hsp70 has also been described for Parkinson's disease, where Hsp70 overexpression reduced α -synuclein accumulation and toxicity in mouse and drosophila models [217, 434]. In all these examples, the protective role of Hsp70 has been described for intracellular Hsp70. However, heat shock proteins are also found extracellularly and numerous studies have demonstrated a protective role for extracellular Hsc70 and Hsp70 against nutrient deprivation in neurons, smooth muscle cells and monocytes (reviewed in [427]). Hsp70 has been shown to be released from some cells,

and taken up by others in a biologically active form [435, 436]. Although the extracellular mechanism of action of Hsp70 protection is unknown, there is evidence to suggest that Hsp70 can be internalised and imported into the cytoplasm and nucleus of various cell types thus increasing their survival (reviewed in [427]). Indeed, exogenous administration of Hsp70 to rat microglial cultures has been demonstrated to enhance the clearance of A β [437]. Extracellular Hsp70 has also been shown to protect against neurodegeneration in a mouse model of amyotrophic lateral sclerosis (ALS) [438].

6.1.2 Hsp70 and its role in lysosomal storage diseases

Lysosomal storage disorders (LSDs) are a group of diverse inherited diseases caused by mutations in lysosomal proteins [430]. In spite of their varied monogenetic origin, LSDs have a number of cellular and clinical manifestations in common [439]. These include perturbed lysosomal trafficking, autophagy dysfunction, increased oxidative stress, disrupted calcium homeostasis, lysosomal destabilisation, enhanced ER-stress responses and cell death [439]. The heat shock response, and in particular the members of the Hsp70 family, influence many of the primary and secondary cellular processes of LSDs, and thus it is unsurprising that emerging evidence implicates a protective role for Hsp70 in LSDs [430]. Disrupted homeostasis due to the presence of dysfunctional, often misfolded, lysosomal proteins as well as the accumulation of potentially toxic substrates with a variety of downstream effects are recurring themes in LSDs [430, 439].

Key functions of the Hsp70 family of molecular chaperones include assisting the folding of newly synthesised or damaged proteins, preventing protein aggregation, and targeting severely damaged proteins for degradation [199]. Hsp70 can therefore play a protective role in disease pathogenesis in LSDs. For example, celastrol, which activates the heat shock response, has been shown to enhance both the quantity and the catalytic activity of the mutated enzyme, glucocerebrosidase in Gaucher's disease models [440]. Hsp70 has also been shown to be protective in models of Niemann Pick disease A and B [441]. In this instance, exogenously applied recombinant Hsp70 was shown to be trafficked to the lysosome and protection was mediated by enhancing the activity of mutated acid sphingomyelinase [441].

Striking similarities between LSDs and amyloid diseases such as Alzheimer's, Parkinson's and Huntington's disease with respect to the involvement of the lysosome are apparent [306]. Hsp70 has been shown to have a protective effect in both amyloidoses and LSDs as discussed above. Taking advantage of the endocytic machinery to traffic recombinant Hsp70 to the lysosome [441], the role of Hsp70 in fibril-mediated lysosomal disruption was investigated.

This was based on the observations of impaired lysosomal function and trafficking of lysosomal membrane proteins by fragmented β_2m fibrils. The Hsp70 used in the experiments described here is the cytosolic stress-inducible Hsp70 (Hsp70(1A), herein referred to as Hsp70) which has been shown to translocate to the lysosomal compartment under conditions of cellular stress [442]. It is the same isoform which has been shown to be trafficked to the lysosome and play a protective role in models of Niemann Pick disease A and B [441]. This chapter describes experiments designed to investigate whether or not Hsp70 is protective against fragmented β_2m fibrils.

6.2 Results

6.2.1 Expression and purification of Hsp70

In order to generate Hsp70 to determine if Hsp70 protected cells against the deleterious effects of amyloid fibrils, recombinant Hsp70 was expressed in BL21 (DE3) pLysS cells carrying the pET28b-Hsp70(1A) plasmid according to an established protocol [333] (Section 2.9 and Figure 6.1). Cells were lysed after induction with IPTG and the soluble fraction of the cell lysate was purified by Ni-NTA chromatography. The protein was eluted via a step gradient and Hsp70 elutes as a single peak at an imidazole concentration of 200 mM (Figure 6.2 and Figure 6.3). Fractions spanning this single peak were pooled and dialysed prior to further purification by size exclusion chromatography.

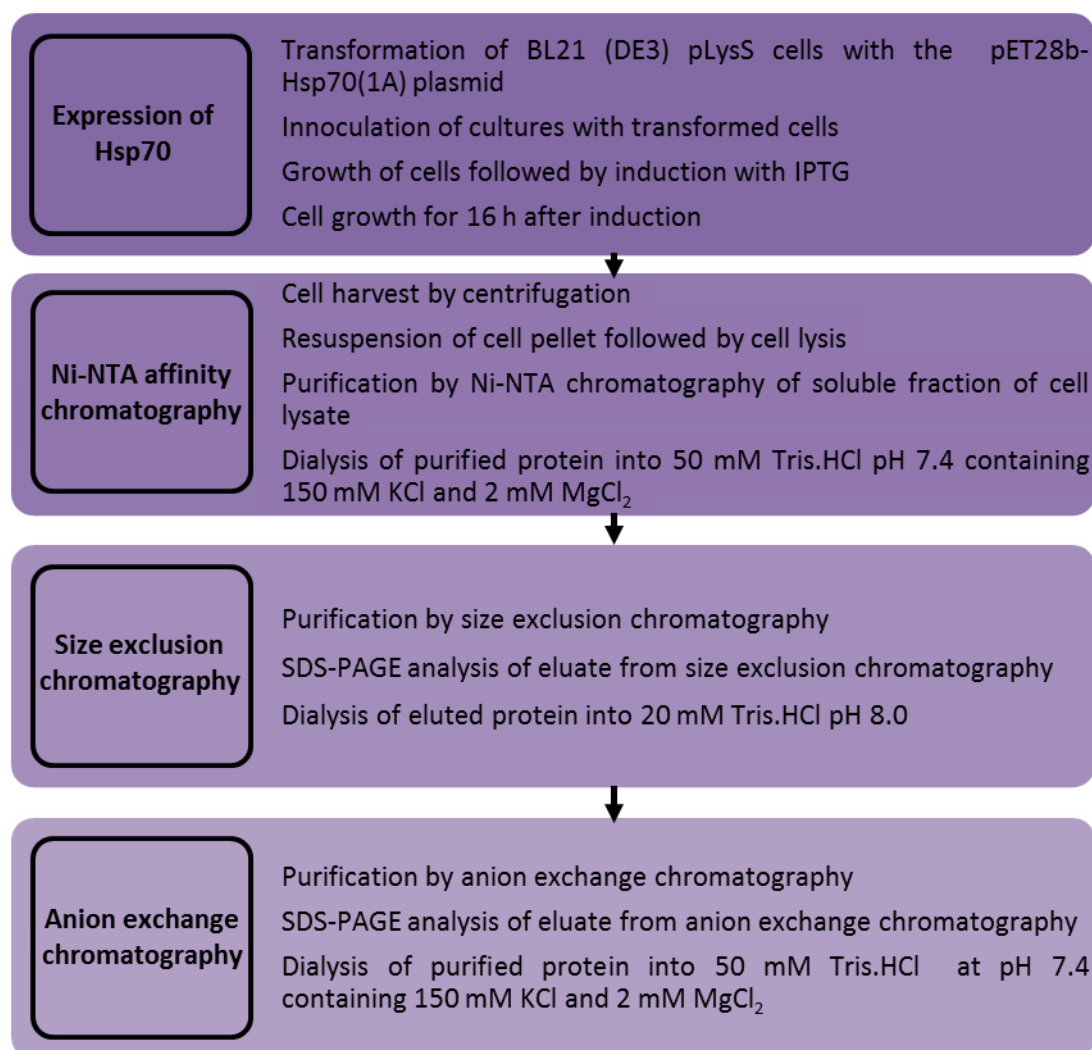


Figure 6.1: Schematic of Hsp70 expression and purification strategy.

This, however, did not successfully separate the protein into well resolved peaks as judged by the size exclusion chromatography profile (Figure 6.4). SDS-PAGE analysis of the size exclusion chromatography eluate shows the presence of a less abundant, lower band which could be a contaminant or a proteolytic fragment of Hsp70 (predicted molecular mass of Hsp70 is 72 KDa) (Figure 6.5). The protein was therefore pooled and dialysed against 20 mM Tris.HCl pH 8.0 prior to further purification by anion exchange chromatography. Purification by anion exchange chromatography separated the protein into sharper, well resolved peaks (Figure 6.6).

Analysis of purity by SDS-PAGE revealed that the second peak corresponds to relatively pure Hsp70 (Figure 6.7). Electrospray ionisation mass spectrometry was used to determine the molecular weight of the purified protein (Figure 6.8). A molecular mass of 72085 Da is consistent with the purified protein being hexa his-tagged monomeric Hsp70 with the N terminal methionine excised (expected mass 72084.36 Da). Excision of the N terminal

methionine has been shown to be a common modification of proteins in the cytosol of *Escherichia coli* [443]. The purified Hsp70 was stored at -80 °C.

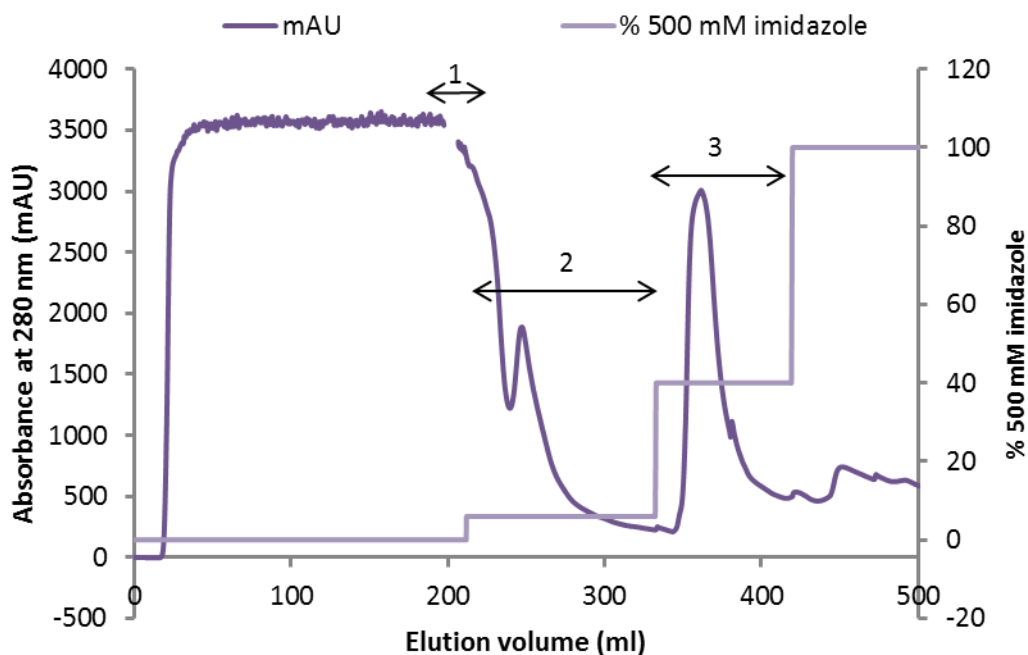


Figure 6.2: Ni-NTA affinity chromatography purification of Hsp70. Recombinant N-hexa-His tagged Hsp70 was overexpressed in BL21 (DE3) pLysS cells transformed with the pET28b-Hsp70(1A) plasmid [333]. Cells were harvested from induced cultures and lysed. Cell lysates were filtered and loaded onto an XK26 column containing 25 ml Ni Sepharose High Performance. 1 indicates a disruption in the absorbance at 280 nm due to accidental loading of air on to the column. 2 indicates a wash step with 40 mM imidazole and 3 indicates an elution step with 200 mM imidazole. Samples from 2 and 3 were collected for SDS-PAGE analysis.

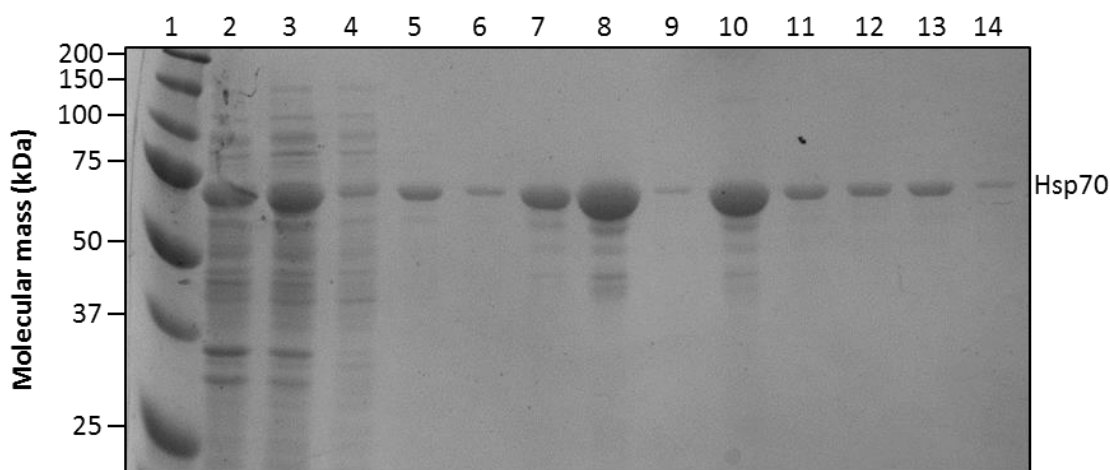


Figure 6.3: SDS-PAGE analysis of Hsp70 purification by Ni-NTA chromatography. Samples were resolved by 10% Tris-glycine SDS-PAGE and visualised by Coomassie Blue. Lane 1 – marker; 2 – whole cell lysate of induced cells; 3 – soluble fraction of whole cell lysate; 4 – flow-through (1 in Figure 6.2) ; 5 – wash with 40 mM imidazole (2 in Figure 6.2); 6 to 14 – samples spanning peak that elutes at 200 mM Imidazole (3 in Figure 6.2).

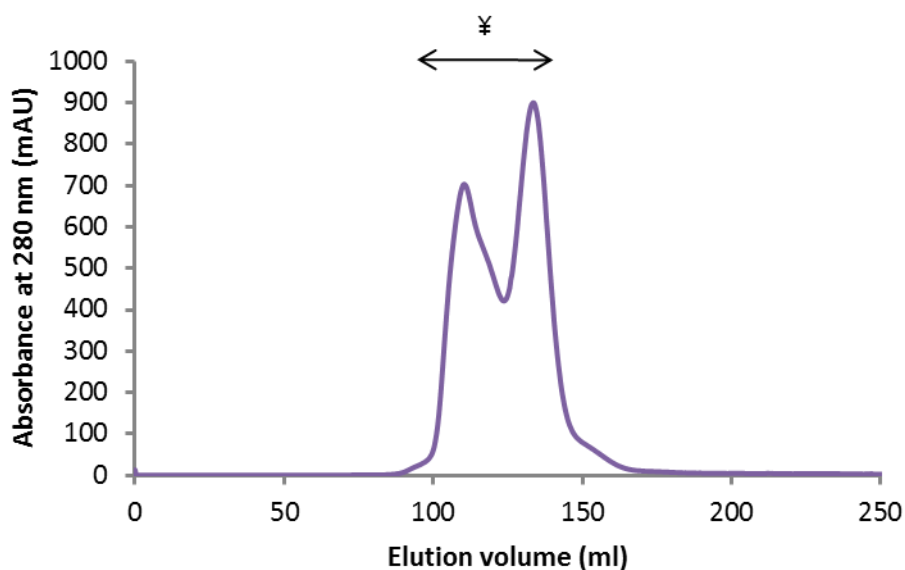


Figure 6.4: Size exclusion chromatography purification of Hsp70. Fractions corresponding to the Ni-NTA affinity chromatography elution peak (3 in Figure 6.2) were pooled and dialysed against 50 mM Tris.HCl pH 7.4 containing 150 mM KCl and 2 mM MgCl₂. Dialysed protein was concentrated to 12 mg/ml prior to loading on to a Superdex 75 HiLoad 26/60 size exclusion column for further purification. Samples spanning both peaks (indicated by ¥) were collected for SDS-PAGE analysis.

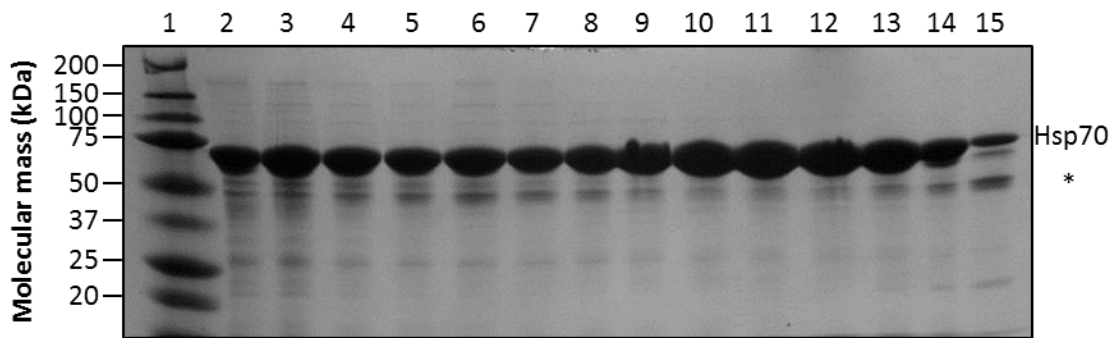


Figure 6.5: SDS-PAGE analysis of size exclusion chromatography purification of Hsp70. Samples were resolved by 10% Tris-glycine SDS-PAGE and visualised by Coomassie Blue. Lane 1 – marker; 2 to 15 samples spanning both peaks from the size exclusion chromatography elution profile (¥ in Figure 6.4). * Indicates a band corresponding to either a contaminant or degradation product of Hsp70.

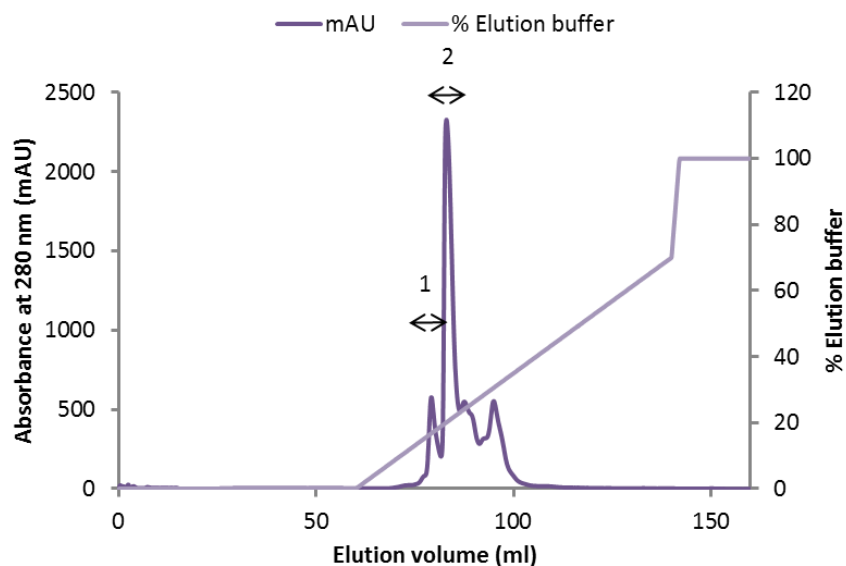


Figure 6.6: Further purification of Hsp70 by anion exchange chromatography. Fractions spanning both peaks from size exclusion chromatography purification (¥ in Figure 6.4) were pooled and dialysed against 20 mM Tris.HCl pH 8.0 and loaded onto a Resource Q anion-exchange column. A linear gradient of 0 – 700 mM NaCl in 20 mM Tris.HCl pH 8.0 over 80 ml was applied to elute the protein. Fractions from peaks 1 and 2 were collected for SDS-PAGE analysis.

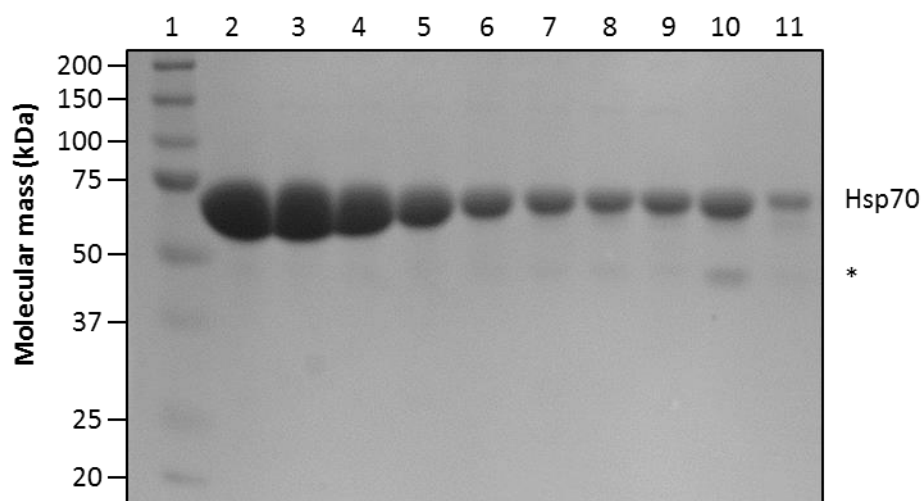


Figure 6.7: SDS-PAGE analysis of anion exchange chromatography purification of Hsp70. Samples were resolved by 10% Tris-glycine SDS-PAGE and visualised by Coomassie Blue. Lane 1 – marker; 2 to 9 – samples spanning the second peak (2 on Figure 6.6); 10-11 – samples spanning the first peak (1 on Figure 6.6). * indicates a band corresponding to a contaminant or degradation product of Hsp70.

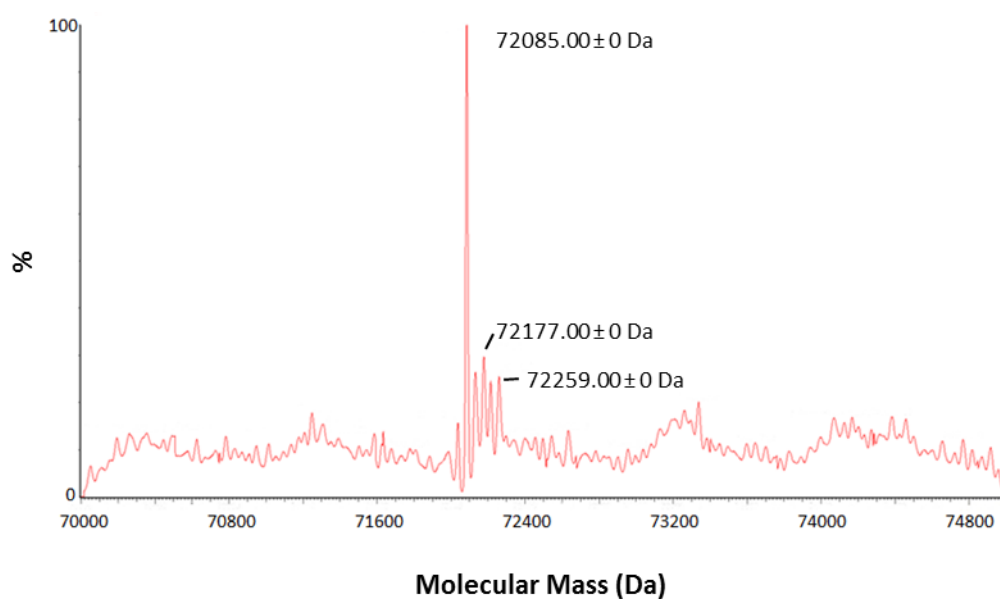


Figure 6.8: Electrospray ionisation mass spectrometry (ESI-MS) analysis of purified Hsp70. Mass profiles generated by Maximum Entropy processing of the ESI-MS m/z spectra. The peak corresponding to 72085.00 ± 0 Da represents hexa-his-tagged monomeric Hsp70. The peaks to the right correspond to Hsp70 bound to sodium and potassium ions. ESI-MS analysis was performed by Dr James Ault (University of Leeds, Astbury mass spectrometry facility manager).

6.2.2 Analysis of the intracellular localisation of recombinant Hsp70

To confirm that exogenously added, purified, recombinant Hsp70 was indeed trafficked to the lysosome as shown previously, its intracellular localisation was analysed by live cell confocal microscopy [441]. Purified Hsp70 was fluorescently labelled with Alexa Fluor® 405 prior to incubation with RAW 264.7 cells for 4 h (Section 2.10.1). Cells were stained with LysoTracker Green and imaged. Labelled Hsp70 was found in intracellular punctate structures which colocalised with LysoTracker Green (Figure 6.9).

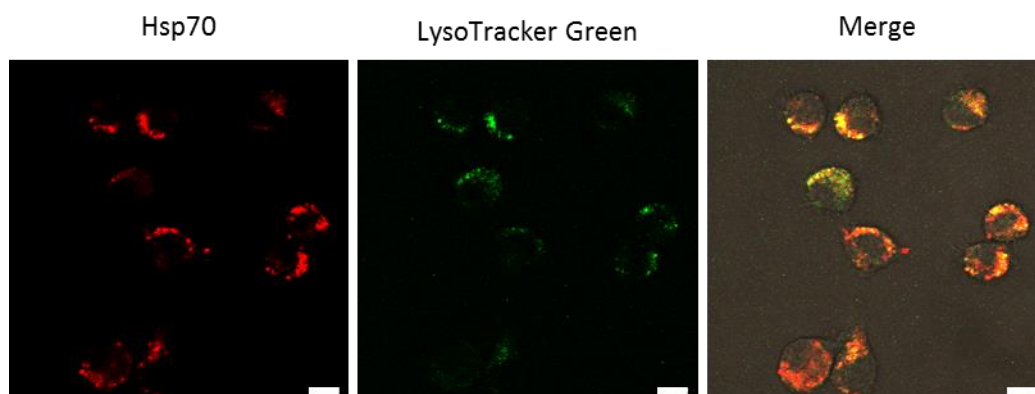


Figure 6.9: Analysis of the internalisation and localisation of labelled Hsp70 in RAW 264.7 cells. RAW 264.7 cells were incubated with 3 μ M Alexa Fluor® 405 Hsp70 for 4 h. Cells were washed and stained with 50 nM LysoTracker Green 30 min prior to imaging. Images were acquired using a Zeiss LSM510 confocal microscope with a 40X objective. Representative confocal images are shown. Scale bar represents 10 μ m.

6.2.3 Investigation of the role of Hsp70 in amyloid-mediated disruption of MTT reduction

To investigate whether Hsp70 could protect against inhibition of MTT reduction by fragmented β_2 m fibrils, RAW 264.7 and SH-SY5Y cells were pre-incubated with Hsp70 4 h (RAW 264.7) or 6 h (SH-SY5Y) prior to incubation with fragmented fibrils (Section 2.10.2). The MTT assay was then employed to measure the effect of Hsp70 on MTT reduction by fibril-treated cells. Pre-incubation of cells with Hsp70 reduced the inhibition of MTT reduction by fragmented β_2 m fibrils in both RAW 264.7 and SH-SY5Y cells (Figure 6.10).

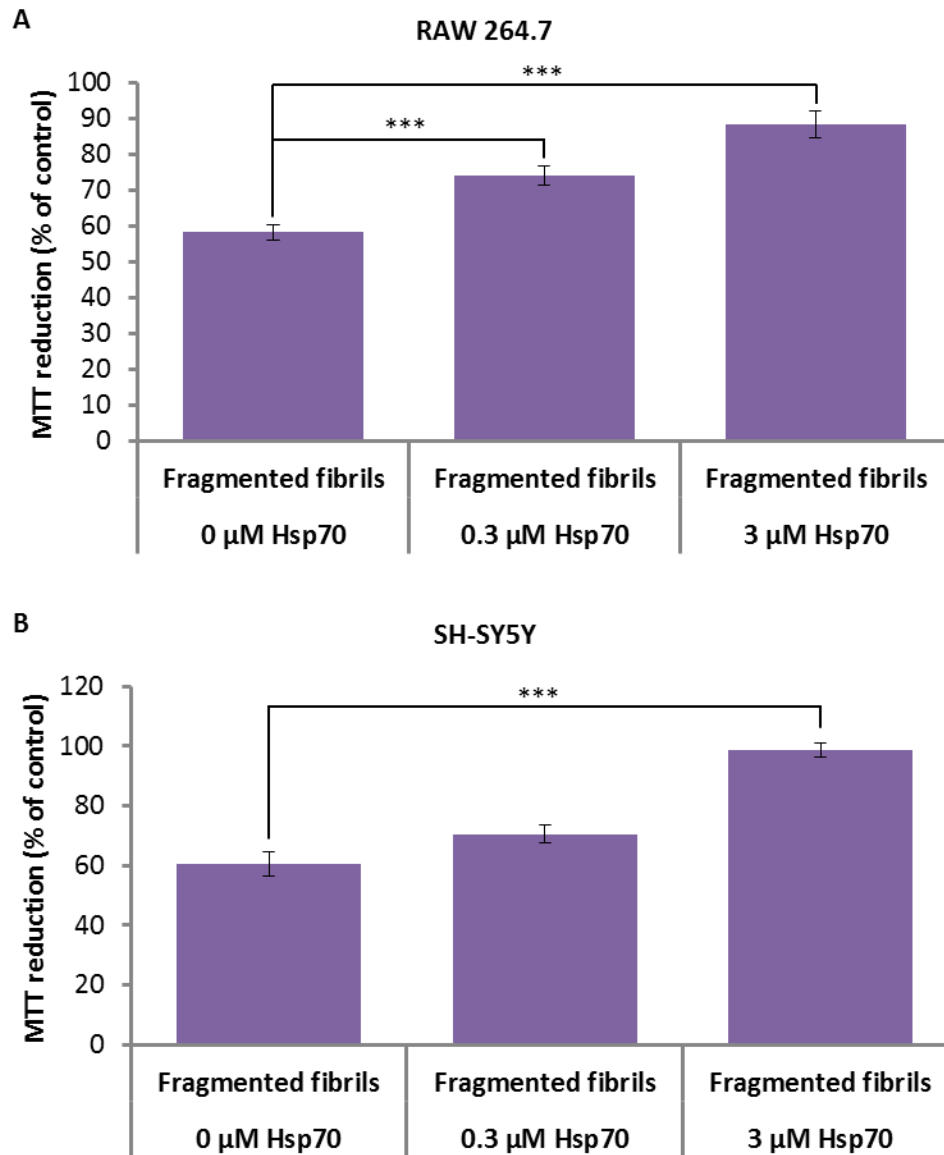


Figure 6.10: Analysis of the effect of Hsp70 on MTT reduction in fibril treated cells. RAW 264.7 (A) and SH-SY5Y (B) were pre-incubated with Hsp70 at the concentrations indicated for 4 h (RAW 264.7) or 6 h (SH-SY5Y). Cells were then incubated with 1.2 μM (monomer equivalent) fragmented $\beta_2\text{m}$ fibrils or fibril growth buffer as a control for 24 h prior to analysis of MTT reduction. MTT reduction (%) was calculated by normalising against cells treated with the respective concentrations of Hsp70 and fibril growth buffer (100 %). Error bars represent one S.E.M. over three independent experiments containing five replicates each. *** signifies a p value of <0.001.

6.2.4 Investigation of the role of W90F Hsp70 in amyloid-mediated disruption of MTT reduction

In addition to its role as a molecular chaperone, Hsp70 is also involved in the regulation of LMP [444]. LMP causes the release of cathepsins and other hydrolases from the lysosomal lumen to the cytosol. It is therefore a potentially lethal event due to digestion of vital proteins as well as activation of additional hydrolases such as caspases [283]. LMP is induced by a range of different stimuli including activation by cell death effectors such as Bax [283]. Exogenously added Hsp70 has been shown to be trafficked to the lysosome and to inhibit LMP by stabilising lysosomes. This stabilising effect is due to the binding of Hsp70 to the endolysosomal lipid bis(monoacylglycero)phosphate (BMP). This interaction enhances sphingomyelin catabolism thus increasing cellular levels of ceramide and resulting in lysosomal stability [441]. By changing the lipid composition of inner lysosomal membranes, sphingolipid catabolism is thought to enhance the stability of the lysosomal membrane [445]. A single point mutation in the ATPase domain of Hsp70 at residue 90, which changes a tryptophan residue to a phenylalanine residue (W90F), has been shown to specifically abolish the interaction between Hsp70 and BMP whilst retaining the structural and functional aspects of the Hsp70 chaperone [441]. W90F Hsp70 is therefore unable to protect against LMP in contrast to wild-type Hsp70 in models of Niemann Pick disease A and B [441]. Recent work in our laboratory has shown that fragmented β_2m fibrils disrupt artificial lipid bilayers which contain BMP [446]. W90F Hsp70 was used as a tool to investigate whether the interaction of Hsp70 and BMP was necessary for protection from fragmented β_2m fibrils.

W90F Hsp70, was expressed in BL21 (DE3) pLysS cells carrying the pET28b-W90F Hsp70(1A) plasmid and then purified using the same protocol as used for wild-type Hsp70 [333] (Figure 6.1 and Section 2.9). The purity of W90F Hsp70 was confirmed by analytical size exclusion chromatography and SDS-PAGE analysis (Figure 6.11 and Figure 6.12).

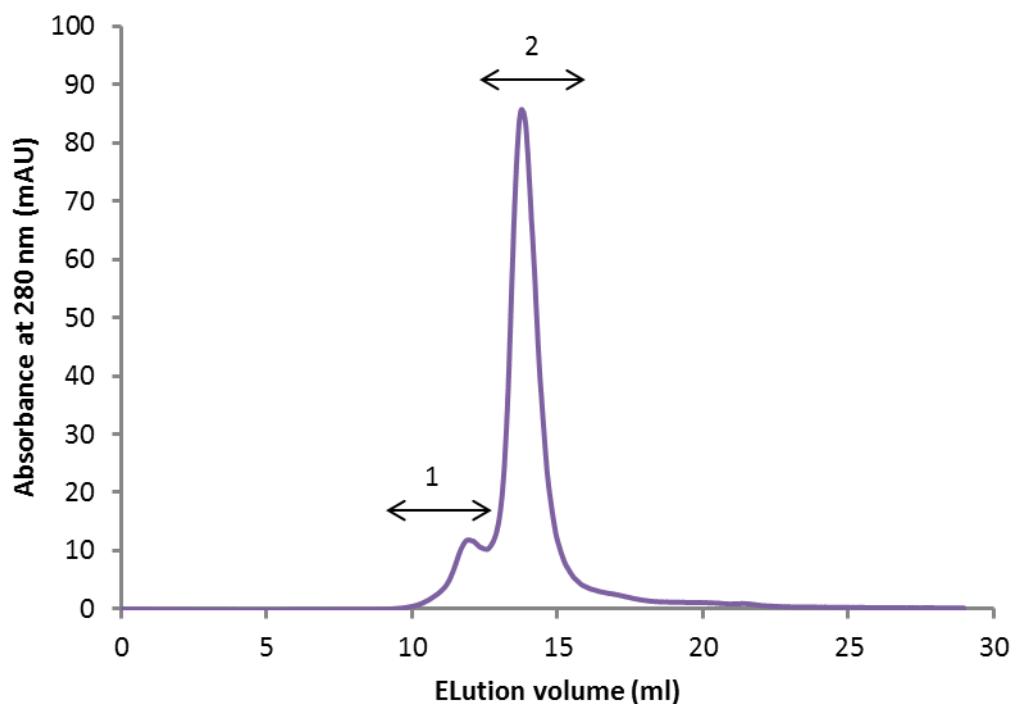


Figure 6.11: Analytical size exclusion chromatography of purified W90F Hsp70. Purified W90F Hsp70 was separated by size exclusion chromatography using an analytical size exclusion column (Superdex 200 10/300 GL). Samples from both peaks (1 and 2) were collected for SDS-PAGE analysis.



Figure 6.12: SDS-PAGE analysis of analytical size exclusion chromatography of purified W90F Hsp70. Samples were resolved by 10% Tris-glycine SDS-PAGE and visualised by Coomassie Blue. 1 – Marker; 2 to 4 samples spanning the first peak from the size exclusion chromatography elution profile (1 in Figure 6.11); 5 to 11 – samples spanning the second peak (2 in Figure 6.11).

The effect of W90F Hsp70 on the inhibition of MTT reduction by fragmented β_2m fibrils was investigated. Cells were pre-incubated with Hsp70 or W90F Hsp70 prior to incubation with fragmented fibrils (Section 2.10.2). W90F Hsp70 also protects against fibril-mediated inhibition in MTT reduction (Figure 6.13). This protection, observed in both RAW 264.7 and SH-SY5Y cells, is comparable to that conferred by wild-type Hsp70. This suggests that Hsp70 rescue is unlikely to require the interaction of Hsp70 with the endolysosomal lipid, BMP.

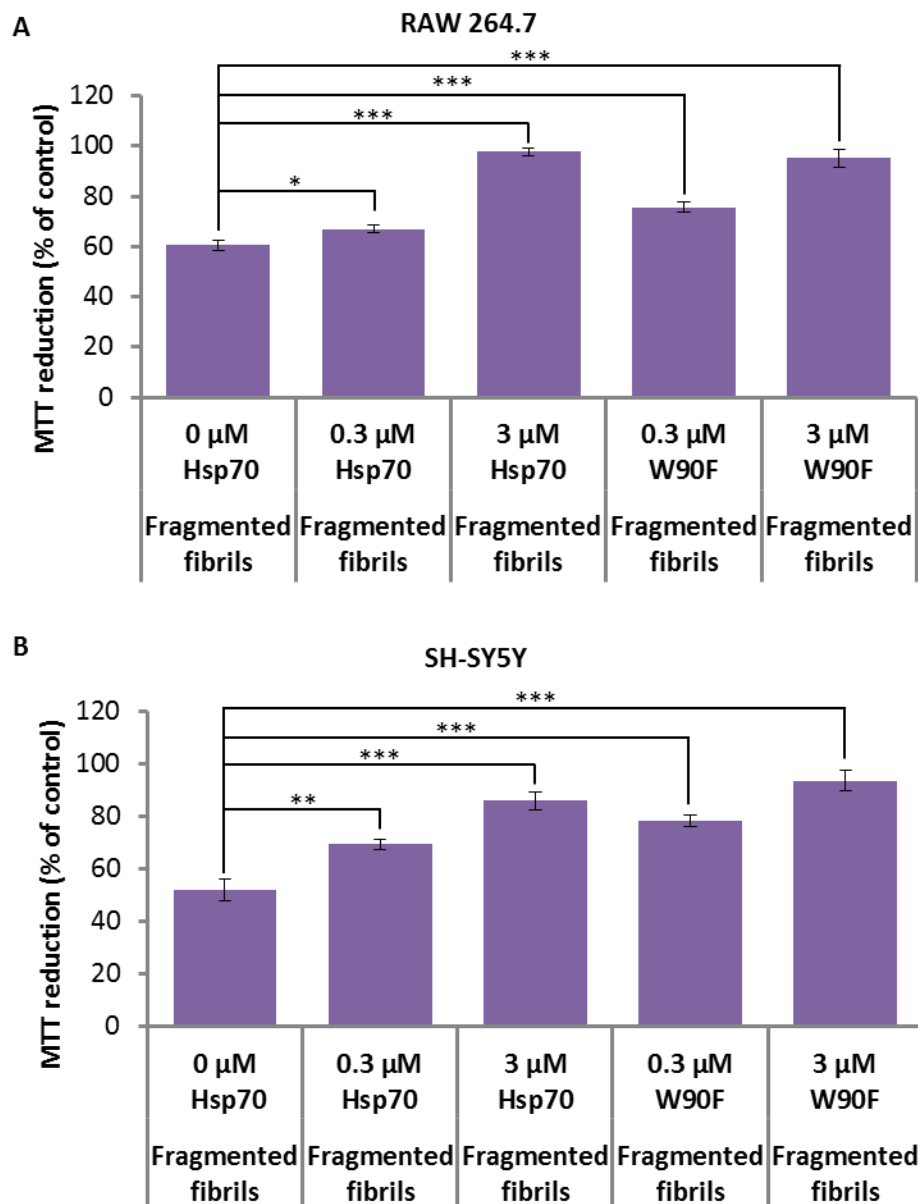


Figure 6.13: Analysis of the effect of W90F Hsp70 on the fibril-mediated disruption of MTT reduction. RAW 264.7 (A) and SH-SY5Y (B) were pre-incubated with Hsp70 or W90F Hsp70 at the concentrations indicated for 4 h (RAW 264.7) or 6 h (SH-SY5Y). Cells were then incubated with 1.2 μM (monomer equivalent) fragmented fibrils or fibril growth buffer as a control for 24 h prior to analysis of MTT reduction. MTT reduction (%) was calculated by normalising against cells treated with the respective concentrations of W90F Hsp70 or Hsp70, and fibril growth buffer. Error bars represent one S.E.M. over three independent experiments containing five replicates each. *, ** and *** signify p values of <0.05, <0.01 and <0.001 respectively.

6.2.5 Investigation of the effect of Hsp70 on fibril-mediated alteration in formazan trafficking

To investigate whether Hsp70 protected against the fibril-mediated alteration in formazan trafficking in the MTT assay, SH-SY5Y cells were pre-incubated with Hsp70 prior to incubation with fragmented fibrils (Section 2.10.3). In the absence of Hsp70, phase contrast microscopy analysis showed accumulation of formazan as extracellular needles in fibril-treated cells and intracellular granules in buffer-treated controls (Figure 6.14). Pre-incubation with Hsp70 had a subtle effect on the production of extracellular needles by fibril-treated cells. Although formazan still accumulated in extracellular needles, intracellular granules were also observed (bottom panel in Figure 6.14). Such intracellular granules are not observed in the absence of Hsp70.

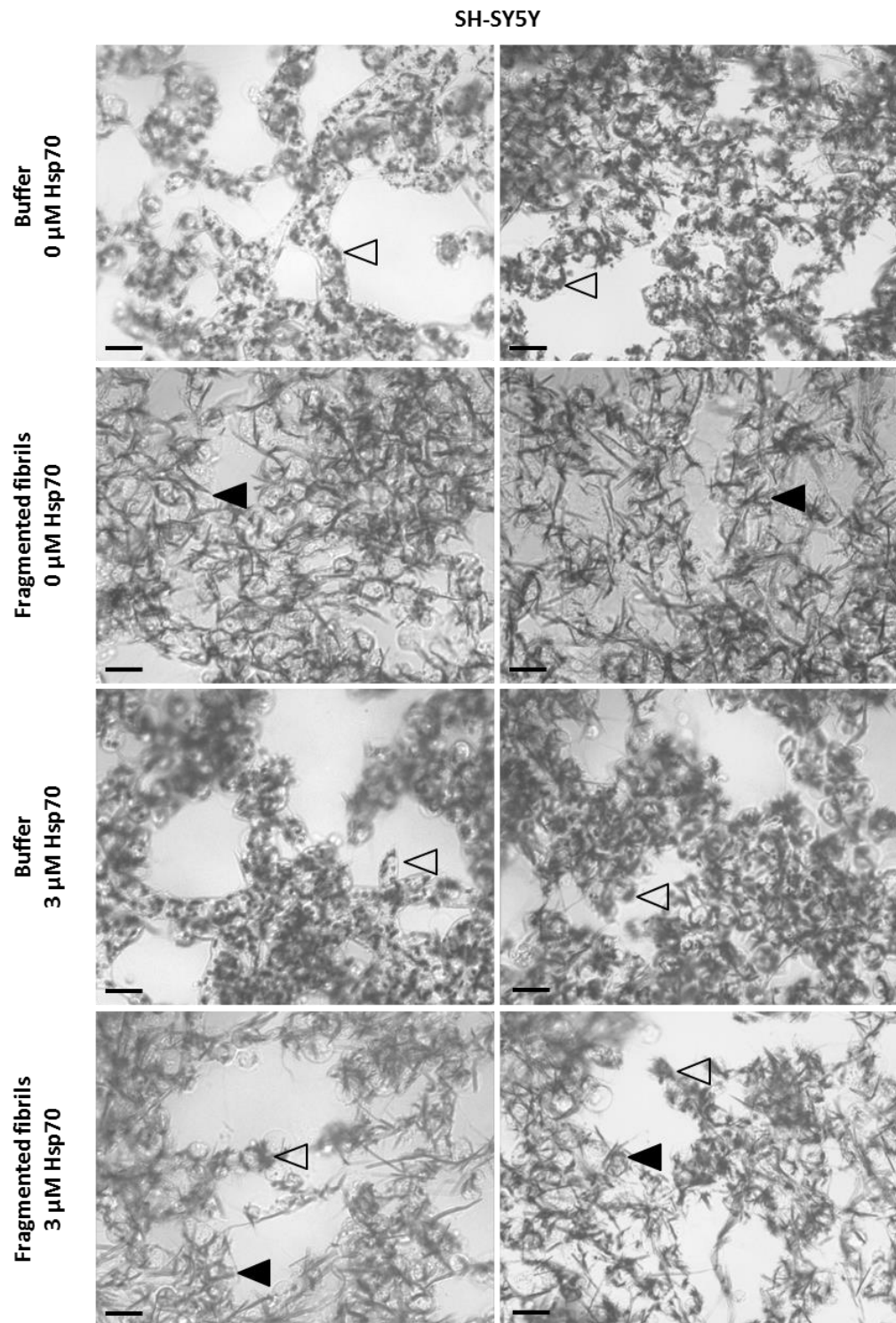


Figure 6.14: Phase contrast microscopy analysis of the effect of Hsp70 on formazan trafficking. SH-SY5Y cells were pre-incubated with either 3 μM Hsp70 or PBS as a control for 6 hours prior to 24 h incubation with 1.2 μM (monomer equivalent) fragmented β_2m fibrils or fibril growth buffer. Cells were incubated with MTT 90 min before imaging by phase contrast microscopy. Reduced formazan was visualised as dark intracellular granules (open triangle) or extracellular needles (filled triangle). Images were acquired on a Leica DM IL inverted contrasting microscope connected to a Leica DC 300F camera (Leica microsystems). Representative images are shown. The scale bar represents 20 μm.

6.2.6 Further investigation into the effect of Hsp70 on fibril-mediated cell disruption

Due to the observation of fibril-mediated perturbation in LAMP-1 trafficking (Figure 5.2), the effect of Hsp70 on the cell-surface expression of LAMP-1 in fibril-treated cells was analysed by flow cytometry (Section 2.10.4). SH-SY5Y cells were pre-incubated with Hsp70 prior to incubation with fragmented β_2m fibrils or controls. Hsp70 did not have a significant effect on the cell surface LAMP-1 expression in cells incubated with fragmented fibrils or controls (Figure 6.15).

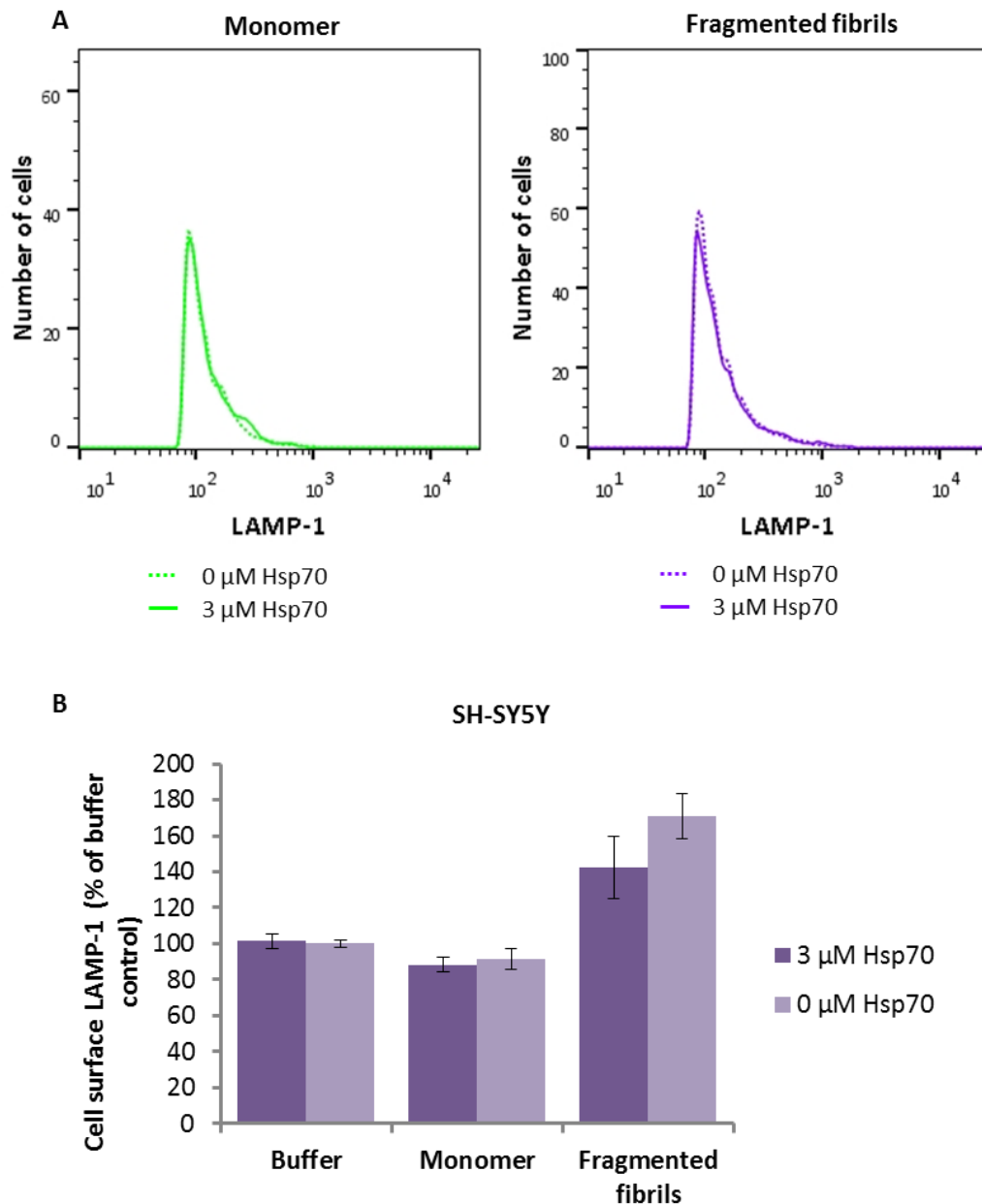


Figure 6.15: Analysis of the effect of Hsp70 on the cell surface expression of LAMP-1. SH-SY5Y cells were pre-incubated with either 3 μ M Hsp70 or PBS as a control prior to incubation with 1.2 μ M (monomer equivalent) fragmented β_2 m fibrils or controls (1.2 μ M β_2 m monomer or fibril growth buffer). Cells were then stained with fluorescently labelled anti-LAMP-1. Cell-associated fluorescence was quantified by flow cytometry. (A) Representative flow cytometry data showing the effect of Hsp70 on cell-surface LAMP-1 expression. (B) Quantification of flow cytometry data. Cell surface LAMP-1 (%) was calculated by normalising to signal from cells that were incubated with fibril growth buffer (100 %). Error bars represent one S.E.M. over three independent experiments each containing three replicates each. Flow cytometry data was collected on a BD LSRFortessa analyser (Becton Dickinson).

In order to further examine the effects of Hsp70 on the fibril-associated disruption of cellular function, its role in ovalbumin degradation in fibril-treated cells was analysed by flow cytometry (Section 2.10.5). This was based on the observation of impairment in degradation of endocytosed proteins in cells incubated with fragmented β_2m fibrils (Figure 4.10 and Figure 4.11). SH-SY5Y cells were pre-incubated with Hsp70 for 6 h before incubation with fragmented fibrils or controls for 24 h. Cells were then pulsed with a fluorescent protein substrate, Alexa Fluor® 647 ovalbumin (AF647-ovalbumin) for 6 h. Following pulse, cells were analysed for cell-associated fluorescence immediately (0 h chase) or cultured for a further 24 h in the absence of AF647-ovalbumin and then analysed (24 h chase). Pre-incubation of cells with Hsp70 restored ovalbumin degradation in fibril-treated cells to levels comparable to controls (Figure 6.16). Hsp70 therefore restores the ability of fibril-treated cells to degrade endocytosed proteins.

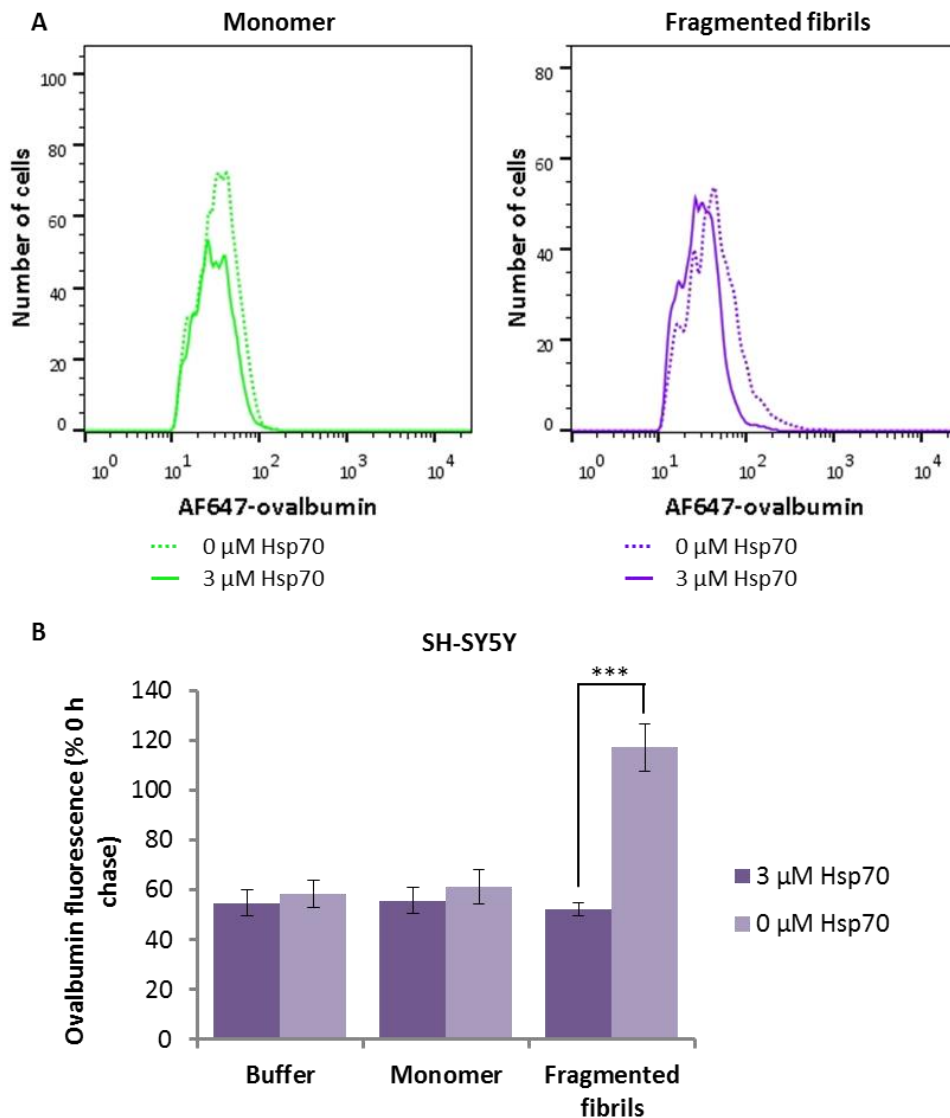


Figure 6.16: Analysis of the effect of Hsp70 on the degradation of fluorescently labelled ovalbumin in fibril treated cells. SH-SY5Y cells were pre-incubated with Hsp70 at the concentrations indicated for 6 h prior to incubation with fragmented fibrils or controls. Cells were then pulsed with A647-ovalbumin and its degradation over time was followed by measuring cell-associated fluorescence immediately after pulsing with labelled ovalbumin (0 h chase) or 24 h later (24 h chase). (A) Representative flow cytometry data showing the effect of Hsp70 on ovalbumin degradation. (B) Quantification of flow cytometry data. Ovalbumin fluorescence (%) was calculated by normalising the fluorescence at 24 h chase to the fluorescence at 0 h chase (100 %). Error bars represent one S.E.M. over three independent experiments containing three replicates each. *** signifies a p value of <0.001. Flow cytometry data was collected on a BD LSRFortessa analyser (Becton Dickinson).

6.3 Discussion

The experiments described here demonstrate protection by Hsp70 from cellular disruption mediated by fragmented fibrils. Pre-incubation of cells with Hsp70 prior to incubation with fragmented fibrils, confers protection against amyloid-mediated impairment in MTT reduction and ovalbumin degradation. As the single point mutant, W90F Hsp70, is also able to protect against amyloid-mediated impairment in MTT reduction, this protection is unlikely to be due to enhancement of acid sphingomyelinase activity through interactions with BMP. Pre-incubation of cells with Hsp70, does not however, protect against fibril-mediated perturbation in LAMP-1 trafficking.

In vitro studies on the effect of Hsp70 on α -synuclein fibril formation have demonstrated that Hsp70 inhibits fibril formation by binding to prefibrillar species [447, 448]. The constitutively expressed member of the Hsp70 family, Hsc70, has also been shown to inhibit α -synuclein fibril formation [449]. Furthermore, Hsc70 was shown to 'coat' α -synuclein fibrils. α -synuclein fibrils coated with Hsp70 were shown to be less toxic than uncoated fibrils [449]. In light of this precedent, it is possible that Hsp70 has a direct effect on β_2m fibrils. β_2m fibrils, like all amyloid fibrils, have the potential to disaggregate and release soluble species. Fibril disaggregation has been demonstrated to be associated with toxicity [166, 191, 192]. Indeed, *in vitro* studies on the effect of Hsp70 on fragmented β_2m fibrils demonstrate a reduction in the rate of fibril disaggregation (Kevin Tipping, personal communications and Figure 6.17). Hsp70 protection could be mediated by its stabilising effect on fibrils thus reducing the release of potentially deleterious, soluble oligomeric species. Alternatively, by interacting with fragmented β_2m fibrils, Hsp70 could mask fibril surfaces, thus preventing abnormal interactions with cellular proteins or lipids.

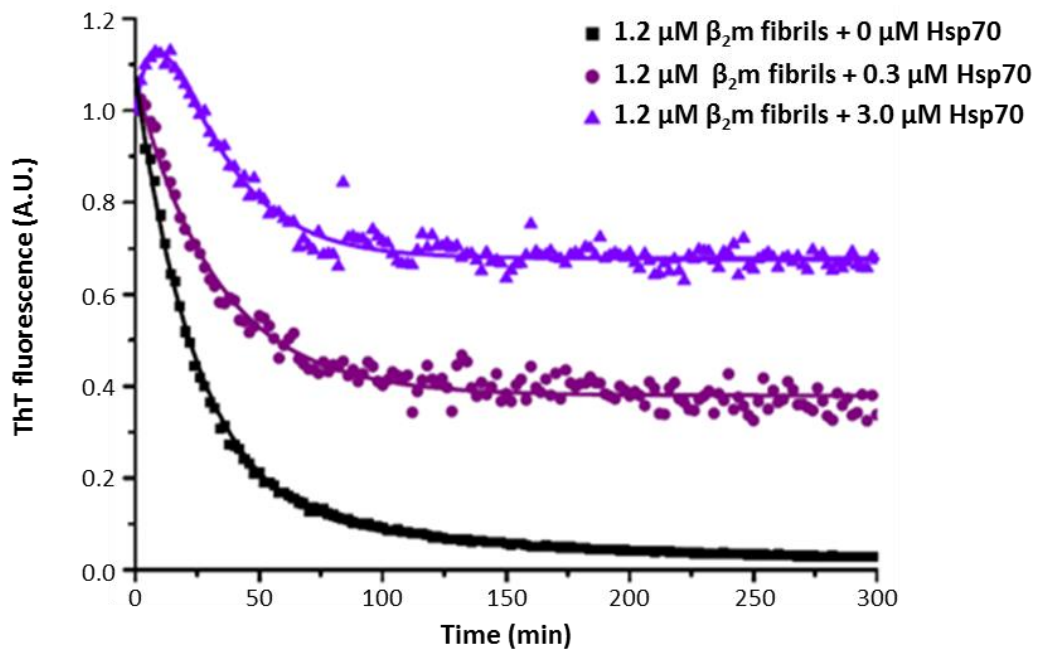


Figure 6.17: Analysis of the effect of Hsp70 on disaggregation of β_2m fibrils. Fibril disaggregation was followed over time by measuring ThT fluorescence. Hsp70 and fragmented β_2m fibrils were diluted in 50 mM sodium phosphate buffer at pH 7.4 containing 10 μM ThT, 30 mM NaCl and 3 mM KCl, to the concentrations indicated. ThT fluorescence was monitored and results were normalised to ThT fluorescence at 0 min for each sample (1.0). Representative data averaged from three independent replicates are shown. ThT was excited at 440 nm and fluorescence measured at 480 nm. Experiment performed by Kevin Tipping, University of Leeds.

However, the experiments described in this chapter differ fundamentally from the studies mentioned above [447, 449]. Both these studies involve pre-incubation of Hsp70/Hsc70 with α -synuclein monomer/fibrils prior to incubation with cells, whereas experiments here involve pre-incubation of cells with Hsp70 prior to incubation with fibrils. Hsp70 presumably only comes into contact with β_2m fibrils in the lysosome. Therefore, although a direct interaction of Hsp70 with β_2m fibrils and a reduction in disaggregation is theoretically plausible, it is likely that other factors are also involved.

It is possible that pre-incubation of cells with Hsp70 could 'coat' inner membranes of endosomes, late endosomes and lysosomes prior to fibril insult. For example, Hsp70 has been shown to bind to membrane lipids and this binding is enhanced at lysosomal pH [441]. Hsp70, by binding to membrane lipids, could therefore obstruct abnormal interactions of fibrils with these lipids. Indeed, fragmented β_2m fibrils have been shown to interact with synthetic liposomes, with fibril-lipid interactions resulting in membrane distortion and blebbing [231]. In addition, recent work in our laboratory has shown that fragmented β_2m fibrils interact with and damage synthetic lipid bilayers [446]. This interaction is dependent on pH, with lipid bilayers being particularly susceptible to damage at low pH [446]. Lipid composition has also been shown to be important and damage by fragmented β_2m fibrils is enhanced in lipid bilayers containing BMP [446]. Although the protection by Hsp70 is unlikely to be via interaction with BMP, it is possible that Hsp70 binds to other membrane lipids. Lysosomal membrane damage is not apparent in cells incubated with fragmented β_2m fibrils (Eric Hewitt, personal communications and Figure 4.17); however, it is possible that β_2m fibrils interact with endosomal, late endosomal and lysosomal membrane lipids in a cellular context. Abnormal interactions with these lipids could result in disruptions in the endolysosomal system.

Hsp70 could also protect cells from the deleterious effects of fragmented β_2m fibrils by enhancing the activities of lysosomal enzymes such as the proteases involved in lysosomal degradation. Indeed, celastrol, which induces Hsp70, has been shown to enhance the enzymatic activity of glucocerebrosidase in models of Gaucher's disease [440]. Hsp70 has also been shown to enhance the activity of acid sphingomyelinase, the enzyme mutated in Niemann Pick disease A and B, and this enhancement leads to protection in models of Niemann Pick disease A and B models [441]. Hsp70 activation has also been demonstrated to boost the activities of enzymes with metabolic disease-causing mutations, such as cystathione β -synthase and methylene tetrahydrofolate reductase [450]. By boosting the activity of lysosomal proteases, Hsp70 could protect against fibril-mediated impairment in degradation of endocytosed proteins. This could also explain why Hsp70 has no effect on LAMP-1 trafficking but restores the degradation of ovalbumin.

The pharmacological enhancement of Hsp70 is an attractive therapeutic strategy and has been explored as treatment for several amyloid diseases [451]. In addition to its efficacy in Gaucher's disease models, celastrol has also been shown to have a protective effect in animal models of Parkinson's disease, Huntington's disease and ALS models with superoxide dismutase-1 (SOD1) mutations [452-454]. 17-N-allylamino-17-demethoxygeldanamycin (17-AAG), an analogue of the Hsp90 inhibitor, geldanamycin, inhibits Hsp90 by blocking the

interaction between Hsp90 and heat shock transcription factor 1 (HSF1) [430]. By doing so, geldanamycin and its derivatives, increase the levels of activated HSF1, thus resulting in the activation of the heat shock response, including activation of Hsp70 [430, 451]. Treatment with 17-AAG has been shown to attenuate the toxicity of α -synuclein in cell models of Parkinson's disease, as well as polyglutamine in mouse models of the polyglutamine disease, SBMA [455, 456]. Finally, arimoclomol has been shown to activate the heat shock response in stressed cells by stabilising activated HSF1 thus resulting in the upregulation of molecular chaperones, including Hsp70 [451]. Arimoclomol has been demonstrated to be protective in mouse models of ALS with SOD1 mutations, as well as mouse models of SBMA [457-459]. Arimoclomol is currently being investigated in phase II clinical trials of ALS [451].

This chapter demonstrates that Hsp70 confers protection against some of the observed deleterious effects of fragmented β_2m fibrils. This adds to the growing body of evidence indicating a protective role for Hsp70 in amyloid disease. A detailed investigation into the mechanism of Hsp70 protection from fragmented β_2m fibrils could inform future therapeutic strategies against amyloid disease.

7 Discussion and future work

Although the close association between appearance of amyloid deposits and onset of pathological events has been clear for many years, the mechanisms of disease pathogenesis remain unclear [79]. Due to the lack of correlation between fibril load and disease severity, research efforts have focused on the investigation of pre-fibrillar aggregates [79, 135, 143-145]. However, accumulating evidence also implicates fibrils as amyloid species with toxic potential [173, 177-186]. The role of amyloid fibrils in disease pathogenesis is being reappraised in light of this accumulating evidence [176]. The experiments described in this thesis investigated the effect of amyloid fibrils on cellular function.

β_2m was used a model to study amyloid disease based on the extensive characterisation of fibril formation pathways, various intermediate species and amyloid fibrils [125, 189, 337, 340, 341, 368]. In addition, β_2m amyloid fibrils formed *in vitro* have been shown to share structural characteristics with *ex vivo* β_2m amyloid fibrils [366]. The β_2m fibrils generated and incorporated in the experiments described here, display characteristic amyloid properties such as binding to ThT and the conformation-specific anti-fibril antibody WO1 [86, 327]. The fragmentation of β_2m fibrils has been shown to yield nanoscale β_2m fibrils which display the same structural characteristics but are of a reduced average length [190]. Fragmented β_2m fibrils have a greater biological activity as evidenced by their ability to inhibit MTT reduction to a greater extent than their unfragmented counterparts [190]. The fragmented β_2m fibrils generated here also display this enhanced biological activity and were therefore selected for further investigation. Previous work in the laboratory using macrophages and primary human monocytes demonstrated that β_2m fibrils are trafficked to the lysosome where they persist [247, 248]. Building on this, the effect of β_2m fibrils on lysosome function was investigated.

7.1 Lysosome dysfunction and its role in amyloid disease

Previous work showed that internalisation of β_2m fibrils was length-dependent with fragmented fibrils being internalised to a greater extent than unfragmented fibrils (Andrew Hellewell, personal communications). This difference in internalisation, and hence access to intracellular organelles such as the lysosome, rationalises the differences in biological activity observed. Lysosomal dysfunction is a recurrent theme in reported mechanisms underlying amyloid diseases [278]. The data presented in this thesis support the notion that lysosomes are a key target in amyloid disease. As protein degradation is a crucial function of the lysosome, the effect of fragmented β_2m fibrils on the ability of lysosomes to perform this function was investigated. Fragmented fibrils were shown to impair the degradation of

endocytosed proteins. However, the proteolysis of the cell permeant Magic Red™ cathepsin B substrate was unaffected by fragmented fibrils. This could be due to a saturating effect on lysosomal proteolytic machinery by fibrils acting on proteases other than cathepsin B or disruption in trafficking of endocytosed cargo to lysosomes. Experiments investigating the effect of fragmented β_2m fibrils on other lysosomal hydrolases show no effect on β -glucocerebrosidase activity and only a modest effect on β -galactosidase activity. This suggests that fragmented fibrils only inhibit the capacity of cells to degrade proteins.

Future work investigating whether fragmented fibrils saturate proteolytic machinery could involve investigation of activities of other lysosomal cysteine proteases such as cathepsin L and K using commercially available cell permeant substrates similar to that used for cathepsin B. Further investigation could also include aspartic and serine proteases. In order to analyse whether fragmented fibrils disrupt the trafficking of endocytosed cargo to lysosomes, the trafficking of endocytosed fluorescently labelled protein substrate could be further characterised. As LysoTracker Green accumulates in acidic vesicles, it does not necessarily distinguish between late endosomes and lysosomes. A more detailed characterisation could involve antibody markers to organelles in the endolysosomal pathway such as the early endosome marker (anti-EEA1), the late endosome marker (anti-Rab7) and the lysosomal marker (anti-LAMP-1). For example, live cell confocal microscopy could be used to analyse and quantify the colocalisation of AF647-ovalbumin with anti-EEA1, anti-Rab7 and anti-LAMP-1 in order to identify the block in trafficking of endocytosed cargo. This could also extend to investigation of the effect of fragmented fibrils on other lysosomal hydrolases using substrates that require targeted delivery to the lysosome.

The inhibition of degradation of endocytosed proteins by fragmented fibrils, and thus their accumulation in cells, has a number of derived consequences. Impairment in degradation could also affect resident cellular proteins whose accumulation could have further reaching consequences. If the function of these resident cellular proteins requires their recycling, their entrapment in dysfunctional lysosomes would influence cellular signalling pathways. Lysosomal dysfunction would also impact upon autophagy and autophagy dysfunction is recurrently reported as a mechanism underlying neurodegenerative diseases such as Alzheimer's, Parkinson's and Huntington's diseases [278].

Indications of altered autophagy are often deduced by observations of autophagosome accumulation [242, 255, 261, 290, 291]. Indeed a preliminary investigation into the effects of fragmented β_2m fibrils indicates altered autophagy; however it is unclear whether this

alteration corresponds to a compensatory upregulation of autophagy or a block in autophagosome clearance. Further investigation into the effect of fibrils on autophagy could involve experiments that distinguish between effects on fusion of autophagosomes to lysosomes to form functional autolysosomes, and the degradation in and clearance of autolysosomes. For example, immunofluorescence microscopy analysis of fixed cells stained with anti-LC3B and anti-cathepsin D should provide information on autophagosome and lysosome fusion. Cathepsin D is a lysosomal hydrolase and therefore antibodies specific for cathepsin D could be used to stain lysosomes. LC3-II, the lipidated form of LC3-I is recruited to active autophagosomes and therefore the anti-LC3B antibody (which recognises both LC3-I and LC3-II) could be used to stain autophagosomes. Activated autophagosomes could be distinguished from non-activated autophagosomes by incorporating a commercially available selective permeabilisation solution which extracts cytosolic LC3-I without affecting LC3-II (Merck Millipore). Co-localisation analysis of cathepsin D and LC3-II could therefore be informative on fusion of autophagosomes and lysosomes. Elucidation of degradation in the autolysosome is more challenging. One approach could involve monitoring the time-dependent decrease of an autophagy-degradable marker in the presence or absence of fibrils. The caveat with this approach, however, is that the marker may be degraded by autophagy-independent mechanisms and of course fibrils may impair the degradation of the marker without impairing autophagy.

Inhibition of lysosomal function has been implicated in the pathogenesis of amyloid disease [278]. This is particularly highlighted by a study using primary mouse cortical neurons which demonstrated that inhibition of lysosomal proteolysis by protease inhibitors or by suppression of lysosomal acidification, retarded transport of autolysosomes, late endosomes and lysosomes and resulted in their accumulation in dystrophic axonal swellings. Interestingly these dystrophic swellings resembled those observed in Alzheimer's disease mouse models and were reversed when lysosomal proteolysis was restored [284].

Lysosomal dysfunction could also contribute to the pathology of DRA. β_2m amyloid fibrils deposit in osteoarticular tissues and result in bone and joint destruction [52, 53]. Macrophages, which infiltrate β_2m amyloid deposits *in vivo*, have been shown to internalise β_2m fibrils and traffic them to the lysosome where they persist [247, 248, 390]. β_2m fibrils in the lysosome could reduce the degradative capacity of these cells whose function relies heavily on degradation. Furthermore, β_2m fibrils have the potential to disrupt bone remodelling due to their demonstrated ability to perturb primary human cells implicated in the pathology of DRA (osteoblasts and osteoclasts) [248]. Bone remodelling requires the concerted

action of osteoclasts (which resorb bone) and osteoblasts (which produce bone) [460]. β_2 m fibrils were shown to inhibit the ability of osteoclasts to resorb bone [248]. Bone resorption by osteoclasts involves lysosome-like organelles and fibril-mediated lysosomal dysfunction could rationalise this inhibition [460].

7.2 Membrane trafficking perturbations and their role in amyloid disease

Accumulating evidence implicates trafficking defects in Alzheimer's, Parkinson's and Huntington's diseases [323, 394, 395, 409-413]. Fragmented fibrils were shown to enhance the expression of the lysosomal membrane proteins, LAMP-1 and CD63 at the cell surface without increasing their expression or inducing a gross re-distribution of existing protein pools. Inhibition of protein synthesis using cycloheximide, inhibited, in part, this increase in LAMP-1 and CD63 at the cell surface suggesting that fragmented fibrils alter the trafficking of newly synthesised LAMP-1 and CD63. This could be due to impairment in trafficking of newly synthesised protein from the TGN to late endosomes. On the other hand, an increase in trafficking of newly synthesised protein to the plasma membrane or the retention of protein at the plasma membrane could rationalise this observation.

A preliminary investigation of the effect of fibrils on fluid phase endocytosis using dextrans indicates that fibrils do not affect the overall uptake of dextrans but may disrupt trafficking of endocytosed cargo to the lysosome. This would rationalise the impairment in ovalbumin degradation and the lack of effect of fibrils on the cleavage of the membrane permeant Magic Red™ cathepsin B substrate. It could also explain the increased levels of LC3-II in fibril treated cells as a perturbation in delivery of cargo (such as autophagosomes) to lysosomes, would result in defective autophagosome clearance.

Amyloid-mediated trafficking defects have been proposed to occur via abnormal interactions with regulatory proteins which mediate trafficking such as α -synuclein interactions with Rab1, Rab3a, Rab5 and Rab8 [409-411]. Reported trafficking defects also include amyloid-mediated inhibition of clathrin-mediated endocytosis by $A\beta$, huntingtin, ataxin-1 and superoxide dismutase-1 amyloid aggregates [323, 413, 414]. It is possible that fragmented fibrils participate in abnormal interactions with other proteins inside trafficking vesicles/endosomes/lysosomes and by doing so, alter the trafficking of LAMP-1 and CD63. Identification of such interacting proteins would be informative on the mechanism of trafficking disruption.

As inhibition of clathrin-mediated endocytosis has been linked to amyloid disease, it would be interesting to see whether fragmented fibrils disrupt clathrin-mediated endocytosis [323, 414]. This could be achieved by measuring the uptake of fluorescently labelled transferrin, which has been shown to occur via binding to the transferrin receptor followed by clathrin-mediated endocytosis of the transferrin-transferrin receptor complex [414, 461]. Future work could also involve the investigation of trafficking of other lysosomal proteins such as lysosomal hydrolases to the lysosome. If fragmented fibrils do indeed block the delivery of cargo to lysosomes, it would be informative to identify the precise step at which this block occurs. This could be inferred from the experiments with labelled ovalbumin and organelle markers suggested above. Alternatively, dextrans could be incorporated into these experiments. Due to their resistance to hydrolysis, dextrans would have the added bonus of being able to distinguish effects on trafficking from effects on lysosome-mediated degradation.

7.3 Future therapeutic strategies for amyloid disease

A large body of evidence indicates that elevation of Hsp70 levels is protective in several models of neurodegeneration [217, 427, 431-434, 437, 438]. The role of Hsp70 in fibril mediated cell-disruption was therefore investigated. Consistent with previous reports, recombinant Hsp70 was internalised by cells and trafficked to intracellular compartments which co-stained with LysoTracker Green [441]. Hsp70 protected cell from fibril-mediated inhibition of MTT reduction and impairment in degradation of endocytosed protein, but did not confer protection against membrane trafficking defects. Protection may be mediated by stabilising fibrils and preventing release of potentially deleterious soluble species, or by masking the fibril surface and preventing abnormal interactions with cellular proteins. Alternatively, Hsp70 has been shown to bind membrane lipids, and may bind to lipids found on the inner membranes of endosomes, late endosomes or lysosomes [441]. By doing so, Hsp70 may prevent fibril-mediated disruption in cargo delivery to the lysosome. Hsp70 could also rescue the degradation of endocytosed protein by enhancing the activity of lysosomal enzymes. Investigation into the interaction partners of Hsp70 in lysosomes isolated from cells pre-incubated with Hsp70 in the presence and absence of fibrils may shed further light on the protection mechanism. The pharmacological and genetic enhancement of molecular chaperones including Hsp70 is being explored as a therapeutic strategy against protein conformational diseases, lysosomal storage diseases (LSDs) and amyloidosis [197, 214, 215, 430, 451]. In addition, the targeted delivery of recombinant Hsp70 is currently in preclinical development for multiple LSDs [462]. This therapeutic strategy could also apply to amyloid diseases. Further characterisation of the mechanism of protection by Hsp70 demonstrated

here would therefore be beneficial, not only in understanding the mechanism by which fibrils mediate cell-disruption but may also inform future therapeutic strategies.

In combination with previous studies, the work described in this thesis implicates the lysosome as a key target in the pathogenesis of amyloid disease, and can be used to inform therapeutic strategies. For example, enhancement of lysosomal function would clear amyloid, counteract the deleterious effects of fibrils and could restore cellular health. The recent discovery of a gene network which globally controls and co-ordinates lysosomal biogenesis, autophagy, exocytosis and endocytosis has shed light on how lysosomes adapt to environmental cues [304]. This lysosomal gene network is referred to as the co-ordinated lysosomal expression and regulation (CLEAR) network and it is controlled by a master regulator, transcription factor EB (TFEB) [304]. TFEB has been shown to positively regulate genes in the CLEAR network, control the number of lysosomes and enhance the clearance of lysosomal substrates [278]. Interestingly, TFEB activation has been investigated as a therapeutic strategy for lysosomal storage diseases as well as neurodegenerative diseases. For example, TFEB gene delivery restored lysosomal levels in a mouse model of Parkinson's disease and diminished dopaminergic neurodegeneration [261]. TFEB was also shown to enhance degradation and decrease neurotoxicity in a mouse model of Huntington's disease [463]. It is predicted that overexpression of TFEB would in turn enhance the expression of lysosomal genes resulting in enhanced lysosomal degradation. It would be interesting to see whether overexpression of TFEB would be protective in the context of impaired degradation of endocytosed proteins in fibril-treated cells. Future work could incorporate cells transfected with TFEB in assays analysing the effect of fragmented fibrils on ovalbumin degradation.

7.4 Summary

In summary, this thesis demonstrates that fragmented β_2m fibrils target the lysosome and disrupt lysosomal function. Fragmented β_2m fibrils also perturb the trafficking of lysosomal membrane proteins. Preliminary work suggests that fragmented β_2m fibrils disrupt delivery of endocytosed cargo to lysosomes and may therefore impact on autophagy. Lysosomal dysfunction and disruptions in trafficking have significant consequences on cellular function. Molecular mechanisms by which nanoscale amyloid fibrils may target the lysosome and endolysosomal pathway thus impacting on disease pathogenesis are depicted in Figure 7.1.

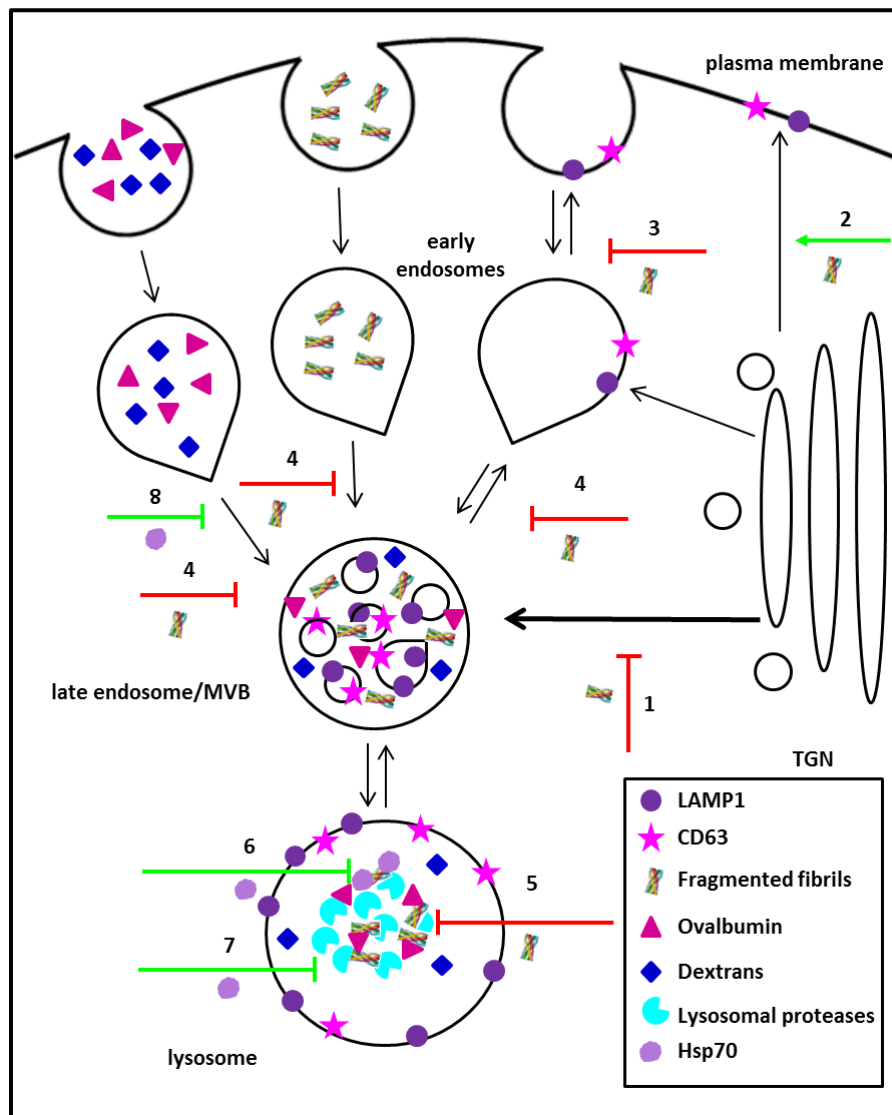


Figure 7.1: Model of cellular disruption by fragmented β_2m amyloid fibrils. β_2m fibrils have been shown to be internalised and trafficked to the lysosome [247, 248] (Andrew Hellewell, personal communications). β_2m fibrils may disrupt cellular function by the following mechanisms. 1) Fragmented fibrils may inhibit the transport of lysosomal membrane proteins such as LAMP-1 and CD63 from the TGN to late endosomes. 2) The trafficking of lysosomal membrane proteins such as LAMP-1 and CD63 to the plasma membrane may be enhanced by fragmented fibrils. 3) Endocytosis of lysosomal membrane proteins at the cell surface may be inhibited by fragmented fibrils. 4) The delivery of contents of early endosomes such as ovalbumin, dextrans and fragmented fibrils may be blocked by fragmented fibrils. 5) Lysosome mediated degradation may be impaired by saturation of the proteolytic machinery by fragmented fibrils. Protection by Hsp70 from fibril-mediated cell disruption could be mediated by the following mechanisms. 6) Hsp70 may stabilise fibrils thus preventing disaggregation or mask fibril surfaces and prevent abnormal interactions with cellular proteins. 7) Hsp70 may enhance lysosomal proteases and thus overcome fibril-mediated inhibition of degradation of endocytosed proteins. 8) Hsp70 may interact with lipids in the inner membranes of endosomes, late endosomes and lysosomes and thus rescue cells from fibril-mediated disruption of endocytosed cargo to lysosomes.

8 References

- 1 Chiti, F. and Dobson, C.M. (2006) Protein misfolding, functional amyloid, and human disease. *Annu Rev Biochem* 75, 333-366
- 2 Hebert, L.E., Weuve, J., Scherr, P.A., and Evans, D.A. (2013) Alzheimer disease in the United States (2010-2050) estimated using the 2010 census. *Neurology* 80, 1778-1783
- 3 Stefani, M. and Dobson, C.M. (2003) Protein aggregation and aggregate toxicity: new insights into protein folding, misfolding diseases and biological evolution. *J Mol Med (Berl)* 81, 678-699
- 4 Sipe, J.D., Benson, M.D., Buxbaum, J.N., Ikeda, S., Merlini, G., Saraiva, M.J., and Westermarck, P. (2012) Amyloid fibril protein nomenclature: 2012 recommendations from the Nomenclature Committee of the International Society of Amyloidosis. *Amyloid* 19, 167-170
- 5 Hardy, J. (2006) A hundred years of Alzheimer's disease research. *Neuron* 52, 3-13
- 6 Anand, R., Gill, K.D., and Mahdi, A.A. (2014) Therapeutics of Alzheimer's disease: Past, present and future. *Neuropharmacology* 76 Pt A, 27-50
- 7 Passmore, M.J., Ho, A., and Gallagher, R. (2012) Behavioral and psychological symptoms in moderate to severe Alzheimer's disease: a palliative care approach emphasizing recognition of personhood and preservation of dignity. *J Alzheimers Dis* 29, 1-13
- 8 Ghidoni, R., Paterlini, A., and Benussi, L. (2013) Translational proteomics in Alzheimer's disease and related disorders. *Clin Biochem* 46, 480-486
- 9 Blessed, G., Tomlinson, B.E., and Roth, M. (1968) The association between quantitative measures of dementia and of senile change in the cerebral grey matter of elderly subjects. *Br J Psychiatry* 114, 797-811
- 10 Glenner, G.G. and Wong, C.W. (1984) Alzheimer's disease: initial report of the purification and characterization of a novel cerebrovascular amyloid protein. *Biochem Biophys Res Commun* 120, 885-890
- 11 Lee, V.M., Balin, B.J., Otvos, L., Jr., and Trojanowski, J.Q. (1991) A68: a major subunit of paired helical filaments and derivatized forms of normal Tau. *Science* 251, 675-678
- 12 Hardy, J.A. and Higgins, G.A. (1992) Alzheimer's disease: the amyloid cascade hypothesis. *Science* 256, 184-185
- 13 Coulson, E.J., Paliga, K., Beyreuther, K., and Masters, C.L. (2000) What the evolution of the amyloid protein precursor supergene family tells us about its function. *Neurochem Int* 36, 175-184

- 14 Nalivaeva, N.N. and Turner, A.J. (2013) The amyloid precursor protein: a biochemical enigma in brain development, function and disease. *FEBS Lett* 587, 2046-2054
- 15 Young-Pearse, T.L., Bai, J., Chang, R., Zheng, J.B., LoTurco, J.J., and Selkoe, D.J. (2007) A critical function for beta-amyloid precursor protein in neuronal migration revealed by in utero RNA interference. *J Neurosci* 27, 14459-14469
- 16 Ross, C.A. and Poirier, M.A. (2004) Protein aggregation and neurodegenerative disease. *Nat Med* 10 Suppl, S10-17
- 17 Esler, W.P. and Wolfe, M.S. (2001) A portrait of Alzheimer secretases--new features and familiar faces. *Science* 293, 1449-1454
- 18 Kaye, R., Head, E., Thompson, J.L., McIntire, T.M., Milton, S.C., Cotman, C.W., and Glabe, C.G. (2003) Common structure of soluble amyloid oligomers implies common mechanism of pathogenesis. *Science* 300, 486-489
- 19 Welander, H., Franberg, J., Graff, C., Sundstrom, E., Winblad, B., and Tjernberg, L.O. (2009) Abeta43 is more frequent than Abeta40 in amyloid plaque cores from Alzheimer disease brains. *J Neurochem* 110, 697-706
- 20 Medeiros, R., Baglietto-Vargas, D., and LaFerla, F.M. (2011) The role of tau in Alzheimer's disease and related disorders. *CNS Neurosci Ther* 17, 514-524
- 21 Dixit, R., Ross, J.L., Goldman, Y.E., and Holzaur, E.L. (2008) Differential regulation of dynein and kinesin motor proteins by tau. *Science* 319, 1086-1089
- 22 Li, H.L., Wang, H.H., Liu, S.J., Deng, Y.Q., Zhang, Y.J., Tian, Q., Wang, X.C., Chen, X.Q., Yang, Y., Zhang, J.Y., Wang, Q., Xu, H., Liao, F.F., and Wang, J.Z. (2007) Phosphorylation of tau antagonizes apoptosis by stabilizing beta-catenin, a mechanism involved in Alzheimer's neurodegeneration. *Proc Natl Acad Sci U S A* 104, 3591-3596
- 23 Van Den Eeden, S.K., Tanner, C.M., Bernstein, A.L., Fross, R.D., Leimpeter, A., Bloch, D.A., and Nelson, L.M. (2003) Incidence of Parkinson's disease: variation by age, gender, and race/ethnicity. *Am J Epidemiol* 157, 1015-1022
- 24 de Lau, L.M. and Breteler, M.M. (2006) Epidemiology of Parkinson's disease. *Lancet Neurol* 5, 525-535
- 25 Shulman, J.M., De Jager, P.L., and Feany, M.B. (2011) Parkinson's disease: genetics and pathogenesis. *Annu Rev Pathol* 6, 193-222
- 26 Fahn, S. (2003) Description of Parkinson's disease as a clinical syndrome. *Ann N Y Acad Sci* 991, 1-14
- 27 Waxman, E.A. and Giasson, B.I. (2009) Molecular mechanisms of alpha-synuclein neurodegeneration. *Biochim Biophys Acta* 1792, 616-624

- 28** Vargas, K.J., Makani, S., Davis, T., Westphal, C.H., Castillo, P.E., and Chandra, S.S. (2014) Synucleins regulate the kinetics of synaptic vesicle endocytosis. *J Neurosci* 34, 9364-9376
- 29** Rodriguez-Oroz, M.C., Jahanshahi, M., Krack, P., Litvan, I., Macias, R., Bezard, E., and Obeso, J.A. (2009) Initial clinical manifestations of Parkinson's disease: features and pathophysiological mechanisms. *Lancet Neurol* 8, 1128-1139
- 30** Dickson, D.W., Braak, H., Duda, J.E., Duyckaerts, C., Gasser, T., Halliday, G.M., Hardy, J., Leverenz, J.B., Del Tredici, K., Wszolek, Z.K., and Litvan, I. (2009) Neuropathological assessment of Parkinson's disease: refining the diagnostic criteria. *Lancet Neurol* 8, 1150-1157
- 31** Hawkes, C.H. (2008) The prodromal phase of sporadic Parkinson's disease: does it exist and if so how long is it? *Mov Disord* 23, 1799-1807
- 32** Brichta, L., Greengard, P., and Flajolet, M. (2013) Advances in the pharmacological treatment of Parkinson's disease: targeting neurotransmitter systems. *Trends Neurosci* 36, 543-554
- 33** Soto, C. (2003) Unfolding the role of protein misfolding in neurodegenerative diseases. *Nat Rev Neurosci* 4, 49-60
- 34** Pillay, K. and Govender, P. (2013) Amylin uncovered: a review on the polypeptide responsible for type II diabetes. *Biomed Res Int* 2013, 826706
- 35** UKPDS (1998) Intensive blood-glucose control with sulphonylureas or insulin compared with conventional treatment and risk of complications in patients with type 2 diabetes (UKPDS 33). UK Prospective Diabetes Study (UKPDS) Group. *Lancet* 352, 837-853
- 36** Westermark, P., Wernstedt, C., Wilander, E., Hayden, D.W., O'Brien, T.D., and Johnson, K.H. (1987) Amyloid fibrils in human insulinoma and islets of Langerhans of the diabetic cat are derived from a neuropeptide-like protein also present in normal islet cells. *Proc Natl Acad Sci U S A* 84, 3881-3885
- 37** Cooper, G.J., Willis, A.C., Clark, A., Turner, R.C., Sim, R.B., and Reid, K.B. (1987) Purification and characterization of a peptide from amyloid-rich pancreases of type 2 diabetic patients. *Proc Natl Acad Sci U S A* 84, 8628-8632
- 38** Rotondo, F., Vidal, S., Bell, D., Horvath, E., Kovacs, K., Scheithauer, B.W., and Lloyd, R.V. (2003) Immunohistochemical localization of amylin in human pancreas, thyroid, pituitary and their tumors. *Acta Histochem* 105, 303-307
- 39** Martin, C. (2006) The physiology of amylin and insulin: maintaining the balance between glucose secretion and glucose uptake. *Diabetes Educ* 32 Suppl 3, 101S-104S
- 40** Cluck, M.W., Chan, C.Y., and Adrian, T.E. (2005) The regulation of amylin and insulin gene expression and secretion. *Pancreas* 30, 1-14

- 41 Hoppener, J.W. and Lips, C.J. (2006) Role of islet amyloid in type 2 diabetes mellitus. *Int J Biochem Cell Biol* 38, 726-736
- 42 Hoppener, J.W., Verbeek, J.S., de Koning, E.J., Oosterwijk, C., van Hulst, K.L., Visser-Vernooy, H.J., Hofhuis, F.M., van Gaalen, S., Berends, M.J., Hackeng, W.H., and et al. (1993) Chronic overproduction of islet amyloid polypeptide/amylin in transgenic mice: lysosomal localization of human islet amyloid polypeptide and lack of marked hyperglycaemia or hyperinsulinaemia. *Diabetologia* 36, 1258-1265
- 43 Rochester, C.D. and Akiyode, O. (2014) Novel and emerging diabetes mellitus drug therapies for the type 2 diabetes patient. *World J Diabetes* 5, 305-315
- 44 Lopes, D.H., Colin, C., Degaki, T.L., de Sousa, A.C., Vieira, M.N., Sebollela, A., Martinez, A.M., Bloch, C., Jr., Ferreira, S.T., and Sogayar, M.C. (2004) Amyloidogenicity and cytotoxicity of recombinant mature human islet amyloid polypeptide (rIAPP). *J Biol Chem* 279, 42803-42810
- 45 Gejyo, F., Odani, S., Yamada, T., Honma, N., Saito, H., Suzuki, Y., Nakagawa, Y., Kobayashi, H., Maruyama, Y., Hirasawa, Y., and et al. (1986) Beta 2-microglobulin: a new form of amyloid protein associated with chronic hemodialysis. *Kidney Int* 30, 385-390
- 46 Pamer, E. and Cresswell, P. (1998) Mechanisms of MHC class I--restricted antigen processing. *Annu Rev Immunol* 16, 323-358
- 47 Rock, K.L. and Goldberg, A.L. (1999) Degradation of cell proteins and the generation of MHC class I-presented peptides. *Annu Rev Immunol* 17, 739-779
- 48 Floege, J., Bartsch, A., Schulze, M., Shaldon, S., Koch, K.M., and Smeby, L.C. (1991) Clearance and synthesis rates of beta 2-microglobulin in patients undergoing hemodialysis and in normal subjects. *J Lab Clin Med* 118, 153-165
- 49 Floege, J. and Ketteler, M. (2001) beta2-microglobulin-derived amyloidosis: an update. *Kidney Int Suppl* 78, S164-171
- 50 Gejyo, F., Homma, N., Suzuki, Y., and Arakawa, M. (1986) Serum levels of beta 2-microglobulin as a new form of amyloid protein in patients undergoing long-term hemodialysis. *N Engl J Med* 314, 585-586
- 51 Rabindranath, K.S., Strippoli, G.F., Daly, C., Roderick, P.J., Wallace, S., and MacLeod, A.M. (2006) Haemodiafiltration, haemofiltration and haemodialysis for end-stage kidney disease. *Cochrane Database Syst Rev*, CD006258
- 52 Otsubo, S., Kimata, N., Okutsu, I., Oshikawa, K., Ueda, S., Sugimoto, H., Mitobe, M., Uchida, K., Otsubo, K., Nitta, K., and Akiba, T. (2009) Characteristics of dialysis-related amyloidosis in patients on haemodialysis therapy for more than 30 years. *Nephrol Dial Transplant* 24, 1593-1598

- 53 Linke, R.P., Schaeffer, J., Gielow, P., Lindner, P., Lottspeich, F., Pluckthun, A., and Weiss, E.H. (2000) Production of recombinant human beta2-microglobulin for scintigraphic diagnosis of amyloidosis in uremia and hemodialysis. *Eur J Biochem* 267, 627-633
- 54 Hodkinson, J.P., Ashcroft, A.E., and Radford, S.E. (2012) Protein misfolding and toxicity in dialysis-related amyloidosis. In *Non-fibrillar amyloidogenic protein assemblies : common cytotoxins underlying degenerative diseases* (Rahimi, F. and Bitan, G., eds), pp. 377-405, Springer
- 55 Saito, A. and Gejyo, F. (2006) Current clinical aspects of dialysis-related amyloidosis in chronic dialysis patients. *Ther Apher Dial* 10, 316-320
- 56 Campistol, J.M. (2001) Dialysis-related amyloidosis after renal transplantation. *Semin Dial* 14, 99-102
- 57 Yamamoto, S., Kazama, J.J., Narita, I., Naiki, H., and Gejyo, F. (2009) Recent progress in understanding dialysis-related amyloidosis. *Bone* 45 Suppl 1, S39-42
- 58 Maury, C.P. (2009) The emerging concept of functional amyloid. *J Intern Med* 265, 329-334
- 59 Chernoff, Y.O. (2004) Amyloidogenic domains, prions and structural inheritance: rudiments of early life or recent acquisition? *Curr Opin Chem Biol* 8, 665-671
- 60 Fowler, D.M., Koulov, A.V., Balch, W.E., and Kelly, J.W. (2007) Functional amyloid--from bacteria to humans. *Trends Biochem Sci* 32, 217-224
- 61 Smith, J.F., Knowles, T.P., Dobson, C.M., Macphee, C.E., and Welland, M.E. (2006) Characterization of the nanoscale properties of individual amyloid fibrils. *Proc Natl Acad Sci U S A* 103, 15806-15811
- 62 Chapman, M.R., Robinson, L.S., Pinkner, J.S., Roth, R., Heuser, J., Hammar, M., Normark, S., and Hultgren, S.J. (2002) Role of *Escherichia coli* curli operons in directing amyloid fiber formation. *Science* 295, 851-855
- 63 Barnhart, M.M. and Chapman, M.R. (2006) Curli biogenesis and function. *Annu Rev Microbiol* 60, 131-147
- 64 Hammar, M., Arnqvist, A., Bian, Z., Olsen, A., and Normark, S. (1995) Expression of two csg operons is required for production of fibronectin- and congo red-binding curli polymers in *Escherichia coli* K-12. *Mol Microbiol* 18, 661-670
- 65 Evans, M.L. and Chapman, M.R. (2014) Curli biogenesis: order out of disorder. *Biochim Biophys Acta* 1843, 1551-1558
- 66 Nenner, A.A., Robinson, L.S., Hammer, N.D., Epstein, E.A., Badtke, M.P., Hultgren, S.J., and Chapman, M.R. (2011) CsgE is a curli secretion specificity factor that prevents amyloid fibre aggregation. *Mol Microbiol* 81, 486-499

- 67 Nenninger, A.A., Robinson, L.S., and Hultgren, S.J. (2009) Localized and efficient curli nucleation requires the chaperone-like amyloid assembly protein CsgF. *Proc Natl Acad Sci U S A* 106, 900-905
- 68 Robinson, L.S., Ashman, E.M., Hultgren, S.J., and Chapman, M.R. (2006) Secretion of curli fibre subunits is mediated by the outer membrane-localized CsgG protein. *Mol Microbiol* 59, 870-881
- 69 Prusiner, S.B. (1982) Novel proteinaceous infectious particles cause scrapie. *Science* 216, 136-144
- 70 Prusiner, S.B. (1998) Prions. *Proc Natl Acad Sci U S A* 95, 13363-13383
- 71 Hofmann, J. and Vorberg, I. (2013) Life cycle of cytosolic prions. *Prion* 7, 369-377
- 72 Uptain, S.M. and Lindquist, S. (2002) Prions as protein-based genetic elements. *Annu Rev Microbiol* 56, 703-741
- 73 True, H.L., Berlin, I., and Lindquist, S.L. (2004) Epigenetic regulation of translation reveals hidden genetic variation to produce complex traits. *Nature* 431, 184-187
- 74 Shorter, J. and Lindquist, S. (2005) Prions as adaptive conduits of memory and inheritance. *Nat Rev Genet* 6, 435-450
- 75 Lian, H.Y., Jiang, Y., Zhang, H., Jones, G.W., and Perrett, S. (2006) The yeast prion protein Ure2: structure, function and folding. *Biochim Biophys Acta* 1764, 535-545
- 76 Wickner, R.B., Edskes, H.K., Roberts, B.T., Baxa, U., Pierce, M.M., Ross, E.D., and Brachmann, A. (2004) Prions: proteins as genes and infectious entities. *Genes Dev* 18, 470-485
- 77 Jensen, M.A., True, H.L., Chernoff, Y.O., and Lindquist, S. (2001) Molecular population genetics and evolution of a prion-like protein in *Saccharomyces cerevisiae*. *Genetics* 159, 527-535
- 78 Chien, P., Weissman, J.S., and DePace, A.H. (2004) Emerging principles of conformation-based prion inheritance. *Annu Rev Biochem* 73, 617-656
- 79 Knowles, T.P., Vendruscolo, M., and Dobson, C.M. (2014) The amyloid state and its association with protein misfolding diseases. *Nat Rev Mol Cell Biol* 15, 384-396
- 80 Hearing, V.J. (2000) The melanosome: the perfect model for cellular responses to the environment. *Pigment Cell Res* 13 Suppl 8, 23-34
- 81 Fowler, D.M., Koulov, A.V., Alory-Jost, C., Marks, M.S., Balch, W.E., and Kelly, J.W. (2006) Functional amyloid formation within mammalian tissue. *PLoS Biol* 4, e6
- 82 Berson, J.F., Theos, A.C., Harper, D.C., Tenza, D., Raposo, G., and Marks, M.S. (2003) Proprotein convertase cleavage liberates a fibrillogenic fragment of a resident glycoprotein to initiate melanosome biogenesis. *J Cell Biol* 161, 521-533

- 83** Maji, S.K., Perrin, M.H., Sawaya, M.R., Jessberger, S., Vadodaria, K., Rissman, R.A., Singru, P.S., Nilsson, K.P., Simon, R., Schubert, D., Eisenberg, D., Rivier, J., Sawchenko, P., Vale, W., and Riek, R. (2009) Functional amyloids as natural storage of peptide hormones in pituitary secretory granules. *Science* 325, 328-332
- 84** Sipe, J.D. and Cohen, A.S. (2000) Review: history of the amyloid fibril. *J Struct Biol* 130, 88-98
- 85** Shewmaker, F., McGlinchey, R.P., and Wickner, R.B. (2011) Structural insights into functional and pathological amyloid. *J Biol Chem* 286, 16533-16540
- 86** Nilsson, M.R. (2004) Techniques to study amyloid fibril formation in vitro. *Methods* 34, 151-160
- 87** Westermark, G.T., Johnson, K.H., and Westermark, P. (1999) Staining methods for identification of amyloid in tissue. *Methods Enzymol* 309, 3-25
- 88** Sunde, M., Serpell, L.C., Bartlam, M., Fraser, P.E., Pepys, M.B., and Blake, C.C. (1997) Common core structure of amyloid fibrils by synchrotron X-ray diffraction. *J Mol Biol* 273, 729-739
- 89** Dobson, C.M. (2003) Protein folding and misfolding. *Nature* 426, 884-890
- 90** Eisenberg, D. and Jucker, M. (2012) The amyloid state of proteins in human diseases. *Cell* 148, 1188-1203
- 91** Serpell, L.C., Sunde, M., Benson, M.D., Tennent, G.A., Pepys, M.B., and Fraser, P.E. (2000) The protofilament substructure of amyloid fibrils. *J Mol Biol* 300, 1033-1039
- 92** Sunde, M. and Blake, C. (1997) The structure of amyloid fibrils by electron microscopy and X-ray diffraction. *Adv Protein Chem* 50, 123-159
- 93** Bauer, H.H., Aebi, U., Haner, M., Hermann, R., Muller, M., and Merkle, H.P. (1995) Architecture and polymorphism of fibrillar supramolecular assemblies produced by in vitro aggregation of human calcitonin. *J Struct Biol* 115, 1-15
- 94** Saiki, M., Honda, S., Kawasaki, K., Zhou, D., Kaito, A., Konakahara, T., and Morii, H. (2005) Higher-order molecular packing in amyloid-like fibrils constructed with linear arrangements of hydrophobic and hydrogen-bonding side-chains. *J Mol Biol* 348, 983-998
- 95** Sawaya, M.R., Sambashivan, S., Nelson, R., Ivanova, M.I., Sievers, S.A., Apostol, M.I., Thompson, M.J., Balbirnie, M., Wiltzius, J.J., McFarlane, H.T., Madsen, A.O., Riek, C., and Eisenberg, D. (2007) Atomic structures of amyloid cross-beta spines reveal varied steric zippers. *Nature* 447, 453-457
- 96** Pedersen, J.S., Andersen, C.B., and Otzen, D.E. (2010) Amyloid structure--one but not the same: the many levels of fibrillar polymorphism. *FEBS J* 277, 4591-4601

- 97** Eanes, E.D. and Glenner, G.G. (1968) X-ray diffraction studies on amyloid filaments. *J Histochem Cytochem* 16, 673-677
- 98** Serpell, L. (2014) Amyloid structure. *Essays Biochem* 56, 1-10
- 99** Makin, O.S. and Serpell, L.C. (2005) Structures for amyloid fibrils. *FEBS J* 272, 5950-5961
- 100** Fitzpatrick, A.W., Debelouchina, G.T., Bayro, M.J., Clare, D.K., Caporini, M.A., Bajaj, V.S., Jaroniec, C.P., Wang, L., Ladizhansky, V., Muller, S.A., MacPhee, C.E., Waudby, C.A., Mott, H.R., De Simone, A., Knowles, T.P., Saibil, H.R., Vendruscolo, M., Orlova, E.V., Griffin, R.G., and Dobson, C.M. (2013) Atomic structure and hierarchical assembly of a cross-beta amyloid fibril. *Proc Natl Acad Sci U S A* 110, 5468-5473
- 101** Marshall, K.E., Marchante, R., Xue, W.F., and Serpell, L.C. (2014) The relationship between amyloid structure and cytotoxicity. *Prion* 8, 5-9
- 102** Petkova, A.T., Ishii, Y., Balbach, J.J., Antzutkin, O.N., Leapman, R.D., Delaglio, F., and Tycko, R. (2002) A structural model for Alzheimer's beta -amyloid fibrils based on experimental constraints from solid state NMR. *Proc Natl Acad Sci U S A* 99, 16742-16747
- 103** Luhrs, T., Ritter, C., Adrian, M., Riek-Loher, D., Bohrmann, B., Dobeli, H., Schubert, D., and Riek, R. (2005) 3D structure of Alzheimer's amyloid-beta(1-42) fibrils. *Proc Natl Acad Sci U S A* 102, 17342-17347
- 104** Lu, J.X., Qiang, W., Yau, W.M., Schwieters, C.D., Meredith, S.C., and Tycko, R. (2013) Molecular structure of beta-amyloid fibrils in Alzheimer's disease brain tissue. *Cell* 154, 1257-1268
- 105** Van Melckebeke, H., Wasmer, C., Lange, A., Ab, E., Loquet, A., Bockmann, A., and Meier, B.H. (2010) Atomic-resolution three-dimensional structure of HET-s(218-289) amyloid fibrils by solid-state NMR spectroscopy. *J Am Chem Soc* 132, 13765-13775
- 106** Makin, O.S., Atkins, E., Sikorski, P., Johansson, J., and Serpell, L.C. (2005) Molecular basis for amyloid fibril formation and stability. *Proc Natl Acad Sci U S A* 102, 315-320
- 107** Morris, K.L., Rodger, A., Hicks, M.R., Debulpaep, M., Schymkowitz, J., Rousseau, F., and Serpell, L.C. (2013) Exploring the sequence-structure relationship for amyloid peptides. *Biochem J* 450, 275-283
- 108** Luheshi, L.M. and Dobson, C.M. (2009) Bridging the gap: from protein misfolding to protein misfolding diseases. *FEBS Lett* 583, 2581-2586
- 109** Xue, W.F., Homans, S.W., and Radford, S.E. (2008) Systematic analysis of nucleation-dependent polymerization reveals new insights into the mechanism of amyloid self-assembly. *Proc Natl Acad Sci U S A* 105, 8926-8931

- 110** Kashchiev, D., Cabriolu, R., and Auer, S. (2013) Confounding the paradigm: peculiarities of amyloid fibril nucleation. *J Am Chem Soc* 135, 1531-1539
- 111** Nesterov, E.E., Skoch, J., Hyman, B.T., Klunk, W.E., Bacskai, B.J., and Swager, T.M. (2005) In vivo optical imaging of amyloid aggregates in brain: design of fluorescent markers. *Angew Chem Int Ed Engl* 44, 5452-5456
- 112** Kaminski Schierle, G.S., van de Linde, S., Erdelyi, M., Esbjorner, E.K., Klein, T., Rees, E., Bertoncini, C.W., Dobson, C.M., Sauer, M., and Kaminski, C.F. (2011) In situ measurements of the formation and morphology of intracellular beta-amyloid fibrils by super-resolution fluorescence imaging. *J Am Chem Soc* 133, 12902-12905
- 113** McGuire, E.K., Motskin, M., Bolognesi, B., Bergin, S.D., Knowles, T.P., Skepper, J., Luheshi, L.M., McComb, D.W., Dobson, C.M., and Porter, A.E. (2012) Selenium-enhanced electron microscopic imaging of different aggregate forms of a segment of the amyloid beta peptide in cells. *ACS Nano* 6, 4740-4747
- 114** Serio, T.R., Cashikar, A.G., Kowal, A.S., Sawicki, G.J., Moslehi, J.J., Serpell, L., Arnsdorf, M.F., and Lindquist, S.L. (2000) Nucleated conformational conversion and the replication of conformational information by a prion determinant. *Science* 289, 1317-1321
- 115** Cheon, M., Chang, I., Mohanty, S., Luheshi, L.M., Dobson, C.M., Vendruscolo, M., and Favrin, G. (2007) Structural reorganisation and potential toxicity of oligomeric species formed during the assembly of amyloid fibrils. *PLoS Comput Biol* 3, 1727-1738
- 116** Dusa, A., Kaylor, J., Edridge, S., Bodner, N., Hong, D.P., and Fink, A.L. (2006) Characterization of oligomers during alpha-synuclein aggregation using intrinsic tryptophan fluorescence. *Biochemistry* 45, 2752-2760
- 117** Stefani, M. (2010) Biochemical and biophysical features of both oligomer/fibril and cell membrane in amyloid cytotoxicity. *FEBS J* 277, 4602-4613
- 118** Woods, L.A., Radford, S.E., and Ashcroft, A.E. (2013) Advances in ion mobility spectrometry-mass spectrometry reveal key insights into amyloid assembly. *Biochim Biophys Acta* 1834, 1257-1268
- 119** Carulla, N., Zhou, M., Arimon, M., Gairi, M., Giralt, E., Robinson, C.V., and Dobson, C.M. (2009) Experimental characterization of disordered and ordered aggregates populated during the process of amyloid fibril formation. *Proc Natl Acad Sci U S A* 106, 7828-7833
- 120** Caughey, B. and Lansbury, P.T. (2003) Protofibrils, pores, fibrils, and neurodegeneration: separating the responsible protein aggregates from the innocent bystanders. *Annu Rev Neurosci* 26, 267-298

- 121** Lashuel, H.A., Hartley, D.M., Petre, B.M., Wall, J.S., Simon, M.N., Walz, T., and Lansbury, P.T., Jr. (2003) Mixtures of wild-type and a pathogenic (E22G) form of Abeta40 in vitro accumulate protofibrils, including amyloid pores. *J Mol Biol* 332, 795-808
- 122** Mastrangelo, I.A., Ahmed, M., Sato, T., Liu, W., Wang, C., Hough, P., and Smith, S.O. (2006) High-resolution atomic force microscopy of soluble Abeta42 oligomers. *J Mol Biol* 358, 106-119
- 123** Ferrone, F. (1999) Analysis of protein aggregation kinetics. *Methods Enzymol* 309, 256-274
- 124** Jarrett, J.T. and Lansbury, P.T., Jr. (1992) Amyloid fibril formation requires a chemically discriminating nucleation event: studies of an amyloidogenic sequence from the bacterial protein OsmB. *Biochemistry* 31, 12345-12352
- 125** Jahn, T.R. and Radford, S.E. (2008) Folding versus aggregation: polypeptide conformations on competing pathways. *Arch Biochem Biophys* 469, 100-117
- 126** Kaye, R., Head, E., Sarsoza, F., Saing, T., Cotman, C.W., Necula, M., Margol, L., Wu, J., Breydo, L., Thompson, J.L., Rasool, S., Gurlo, T., Butler, P., and Glabe, C.G. (2007) Fibril specific, conformation dependent antibodies recognize a generic epitope common to amyloid fibrils and fibrillar oligomers that is absent in prefibrillar oligomers. *Mol Neurodegener* 2, 18
- 127** Glabe, C.G. (2008) Structural classification of toxic amyloid oligomers. *J Biol Chem* 283, 29639-29643
- 128** Hardy, J. and Selkoe, D.J. (2002) The amyloid hypothesis of Alzheimer's disease: progress and problems on the road to therapeutics. *Science* 297, 353-356
- 129** Lansbury, P.T. and Lashuel, H.A. (2006) A century-old debate on protein aggregation and neurodegeneration enters the clinic. *Nature* 443, 774-779
- 130** Pike, C.J., Walencewicz, A.J., Glabe, C.G., and Cotman, C.W. (1991) In vitro aging of beta-amyloid protein causes peptide aggregation and neurotoxicity. *Brain Res* 563, 311-314
- 131** Geula, C., Wu, C.K., Saroff, D., Lorenzo, A., Yuan, M., and Yankner, B.A. (1998) Aging renders the brain vulnerable to amyloid beta-protein neurotoxicity. *Nat Med* 4, 827-831
- 132** Lorenzo, A., Razzaboni, B., Weir, G.C., and Yankner, B.A. (1994) Pancreatic islet cell toxicity of amylin associated with type-2 diabetes mellitus. *Nature* 368, 756-760
- 133** Lorenzo, A. and Yankner, B.A. (1994) Beta-amyloid neurotoxicity requires fibril formation and is inhibited by congo red. *Proc Natl Acad Sci U S A* 91, 12243-12247
- 134** Naslund, J., Haroutunian, V., Mohs, R., Davis, K.L., Davies, P., Greengard, P., and Buxbaum, J.D. (2000) Correlation between elevated levels of amyloid beta-peptide in the brain and cognitive decline. *JAMA* 283, 1571-1577

- 135** Lue, L.F., Kuo, Y.M., Roher, A.E., Brachova, L., Shen, Y., Sue, L., Beach, T., Kurth, J.H., Rydel, R.E., and Rogers, J. (1999) Soluble amyloid beta peptide concentration as a predictor of synaptic change in Alzheimer's disease. *Am J Pathol* 155, 853-862
- 136** McLean, C.A., Cherny, R.A., Fraser, F.W., Fuller, S.J., Smith, M.J., Beyreuther, K., Bush, A.I., and Masters, C.L. (1999) Soluble pool of Abeta amyloid as a determinant of severity of neurodegeneration in Alzheimer's disease. *Ann Neurol* 46, 860-866
- 137** Wang, J., Dickson, D.W., Trojanowski, J.Q., and Lee, V.M. (1999) The levels of soluble versus insoluble brain Abeta distinguish Alzheimer's disease from normal and pathologic aging. *Exp Neurol* 158, 328-337
- 138** Moechars, D., Dewachter, I., Lorent, K., Reverse, D., Baekelandt, V., Naidu, A., Tesseur, I., Spittaels, K., Haute, C.V., Checler, F., Godaux, E., Cordell, B., and Van Leuven, F. (1999) Early phenotypic changes in transgenic mice that overexpress different mutants of amyloid precursor protein in brain. *J Biol Chem* 274, 6483-6492
- 139** Dickson, D.W., Crystal, H.A., Mattiace, L.A., Masur, D.M., Blau, A.D., Davies, P., Yen, S.H., and Aronson, M.K. (1992) Identification of normal and pathological aging in prospectively studied nondemented elderly humans. *Neurobiol Aging* 13, 179-189
- 140** Haass, C. and Selkoe, D.J. (2007) Soluble protein oligomers in neurodegeneration: lessons from the Alzheimer's amyloid beta-peptide. *Nat Rev Mol Cell Biol* 8, 101-112
- 141** Campioni, S., Mannini, B., Zampagni, M., Pensalfini, A., Parrini, C., Evangelisti, E., Relini, A., Stefani, M., Dobson, C.M., Cecchi, C., and Chiti, F. (2010) A causative link between the structure of aberrant protein oligomers and their toxicity. *Nat Chem Biol* 6, 140-147
- 142** Bucciantini, M., Giannoni, E., Chiti, F., Baroni, F., Formigli, L., Zurdo, J., Taddei, N., Ramponi, G., Dobson, C.M., and Stefani, M. (2002) Inherent toxicity of aggregates implies a common mechanism for protein misfolding diseases. *Nature* 416, 507-511
- 143** Slow, E.J., Graham, R.K., Osmand, A.P., Devon, R.S., Lu, G., Deng, Y., Pearson, J., Vaid, K., Bissada, N., Wetzel, R., Leavitt, B.R., and Hayden, M.R. (2005) Absence of behavioral abnormalities and neurodegeneration in vivo despite widespread neuronal huntingtin inclusions. *Proc Natl Acad Sci U S A* 102, 11402-11407
- 144** Arrasate, M., Mitra, S., Schweitzer, E.S., Segal, M.R., and Finkbeiner, S. (2004) Inclusion body formation reduces levels of mutant huntingtin and the risk of neuronal death. *Nature* 431, 805-810
- 145** Bowman, A.B., Yoo, S.Y., Dantuma, N.P., and Zoghbi, H.Y. (2005) Neuronal dysfunction in a polyglutamine disease model occurs in the absence of ubiquitin-proteasome system impairment and inversely correlates with the degree of nuclear inclusion formation. *Hum Mol Genet* 14, 679-691

- 146** Roher, A.E. and Kuo, Y.M. (1999) Isolation of amyloid deposits from brain. *Methods Enzymol* 309, 58-67
- 147** Harper, J.D., Wong, S.S., Lieber, C.M., and Lansbury, P.T. (1997) Observation of metastable A β amyloid protofibrils by atomic force microscopy. *Chem Biol* 4, 119-125
- 148** Walsh, D.M., Lomakin, A., Benedek, G.B., Condron, M.M., and Teplow, D.B. (1997) Amyloid beta-protein fibrillogenesis. Detection of a protofibrillar intermediate. *J Biol Chem* 272, 22364-22372
- 149** Rochet, J.C., Conway, K.A., and Lansbury, P.T., Jr. (2000) Inhibition of fibrillization and accumulation of prefibrillar oligomers in mixtures of human and mouse alpha-synuclein. *Biochemistry* 39, 10619-10626
- 150** Poirier, M.A., Li, H., Macosko, J., Cai, S., Amzel, M., and Ross, C.A. (2002) Huntingtin spheroids and protofibrils as precursors in polyglutamine fibrilization. *J Biol Chem* 277, 41032-41037
- 151** Green, J.D., Goldsbury, C., Kistler, J., Cooper, G.J., and Aebi, U. (2004) Human amylin oligomer growth and fibril elongation define two distinct phases in amyloid formation. *J Biol Chem* 279, 12206-12212
- 152** Woods, L.A., Platt, G.W., Hellewell, A.L., Hewitt, E.W., Homans, S.W., Ashcroft, A.E., and Radford, S.E. (2011) Ligand binding to distinct states diverts aggregation of an amyloid-forming protein. *Nat Chem Biol* 7, 730-739
- 153** Mukai, H., Isagawa, T., Goyama, E., Tanaka, S., Bence, N.F., Tamura, A., Ono, Y., and Kopito, R.R. (2005) Formation of morphologically similar globular aggregates from diverse aggregation-prone proteins in mammalian cells. *Proc Natl Acad Sci U S A* 102, 10887-10892
- 154** Lee, H.J. and Lee, S.J. (2002) Characterization of cytoplasmic alpha-synuclein aggregates. Fibril formation is tightly linked to the inclusion-forming process in cells. *J Biol Chem* 277, 48976-48983
- 155** Townsend, M., Shankar, G.M., Mehta, T., Walsh, D.M., and Selkoe, D.J. (2006) Effects of secreted oligomers of amyloid beta-protein on hippocampal synaptic plasticity: a potent role for trimers. *J Physiol* 572, 477-492
- 156** Cleary, J.P., Walsh, D.M., Hofmeister, J.J., Shankar, G.M., Kuskowski, M.A., Selkoe, D.J., and Ashe, K.H. (2005) Natural oligomers of the amyloid-beta protein specifically disrupt cognitive function. *Nat Neurosci* 8, 79-84
- 157** Walsh, D.M., Klyubin, I., Fadeeva, J.V., Cullen, W.K., Anwyl, R., Wolfe, M.S., Rowan, M.J., and Selkoe, D.J. (2002) Naturally secreted oligomers of amyloid beta protein potently inhibit hippocampal long-term potentiation in vivo. *Nature* 416, 535-539

- 158** Lesne, S., Koh, M.T., Kotilinek, L., Kaye, R., Glabe, C.G., Yang, A., Gallagher, M., and Ashe, K.H. (2006) A specific amyloid-beta protein assembly in the brain impairs memory. *Nature* 440, 352-357
- 159** Pountney, D.L., Lowe, R., Quilty, M., Vickers, J.C., Voelcker, N.H., and Gai, W.P. (2004) Annular alpha-synuclein species from purified multiple system atrophy inclusions. *J Neurochem* 90, 502-512
- 160** Klyubin, I., Betts, V., Welzel, A.T., Blennow, K., Zetterberg, H., Wallin, A., Lemere, C.A., Cullen, W.K., Peng, Y., Wisniewski, T., Selkoe, D.J., Anwyl, R., Walsh, D.M., and Rowan, M.J. (2008) Amyloid beta protein dimer-containing human CSF disrupts synaptic plasticity: prevention by systemic passive immunization. *J Neurosci* 28, 4231-4237
- 161** Broersen, K., Rousseau, F., and Schymkowitz, J. (2010) The culprit behind amyloid beta peptide related neurotoxicity in Alzheimer's disease: oligomer size or conformation? *Alzheimers Res Ther* 2, 12
- 162** Hoshi, M., Sato, M., Matsumoto, S., Noguchi, A., Yasutake, K., Yoshida, N., and Sato, K. (2003) Spherical aggregates of beta-amyloid (amylospheroid) show high neurotoxicity and activate tau protein kinase I/glycogen synthase kinase-3beta. *Proc Natl Acad Sci U S A* 100, 6370-6375
- 163** White, J.A., Manelli, A.M., Holmberg, K.H., Van Eldik, L.J., and Ladu, M.J. (2005) Differential effects of oligomeric and fibrillar amyloid-beta 1-42 on astrocyte-mediated inflammation. *Neurobiol Dis* 18, 459-465
- 164** Billings, L.M., Oddo, S., Green, K.N., McGaugh, J.L., and LaFerla, F.M. (2005) Intraneuronal A β causes the onset of early Alzheimer's disease-related cognitive deficits in transgenic mice. *Neuron* 45, 675-688
- 165** Koffie, R.M., Meyer-Luehmann, M., Hashimoto, T., Adams, K.W., Mielke, M.L., Garcia-Alloza, M., Micheva, K.D., Smith, S.J., Kim, M.L., Lee, V.M., Hyman, B.T., and Spires-Jones, T.L. (2009) Oligomeric amyloid beta associates with postsynaptic densities and correlates with excitatory synapse loss near senile plaques. *Proc Natl Acad Sci U S A* 106, 4012-4017
- 166** Cremades, N., Cohen, S.I., Deas, E., Abramov, A.Y., Chen, A.Y., Orte, A., Sandal, M., Clarke, R.W., Dunne, P., Aprile, F.A., Bertocini, C.W., Wood, N.W., Knowles, T.P., Dobson, C.M., and Klenerman, D. (2012) Direct observation of the interconversion of normal and toxic forms of alpha-synuclein. *Cell* 149, 1048-1059
- 167** Gosavi, N., Lee, H.J., Lee, J.S., Patel, S., and Lee, S.J. (2002) Golgi fragmentation occurs in the cells with prefibrillar alpha-synuclein aggregates and precedes the formation of fibrillar inclusion. *J Biol Chem* 277, 48984-48992

- 168** Winner, B., Jappelli, R., Maji, S.K., Desplats, P.A., Boyer, L., Aigner, S., Hetzer, C., Loher, T., Vilar, M., Campioni, S., Tzitzilonis, C., Soragni, A., Jessberger, S., Mira, H., Consiglio, A., Pham, E., Masliah, E., Gage, F.H., and Riek, R. (2011) In vivo demonstration that alpha-synuclein oligomers are toxic. *Proc Natl Acad Sci U S A* 108, 4194-4199
- 169** Lindersson, E., Beedholm, R., Hojrup, P., Moos, T., Gai, W., Hendil, K.B., and Jensen, P.H. (2004) Proteasomal inhibition by alpha-synuclein filaments and oligomers. *J Biol Chem* 279, 12924-12934
- 170** Nucifora, L.G., Burke, K.A., Feng, X., Arbez, N., Zhu, S., Miller, J., Yang, G., Ratovitski, T., Delannoy, M., Muchowski, P.J., Finkbeiner, S., Legleiter, J., Ross, C.A., and Poirier, M.A. (2012) Identification of novel potentially toxic oligomers formed in vitro from mammalian-derived expanded huntingtin exon-1 protein. *J Biol Chem* 287, 16017-16028
- 171** Demuro, A., Mina, E., Kaye, R., Milton, S.C., Parker, I., and Glabe, C.G. (2005) Calcium dysregulation and membrane disruption as a ubiquitous neurotoxic mechanism of soluble amyloid oligomers. *J Biol Chem* 280, 17294-17300
- 172** Reixach, N., Deechongkit, S., Jiang, X., Kelly, J.W., and Buxbaum, J.N. (2004) Tissue damage in the amyloidoses: Transthyretin monomers and nonnative oligomers are the major cytotoxic species in tissue culture. *Proc Natl Acad Sci U S A* 101, 2817-2822
- 173** Gharibyan, A.L., Zamotin, V., Yanamandra, K., Moskaleva, O.S., Margulis, B.A., Kostanyan, I.A., and Morozova-Roche, L.A. (2007) Lysozyme amyloid oligomers and fibrils induce cellular death via different apoptotic/necrotic pathways. *J Mol Biol* 365, 1337-1349
- 174** Anderluh, G., Gutierrez-Aguirre, I., Rabzelj, S., Ceru, S., Kopitar-Jerala, N., Macek, P., Turk, V., and Zerovnik, E. (2005) Interaction of human stefin B in the prefibrillar oligomeric form with membranes. Correlation with cellular toxicity. *FEBS J* 272, 3042-3051
- 175** Rigacci, S., Bucciantini, M., Relini, A., Pesce, A., Gliozzi, A., Berti, A., and Stefani, M. (2008) The (1-63) region of the p53 transactivation domain aggregates in vitro into cytotoxic amyloid assemblies. *Biophys J* 94, 3635-3646
- 176** Gilbert, B.J. (2013) The role of amyloid beta in the pathogenesis of Alzheimer's disease. *J Clin Pathol* 66, 362-366
- 177** Petkova, A.T., Leapman, R.D., Guo, Z., Yau, W.M., Mattson, M.P., and Tycko, R. (2005) Self-propagating, molecular-level polymorphism in Alzheimer's beta-amyloid fibrils. *Science* 307, 262-265

- 178** Qiang, W., Yau, W.M., Luo, Y., Mattson, M.P., and Tycko, R. (2012) Antiparallel beta-sheet architecture in Iowa-mutant beta-amyloid fibrils. *Proc Natl Acad Sci U S A* 109, 4443-4448
- 179** Picone, P., Carrotta, R., Montana, G., Nobile, M.R., San Biagio, P.L., and Di Carlo, M. (2009) Abeta oligomers and fibrillar aggregates induce different apoptotic pathways in LAN5 neuroblastoma cell cultures. *Biophys J* 96, 4200-4211
- 180** Mossuto, M.F., Dhulesia, A., Devlin, G., Frare, E., Kumita, J.R., de Laureto, P.P., Dumoulin, M., Fontana, A., Dobson, C.M., and Salvatella, X. (2010) The non-core regions of human lysozyme amyloid fibrils influence cytotoxicity. *J Mol Biol* 402, 783-796
- 181** Mossuto, M.F., Bolognesi, B., Guixer, B., Dhulesia, A., Agostini, F., Kumita, J.R., Tartaglia, G.G., Dumoulin, M., Dobson, C.M., and Salvatella, X. (2011) Disulfide bonds reduce the toxicity of the amyloid fibrils formed by an extracellular protein. *Angew Chem Int Ed Engl* 50, 7048-7051
- 182** Novitskaya, V., Bocharova, O.V., Bronstein, I., and Baskakov, I.V. (2006) Amyloid fibrils of mammalian prion protein are highly toxic to cultured cells and primary neurons. *J Biol Chem* 281, 13828-13836
- 183** Lee, Y.J., Savtchenko, R., Ostapchenko, V.G., Makarava, N., and Baskakov, I.V. (2011) Molecular structure of amyloid fibrils controls the relationship between fibrillar size and toxicity. *PLoS One* 6, e20244
- 184** Engel, M.F., Khemtémourian, L., Kleijer, C.C., Meeldijk, H.J., Jacobs, J., Verkleij, A.J., de Kruijff, B., Killian, J.A., and Hoppener, J.W. (2008) Membrane damage by human islet amyloid polypeptide through fibril growth at the membrane. *Proc Natl Acad Sci U S A* 105, 6033-6038
- 185** Bucciantini, M., Nosi, D., Forzan, M., Russo, E., Calamai, M., Pieri, L., Formigli, L., Quercioli, F., Soria, S., Pavone, F., Savistchenko, J., Melki, R., and Stefani, M. (2012) Toxic effects of amyloid fibrils on cell membranes: the importance of ganglioside GM1. *FASEB J* 26, 818-831
- 186** Pieri, L., Bucciantini, M., Nosi, D., Formigli, L., Savistchenko, J., Melki, R., and Stefani, M. (2006) The yeast prion Ure2p native-like assemblies are toxic to mammalian cells regardless of their aggregation state. *J Biol Chem* 281, 15337-15344
- 187** Stokin, G.B., Lillo, C., Falzone, T.L., Brusch, R.G., Rockenstein, E., Mount, S.L., Raman, R., Davies, P., Masliah, E., Williams, D.S., and Goldstein, L.S. (2005) Axonopathy and transport deficits early in the pathogenesis of Alzheimer's disease. *Science* 307, 1282-1288

- 188** Meyer-Luehmann, M., Spires-Jones, T.L., Prada, C., Garcia-Alloza, M., de Calignon, A., Rozkalne, A., Koenigsnecht-Talboo, J., Holtzman, D.M., Bacskai, B.J., and Hyman, B.T. (2008) Rapid appearance and local toxicity of amyloid-beta plaques in a mouse model of Alzheimer's disease. *Nature* 451, 720-724
- 189** Gosal, W.S., Morten, I.J., Hewitt, E.W., Smith, D.A., Thomson, N.H., and Radford, S.E. (2005) Competing pathways determine fibril morphology in the self-assembly of beta2-microglobulin into amyloid. *J Mol Biol* 351, 850-864
- 190** Xue, W.F., Hellewell, A.L., Gosal, W.S., Homans, S.W., Hewitt, E.W., and Radford, S.E. (2009) Fibril fragmentation enhances amyloid cytotoxicity. *J Biol Chem* 284, 34272-34282
- 191** Martins, I.C., Kuperstein, I., Wilkinson, H., Maes, E., Vanbrabant, M., Jonckheere, W., Van Gelder, P., Hartmann, D., D'Hooge, R., De Strooper, B., Schymkowitz, J., and Rousseau, F. (2008) Lipids revert inert Abeta amyloid fibrils to neurotoxic protofibrils that affect learning in mice. *EMBO J* 27, 224-233
- 192** Picotti, P., De Franceschi, G., Frare, E., Spolaore, B., Zambonin, M., Chiti, F., de Laureto, P.P., and Fontana, A. (2007) Amyloid fibril formation and disaggregation of fragment 1-29 of apomyoglobin: insights into the effect of pH on protein fibrillogenesis. *J Mol Biol* 367, 1237-1245
- 193** Olzscha, H., Schermann, S.M., Woerner, A.C., Pinkert, S., Hecht, M.H., Tartaglia, G.G., Vendruscolo, M., Hayer-Hartl, M., Hartl, F.U., and Vabulas, R.M. (2011) Amyloid-like aggregates sequester numerous metastable proteins with essential cellular functions. *Cell* 144, 67-78
- 194** Bolognesi, B., Kumita, J.R., Barros, T.P., Esbjorner, E.K., Luheshi, L.M., Crowther, D.C., Wilson, M.R., Dobson, C.M., Favrin, G., and Yerbury, J.J. (2010) ANS binding reveals common features of cytotoxic amyloid species. *ACS Chem Biol* 5, 735-740
- 195** Zampagni, M., Cascella, R., Casamenti, F., Grossi, C., Evangelisti, E., Wright, D., Becatti, M., Liguri, G., Mannini, B., Campioni, S., Chiti, F., and Cecchi, C. (2011) A comparison of the biochemical modifications caused by toxic and non-toxic protein oligomers in cells. *J Cell Mol Med* 15, 2106-2116
- 196** Virok, D.P., Simon, D., Bozso, Z., Rajko, R., Datki, Z., Balint, E., Szegedi, V., Janaky, T., Penke, B., and Fulop, L. (2011) Protein array based interactome analysis of amyloid-beta indicates an inhibition of protein translation. *J Proteome Res* 10, 1538-1547
- 197** Balch, W.E., Morimoto, R.I., Dillin, A., and Kelly, J.W. (2008) Adapting proteostasis for disease intervention. *Science* 319, 916-919

- 198** Koga, H., Kaushik, S., and Cuervo, A.M. (2011) Protein homeostasis and aging: The importance of exquisite quality control. *Ageing Res Rev* 10, 205-215
- 199** Kim, Y.E., Hipp, M.S., Bracher, A., Hayer-Hartl, M., and Hartl, F.U. (2013) Molecular chaperone functions in protein folding and proteostasis. *Annu Rev Biochem* 82, 323-355
- 200** Ciechanover, A., Orian, A., and Schwartz, A.L. (2000) Ubiquitin-mediated proteolysis: biological regulation via destruction. *Bioessays* 22, 442-451
- 201** Bence, N.F., Sampat, R.M., and Kopito, R.R. (2001) Impairment of the ubiquitin-proteasome system by protein aggregation. *Science* 292, 1552-1555
- 202** Shimura, H., Hattori, N., Kubo, S., Mizuno, Y., Asakawa, S., Minoshima, S., Shimizu, N., Iwai, K., Chiba, T., Tanaka, K., and Suzuki, T. (2000) Familial Parkinson disease gene product, parkin, is a ubiquitin-protein ligase. *Nat Genet* 25, 302-305
- 203** McNaught, K.S., Perl, D.P., Brownell, A.L., and Olanow, C.W. (2004) Systemic exposure to proteasome inhibitors causes a progressive model of Parkinson's disease. *Ann Neurol* 56, 149-162
- 204** Anfinsen, C.B. (1973) Principles that govern the folding of protein chains. *Science* 181, 223-230
- 205** Ellis, R.J. and Minton, A.P. (2006) Protein aggregation in crowded environments. *Biol Chem* 387, 485-497
- 206** Ellis, R.J. (2001) Macromolecular crowding: an important but neglected aspect of the intracellular environment. *Curr Opin Struct Biol* 11, 114-119
- 207** Hartl, F.U. and Hayer-Hartl, M. (2002) Molecular chaperones in the cytosol: from nascent chain to folded protein. *Science* 295, 1852-1858
- 208** Bukau, B., Weissman, J., and Horwich, A. (2006) Molecular chaperones and protein quality control. *Cell* 125, 443-451
- 209** Wilhelmus, M.M., Otte-Holler, I., Wesseling, P., de Waal, R.M., Boelens, W.C., and Verbeek, M.M. (2006) Specific association of small heat shock proteins with the pathological hallmarks of Alzheimer's disease brains. *Neuropathol Appl Neurobiol* 32, 119-130
- 210** Fargnoli, J., Kunisada, T., Fornace, A.J., Jr., Schneider, E.L., and Holbrook, N.J. (1990) Decreased expression of heat shock protein 70 mRNA and protein after heat treatment in cells of aged rats. *Proc Natl Acad Sci U S A* 87, 846-850
- 211** Hall, D.M., Xu, L., Drake, V.J., Oberley, L.W., Oberley, T.D., Moseley, P.L., and Kregel, K.C. (2000) Aging reduces adaptive capacity and stress protein expression in the liver after heat stress. *J Appl Physiol* (1985) 89, 749-759

- 212** Pahlavani, M.A., Harris, M.D., Moore, S.A., Weindruch, R., and Richardson, A. (1995) The expression of heat shock protein 70 decreases with age in lymphocytes from rats and rhesus monkeys. *Exp Cell Res* 218, 310-318
- 213** Gidalevitz, T., Ben-Zvi, A., Ho, K.H., Brignull, H.R., and Morimoto, R.I. (2006) Progressive disruption of cellular protein folding in models of polyglutamine diseases. *Science* 311, 1471-1474
- 214** Westerheide, S.D. and Morimoto, R.I. (2005) Heat shock response modulators as therapeutic tools for diseases of protein conformation. *J Biol Chem* 280, 33097-33100
- 215** Mu, T.W., Ong, D.S., Wang, Y.J., Balch, W.E., Yates, J.R., 3rd, Segatori, L., and Kelly, J.W. (2008) Chemical and biological approaches synergize to ameliorate protein-folding diseases. *Cell* 134, 769-781
- 216** Lotz, G.P., Legleiter, J., Aron, R., Mitchell, E.J., Huang, S.Y., Ng, C., Glabe, C., Thompson, L.M., and Muchowski, P.J. (2010) Hsp70 and Hsp40 functionally interact with soluble mutant huntingtin oligomers in a classic ATP-dependent reaction cycle. *J Biol Chem* 285, 38183-38193
- 217** Auluck, P.K., Chan, H.Y., Trojanowski, J.Q., Lee, V.M., and Bonini, N.M. (2002) Chaperone suppression of alpha-synuclein toxicity in a Drosophila model for Parkinson's disease. *Science* 295, 865-868
- 218** Hageman, J., Rujano, M.A., van Waarde, M.A., Kakkar, V., Dirks, R.P., Govorukhina, N., Oosterveld-Hut, H.M., Lubsen, N.H., and Kampinga, H.H. (2010) A DNAJB chaperone subfamily with HDAC-dependent activities suppresses toxic protein aggregation. *Mol Cell* 37, 355-369
- 219** Berthelot, K., Cullin, C., and Lecomte, S. (2013) What does make an amyloid toxic: morphology, structure or interaction with membrane? *Biochimie* 95, 12-19
- 220** Williams, T.L. and Serpell, L.C. (2011) Membrane and surface interactions of Alzheimer's Abeta peptide--insights into the mechanism of cytotoxicity. *FEBS J* 278, 3905-3917
- 221** Necula, M., Chirita, C.N., and Kuret, J. (2003) Rapid anionic micelle-mediated alpha-synuclein fibrillization in vitro. *J Biol Chem* 278, 46674-46680
- 222** Knight, J.D. and Miranker, A.D. (2004) Phospholipid catalysis of diabetic amyloid assembly. *J Mol Biol* 341, 1175-1187
- 223** Choo-Smith, L.P., Garzon-Rodriguez, W., Glabe, C.G., and Surewicz, W.K. (1997) Acceleration of amyloid fibril formation by specific binding of Abeta-(1-40) peptide to ganglioside-containing membrane vesicles. *J Biol Chem* 272, 22987-22990
- 224** Lashuel, H.A. and Lansbury, P.T., Jr. (2006) Are amyloid diseases caused by protein aggregates that mimic bacterial pore-forming toxins? *Q Rev Biophys* 39, 167-201

- 225** Hebda, J.A. and Miranker, A.D. (2009) The interplay of catalysis and toxicity by amyloid intermediates on lipid bilayers: insights from type II diabetes. *Annu Rev Biophys* 38, 125-152
- 226** Green, J.D., Kreplak, L., Goldsbury, C., Li Blatter, X., Stolz, M., Cooper, G.S., Seelig, A., Kistler, J., and Aebi, U. (2004) Atomic force microscopy reveals defects within mica supported lipid bilayers induced by the amyloidogenic human amylin peptide. *J Mol Biol* 342, 877-887
- 227** Ta, H.P., Berthelot, K., Couлары-Salin, B., Castano, S., Desbat, B., Bonnafous, P., Lambert, O., Alves, I., Cullin, C., and Lecomte, S. (2012) A yeast toxic mutant of HET-s amyloid disrupts membrane integrity. *Biochim Biophys Acta* 1818, 2325-2334
- 228** Zhang, Y.J., Shi, J.M., Bai, C.J., Wang, H., Li, H.Y., Wu, Y., and Ji, S.R. (2012) Intra-membrane oligomerization and extra-membrane oligomerization of amyloid-beta peptide are competing processes as a result of distinct patterns of motif interplay. *J Biol Chem* 287, 748-756
- 229** Shai, Y. (1999) Mechanism of the binding, insertion and destabilization of phospholipid bilayer membranes by alpha-helical antimicrobial and cell non-selective membrane-lytic peptides. *Biochim Biophys Acta* 1462, 55-70
- 230** Sparr, E., Engel, M.F., Sakharov, D.V., Sprong, M., Jacobs, J., de Kruijff, B., Hoppener, J.W., and Killian, J.A. (2004) Islet amyloid polypeptide-induced membrane leakage involves uptake of lipids by forming amyloid fibers. *FEBS Lett* 577, 117-120
- 231** Milanesi, L., Sheynis, T., Xue, W.F., Orlova, E.V., Hellewell, A.L., Jelinek, R., Hewitt, E.W., Radford, S.E., and Saibil, H.R. (2012) Direct three-dimensional visualization of membrane disruption by amyloid fibrils. *Proc Natl Acad Sci U S A* 109, 20455-20460
- 232** Petersen, O.H., Michalak, M., and Verkhratsky, A. (2005) Calcium signalling: past, present and future. *Cell Calcium* 38, 161-169
- 233** Glabe, C.G. (2006) Common mechanisms of amyloid oligomer pathogenesis in degenerative disease. *Neurobiol Aging* 27, 570-575
- 234** Ding, T.T., Lee, S.J., Rochet, J.C., and Lansbury, P.T., Jr. (2002) Annular alpha-synuclein protofibrils are produced when spherical protofibrils are incubated in solution or bound to brain-derived membranes. *Biochemistry* 41, 10209-10217
- 235** Lashuel, H.A., Petre, B.M., Wall, J., Simon, M., Nowak, R.J., Walz, T., and Lansbury, P.T., Jr. (2002) Alpha-synuclein, especially the Parkinson's disease-associated mutants, forms pore-like annular and tubular protofibrils. *J Mol Biol* 322, 1089-1102

- 236** Wacker, J.L., Zareie, M.H., Fong, H., Sarikaya, M., and Muchowski, P.J. (2004) Hsp70 and Hsp40 attenuate formation of spherical and annular polyglutamine oligomers by partitioning monomer. *Nat Struct Mol Biol* 11, 1215-1222
- 237** Lal, R., Lin, H., and Quist, A.P. (2007) Amyloid beta ion channel: 3D structure and relevance to amyloid channel paradigm. *Biochim Biophys Acta* 1768, 1966-1975
- 238** Volles, M.J. and Lansbury, P.T., Jr. (2002) Vesicle permeabilization by protofibrillar alpha-synuclein is sensitive to Parkinson's disease-linked mutations and occurs by a pore-like mechanism. *Biochemistry* 41, 4595-4602
- 239** Kagan, B.L., Hirakura, Y., Azimov, R., and Azimova, R. (2001) The channel hypothesis of Huntington's disease. *Brain Res Bull* 56, 281-284
- 240** Chafekar, S.M., Baas, F., and Scheper, W. (2008) Oligomer-specific Abeta toxicity in cell models is mediated by selective uptake. *Biochim Biophys Acta* 1782, 523-531
- 241** Zhao, W.Q., Santini, F., Breese, R., Ross, D., Zhang, X.D., Stone, D.J., Ferrer, M., Townsend, M., Wolfe, A.L., Seager, M.A., Kinney, G.G., Shughrue, P.J., and Ray, W.J. (2010) Inhibition of calcineurin-mediated endocytosis and alpha-amino-3-hydroxy-5-methyl-4-isoxazolepropionic acid (AMPA) receptors prevents amyloid beta oligomer-induced synaptic disruption. *J Biol Chem* 285, 7619-7632
- 242** Soura, V., Stewart-Parker, M., Williams, T.L., Ratnayaka, A., Atherton, J., Gorringer, K., Tuffin, J., Darwent, E., Rambaran, R., Klein, W., Lacor, P., Staras, K., Thorpe, J., and Serpell, L.C. (2012) Visualization of co-localization in Abeta42-administered neuroblastoma cells reveals lysosome damage and autophagosome accumulation related to cell death. *Biochem J* 441, 579-590
- 243** Lee, H.J., Patel, S., and Lee, S.J. (2005) Intravesicular localization and exocytosis of alpha-synuclein and its aggregates. *J Neurosci* 25, 6016-6024
- 244** Sung, J.Y., Kim, J., Paik, S.R., Park, J.H., Ahn, Y.S., and Chung, K.C. (2001) Induction of neuronal cell death by Rab5A-dependent endocytosis of alpha-synuclein. *J Biol Chem* 276, 27441-27448
- 245** Freeman, D., Cedillos, R., Choyke, S., Lukic, Z., McGuire, K., Marvin, S., Burrage, A.M., Sudholt, S., Rana, A., O'Connor, C., Wiethoff, C.M., and Campbell, E.M. (2013) Alpha-synuclein induces lysosomal rupture and cathepsin dependent reactive oxygen species following endocytosis. *PLoS One* 8, e62143
- 246** Ren, P.H., Lauckner, J.E., Kachirskaja, I., Heuser, J.E., Melki, R., and Kopito, R.R. (2009) Cytoplasmic penetration and persistent infection of mammalian cells by polyglutamine aggregates. *Nat Cell Biol* 11, 219-225

- 247** Morten, I.J., Gosal, W.S., Radford, S.E., and Hewitt, E.W. (2007) Investigation into the role of macrophages in the formation and degradation of beta2-microglobulin amyloid fibrils. *J Biol Chem* 282, 29691-29700
- 248** Porter, M.Y., Routledge, K.E., Radford, S.E., and Hewitt, E.W. (2011) Characterization of the response of primary cells relevant to dialysis-related amyloidosis to beta2-microglobulin monomer and fibrils. *PLoS One* 6, e27353
- 249** Barbero-Camps, E., Fernandez, A., Baulies, A., Martinez, L., Fernandez-Checa, J.C., and Colell, A. (2014) Endoplasmic Reticulum Stress Mediates Amyloid beta Neurotoxicity via Mitochondrial Cholesterol Trafficking. *Am J Pathol* 184, 2066-2081
- 250** Li, J.Q., Yu, J.T., Jiang, T., and Tan, L. (2014) Endoplasmic Reticulum Dysfunction in Alzheimer's Disease. *Mol Neurobiol*
- 251** Umeda, T., Tomiyama, T., Sakama, N., Tanaka, S., Lambert, M.P., Klein, W.L., and Mori, H. (2011) Intraneuronal amyloid beta oligomers cause cell death via endoplasmic reticulum stress, endosomal/lysosomal leakage, and mitochondrial dysfunction in vivo. *J Neurosci Res* 89, 1031-1042
- 252** Bennett, E.J., Shaler, T.A., Woodman, B., Ryu, K.Y., Zaitseva, T.S., Becker, C.H., Bates, G.P., Schulman, H., and Kopito, R.R. (2007) Global changes to the ubiquitin system in Huntington's disease. *Nature* 448, 704-708
- 253** Schmidt, M. and Finley, D. (2014) Regulation of proteasome activity in health and disease. *Biochim Biophys Acta* 1843, 13-25
- 254** Huang, Q. and Figueiredo-Pereira, M.E. (2010) Ubiquitin/proteasome pathway impairment in neurodegeneration: therapeutic implications. *Apoptosis* 15, 1292-1311
- 255** Wong, E. and Cuervo, A.M. (2010) Autophagy gone awry in neurodegenerative diseases. *Nat Neurosci* 13, 805-811
- 256** Nixon, R.A. (2013) The role of autophagy in neurodegenerative disease. *Nat Med* 19, 983-997
- 257** Schon, E.A. and Przedborski, S. (2011) Mitochondria: the next (neurode)generation. *Neuron* 70, 1033-1053
- 258** Sarafian, T.A., Ryan, C.M., Souda, P., Masliah, E., Kar, U.K., Vinters, H.V., Mathern, G.W., Faull, K.F., Whitelegge, J.P., and Watson, J.B. (2013) Impairment of mitochondria in adult mouse brain overexpressing predominantly full-length, N-terminally acetylated human alpha-synuclein. *PLoS One* 8, e63557
- 259** Maruszak, A. and Zekanowski, C. (2011) Mitochondrial dysfunction and Alzheimer's disease. *Prog Neuropsychopharmacol Biol Psychiatry* 35, 320-330

- 260** Boland, B. and Campbell, V. (2004) Abeta-mediated activation of the apoptotic cascade in cultured cortical neurones: a role for cathepsin-L. *Neurobiol Aging* 25, 83-91
- 261** Dehay, B., Bove, J., Rodriguez-Muela, N., Perier, C., Recasens, A., Boya, P., and Vila, M. (2010) Pathogenic lysosomal depletion in Parkinson's disease. *J Neurosci* 30, 12535-12544
- 262** Ji, Z.S., Miranda, R.D., Newhouse, Y.M., Weisgraber, K.H., Huang, Y., and Mahley, R.W. (2002) Apolipoprotein E4 potentiates amyloid beta peptide-induced lysosomal leakage and apoptosis in neuronal cells. *J Biol Chem* 277, 21821-21828
- 263** Ditaranto, K., Tekirian, T.L., and Yang, A.J. (2001) Lysosomal membrane damage in soluble Abeta-mediated cell death in Alzheimer's disease. *Neurobiol Dis* 8, 19-31
- 264** Liu, R.Q., Zhou, Q.H., Ji, S.R., Zhou, Q., Feng, D., Wu, Y., and Sui, S.F. (2010) Membrane localization of beta-amyloid 1-42 in lysosomes: a possible mechanism for lysosome labilization. *J Biol Chem* 285, 19986-19996
- 265** De Kimpe, L., van Haastert, E.S., Kaminari, A., Zwart, R., Rutjes, H., Hoozemans, J.J., and Scheper, W. (2013) Intracellular accumulation of aggregated pyroglutamate amyloid beta: convergence of aging and Abeta pathology at the lysosome. *Age (Dordr)* 35, 673-687
- 266** Rugarli, E.I. and Langer, T. (2012) Mitochondrial quality control: a matter of life and death for neurons. *EMBO J* 31, 1336-1349
- 267** Li, Z., Okamoto, K., Hayashi, Y., and Sheng, M. (2004) The importance of dendritic mitochondria in the morphogenesis and plasticity of spines and synapses. *Cell* 119, 873-887
- 268** MacAskill, A.F. and Kittler, J.T. (2010) Control of mitochondrial transport and localization in neurons. *Trends Cell Biol* 20, 102-112
- 269** Menzies, R.A. and Gold, P.H. (1971) The turnover of mitochondria in a variety of tissues of young adult and aged rats. *J Biol Chem* 246, 2425-2429
- 270** Miwa, S., Lawless, C., and von Zglinicki, T. (2008) Mitochondrial turnover in liver is fast in vivo and is accelerated by dietary restriction: application of a simple dynamic model. *Aging Cell* 7, 920-923
- 271** Kaplan, B.B., Gioio, A.E., Hillefors, M., and Aschrafi, A. (2009) Axonal protein synthesis and the regulation of local mitochondrial function. *Results Probl Cell Differ* 48, 225-242
- 272** Brown, M.R., Sullivan, P.G., and Geddes, J.W. (2006) Synaptic mitochondria are more susceptible to Ca²⁺ overload than nonsynaptic mitochondria. *J Biol Chem* 281, 11658-11668

- 273** Wang, Q.J., Ding, Y., Kohtz, D.S., Mizushima, N., Cristea, I.M., Rout, M.P., Chait, B.T., Zhong, Y., Heintz, N., and Yue, Z. (2006) Induction of autophagy in axonal dystrophy and degeneration. *J Neurosci* 26, 8057-8068
- 274** Alikhani, N., Guo, L., Yan, S., Du, H., Pinho, C.M., Chen, J.X., Glaser, E., and Yan, S.S. (2011) Decreased proteolytic activity of the mitochondrial amyloid-beta degrading enzyme, PreP peptidasome, in Alzheimer's disease brain mitochondria. *J Alzheimers Dis* 27, 75-87
- 275** Kitada, T., Pisani, A., Porter, D.R., Yamaguchi, H., Tscherter, A., Martella, G., Bonsi, P., Zhang, C., Pothos, E.N., and Shen, J. (2007) Impaired dopamine release and synaptic plasticity in the striatum of PINK1-deficient mice. *Proc Natl Acad Sci U S A* 104, 11441-11446
- 276** Valente, E.M., Abou-Sleiman, P.M., Caputo, V., Muqit, M.M., Harvey, K., Gispert, S., Ali, Z., Del Turco, D., Bentivoglio, A.R., Healy, D.G., Albanese, A., Nussbaum, R., Gonzalez-Maldonado, R., Deller, T., Salvi, S., Cortelli, P., Gilks, W.P., Latchman, D.S., Harvey, R.J., Dallapiccola, B., Auburger, G., and Wood, N.W. (2004) Hereditary early-onset Parkinson's disease caused by mutations in PINK1. *Science* 304, 1158-1160
- 277** Vives-Bauza, C. and Przedborski, S. (2011) Mitophagy: the latest problem for Parkinson's disease. *Trends Mol Med* 17, 158-165
- 278** Settembre, C., Fraldi, A., Medina, D.L., and Ballabio, A. (2013) Signals from the lysosome: a control centre for cellular clearance and energy metabolism. *Nat Rev Mol Cell Biol* 14, 283-296
- 279** de Duve, C. (2005) The lysosome turns fifty. *Nat Cell Biol* 7, 847-849
- 280** Saftig, P. and Klumperman, J. (2009) Lysosome biogenesis and lysosomal membrane proteins: trafficking meets function. *Nat Rev Mol Cell Biol* 10, 623-635
- 281** Kaushik, S. and Cuervo, A.M. (2012) Chaperone-mediated autophagy: a unique way to enter the lysosome world. *Trends Cell Biol* 22, 407-417
- 282** Luzio, J.P., Pryor, P.R., and Bright, N.A. (2007) Lysosomes: fusion and function. *Nat Rev Mol Cell Biol* 8, 622-632
- 283** Boya, P. and Kroemer, G. (2008) Lysosomal membrane permeabilization in cell death. *Oncogene* 27, 6434-6451
- 284** Lee, S., Sato, Y., and Nixon, R.A. (2011) Lysosomal proteolysis inhibition selectively disrupts axonal transport of degradative organelles and causes an Alzheimer's-like axonal dystrophy. *J Neurosci* 31, 7817-7830
- 285** Lai, A.Y., Lan, C.P., Hasan, S., Brown, M.E., and McLaurin, J. (2014) scyllo-Inositol promotes robust mutant Huntingtin protein degradation. *J Biol Chem* 289, 3666-3676

- 286** McLaurin, J., Golomb, R., Jurewicz, A., Antel, J.P., and Fraser, P.E. (2000) Inositol stereoisomers stabilize an oligomeric aggregate of Alzheimer amyloid beta peptide and inhibit abeta -induced toxicity. *J Biol Chem* 275, 18495-18502
- 287** Tsunemi, T. and Krainc, D. (2014) Zn(2)(+) dyshomeostasis caused by loss of ATP13A2/PARK9 leads to lysosomal dysfunction and alpha-synuclein accumulation. *Hum Mol Genet* 23, 2791-2801
- 288** Mazzulli, J.R., Xu, Y.H., Sun, Y., Knight, A.L., McLean, P.J., Caldwell, G.A., Sidransky, E., Grabowski, G.A., and Krainc, D. (2011) Gaucher disease glucocerebrosidase and alpha-synuclein form a bidirectional pathogenic loop in synucleinopathies. *Cell* 146, 37-52
- 289** Rivera, J.F., Gurlo, T., Daval, M., Huang, C.J., Matveyenko, A.V., Butler, P.C., and Costes, S. (2011) Human-IAPP disrupts the autophagy/lysosomal pathway in pancreatic beta-cells: protective role of p62-positive cytoplasmic inclusions. *Cell Death Differ* 18, 415-426
- 290** Nixon, R.A., Wegiel, J., Kumar, A., Yu, W.H., Peterhoff, C., Cataldo, A., and Cuervo, A.M. (2005) Extensive involvement of autophagy in Alzheimer disease: an immuno-electron microscopy study. *J Neuropathol Exp Neurol* 64, 113-122
- 291** Kegel, K.B., Kim, M., Sapp, E., McIntyre, C., Castano, J.G., Aronin, N., and DiFiglia, M. (2000) Huntingtin expression stimulates endosomal-lysosomal activity, endosome tubulation, and autophagy. *J Neurosci* 20, 7268-7278
- 292** Boland, B., Kumar, A., Lee, S., Platt, F.M., Wegiel, J., Yu, W.H., and Nixon, R.A. (2008) Autophagy induction and autophagosome clearance in neurons: relationship to autophagic pathology in Alzheimer's disease. *J Neurosci* 28, 6926-6937
- 293** Rubinsztein, D.C., Cuervo, A.M., Ravikumar, B., Sarkar, S., Korolchuk, V., Kaushik, S., and Klionsky, D.J. (2009) In search of an "autophagometer". *Autophagy* 5, 585-589
- 294** Settembre, C., Fraldi, A., Jahreiss, L., Spampinato, C., Venturi, C., Medina, D., de Pablo, R., Tacchetti, C., Rubinsztein, D.C., and Ballabio, A. (2008) A block of autophagy in lysosomal storage disorders. *Hum Mol Genet* 17, 119-129
- 295** Mizushima, N., Levine, B., Cuervo, A.M., and Klionsky, D.J. (2008) Autophagy fights disease through cellular self-digestion. *Nature* 451, 1069-1075
- 296** He, C. and Klionsky, D.J. (2009) Regulation mechanisms and signaling pathways of autophagy. *Annu Rev Genet* 43, 67-93
- 297** Cuervo, A.M. (2010) Chaperone-mediated autophagy: selectivity pays off. *Trends Endocrinol Metab* 21, 142-150
- 298** Massey, A.C., Kaushik, S., Sovak, G., Kiffin, R., and Cuervo, A.M. (2006) Consequences of the selective blockage of chaperone-mediated autophagy. *Proc Natl Acad Sci U S A* 103, 5805-5810

- 299** Nedelsky, N.B., Todd, P.K., and Taylor, J.P. (2008) Autophagy and the ubiquitin-proteasome system: collaborators in neuroprotection. *Biochim Biophys Acta* 1782, 691-699
- 300** Cuervo, A.M., Stefanis, L., Fredenburg, R., Lansbury, P.T., and Sulzer, D. (2004) Impaired degradation of mutant alpha-synuclein by chaperone-mediated autophagy. *Science* 305, 1292-1295
- 301** Wang, Y., Martinez-Vicente, M., Kruger, U., Kaushik, S., Wong, E., Mandelkow, E.M., Cuervo, A.M., and Mandelkow, E. (2009) Tau fragmentation, aggregation and clearance: the dual role of lysosomal processing. *Hum Mol Genet* 18, 4153-4170
- 302** Lee, J.A. and Gao, F.B. (2009) Inhibition of autophagy induction delays neuronal cell loss caused by dysfunctional ESCRT-III in frontotemporal dementia. *J Neurosci* 29, 8506-8511
- 303** Filimonenko, M., Stuffers, S., Raiborg, C., Yamamoto, A., Malerod, L., Fisher, E.M., Isaacs, A., Brech, A., Stenmark, H., and Simonsen, A. (2007) Functional multivesicular bodies are required for autophagic clearance of protein aggregates associated with neurodegenerative disease. *J Cell Biol* 179, 485-500
- 304** Sardiello, M., Palmieri, M., di Ronza, A., Medina, D.L., Valenza, M., Gennarino, V.A., Di Malta, C., Donaudy, F., Embrione, V., Polishchuk, R.S., Banfi, S., Parenti, G., Cattaneo, E., and Ballabio, A. (2009) A gene network regulating lysosomal biogenesis and function. *Science* 325, 473-477
- 305** Schultz, M.L., Tecedor, L., Chang, M., and Davidson, B.L. (2011) Clarifying lysosomal storage diseases. *Trends Neurosci* 34, 401-410
- 306** Settembre, C., Fraldi, A., Rubinsztein, D.C., and Ballabio, A. (2008) Lysosomal storage diseases as disorders of autophagy. *Autophagy* 4, 113-114
- 307** Futerman, A.H. and van Meer, G. (2004) The cell biology of lysosomal storage disorders. *Nat Rev Mol Cell Biol* 5, 554-565
- 308** Ravikumar, B., Duden, R., and Rubinsztein, D.C. (2002) Aggregate-prone proteins with polyglutamine and polyalanine expansions are degraded by autophagy. *Hum Mol Genet* 11, 1107-1117
- 309** Settembre, C., Annunziata, I., Spampinato, C., Zarccone, D., Cobellis, G., Nusco, E., Zito, E., Tacchetti, C., Cosma, M.P., and Ballabio, A. (2007) Systemic inflammation and neurodegeneration in a mouse model of multiple sulfatase deficiency. *Proc Natl Acad Sci U S A* 104, 4506-4511
- 310** Grabowski, G.A. (2008) Phenotype, diagnosis, and treatment of Gaucher's disease. *Lancet* 372, 1263-1271

- 311** Stern, G. (2014) Niemann-Pick's and Gaucher's diseases. *Parkinsonism Relat Disord* 20 Suppl 1, S143-146
- 312** Neudorfer, O., Giladi, N., Elstein, D., Abrahamov, A., Turezkite, T., Aghai, E., Reches, A., Bembi, B., and Zimran, A. (1996) Occurrence of Parkinson's syndrome in type I Gaucher disease. *QJM* 89, 691-694
- 313** Tayebi, N., Walker, J., Stubblefield, B., Orvisky, E., LaMarca, M.E., Wong, K., Rosenbaum, H., Schiffmann, R., Bembi, B., and Sidransky, E. (2003) Gaucher disease with parkinsonian manifestations: does glucocerebrosidase deficiency contribute to a vulnerability to parkinsonism? *Mol Genet Metab* 79, 104-109
- 314** Sidransky, E. (2005) Gaucher disease and parkinsonism. *Mol Genet Metab* 84, 302-304
- 315** Wong, K., Sidransky, E., Verma, A., Mixon, T., Sandberg, G.D., Wakefield, L.K., Morrison, A., Lwin, A., Colegial, C., Allman, J.M., and Schiffmann, R. (2004) Neuropathology provides clues to the pathophysiology of Gaucher disease. *Mol Genet Metab* 82, 192-207
- 316** Sidransky, E., Nalls, M.A., Aasly, J.O., Aharon-Peretz, J., Annesi, G., Barbosa, E.R., Bar-Shira, A., Berg, D., Bras, J., Brice, A., Chen, C.M., Clark, L.N., Condroyer, C., De Marco, E.V., Durr, A., Eblan, M.J., Fahn, S., Farrer, M.J., Fung, H.C., Gan-Or, Z., Gasser, T., Gershoni-Baruch, R., Giladi, N., Griffith, A., Gurevich, T., Januario, C., Kropp, P., Lang, A.E., Lee-Chen, G.J., Lesage, S., Marder, K., Mata, I.F., Mirelman, A., Mitsui, J., Mizuta, I., Nicoletti, G., Oliveira, C., Ottman, R., Orr-Urtreger, A., Pereira, L.V., Quattrone, A., Rogaeva, E., Rolfs, A., Rosenbaum, H., Rozenberg, R., Samii, A., Samaddar, T., Schulte, C., Sharma, M., Singleton, A., Spitz, M., Tan, E.K., Tayebi, N., Toda, T., Troiano, A.R., Tsuji, S., Wittstock, M., Wolfsberg, T.G., Wu, Y.R., Zabetian, C.P., Zhao, Y., and Ziegler, S.G. (2009) Multicenter analysis of glucocerebrosidase mutations in Parkinson's disease. *N Engl J Med* 361, 1651-1661
- 317** Nixon, R.A. (2004) Niemann-Pick Type C disease and Alzheimer's disease: the APP-endosome connection fattens up. *Am J Pathol* 164, 757-761
- 318** Yamazaki, T., Chang, T.Y., Haass, C., and Ihara, Y. (2001) Accumulation and aggregation of amyloid beta-protein in late endosomes of Niemann-pick type C cells. *J Biol Chem* 276, 4454-4460
- 319** Jin, L.W., Shie, F.S., Maezawa, I., Vincent, I., and Bird, T. (2004) Intracellular accumulation of amyloidogenic fragments of amyloid-beta precursor protein in neurons with Niemann-Pick type C defects is associated with endosomal abnormalities. *Am J Pathol* 164, 975-985
- 320** Love, S., Bridges, L.R., and Case, C.P. (1995) Neurofibrillary tangles in Niemann-Pick disease type C. *Brain* 118 (Pt 1), 119-129

- 321** Suzuki, K., Parker, C.C., Pentchev, P.G., Katz, D., Ghetti, B., D'Agostino, A.N., and Carstea, E.D. (1995) Neurofibrillary tangles in Niemann-Pick disease type C. *Acta Neuropathol* 89, 227-238
- 322** Poirier, J. (2003) Apolipoprotein E and cholesterol metabolism in the pathogenesis and treatment of Alzheimer's disease. *Trends Mol Med* 9, 94-101
- 323** Treusch, S., Hamamichi, S., Goodman, J.L., Matlack, K.E., Chung, C.Y., Baru, V., Shulman, J.M., Parrado, A., Bevis, B.J., Valastyan, J.S., Han, H., Lindhagen-Persson, M., Reiman, E.M., Evans, D.A., Bennett, D.A., Olofsson, A., DeJager, P.L., Tanzi, R.E., Caldwell, K.A., Caldwell, G.A., and Lindquist, S. (2011) Functional links between Abeta toxicity, endocytic trafficking, and Alzheimer's disease risk factors in yeast. *Science* 334, 1241-1245
- 324** Sorrentino, P., Iuliano, A., Polverino, A., Jacini, F., and Sorrentino, G. (2014) The dark sides of amyloid in Alzheimer's disease pathogenesis. *FEBS Lett* 588, 641-652
- 325** Kad, N.M., Thomson, N.H., Smith, D.P., Smith, D.A., and Radford, S.E. (2001) Beta(2)-microglobulin and its deamidated variant, N17D form amyloid fibrils with a range of morphologies in vitro. *J Mol Biol* 313, 559-571
- 326** Gill, S.C. and von Hippel, P.H. (1989) Calculation of protein extinction coefficients from amino acid sequence data. *Anal Biochem* 182, 319-326
- 327** O'Nuallain, B. and Wetzel, R. (2002) Conformational Abs recognizing a generic amyloid fibril epitope. *Proc Natl Acad Sci U S A* 99, 1485-1490
- 328** Xue, W.F., Homans, S.W., and Radford, S.E. (2009) Amyloid fibril length distribution quantified by atomic force microscopy single-particle image analysis. *Protein Eng Des Sel* 22, 489-496
- 329** Bolte, S. and Cordelieres, F.P. (2006) A guided tour into subcellular colocalization analysis in light microscopy. *J Microsc* 224, 213-232
- 330** Dunn, K.W., Kamocka, M.M., and McDonald, J.H. (2011) A practical guide to evaluating colocalization in biological microscopy. *Am J Physiol Cell Physiol* 300, C723-742
- 331** Costes, S.V., Daelemans, D., Cho, E.H., Dobbin, Z., Pavlakis, G., and Lockett, S. (2004) Automatic and quantitative measurement of protein-protein colocalization in live cells. *Biophys J* 86, 3993-4003
- 332** Manders, E.M.M., Verbeek, F.J., and Aten, J.A. (1993) Measurement of co-localization of objects in dual-colour confocal images. *Journal of Microscopy* 169, 375-382
- 333** Roodveldt, C., Bertocini, C.W., Andersson, A., van der Goot, A.T., Hsu, S.T., Fernandez-Montesinos, R., de Jong, J., van Ham, T.J., Nollen, E.A., Pozo, D., Christodoulou, J., and

- Dobson, C.M. (2009) Chaperone proteostasis in Parkinson's disease: stabilization of the Hsp70/alpha-synuclein complex by Hip. *EMBO J* 28, 3758-3770
- 334** Trinh, C.H., Smith, D.P., Kalverda, A.P., Phillips, S.E., and Radford, S.E. (2002) Crystal structure of monomeric human beta-2-microglobulin reveals clues to its amyloidogenic properties. *Proc Natl Acad Sci U S A* 99, 9771-9776
- 335** Khan, A.R., Baker, B.M., Ghosh, P., Biddison, W.E., and Wiley, D.C. (2000) The structure and stability of an HLA-A*0201/octameric tax peptide complex with an empty conserved peptide-N-terminal binding site. *J Immunol* 164, 6398-6405
- 336** Verdone, G., Corazza, A., Viglino, P., Pettirossi, F., Giorgetti, S., Mangione, P., Andreola, A., Stoppini, M., Bellotti, V., and Esposito, G. (2002) The solution structure of human beta2-microglobulin reveals the prodromes of its amyloid transition. *Protein Sci* 11, 487-499
- 337** Eichner, T. and Radford, S.E. (2011) Understanding the complex mechanisms of beta2-microglobulin amyloid assembly. *FEBS J* 278, 3868-3883
- 338** Jahn, T.R., Parker, M.J., Homans, S.W., and Radford, S.E. (2006) Amyloid formation under physiological conditions proceeds via a native-like folding intermediate. *Nat Struct Mol Biol* 13, 195-201
- 339** Borbulevych, O.Y., Do, P., and Baker, B.M. (2010) Structures of native and affinity-enhanced WT1 epitopes bound to HLA-A*0201: implications for WT1-based cancer therapeutics. *Mol Immunol* 47, 2519-2524
- 340** Eichner, T., Kalverda, A.P., Thompson, G.S., Homans, S.W., and Radford, S.E. (2011) Conformational conversion during amyloid formation at atomic resolution. *Mol Cell* 41, 161-172
- 341** Platt, G.W. and Radford, S.E. (2009) Glimpses of the molecular mechanisms of beta2-microglobulin fibril formation in vitro: aggregation on a complex energy landscape. *FEBS Lett* 583, 2623-2629
- 342** Rosano, C., Zuccotti, S., Mangione, P., Giorgetti, S., Bellotti, V., Pettirossi, F., Corazza, A., Viglino, P., Esposito, G., and Bolognesi, M. (2004) beta2-microglobulin H31Y variant 3D structure highlights the protein natural propensity towards intermolecular aggregation. *J Mol Biol* 335, 1051-1064
- 343** Esposito, G., Ricagno, S., Corazza, A., Rennella, E., Gumral, D., Mimmi, M.C., Betto, E., Pucillo, C.E., Fogolari, F., Viglino, P., Raimondi, S., Giorgetti, S., Bolognesi, B., Merlini, G., Stoppini, M., Bolognesi, M., and Bellotti, V. (2008) The controlling roles of Trp60 and Trp95 in beta2-microglobulin function, folding and amyloid aggregation properties. *J Mol Biol* 378, 887-897

- 344** Calabrese, M.F., Eakin, C.M., Wang, J.M., and Miranker, A.D. (2008) A regulatable switch mediates self-association in an immunoglobulin fold. *Nat Struct Mol Biol* 15, 965-971
- 345** Kihara, M., Chatani, E., Iwata, K., Yamamoto, K., Matsuura, T., Nakagawa, A., Naiki, H., and Goto, Y. (2006) Conformation of amyloid fibrils of beta2-microglobulin probed by tryptophan mutagenesis. *J Biol Chem* 281, 31061-31069
- 346** Iwata, K., Matsuura, T., Sakurai, K., Nakagawa, A., and Goto, Y. (2007) High-resolution crystal structure of beta2-microglobulin formed at pH 7.0. *J Biochem* 142, 413-419
- 347** Ricagno, S., Colombo, M., de Rosa, M., Sangiovanni, E., Giorgetti, S., Raimondi, S., Bellotti, V., and Bolognesi, M. (2008) DE loop mutations affect beta2-microglobulin stability and amyloid aggregation. *Biochem Biophys Res Commun* 377, 146-150
- 348** Santambrogio, C., Ricagno, S., Colombo, M., Barbiroli, A., Bonomi, F., Bellotti, V., Bolognesi, M., and Grandori, R. (2010) DE-loop mutations affect beta2 microglobulin stability, oligomerization, and the low-pH unfolded form. *Protein Sci* 19, 1386-1394
- 349** Eakin, C.M., Berman, A.J., and Miranker, A.D. (2006) A native to amyloidogenic transition regulated by a backbone trigger. *Nat Struct Mol Biol* 13, 202-208
- 350** Eakin, C.M. and Miranker, A.D. (2005) From chance to frequent encounters: origins of beta2-microglobulin fibrillogenesis. *Biochim Biophys Acta* 1753, 92-99
- 351** Yamamoto, S., Hasegawa, K., Yamaguchi, I., Tsutsumi, S., Kardos, J., Goto, Y., Gejyo, F., and Naiki, H. (2004) Low concentrations of sodium dodecyl sulfate induce the extension of beta 2-microglobulin-related amyloid fibrils at a neutral pH. *Biochemistry* 43, 11075-11082
- 352** Yamamoto, S., Yamaguchi, I., Hasegawa, K., Tsutsumi, S., Goto, Y., Gejyo, F., and Naiki, H. (2004) Glycosaminoglycans enhance the trifluoroethanol-induced extension of beta 2-microglobulin-related amyloid fibrils at a neutral pH. *J Am Soc Nephrol* 15, 126-133
- 353** Smith, D.P., Jones, S., Serpell, L.C., Sunde, M., and Radford, S.E. (2003) A systematic investigation into the effect of protein destabilisation on beta 2-microglobulin amyloid formation. *J Mol Biol* 330, 943-954
- 354** Kozhukh, G.V., Hagihara, Y., Kawakami, T., Hasegawa, K., Naiki, H., and Goto, Y. (2002) Investigation of a peptide responsible for amyloid fibril formation of beta 2-microglobulin by achromobacter protease I. *J Biol Chem* 277, 1310-1315
- 355** Jones, S., Manning, J., Kad, N.M., and Radford, S.E. (2003) Amyloid-forming peptides from beta2-microglobulin-Insights into the mechanism of fibril formation in vitro. *J Mol Biol* 325, 249-257

- 356** Platt, G.W., Routledge, K.E., Homans, S.W., and Radford, S.E. (2008) Fibril growth kinetics reveal a region of beta2-microglobulin important for nucleation and elongation of aggregation. *J Mol Biol* 378, 251-263
- 357** Routledge, K.E., Tartaglia, G.G., Platt, G.W., Vendruscolo, M., and Radford, S.E. (2009) Competition between intramolecular and intermolecular interactions in an amyloid-forming protein. *J Mol Biol* 389, 776-786
- 358** Ivanova, M.I., Sawaya, M.R., Gingery, M., Attinger, A., and Eisenberg, D. (2004) An amyloid-forming segment of beta2-microglobulin suggests a molecular model for the fibril. *Proc Natl Acad Sci U S A* 101, 10584-10589
- 359** Esposito, G., Michelutti, R., Verdone, G., Viglino, P., Hernandez, H., Robinson, C.V., Amoresano, A., Dal Piaz, F., Monti, M., Pucci, P., Mangione, P., Stoppini, M., Merlini, G., Ferri, G., and Bellotti, V. (2000) Removal of the N-terminal hexapeptide from human beta2-microglobulin facilitates protein aggregation and fibril formation. *Protein Sci* 9, 831-845
- 360** Bellotti, V., Stoppini, M., Mangione, P., Sunde, M., Robinson, C., Asti, L., Brancaccio, D., and Ferri, G. (1998) Beta2-microglobulin can be refolded into a native state from ex vivo amyloid fibrils. *Eur J Biochem* 258, 61-67
- 361** Giorgetti, S., Rossi, A., Mangione, P., Raimondi, S., Marini, S., Stoppini, M., Corazza, A., Viglino, P., Esposito, G., Cetta, G., Merlini, G., and Bellotti, V. (2005) Beta2-microglobulin isoforms display an heterogeneous affinity for type I collagen. *Protein Sci* 14, 696-702
- 362** Eichner, T. and Radford, S.E. (2009) A generic mechanism of beta2-microglobulin amyloid assembly at neutral pH involving a specific proline switch. *J Mol Biol* 386, 1312-1326
- 363** Stoppini, M., Mangione, P., Monti, M., Giorgetti, S., Marchese, L., Arcidiaco, P., Verga, L., Segagni, S., Pucci, P., Merlini, G., and Bellotti, V. (2005) Proteomics of beta2-microglobulin amyloid fibrils. *Biochim Biophys Acta* 1753, 23-33
- 364** Monti, M., Amoresano, A., Giorgetti, S., Bellotti, V., and Pucci, P. (2005) Limited proteolysis in the investigation of beta2-microglobulin amyloidogenic and fibrillar states. *Biochim Biophys Acta* 1753, 44-50
- 365** McParland, V.J., Kad, N.M., Kalverda, A.P., Brown, A., Kirwin-Jones, P., Hunter, M.G., Sunde, M., and Radford, S.E. (2000) Partially unfolded states of beta(2)-microglobulin and amyloid formation in vitro. *Biochemistry* 39, 8735-8746
- 366** Jahn, T.R., Tennent, G.A., and Radford, S.E. (2008) A common beta-sheet architecture underlies in vitro and in vivo beta2-microglobulin amyloid fibrils. *J Biol Chem* 283, 17279-17286

- 367** Myers, S.L., Jones, S., Jahn, T.R., Morten, I.J., Tennent, G.A., Hewitt, E.W., and Radford, S.E. (2006) A systematic study of the effect of physiological factors on beta2-microglobulin amyloid formation at neutral pH. *Biochemistry* 45, 2311-2321
- 368** Radford, S.E., Gosal, W.S., and Platt, G.W. (2005) Towards an understanding of the structural molecular mechanism of beta(2)-microglobulin amyloid formation in vitro. *Biochim Biophys Acta* 1753, 51-63
- 369** Biancalana, M. and Koide, S. (2010) Molecular mechanism of Thioflavin-T binding to amyloid fibrils. *Biochim Biophys Acta* 1804, 1405-1412
- 370** Zhang, C., Jackson, A.P., Zhang, Z.R., Han, Y., Yu, S., He, R.Q., and Perrett, S. (2010) Amyloid-like aggregates of the yeast prion protein ure2 enter vertebrate cells by specific endocytotic pathways and induce apoptosis. *PLoS One* 5
- 371** Cecchi, C., Nichino, D., Zampagni, M., Bernacchioni, C., Evangelisti, E., Pensalfini, A., Liguri, G., Gliozzi, A., Stefani, M., and Relini, A. (2009) A protective role for lipid raft cholesterol against amyloid-induced membrane damage in human neuroblastoma cells. *Biochim Biophys Acta* 1788, 2204-2216
- 372** Mena, C., Esser, E., and Sprague, S.M. (2008) Beta2-microglobulin stimulates osteoclast formation. *Kidney Int* 73, 1275-1281
- 373** Mosmann, T. (1983) Rapid colorimetric assay for cellular growth and survival: application to proliferation and cytotoxicity assays. *J Immunol Methods* 65, 55-63
- 374** Acerra, N., Kad, N.M., Cheruvara, H., and Mason, J.M. (2014) Intracellular selection of peptide inhibitors that target disulphide-bridged Abeta oligomers. *Protein Sci*
- 375** Cipriani, S., Bakshi, R., and Schwarzschild, M.A. (2014) Protection by inosine in a cellular model of Parkinson's disease. *Neuroscience* 274C, 242-249
- 376** Zhao, Y., Zhao, H., Lobo, N., Guo, X., Gentleman, S.M., and Ma, D. (2014) Celastrol Enhances Cell Viability and Inhibits Amyloid-beta Production Induced by Lipopolysaccharide In Vitro. *J Alzheimers Dis*
- 377** Berridge, M.V., Herst, P.M., and Tan, A.S. (2005) Tetrazolium dyes as tools in cell biology: new insights into their cellular reduction. *Biotechnol Annu Rev* 11, 127-152
- 378** Liu, Y., Peterson, D.A., Kimura, H., and Schubert, D. (1997) Mechanism of cellular 3-(4,5-dimethylthiazol-2-yl)-2,5-diphenyltetrazolium bromide (MTT) reduction. *J Neurochem* 69, 581-593
- 379** Liu, Y. and Schubert, D. (1997) Cytotoxic amyloid peptides inhibit cellular 3-(4,5-dimethylthiazol-2-yl)-2,5-diphenyltetrazolium bromide (MTT) reduction by enhancing MTT formazan exocytosis. *J Neurochem* 69, 2285-2293

- 380** Isobe, I., Michikawa, M., and Yanagisawa, K. (1999) Enhancement of MTT, a tetrazolium salt, exocytosis by amyloid beta-protein and chloroquine in cultured rat astrocytes. *Neurosci Lett* 266, 129-132
- 381** Liu, M.L. and Hong, S.T. (2005) Early phase of amyloid beta42-induced cytotoxicity in neuronal cells is associated with vacuole formation and enhancement of exocytosis. *Exp Mol Med* 37, 559-566
- 382** Wogulis, M., Wright, S., Cunningham, D., Chilcote, T., Powell, K., and Rydel, R.E. (2005) Nucleation-dependent polymerization is an essential component of amyloid-mediated neuronal cell death. *J Neurosci* 25, 1071-1080
- 383** Hertel, C., Hauser, N., Schubengel, R., Seilheimer, B., and Kemp, J.A. (1996) Beta-amyloid-induced cell toxicity: enhancement of 3-(4,5-dimethylthiazol-2-yl)-2,5-diphenyltetrazolium bromide-dependent cell death. *J Neurochem* 67, 272-276
- 384** Xue, W.F. and Radford, S.E. (2013) An imaging and systems modeling approach to fibril breakage enables prediction of amyloid behavior. *Biophys J* 105, 2811-2819
- 385** Shorter, J. and Lindquist, S. (2004) Hsp104 catalyzes formation and elimination of self-replicating Sup35 prion conformers. *Science* 304, 1793-1797
- 386** Hellewell, A. (2011) The Cytotoxicity of Amyloid Fibrils. In *Faculty of Biological Sciences*, University of Leeds
- 387** Crouch, S.P., Kozlowski, R., Slater, K.J., and Fletcher, J. (1993) The use of ATP bioluminescence as a measure of cell proliferation and cytotoxicity. *J Immunol Methods* 160, 81-88
- 388** Ghavami, S., Shojaei, S., Yeganeh, B., Ande, S.R., Jangamreddy, J.R., Mehrpour, M., Christoffersson, J., Chaabane, W., Moghadam, A.R., Kashani, H.H., Hashemi, M., Owji, A.A., and Los, M.J. (2014) Autophagy and apoptosis dysfunction in neurodegenerative disorders. *Prog Neurobiol* 112, 24-49
- 389** McBrayer, M. and Nixon, R.A. (2013) Lysosome and calcium dysregulation in Alzheimer's disease: partners in crime. *Biochem Soc Trans* 41, 1495-1502
- 390** Garcia-Garcia, M., Argiles, Gouin-Charnet, A., Durfort, M., Garcia-Valero, J., and Mourad, G. (1999) Impaired lysosomal processing of beta2-microglobulin by infiltrating macrophages in dialysis amyloidosis. *Kidney Int* 55, 899-906
- 391** Kornfeld, S. and Mellman, I. (1989) The biogenesis of lysosomes. *Annu Rev Cell Biol* 5, 483-525
- 392** Macdonald, P.M. (1992) The *Drosophila pumilio* gene: an unusually long transcription unit and an unusual protein. *Development* 114, 221-232

- 393** Zhang, T., Maekawa, Y., Hanba, J., Dainichi, T., Nashed, B.F., Hisaeda, H., Sakai, T., Asao, T., Himeno, K., Good, R.A., and Katunuma, N. (2000) Lysosomal cathepsin B plays an important role in antigen processing, while cathepsin D is involved in degradation of the invariant chain in ovalbumin-immunized mice. *Immunology* 100, 13-20
- 394** Hardy, J., Bogdanovic, N., Winblad, B., Portelius, E., Andreasen, N., Cedazo-Minguez, A., and Zetterberg, H. (2014) Pathways to Alzheimer's disease. *J Intern Med* 275, 296-303
- 395** Hoang, Q.Q. (2014) Pathway for Parkinson disease. *Proc Natl Acad Sci U S A* 111, 2402-2403
- 396** Tanida, I., Ueno, T., and Kominami, E. (2008) LC3 and Autophagy. *Methods Mol Biol* 445, 77-88
- 397** Lorincz, M., Herzenberg, L.A., Diwu, Z., Barranger, J.A., and Kerr, W.G. (1997) Detection and isolation of gene-corrected cells in Gaucher disease via a fluorescence-activated cell sorter assay for lysosomal glucocerebrosidase activity. *Blood* 89, 3412-3420
- 398** Boot, R.G., Verhoek, M., Donker-Koopman, W., Strijland, A., van Marle, J., Overkleeft, H.S., Wennekes, T., and Aerts, J.M. (2007) Identification of the non-lysosomal glucosylceramidase as beta-glucosidase 2. *J Biol Chem* 282, 1305-1312
- 399** Zong, D., Zielinska-Chomej, K., Juntti, T., Mork, B., Lewensohn, R., Haag, P., and Viktorsson, K. (2014) Harnessing the lysosome-dependent antitumor activity of phenothiazines in human small cell lung cancer. *Cell Death Dis* 5, e1111
- 400** Li, Y., Cheng, D., Cheng, R., Zhu, X., Wan, T., Liu, J., and Zhang, R. (2014) Mechanisms of U87 astrocytoma cell uptake and trafficking of monomeric versus protofibril Alzheimer's disease amyloid-beta proteins. *PLoS One* 9, e99939
- 401** Borghi, R., Marchese, R., Negro, A., Marinelli, L., Forloni, G., Zaccheo, D., Abbruzzese, G., and Tabaton, M. (2000) Full length alpha-synuclein is present in cerebrospinal fluid from Parkinson's disease and normal subjects. *Neurosci Lett* 287, 65-67
- 402** Visanji, N.P., Brooks, P.L., Hazrati, L.N., and Lang, A.E. (2013) The prion hypothesis in Parkinson's disease: Braak to the future. *Acta Neuropathol Commun* 1, 2
- 403** Yu, W.H., Cuervo, A.M., Kumar, A., Peterhoff, C.M., Schmidt, S.D., Lee, J.H., Mohan, P.S., Mercken, M., Farmery, M.R., Tjernberg, L.O., Jiang, Y., Duff, K., Uchiyama, Y., Naslund, J., Mathews, P.M., Cataldo, A.M., and Nixon, R.A. (2005) Macroautophagy--a novel Beta-amyloid peptide-generating pathway activated in Alzheimer's disease. *J Cell Biol* 171, 87-98
- 404** Howell, G.J., Holloway, Z.G., Cobbald, C., Monaco, A.P., and Ponnambalam, S. (2006) Cell biology of membrane trafficking in human disease. *Int Rev Cytol* 252, 1-69

- 405** Palade, G. (1975) Intracellular aspects of the process of protein synthesis. *Science* 189, 347-358
- 406** Sollner, T., Whiteheart, S.W., Brunner, M., Erdjument-Bromage, H., Geromanos, S., Tempst, P., and Rothman, J.E. (1993) SNAP receptors implicated in vesicle targeting and fusion. *Nature* 362, 318-324
- 407** Bennett, M.K. (1995) SNAREs and the specificity of transport vesicle targeting. *Curr Opin Cell Biol* 7, 581-586
- 408** Hutagalung, A.H. and Novick, P.J. (2011) Role of Rab GTPases in membrane traffic and cell physiology. *Physiol Rev* 91, 119-149
- 409** Dalfo, E., Gomez-Isla, T., Rosa, J.L., Nieto Bodelon, M., Cuadrado Tejedor, M., Barrachina, M., Ambrosio, S., and Ferrer, I. (2004) Abnormal alpha-synuclein interactions with Rab proteins in alpha-synuclein A30P transgenic mice. *J Neuropathol Exp Neurol* 63, 302-313
- 410** Cooper, A.A., Gitler, A.D., Cashikar, A., Haynes, C.M., Hill, K.J., Bhullar, B., Liu, K., Xu, K., Strathearn, K.E., Liu, F., Cao, S., Caldwell, K.A., Caldwell, G.A., Marsischky, G., Kolodner, R.D., Labaer, J., Rochet, J.C., Bonini, N.M., and Lindquist, S. (2006) Alpha-synuclein blocks ER-Golgi traffic and Rab1 rescues neuron loss in Parkinson's models. *Science* 313, 324-328
- 411** Gitler, A.D., Bevis, B.J., Shorter, J., Strathearn, K.E., Hamamichi, S., Su, L.J., Caldwell, K.A., Caldwell, G.A., Rochet, J.C., McCaffery, J.M., Barlowe, C., and Lindquist, S. (2008) The Parkinson's disease protein alpha-synuclein disrupts cellular Rab homeostasis. *Proc Natl Acad Sci U S A* 105, 145-150
- 412** MacLeod, D.A., Rhinn, H., Kuwahara, T., Zolin, A., Di Paolo, G., McCabe, B.D., Marder, K.S., Honig, L.S., Clark, L.N., Small, S.A., and Abeliovich, A. (2013) RAB7L1 interacts with LRRK2 to modify intraneuronal protein sorting and Parkinson's disease risk. *Neuron* 77, 425-439
- 413** Matlack, K.E., Tardiff, D.F., Narayan, P., Hamamichi, S., Caldwell, K.A., Caldwell, G.A., and Lindquist, S. (2014) Clioquinol promotes the degradation of metal-dependent amyloid-beta (Abeta) oligomers to restore endocytosis and ameliorate Abeta toxicity. *Proc Natl Acad Sci U S A* 111, 4013-4018
- 414** Yu, A., Shibata, Y., Shah, B., Calamini, B., Lo, D.C., and Morimoto, R.I. (2014) Protein aggregation can inhibit clathrin-mediated endocytosis by chaperone competition. *Proc Natl Acad Sci U S A* 111, E1481-1490
- 415** Pols, M.S. and Klumperman, J. (2009) Trafficking and function of the tetraspanin CD63. *Exp Cell Res* 315, 1584-1592

- 416** Eskelinen, E.L., Tanaka, Y., and Saftig, P. (2003) At the acidic edge: emerging functions for lysosomal membrane proteins. *Trends Cell Biol* 13, 137-145
- 417** Akasaki, K., Michihara, A., Mibuka, K., Fujiwara, Y., and Tsuji, H. (1995) Biosynthetic transport of a major lysosomal membrane glycoprotein, lamp-1: convergence of biosynthetic and endocytic pathways occurs at three distinctive points. *Exp Cell Res* 220, 464-473
- 418** Medina, D.L., Fraldi, A., Bouche, V., Annunziata, F., Mansueto, G., Spampanato, C., Puri, C., Pignata, A., Martina, J.A., Sardiello, M., Palmieri, M., Polishchuk, R., Puertollano, R., and Ballabio, A. (2011) Transcriptional activation of lysosomal exocytosis promotes cellular clearance. *Dev Cell* 21, 421-430
- 419** Reddy, A., Caler, E.V., and Andrews, N.W. (2001) Plasma membrane repair is mediated by Ca(2+)-regulated exocytosis of lysosomes. *Cell* 106, 157-169
- 420** van der Sluijs, P., Zibouche, M., and van Kerkhof, P. (2013) Late steps in secretory lysosome exocytosis in cytotoxic lymphocytes. *Front Immunol* 4, 359
- 421** Khalikova, E., Susi, P., and Korpela, T. (2005) Microbial dextran-hydrolyzing enzymes: fundamentals and applications. *Microbiol Mol Biol Rev* 69, 306-325
- 422** Ben-Yoseph, Y., Potier, M., Mitchell, D.A., Pack, B.A., Melancon, S.B., and Nadler, H.L. (1987) Altered molecular size of N-acetylglucosamine 1-phosphotransferase in I-cell disease and pseudo-Hurler polydystrophy. *Biochem J* 248, 697-701
- 423** Settembre, C. and Ballabio, A. (2013) New targets for old diseases: lessons from mucopolidosis type II. *EMBO Mol Med* 5, 1801-1803
- 424** Braulke, T. and Bonifacino, J.S. (2009) Sorting of lysosomal proteins. *Biochim Biophys Acta* 1793, 605-614
- 425** Dell'Angelica, E.C., Shotelersuk, V., Aguilar, R.C., Gahl, W.A., and Bonifacino, J.S. (1999) Altered trafficking of lysosomal proteins in Hermansky-Pudlak syndrome due to mutations in the beta 3A subunit of the AP-3 adaptor. *Mol Cell* 3, 11-21
- 426** Doherty, G.J. and McMahon, H.T. (2009) Mechanisms of endocytosis. *Annu Rev Biochem* 78, 857-902
- 427** Turturici, G., Sconzo, G., and Geraci, F. (2011) Hsp70 and its molecular role in nervous system diseases. *Biochem Res Int* 2011, 618127
- 428** Uversky, V.N. (2011) Flexible nets of malleable guardians: intrinsically disordered chaperones in neurodegenerative diseases. *Chem Rev* 111, 1134-1166
- 429** Fink, A.L. (1999) Chaperone-mediated protein folding. *Physiol Rev* 79, 425-449
- 430** Ingemann, L. and Kirkegaard, T. (2014) Lysosomal Storage Diseases and the Heat Shock Response: Convergences and Therapeutic Opportunities. *J Lipid Res*

- 431** Warrick, J.M., Chan, H.Y., Gray-Board, G.L., Chai, Y., Paulson, H.L., and Bonini, N.M. (1999) Suppression of polyglutamine-mediated neurodegeneration in *Drosophila* by the molecular chaperone HSP70. *Nat Genet* 23, 425-428
- 432** Cummings, C.J., Sun, Y., Opal, P., Antalffy, B., Mestril, R., Orr, H.T., Dillmann, W.H., and Zoghbi, H.Y. (2001) Over-expression of inducible HSP70 chaperone suppresses neuropathology and improves motor function in SCA1 mice. *Hum Mol Genet* 10, 1511-1518
- 433** Adachi, H., Katsuno, M., Minamiyama, M., Sang, C., Pagoulatos, G., Angelidis, C., Kusakabe, M., Yoshiki, A., Kobayashi, Y., Doyu, M., and Sobue, G. (2003) Heat shock protein 70 chaperone overexpression ameliorates phenotypes of the spinal and bulbar muscular atrophy transgenic mouse model by reducing nuclear-localized mutant androgen receptor protein. *J Neurosci* 23, 2203-2211
- 434** Klucken, J., Shin, Y., Masliah, E., Hyman, B.T., and McLean, P.J. (2004) Hsp70 Reduces alpha-Synuclein Aggregation and Toxicity. *J Biol Chem* 279, 25497-25502
- 435** Guzhova, I., Kislyakova, K., Moskaliova, O., Fridlanskaya, I., Tytell, M., Cheetham, M., and Margulis, B. (2001) In vitro studies show that Hsp70 can be released by glia and that exogenous Hsp70 can enhance neuronal stress tolerance. *Brain Res* 914, 66-73
- 436** Hightower, L.E. and Guidon, P.T., Jr. (1989) Selective release from cultured mammalian cells of heat-shock (stress) proteins that resemble glia-axon transfer proteins. *J Cell Physiol* 138, 257-266
- 437** Kakimura, J., Kitamura, Y., Takata, K., Umeki, M., Suzuki, S., Shibagaki, K., Taniguchi, T., Nomura, Y., Gebicke-Haerter, P.J., Smith, M.A., Perry, G., and Shimohama, S. (2002) Microglial activation and amyloid-beta clearance induced by exogenous heat-shock proteins. *FASEB J* 16, 601-603
- 438** Gifondorwa, D.J., Robinson, M.B., Hayes, C.D., Taylor, A.R., Pevette, D.M., Oppenheim, R.W., Caress, J., and Milligan, C.E. (2007) Exogenous delivery of heat shock protein 70 increases lifespan in a mouse model of amyotrophic lateral sclerosis. *J Neurosci* 27, 13173-13180
- 439** Vitner, E.B., Platt, F.M., and Futerman, A.H. (2010) Common and uncommon pathogenic cascades in lysosomal storage diseases. *J Biol Chem* 285, 20423-20427
- 440** Yang, C., Swallows, C.L., Zhang, C., Lu, J., Xiao, H., Brady, R.O., and Zhuang, Z. (2014) Celastrol increases glucocerebrosidase activity in Gaucher disease by modulating molecular chaperones. *Proc Natl Acad Sci U S A* 111, 249-254
- 441** Kirkegaard, T., Roth, A.G., Petersen, N.H., Mahalka, A.K., Olsen, O.D., Moilanen, I., Zyllicz, A., Knudsen, J., Sandhoff, K., Arenz, C., Kinnunen, P.K., Nylandsted, J., and Jaattela, M.

- (2010) Hsp70 stabilizes lysosomes and reverts Niemann-Pick disease-associated lysosomal pathology. *Nature* 463, 549-553
- 442** Mambula, S.S. and Calderwood, S.K. (2006) Heat shock protein 70 is secreted from tumor cells by a nonclassical pathway involving lysosomal endosomes. *J Immunol* 177, 7849-7857
- 443** Hirel, P.H., Schmitter, M.J., Dessen, P., Fayat, G., and Blanquet, S. (1989) Extent of N-terminal methionine excision from *Escherichia coli* proteins is governed by the side-chain length of the penultimate amino acid. *Proc Natl Acad Sci U S A* 86, 8247-8251
- 444** Nylandsted, J., Gyrd-Hansen, M., Danielewicz, A., Fehrenbacher, N., Lademann, U., Hoyer-Hansen, M., Weber, E., Multhoff, G., Rohde, M., and Jaattela, M. (2004) Heat shock protein 70 promotes cell survival by inhibiting lysosomal membrane permeabilization. *J Exp Med* 200, 425-435
- 445** Petersen, N.H., Kirkegaard, T., Olsen, O.D., and Jaattela, M. (2010) Connecting Hsp70, sphingolipid metabolism and lysosomal stability. *Cell Cycle* 9, 2305-2309
- 446** Goodchild, S.C., Sheynis, T., Thompson, R., Tipping, K.W., Xue, W.F., Ranson, N.A., Beales, P.A., Hewitt, E.W., and Radford, S.E. (2014) beta2-Microglobulin Amyloid Fibril-Induced Membrane Disruption Is Enhanced by Endosomal Lipids and Acidic pH. *PLoS One* 9, e104492
- 447** Dedmon, M.M., Christodoulou, J., Wilson, M.R., and Dobson, C.M. (2005) Heat shock protein 70 inhibits alpha-synuclein fibril formation via preferential binding to prefibrillar species. *J Biol Chem* 280, 14733-14740
- 448** Huang, C., Cheng, H., Hao, S., Zhou, H., Zhang, X., Gao, J., Sun, Q.H., Hu, H., and Wang, C.C. (2006) Heat shock protein 70 inhibits alpha-synuclein fibril formation via interactions with diverse intermediates. *J Mol Biol* 364, 323-336
- 449** Pemberton, S., Madiona, K., Pieri, L., Kabani, M., Bousset, L., and Melki, R. (2011) Hsc70 protein interaction with soluble and fibrillar alpha-synuclein. *J Biol Chem* 286, 34690-34699
- 450** Singh, L.R., Gupta, S., Honig, N.H., Kraus, J.P., and Kruger, W.D. (2010) Activation of mutant enzyme function in vivo by proteasome inhibitors and treatments that induce Hsp70. *PLoS Genet* 6, e1000807
- 451** Kalmar, B., Lu, C.H., and Greensmith, L. (2014) The role of heat shock proteins in Amyotrophic Lateral Sclerosis: The therapeutic potential of Arimoclomol. *Pharmacol Ther* 141, 40-54
- 452** Cleren, C., Calingasan, N.Y., Chen, J., and Beal, M.F. (2005) Celastrol protects against MPTP- and 3-nitropropionic acid-induced neurotoxicity. *J Neurochem* 94, 995-1004

- 453** Wang, J., Gines, S., MacDonald, M.E., and Gusella, J.F. (2005) Reversal of a full-length mutant huntingtin neuronal cell phenotype by chemical inhibitors of polyglutamine-mediated aggregation. *BMC Neurosci* 6, 1
- 454** Kiaei, M., Kipiani, K., Petri, S., Chen, J., Calingasan, N.Y., and Beal, M.F. (2005) Celastrol blocks neuronal cell death and extends life in transgenic mouse model of amyotrophic lateral sclerosis. *Neurodegener Dis* 2, 246-254
- 455** Riedel, M., Goldbaum, O., Schwarz, L., Schmitt, S., and Richter-Landsberg, C. (2010) 17-AAG induces cytoplasmic alpha-synuclein aggregate clearance by induction of autophagy. *PLoS One* 5, e8753
- 456** Waza, M., Adachi, H., Katsuno, M., Minamiyama, M., Sang, C., Tanaka, F., Inukai, A., Doyu, M., and Sobue, G. (2005) 17-AAG, an Hsp90 inhibitor, ameliorates polyglutamine-mediated motor neuron degeneration. *Nat Med* 11, 1088-1095
- 457** Kieran, D., Kalmar, B., Dick, J.R., Riddoch-Contreras, J., Burnstock, G., and Greensmith, L. (2004) Treatment with arimoclomol, a coinducer of heat shock proteins, delays disease progression in ALS mice. *Nat Med* 10, 402-405
- 458** Kalmar, B., Novoselov, S., Gray, A., Cheetham, M.E., Margulis, B., and Greensmith, L. (2008) Late stage treatment with arimoclomol delays disease progression and prevents protein aggregation in the SOD1 mouse model of ALS. *J Neurochem* 107, 339-350
- 459** Malik, B., Nirmalanathan, N., Gray, A.L., La Spada, A.R., Hanna, M.G., and Greensmith, L. (2013) Co-induction of the heat shock response ameliorates disease progression in a mouse model of human spinal and bulbar muscular atrophy: implications for therapy. *Brain* 136, 926-943
- 460** Sims, N.A. and Gooi, J.H. (2008) Bone remodeling: Multiple cellular interactions required for coupling of bone formation and resorption. *Semin Cell Dev Biol* 19, 444-451
- 461** Motley, A., Bright, N.A., Seaman, M.N., and Robinson, M.S. (2003) Clathrin-mediated endocytosis in AP-2-depleted cells. *J Cell Biol* 162, 909-918
- 462** Kirkegaard, T. (2013) Emerging therapies and therapeutic concepts for lysosomal storage diseases. *Expert Opinion on Orphan Drugs* 1, 385-404
- 463** Tsunemi, T., Ashe, T.D., Morrison, B.E., Soriano, K.R., Au, J., Roque, R.A., Lazarowski, E.R., Damian, V.A., Masliah, E., and La Spada, A.R. (2012) PGC-1alpha rescues Huntington's disease proteotoxicity by preventing oxidative stress and promoting TFEB function. *Sci Transl Med* 4, 142ra197